CLIMATE CHANGE IMPACTS on HYDROLOGICAL PROCESSES and WATER DEMAND SCENARIO in the WEYIB RIVER BASIN, SOUTHEASTERN ETHIOPIA

A Thesis Submitted in Partial Fulfillment of the Requirements
for the Award of the Degree of

DOCTOR OF PHILOSOPHY

in

Civil Engineering

by

ABDULKERIM BEDEWI SERUR
(Roll No. 136104030)

Under the Supervision of
PROFESSOR ARUP KUMAR SARMA

DEPARTMENT OF CIVIL ENGINEERING
INDIAN INSTITUTE OF TECHNOLOGY GUWAHATI
GUWAHATI-781039, ASSAM, INDIA
JULY, 2017

STATEMENT OF THE AUTHOR

The work contained in this thesis entitled **'Climate Change Impacts on Hydrological Processes and Water Demand Scenario in the Weyib River Basin, Southeastern Ethiopia'** has been carried out by me under the supervision of **Professor Arup Kumar Sarma**, **Department of Civil Engineering, Indian Institute of Technology Guwahati**. I affirm that this thesis is my bonafide work and all sources of materials used for it have been duly acknowledged. I solemnly declare that this thesis is not submitted to any other university or institute for award of any academic degree, diploma, or certificate.

Abdulkerim Bedewi Serur
IIT Guwahati
July, 2017

Prof. A. K. Sarma, PhD
B.P.Chaliha Chair Professor
for Water Resources

Indian Institute of Technology
Guwahati,
Guwahati-781 039

Phones: 0361- 2582409 (O)
0361- 2584409 (R)
0361- 2690953 (R)
9435732225 (m)
Fax: 0361- 2582440
E-mail: aks@iitg.ernet.in

DEPARTMENT OF CIVIL ENGINEERING

Date: 25th July 2017

CERTIFICATE

This is to certify that the thesis entitled '**Climate Change Impacts on Hydrological Processes and Water Demand Scenario in the Weyib River Basin, Southeastern Ethiopia'** submitted by **Mr. Abdulkerim Bedewi Serur** to the **Indian Institute of Technology Guwahati** for the degree of **Doctor of Philosophy** in **Civil Engineering** is a record of bonafide research work carried out by him under my supervision.

The results contained in this thesis have not been submitted in part or full to any other university or institute for award of any academic degree, diploma, or certificate.

Professor Arup Kumar Sarma
IIT Guwahati
July, 2017

DEDICATION

I dedicate my thesis manuscript to my wife, Ametulah Kedir and my daughter, Aaroma and my Son, Moukid to express the love I have for them forever. I also dedicate this thesis manuscript to my families and friends whose words of encouragement and push for tenacity ring in my ears; love you all guys!

LIST OF ACRONYMS

A1B Scenario	Future World of Very Rapid Economic Growth and Global Population with Balanced Across Energy Sources
A1FI Scenario	Future World of Very Rapid Economic Growth and Global Population with Alternative Developments of Energy Technologies (Fossil Intensive)
A2 Scenario	Very Heterogeneous World with Continuously Increasing Global Population
ABT	Aggregated Boosted Trees
ACCES	Africa Climate Change Environment Security
ADD	Average Daily Demand
AGCM	Atmospheric Global Climate Model
AGNPS	Agricultural Nonpoint Source Pollution Model
AIM	Asian Pacific Integrated Model
Alpha_Bf	Baseflow Alpha Factor
ANN	Artificial Neural Network
ANSWERS	Areal Nonpoint Source Watershed Environmental Response Simulation
AOGCMs	Atmospheric-Ocean Global Circulation Models
AR3, 4 and 5	3^{rd} , 4^{th} and 5^{th} IPCC Assessment Reports
ArcGIS	Suit consisting of Geographical Information System software
ArcSWAT	ArcGIS Integrated SWAT Hydrological Model
ARS	Agricultural Research Service
ASD	Autism Spectrum Disorder
ASTER	Advanced Spaceborne Thermal Emission and Reflection Radiometer
AWD	Annual Water Demand
BMNP	Bale Mountainous National Park
B-circ	Vorticity Binning Method
Blai	Maximum Potential Leaf Area Index
BP	Base Period
B1 Scenario	Convergent World with Very Rapid Global Population but With Rapid Changes in Economic Structures
B2 Scenario	A World Which Emphasis on Local Solutions to Economic, Social, and Environmental Sustainability
CanESM2	Canadian Earth System Model-Second Generation
Canmx	Maximum Canopy Storage
CCA	Canonical Correlation Analysis
CCCMA	Canadian Centre for Climate Modelling and Analysis
C-circ	Continuous Velocity Method
CGCM3	Third Generation of Coupled Global Climate Model
CGCM1	First Generation of Coupled Global Climate Model
Ch_K2	Effective Hydraulic Conductivity in Main Channel Alluvium
CIWD	Commercial and Industrial Water Demand
CMIP3, 4 and 5	Coupled Model Inter-Comparison Project Phase 3, 4 and 5
Cn2	SCS Runoff Curve Number for Moisture Condition II
CREAMS	Chemicals, Runoff, and Erosion from Agricultural Management Systems
CSIRO	Commonwealth Scientific and Industrial Research Organization
CTP	Current Total Population
DEM	Digital Elevation Model
DWD	Domestic Water Demand
EB	Entire Basin
ECPs	Extended Concentration Pathways
EMPs	Ecological Management Practices
Esco	Soil Evaporation Compensation Factor
ESMs	Earth System Models
ET	Actual Evapotranspiration
EUROSEM	European Soil Erosion Model

LIST OF ACRONYMS *(Continued)*

GAM	Generalized Additive Model
GDEM	Global Digital Elevation Model
GDMPD	Genal-Dawa River Basin Master Plan Development
GCM	Global Circulation Model
GFDL	Geophysical Fluid Dynamics Laboratory
GFDLESM2M/2G	Geophysical Fluid Dynamics Laboratory Earth System Model 2M/2G
GHG	Greenhouse Gas
GIS	Geographic Information System
GLM	Generalized Linear Model
Gwgmn	Threshold Depth of Water in the Shallow Aquifer Required for Return Flow to Occur
GW_Revap	Groundwater "Revap" Coefficient
GWQ	Groundwater Contribution to Streamflow
HadCM3	Hadley Centre Coupled Model version 3
HadGEM1	Hadley Centre Global Environmental Model, version 1
HadGEM2-ES	Hadley Centre Global Environmental Model, version 1-Earth System
HadRM2	Hadley Centre Regional climate Model, version 2
HBV	Hydrologiska Byråns Vattenbalansavdelning
HEC	Hydrologic Engineering Centre
HMS	Hydrologic Modelling System
HRUs	Hydrologic Response Units
IAMs	Integrated Assessment Models
IIASA	International Institute for Applied Systems Analysis
IMAGE	Integrated Model to Assess the Global Environment
INCCA	Indian Network for Climate Change Assessment
IPCC	Intergovernmental Panel on Climate Change
IPSL	Institut Pierre Simon Laplace
IPSL-CM5ALR	Institut Pierre Simon Laplace-
IWD	Institutional Water Demand
JGCRI	Joint Global Change Research Institute
LH-OAT	Latin Hypercube One-Factor-At-a-Time
LULC	Land Use Land Cover
lpcd	Liter per Capita per Day
LWD	livestock Water Demand
MAGICC	Model for the Assessment of Greenhouse-gas Induced Climate Change
MDD	Maximum Daily Demand
MIKE-SHE	System Hydrologique European
MiniCAM	Mini-Climate Assessment Model
MIRCO-ESM-CHEM	Meteorological Institute of Research and Community Organization-Earth System Model-Chemistry
Mm^3	Million Cubic Meter
MoWE	Ministry of Water and Energy of Ethiopia
m^3 *pcy*	Cubic Meter Per Capita Per Year
MRI-CGCM	Meteorological Research Institute-Coupled Global Climate Model
NCEP-NCAR	National Centre For Environmental Prediction-National Centre for Atmospheric Research
NIES	National Institute for Environmental Studies
NMSA	National Meteorological Service Agency of Ethiopia
NOAA	National Oceanic and Atmospheric Administration
NorESM1-M	Norwegian Earth System Model- Medium Resolution Version
NSE	Nash-Sutcliffe Evaluation Coefficient
OGCM	Oceanic Global Climate Model
ParaSol	Parameter Solutions
Pbias	Percent Bias

LIST OF ACRONYMS *(Continued)*

PCA	Principal Component Analysis
PCM	Parallel Climate Model
PCP	Precipitation
PERC	Percolation to the Shallow Aquifer
PET	Potential Evapotranspiration
PRECIP	Precipitation
PRECIS	Providing REgional Climate for Impact Studies
PTP	Projected Total Population
R^2	Coefficient of Determination
RCM	Regional Climate Model
RCPs	Representative Concentration Pathways
RCP8.5, 4.5 and 2.6	Representative Concentration Pathway of Radiative Forcing Levels 8.5, 4.5 and 2.6 W/m^2 by the year 2100
Revapmn	Threshold Depth of Water in the Shallow Aquifer For "Revap" to Occur
RF	Rainfall
RMSE	Root Mean Square Error
RSM	Regional Spectrum Model
RSR	Ratio of Root Mean Square Error and Standard Deviation of Observation Values
SACZ	South Atlantic Convergence Zone
SB1	Sub-basin 1
SB2	Sub-basin 2
SB3	Sub-basin 3
SB4	Sub-basin 4
SB5	Sub-basin 5
SB6	Sub-basin 6
SCS	Soil Conservation Service
SDSM	Statistical Downscaling Model
Slope	Average Slope Steepness
Sol_Awc	Available Water Capacity of the Soil Layer
Sol_K	Saturated Hydraulic Conductivity
Sol_Z	Depth from Soil Surface to Bottom of Layer
SRES	Special Report on Emission Scenarios
SRTM	Shuttle Radar Topographic Mission
SURFQ	Surface Runoff Contribution to Streamflow
SW	Soil Water Content
SWAT	Soil and Water Assessment Tool
SWIM	Soil and Water Integrated Model
Temp	Temperature
Tmax	Maximum Temperature
Tmin	Minimum Temperature
TP	Total Population
UNFCCC	United Nations Framework Convention on Climate Change
U.S.	United States
USDA	United States Department of Agriculture
UTM	Universal Transverse Mercator
VIC	Variable Infiltration Capacity
WATCH	Water and Global Change
WD	Water Demand
WEAP	Water Evaluation and Planning System
WGEN	Weather GENerator
W/m^2	Watts per Meter Square
WT	Weather Typing
WYLD	Net Water Yield/Availability

ACKNOWLEDGEMENTS

Pursuing a Ph.D. project is a both painful and enjoyable experience. It's just like climbing a high peak, step by step, accompanied with bitterness, hardships, frustration, encouragement and trust with so many people's kind help. Though it will not be enough to express my gratitude in words to all those people who helped me, I would still like to give my many, many thanks to all these people.

Special mention goes to my enthusiastic supervisor, Professor Arup Kumar Sarma for his consistent support, and providing sincere, faithful and immense advice and guidance from the inception until the completion of the work to bring this study to this form at the expense of his invaluable time which enriched my professional performance a lot. To put it in a nut shell, this thesis paper would not have been completed like this without his aforementioned contributions. He was always willing to help me from inception to the end of thesis write-up in all aspects and extremely helpful in correcting the technical problems throughout the work and I have learned many things since I became his student. Thank you very much, Sir. I further take this opportunity to express my deep feelings and gratitude to my Doctoral Committee Members; Professor Subashisa Dutta (Chairman), Dr. Sreeja P. and Dr. Manish Kumar Goyal for their technical constrictive comments throughout the period that I spent in PhD program. Thanks for your help on getting this study into this shape; you have put a great part on it.

I would also like to express my gratitude to Ethiopian Ministry of Education (MoE) for awarding me a scholarship to pursue my PhD study at Civil Engineering Department of Indian Institute of Technology Guwahati, Assam, India and it enabled me to perform the hard tasks related with this research works in a sound way. I'm grateful to Maddawalabu University for allowing me to continue my PhD studies. I am very grateful to Ethiopian National Meteorological Services Agency and Ministry of Water Resources and Energy for providing me a meteorological, hydrological, and spatial data as well as some technical report documents. During in my stay at IIT Guwahati, many friends are helpful to color my life. However, I am hugely appreciative to Vishal Singh, Shivam Gupta and Alemayehu Abate for sharing their ArcSWAT hydrologic model expertise so willingly. I have to acknowledge all my research group mates in catchment hydrology room at water resources engineering lab for their assistances in many aspects that I cannot list them all because of limited space.

Most importantly, I would like to forward the leading and loving thanks to my helpful wife Ametulah Kedir for her never ending concern, support and encouragement. Being both a father and mother while I was away was not an easy thing for my wife. She took every responsibility and suffered all the bitterness to take care of my daughter and my son. Amy, without your love, support, understanding and patience this achievement would have not been possible. The success belongs to both of us. Special thanks go to my lovely kids, Aaroma and Moukid. They are always the source of my strength, happiness and permanent inspirations. Lastly, above all, I want to thank Allah for helping me endures the rigorous of everyday life and to overcome the challenges of PhD studies. Without Him nothing is happened. So I want to say Alhamdulillah**!!**

Abdulkerim Bedewi Serur
July, 2017

TABLE OF CONTENTS

STATEMENT OF THE AUTHOR ii
CERTIFICATE iii
DEDICATION iv
LIST OF ACRONYMS v
ACKNOWLEDGEMENTS viii
LIST OF TABLES xii
LIST OF FIGURES xiii
LIST OF TABLES IN THE APPENDIX xvi
LIST OF FIGURES IN THE APPENDIX xvii
LIST OF PHOTOS IN THE APPENDIX xviii
ABSTRACT xix

Chapter 1: Introduction 1

1.1 Introduction 1
1.2 Background of the Study 1
1.3 Statement of the Problem 4
1.4 Significance of the Study 5
1.5 Research Questions 7
1.6 Research Objectives 8
1.6.1. Broad objective 8
1.6.2. Specific objectives 8
1.7 Organization of the Thesis 8

Chapter 2: Literature Review 11

2.1. Introduction 11
2.2. Climate Change Impacts on the Hydrology and Water Resources 11
2.2.1. Climate change impacts on the hydrologic cycle 11
2.2.2. Climate change impacts on the water resources management 14
2.3. Climate Change Impact in Ethiopia and Africa 17
2.4. General Circulation Model (GCMs) and Earth System Models (ESMs) 19
2.5. Future Emission Scenarios 20
2.5.1. Update on scenario development: from SRES to RCPs 20
2.5.2. The newly developed representative concentration pathway scenarios (RCPs) 20
2.5.3. Benefits of using RCPs 22
2.6. Review of Downscaling Approaches 22
2.6.1. Dynamical downscaling (DD) 23
2.6.2. Statistical downscaling (SD) 23
2.7. Hydrology and Water Resources Modeling 26
2.8. Water Demand Assessment for Selected and Weyib River Basin 27

Chapter 3: Statistical Downscaling of Daily Temperatures and Precipitation Data from CMIP5-ESMs-RCPs Experiment: in Weyib River Basin, Southeastern Ethiopia 30

3.1. Introduction 30
3.2. Materials and Methods 31
3.2.1. Description of study area (Weyib River basin) 31

TABLE OF CONTENTS *(Continued)*

3.2.2. Types of Earth System Models (ESMs) and RCP scenarios used 33
3.2.3. Types of data used 34
3.2.4. Downscaling methods 34
3.2.5. Statistical downscaling model (SDSM) 35
3.2.6. Statistical downscaling model setup (Model Approach) 36
3.2.7. SDSM performance evaluation 39
3.2.8. Statistical bias correction 40
3.2.9. Precipitation and temperatures scenario statistics 40
3.2.10. Mann-Kendall trends test 41
3.3. Results and Discussion 42
3.3.1. Selected common potential predictor variables 42
3.3.2. Calibration and validation of SDSM for both temperatures and precipitation 44
3.3.3. Scenarios developed for future temperatures and precipitation (2006-2100) for twelve averaged spatial weather stations 45
3.3.4. Mann-Kendall trend test of future temperatures and precipitation (2006-2100) 56
3.3.5. Scenarios developed for future temperatures and precipitation (2006-2100) for six averaged arbitrary spatial weather stations 56
3.3.6. Scenarios developed for future temperatures and precipitation (2006-2100) for three averaged arbitrary spatial weather stations 60
3.3.7. Scenarios developed for future temperatures and precipitation (2006-2100) for a single (Goba) weather station 63
3.4. Conclusion 67

Chapter 4: Evaluation of the ArcSWAT Model in Simulating Catchment Hydrology: in Weyib River Basin, Southeastern Ethiopia 68

4.1. Introduction 68
4.2. Materials and Methods 69
4.2.1. Materials and software program used 69
4.2.2. SWAT model description 70
4.2.3. SWAT model approach 71
4.2.4. Hydrological components of SWAT model 71
4.2.5. SWAT model inputs 73
4.2.6. SWAT model setup 75
4.2.7. Model performance evaluation 77
4.3. Results and Discussion 79
4.3.1. Simulation of the hydrology of the Weyib River catchment 79
4.3.2. Parameters sensitivity analysis 81
4.3.3. SWAT model calibration and validation 82
4.4. Conclusion 86

Chapter 5: Climate Change Impact Analysis on Hydrological Processes of the Weyib River Basin, Southeastern Ethiopia 87

5.1. Introduction 87
5.2. Materials and methods 87
5.2.1. Drainage area and hydrologic response unit description (HRUs) 87
5.2.2. The Earth System Models (ESMs) and RCP scenarios 88

TABLE OF CONTENTS *(Continued)*

5.2.3. The ArcSWAT hydrologic model 88
5.2.4. Investigation of future climate changes impact on hydrological processes 89
5.3. Results and Discussion 89
5.3.1. Entire river basin and sub-basin scale current annual hydrological processes 89
5.3.2. Entire river basin and sub-basin scale average annual future changes in hydrological processes under climate change scenarios 95
5.3.3. Entire river basin and sub-basin scale mean monthly and seasonal future changes net water availability under climate change scenarios 98
5.4. Conclusion 114

Chapter 6: Current and Projected Water Demand and Water Availability Estimates under Climate Change Scenarios in the Weyib River Basin, Southeastern Ethiopia 116

6.1. Introduction 116
6.2. Materials and Methods 117
6.2.1. Spatial distribution of current (2005) and projected (in the 2020s, 2050s, and 2080s) total population of Weyib River basin 117
6.2.2. Total annual water demand estimates of Weyib River basin 117
6.2.3. Water availability estimates of Weyib River basin 119
6.3. Results and Discussion 120
6.3.1. Spatial distribution of current (2005) and projected (in the 2020s, 2050s, and 2080s) total population of Weyib River basin 120
6.3.2. Weyib River basin total annual water demand estimates 121
6.3.3. Average annual total water availability estimates of Weyib River basin 122
6.3.4. Water stress index estimates (in m^3per capita per year) of Weyib River basin 124
6.4. Conclusion 127

Chapter 7: Summary, Conclusions, and Recommendations 129

7.1 Summary and Conclusions 129
7.2 Recommendations 137

References 139

Appendices 148

Appendix A 148
Appendix B 159
Appendix C 164

LIST OF TABLES

Table **Page**

2.1 Types of representative concentration pathways (IPCC, 2013b) ---------- 21
3.1 The CMIP5 Earth System Models used in this study----------33
3.2 Details of the 12 meteorological stations and their data records.....34
3.3 Example, correlation matrix obtained from SDSM for minimum temperature.....38
3.4 List of selected common potential predictor variables that gave better correlation results at p<0.05 from CanESM2-historical model for study area of Weyib River basin.....42
3. 5 List of selected common potential predictor variables that gave better correlation results at p<0.05 from GFDL-ESM2M-historical model for study area of Weyib River basin.....43
3.6 List of selected common potential predictor variables that gave better correlation results at p<0.05 from GFDL-ESM2G-historical model for study area of Weyib River basin.....43
3.7 Absolute changes in mean seasonal maximum temperature (°C) at different time slices from the base period.....47
3.8 Absolute changes in mean seasonal minimum temperature (°C) at different time slices from the base period.....50
3.9 Percentage change in mean seasonal precipitation at different time slices from the base period ...54
3.10 Mann-Kendall trend test for future average annual both temperatures and precipitation under three RCP scenarios for mean of 3 ESMs.....56
3.11 Comparison of current and future projections of mean of 3ESMs with three RCPs for annual mean daily maximum temperature (°C) at different averaged spatial observation stations in Weyib River basin.....66
3.12 Comparison of current and future projections of mean of 3ESMs with three RCPs for annual mean daily minimum temperature (°C) at different averaged spatial observation stations in Weyib River basin.....66
3.13 Comparison of current and future projections of mean of 3ESMs with three RCPs for annual mean daily precipitation (mm) at different averaged spatial observation stations in Weyib River basin.....66
4.1 General model performance ratings for recommended statistics for a monthly time step (Moriasi et al., 2007)---------- 79
4.2 Major soil unit of Weyib catchment and their areal coverage in the catchment 80
4.3 Major Landuses of Weyib catchment and their areal coverage in the catchment 80
4.4 Land slope classes of Weyib catchment and their areal coverage in the catchment 80
4.5 SWAT's most sensitive streamflow parameters and final calibrated fitted values 82
4.6 Summary of model performance ratings for simulations of streamflow.....85
5.1 Entire river basin and sub-basin scale analysis of mean annual simulated hydrological processes during baseline (1984-2004) and future period (2010-2100) simulation under Ensembles of ESMs for the RCP8.5, RCP4.5, and RCP2.6 scenarios----------96
6.1 Spatial distribution of current (2005) and projected (2020s, 2050s, and 2080s) total population of Weyib River basin----------120
6.2 The annual total irrigation water requirement of three irrigation schemes in Weyib river basin..121
6.3 Spatial distribution of current (2005) and projected (2020s, 2050s, and 2080s) total annual water demand estimates of Weyib River basin.....122
6.4 Current and future average annual total water availability (mean of 3ESMs) in three future times slice under three RCP scenarios of Weyib River basin 123
6.5 Weyib River basin current and future (mean of 3ESMs) total yearly water availability in three future time slice under three RCP scenarios.....124
6.6 Estimates of water stress index (m^3per capita per year) in Weyib River basin.....125

LIST OF FIGURES

Figure **Page**

3.1 Location map, reaches and some of the weather stations in the study area----------32
3.2 Spatial distribution of temperatures and rainfall characteristics of Weyib River basin----------32
3. A comprehensive flow chart of SDSM downscaling processes, ArcSWAT hydrologic modeling, water demand analysis and water stress estimation---------- 39
3.3a (top left): Calibration result of SDSM for maximum temperature from average of 3 ESMs (1981-1993), b (top right): same as fig 3.3a but for validation period (1994-2005), c (middle left): Calibration result of SDSM for minimum temperature, d (middle right): same as c but for validation period, e (bottom left): Calibration result of SDSM for precipitation, f (bottom right): same as e but for validation period----------45
3.4 Absolute change from baseline simulation of annual maximum temperature in all the ESM-RCP scenarios in the 2020s, 2050s and 2080s time slices ----------46
3.5 Future trend of mean annual maximum temperature (°C) in all the ESM-RCP scenarios----------46
3.6a (top left): Maximum temperature (monthly and seasonal mean daily) during baseline (1981-2005) simulation and three future time slice under RCP2.6 scenario for twelve averaged spatial stations, b (top right): same as fig 3.6a but under RCP4.5, c (bottom left): same as fig 3.6a but under RCP8.5, d (bottom right): same as fig 3.6a but without time slice under RCP2.6, RCP4.5 and RCP8.5 scenarios. ----------48
3.7 Absolute changes from baseline simulation of annual minimum temperature in all the ESM-RCP scenarios in the 2020s, 2050s and 2080s time slices----------49
3.8 Future trend of mean annual minimum temperature (°C) in all the ESM-RCP scenarios ----------49
3.9a (top left): Minimum temperature (monthly and seasonal mean daily) during baseline (1981-2005) simulation and three future time slice under RCP2.6 scenario for twelve averaged spatial stations, b (top right): same as fig 3.9a but under RCP4.5, c (bottom left): same as fig 3.9a but under RCP8.5, d (bottom right): same as fig 3.9a but without time slice under RCP2.6, RCP4.5 and RCP8.5 scenarios.----------51
3.10 Percentage change from baseline simulation of annual precipitation in all the ESM-RCP scenarios in the 2020s, 2050s and 2080s time slices ----------53
3.11 Future trend of mean annual total precipitation (mm) in all the ESM-RCP scenarios----------53
3.12a (top left): Precipitation (monthly and seasonal mean daily) during baseline period (1981-2005) simulation and three future time slice under RCP2.6 scenario for twelve averaged spatial stations, b (top right): same as fig 3.12a but under RCP4.5, c (bottom left): same as fig 3.12a but under RCP8.5, d (bottom right): same as fig 3.12a but without time slice under RCP2.6, RCP4.5 and RCP8.5 scenarios ----------55
3.13a (top left): Monthly mean daily absolute change in maximum temperature from base period in three future time slice under RCP2.6 scenario for six averaged spatial stations, b (top right): same as fig 3.13a but for RCP4.5, c (bottom left): same as fig 3.13a but for RCP8.5, d (bottom right): future trend of mean annual maximum temperature for six averaged spatial stations----59
3.14a (top left): Monthly mean daily absolute change in minimum temperature from base period in three future time slice under RCP2.6 scenario for six averaged spatial stations, b (top right): same as fig 3.14a but for RCP4.5, c (bottom left): same as fig 3.14a but for RCP8.5, d (bottom right): future trend of mean annual minimum temperature for six averaged spatial stations-----59
3.15a (top left): Monthly mean daily percentage change in precipitation from base period in three future time slice under RCP2.6 scenario for six averaged spatial stations, b (top right): same as fig 3.15a but for RCP4.5, c (bottom left): same as fig 3.15a but for RCP8.5, d (bottom right): future trend of mean annual precipitation for six averaged spatial stations ----------59
3.16a (top left): Monthly mean daily absolute change in maximum temperature from base period in three future time slice under RCP2.6 scenario for three averaged spatial stations, b (top right): same as fig 3.16a but for RCP4.5, c (bottom left): same as fig 3.16a but for RCP8.5, d (bottom right): future trend of mean annual maximum temperature for three averaged spatial stations--62

LIST OF FIGURES *(Continued)*

3.17a (top left): Monthly mean daily absolute change in minimum temperature from base period in three future time slice under RCP2.6 scenario for three averaged spatial stations, b (top right): same as fig 3.17a but for RCP4.5, c (bottom left): same as fig 3.17a but for RCP8.5, d (bottom right): future trend of mean annual minimum temperature for three averaged spatial stations --62
3.18a (top left): Monthly mean daily percentage change in precipitation from base period in three future time slice under RCP2.6 scenario for three averaged spatial stations, b (top right): same as fig 3.18a but for RCP4.5, c (bottom left): same as fig 3.18a but for RCP8.5, d (bottom right): future trend of mean annual precipitation for three averaged spatial stations ----------62
3.19a (top left): Monthly mean daily absolute change in maximum temperature from base period in three future time slice under RCP2.6 scenario for single station (Goba), b (top right): same as fig 3.19a but for RCP4.5, c (bottom left): same as fig 3.19a but for RCP8.5, d (bottom right): future trend of mean annual maximum temperature for single station (Goba)----------65
3.20a (top left): Monthly mean daily absolute change in minimum temperature from base period in three future time slice under RCP2.6 scenario for single station (Goba), b (top right): same as fig 3.20a but for RCP4.5, c (bottom left): same as fig 3.20a but for RCP8.5, d (bottom right): future trend of mean annual minimum temperature for single station (Goba) ----------65
3.21a (top left): Monthly mean daily percentage change in precipitation from base period in three future time slice under RCP2.6 scenario for single station (Goba), b (top right): same as fig 3.21a but for RCP4.5, c (bottom left): same as fig 3.21a but for RCP8.5, d (bottom right): future trend of mean annual precipitation single station (Goba) ----------65
4.1 Study area: location map and weather stations of the study area----------69
4.2a (top left): Soil map and its spatial distribution over the Weyib catchment, b (top right): the same as Fig.4.2a but for land use map, c (bottom left): the same as Fig.4.2a but for land slope map, d (bottom right): the same as Fig.4.2a but for DEM map (30mr) 81
4.3 Hydrograph of the observed and simulated streamflow using calibrated parameters for the calibration period (1984-1994) 83
4.4 Regression line fit between observed and simulated streamflow during calibration period 83
4.5 Hydrograph of the observed and simulated streamflow using calibrated parameters for the validation period (1995-2004) 84
4. 6 Regression line fit between observed and simulated streamflow during validation period 84
5.1 Entire basin, sub-basin and reach delineation, longest path, and selected weather stations---------88
5.2a (top middle): Temporal variation of hydrological processes during base period (1984-2004) simulation for entire river basin, b (top left): same as fig 5.2a but for sub-basin 1, c (top right): same as fig 5.2a but for sub-basin 2, d (middle right): same as fig 5.2a but for sub-basin 3, e (middle left): same as fig 5.2a but for sub-basin 4, f (bottom left): same as fig 5.2a but for sub-basin 5, g (bottom right): same as fig 5.2a but for sub-basin 6 91
5.3a (top left): Spatial and temporal variation of total yearly precipitation (PRECIP) during baseline (1984-2004) simulation, b (top right): same as fig 5.3a but for actual evapotranspiration (ET), c (bottom left): same as fig 5.3a but for potential evapotranspiration (PET), d (bottom right): same as fig 5.3a but for surface runoff contribution to the streamflow (SURFQ) 94
5.4a (top left): Spatial and temporal variation of total yearly soil water content (SW) during baseline (1984-2004) simulation, b (top right): same as fig 5.4a but for groundwater contribution to streamflow (GWQ), c (bottom left): same as fig 5.4a but for percolation (PERC), d (bottom right): same as fig 5.4a but for net amount of water availability (WYLD)....94
5.5a (top center): Percentage change from baseline simulation in the mean of three ESMs hydrological processes for the three RCP scenarios in the entire river basin, b (top left): same as fig 5.5a but for sub-basin 1, c (top right): same as fig 5.5a but for sub-basin 2, d (middle left): same as fig 5.5a but for sub-basin 3, e (middle right): same as fig 5.5a but for sub-basin 4, f (bottom left): same as fig 5.5a but for sub-basin 5, g (bottom right): same as fig 5.5a but for sub-basin 6. Legend given in (a) is the same as in all figures 97

LIST OF FIGURES *(Continued)*

5.6a (top center): Entire river basin surface runoff (monthly and seasonal mean daily) during baseline (1984-2004) simulation and three future time slice under mean of 3 ESMs for the RCP2.6 scenario, b (top left): same as fig 5.6a but for RCP4.5 scenario, c (top right): same as fig 5.6a but for RCP8.5 scenario, d (middle center): same as fig 5.6a but for lateral flow RCP 2.6 scenario, e (bottom left): same as fig 5.6d but RCP4.5 scenario, f (bottom right): same as fig 5.6d but RCP8.5 scenario. Legend given in (a) is the same in all figures.....101

5.7a (top center): Entire river basin groundwater flow (monthly and seasonal mean daily) during baseline (1984-2004) simulation and three future time slice under mean of 3 ESMs for theRCP2.6 scenario, b (top left): same as fig 5.7a but for RCP4.5 scenario, c (top right): same as fig 5.7a but for RCP8.5 scenario, d (middle center): same as fig 5.7a but for net water availability RCP 2.6 scenario, e (bottom left): same as fig 5.7d but RCP4.5 scenario, f (bottom right): same as fig 5.7d but RCP8.5 scenario. Legend given in (a) is the same in all figures.....104

5.8a (top left): Sub-basin 1 water availability (monthly and seasonal mean daily) during baseline (1984-2004) simulation and three future time slice under mean of 3 ESMs for RCP2.6 scenario, b (top right): same as fig 5.8a but for RCP4.5 scenario, c (bottom left): same as fig 5.8a but for RCP8.5 scenario, d (bottom right): same as fig 5.8a but without time slice under RCP2.6, RCP4.5 and RCP8.5 scenarios.....108

5.9a (top left): Sub-basin 2 water availability (monthly and seasonal mean daily) during baseline (1984-2004) simulation and three future time slice under mean of 3 ESMs for RCP2.6 scenario, b (top right): same as fig 5.9a but for RCP4.5 scenario, c (bottom left): same as fig 5.9a but for RCP8.5 scenario, d (bottom right): same as fig 5.9a but without time slice under RCP2.6, RCP4.5 and RCP8.5 scenarios.....108

5.10a (top left): Sub-basin 3 water availability (monthly and seasonal mean daily) during baseline (1984-2004) simulation and three future time slice under mean of 3 ESMs for RCP2.6 scenario, b (top right): same as fig 5.10a but for RCP4.5 scenario, c (bottom left): same as fig 5.10a but for RCP8.5 scenario, d (bottom right): same as fig 5.10a but without time slice under RCP2.6, RCP4.5 and RCP8.5 scenarios.....108

5.11a (top left): Sub-basin 4 water availability (monthly and seasonal mean daily) during baseline (1984-2004) simulation and three future time slice under mean of 3 ESMs for RCP2.6 scenario, b (top right): same as fig 5.11a but for RCP4.5 scenario, c (bottom left): same as fig 5.11a but for RCP8.5 scenario, d (bottom right): same as fig 5.11a but without time slice under RCP2.6, RCP4.5 and RCP8.5 scenarios.....112

5.12a (top left): Sub-basin 5 water availability (monthly and seasonal mean daily) during baseline (1984-2004) simulation and three future time slice under mean of 3 ESMs for RCP2.6 scenario, b (top right): same as fig 5.12a but for RCP4.5 scenario, c (bottom left): same as fig 5.12a but for RCP8.5 scenario, d (bottom right): same as fig 5.12a but without time slice under RCP2.6, RCP4.5 and RCP8.5 scenarios.....112

5.13a (top left): Sub-basin 6 water availability (monthly and seasonal mean daily) during baseline (1984-2004) simulation and three future time slice under mean of 3 ESMs for RCP2.6 scenario, b (top right): same as fig 5.13a but for RCP4.5 scenario, c (bottom left): same as fig 5.13a but for RCP8.5 scenario, d (bottom right): same as fig 5.13a but without time slice under RCP2.6, RCP4.5 and RCP8.5 scenarios.....112

6 Spatial distribution of water availability (a), water demand (b) and water stress (water resources status of the basin) (c) during baseline and future time periods (in the 2020s, 2050s and 2080s time slices) of Weyib River basin---------- 124

LIST OF TABLES IN THE APPENDIX

Appendix Table **Page**

1 Lists of selected potential predictor variables from CanESM2-historical model for station: Adaba -----148
2 Lists of selected potential predictor variables from GFDL_ESM2M-historical model for station: Adaba ----------148
3 Lists of selected potential predictor variables from GFDL_ESM2G-historical model for station: Adaba ----------148
4 Lists of selected predictor variables from CanESM2-historical model for station: Agarfa ----------149
5 Lists of selected predictor variables from GFDL_ESM2M-historical model for station: Agarfa---------149
6 Lists of selected potential predictor variables from GFDL_ESM2G-historical model for station: Agarfa ----------149
7 Lists of selected predictor variables from CanESM2-historical model for station: Dinsho ----------150
8 Lists of selected predictor variables from GFDL_ESM2M-historical model for station: Dinsho---------150
9 Lists of selected potential predictor variables from GFDL_ESM2G-historical model for station: Dinsho ----------151
10 Lists of selected predictor variables from CanESM2-historical model for station: Gassera----------151
11 Lists of selected predictor variables from GFDL_ESM2M-historical model for station: Gassera ------151
12 Lists of selected potential predictor variables from GFDL_ESM2G-historical model for station: Gassera ----------151
13 Lists of selected predictor variables from CanESM2-historical model for station: Ginnir ----------151
14 Lists of selected predictor variables from GFDL_ESM2M-historical model for station: Ginnir--------152
15 Lists of selected potential predictor variables from GFDL_ESM2G-historical model for station: Ginnir ----------152
16 Lists of selected predictor variables from CanESM2-historical model for station: Goba----------152
17 Lists of selected predictor variables from GFDL_ESM2M-historical model for station: Goba ---------153
18 Lists of selected potential predictor variables from GFDL_ESM2G-historical model for station: Goba ----------153
19 Lists of selected predictor variables from CanESM2-historical model for station: Goro ----------153
20 Lists of selected predictor variables from GFDL_ESM2M-historical model for station: Goro---------154
21 Lists of selected potential predictor variables from GFDL_ESM2G-historical model for station: Goro ----------154
22 Lists of selected predictor variables from CanESM2-historical model for station: Homa----------154
23 Lists of selected predictor variables from GFDL_ESM2M-historical model for station: Homa --------154
24 Lists of selected potential predictor variables from GFDL_ESM2G-historical model for station: Homa ----------155
25 Lists of selected predictor variables from CanESM2-historical model for station: Hunte----------155
26 Lists selected predictor variables from GFDL_ESM2M-historical model for station: Hunte----------155
27 Lists of selected potential predictor variables from GFDL_ESM2G-historical model for station: Hunte ----------156
28 Lists of selected predictor variables from CanESM2-historical model for station: Ali----------156
29 Lists of selected predictor variables from GFDL_ESM2M-historical model for station: Ali----------156
30 Lists of selected potential predictor variables from GFDL_ESM2G-historical model for station: Ali-156
31 Lists of selected predictor variables from CanESM2-historical model for station: Robe----------156
32 Lists of selected predictor variables from GFDL_ESM2M-historical model for station: Robe ---------157
33 Lists of selected potential predictor variables from GFDL_ESM2G-historical model for station: Robe ----------157
34 Lists of selected predictor variables from CanESM2-historical model for station: Sinnana ----------157
35 Lists of selected predictor variables from GFDL_ESM2M-historical model for station: Sinnana------158
36 Lists of selected potential predictor variables from GFDL_ESM2G-historical model for station: Sinnana ----------158
37 Morphological characteristics for the major soils of Weyib River basin----------158
38 Detail descriptions of soil physical and chemical characteristics of Weyib River basin used as an input for SWAT model ----------159

LIST OF FIGURES IN THE APPENDIX

Appendix Figure **Page**

1 Homogeneity test of annual precipitation series at station Adaba (homogeneous) --- 159
2 Homogeneity test of annual precipitation series at station Sinnana (homogeneous) --- 160
3 Homogeneity test of annual precipitation series at station Agarfa (homogeneous) --- 160
4 Homogeneity test of annual precipitation series at station Goba (homogeneous) --- 160
5 Homogeneity test of annual precipitation series at station Goro (homogeneous)--- 161
6 Homogeneity test of annual precipitation series at station Hunte (homogeneous) --- 161
7 Homogeneity test of annual precipitation series at station Meliyu (homogeneous) --- 161
8 Homogeneity test of annual precipitation series at station Robe (homogeneous) --- 162
9 Homogeneity test of annual precipitation series at station Homa (non-homogeneous) --- 162
10 Homogeneity test of annual precipitation series at station Dinsho (non-homogeneous) - 162
11 Homogeneity test of annual precipitation series at station Ginnir (non-homogeneous) -- 163
12 Homogeneity test of annual precipitation series at station Gassera (non-homogeneous) 163
13 Demonstration of ArcSWAT model for Weyib River Basin --- 163

LIST OF PHOTOS IN THE APPENDIX

Appendix Photo **Page**

1 Bread wheat varieties in Sinana Research Station, Bale Zone of Southern Ethiopia, in side Weyib River basin ----------164
2 Tegona river section, a tributary of Weyib River basin ----------164
3 Shaya river section, a tributary of Weyib River basin----------164
4 Recent bale-robe flash flood, inside Weyib River basin ----------165
5 Mountain Nyala, Bale Mountains National park, Oromia regional state, inside Weyib River basin ----------165

CLIMATE CHANGE IMPACTS on HYDROLOGICAL PROCESSES and WATER DEMAND SCENARIO in the WEYIB RIVER BASIN, SOUTHEASTERN ETHIOPIA

ABSTRACT

Future water availability and water demand scenario of any river basin is expected to change under the impact of climate change. The Weyib River, water from which is utilized for diverse water resources schemes, is one of the important rivers of Ethiopia. However, increase in temperature and change in both magnitude and its spatiotemporal distribution of rainfall under changing climate are adversely affecting the water resources scenario. Prior understanding of such change is crucial for water resources planning and management.

The main objective of this study was to investigate the spatial and temporal variation of current and projected hydrological processes, water demand and water availability under climate change scenarios in Weyib River basin, Bale mountainous area of Southeastern Ethiopia. The impact of climate change on the temperatures and precipitation characteristics of the Weyib River basin has been investigated using GFDL-ESM2M, CanESM2, and GFDL-ESM2G models output for the RCP2.6, RCP4.5, and RCP8.5 scenarios from coupled model inter-comparison project 5 (CMIP5). The statistical downscaling model calibrated and validated using the observed daily data of twelve meteorological stations was used to generate the future scenarios. The ArcSWAT hydrologic model calibrated and validated using the observed daily streamflow data for historical time period was employed to simulate current and projected future hydrological processes and hence to evaluate water availability. Current and projected population of the basin is considered to estimate the annual water demand thereby status of water resources need of the basin was estimated based on water stress index analysis. The analysis of both climate variables and hydrological processes were then carried out in an annual, seasonal, and monthly basis in the 2020s, 2050s, and 2080s time slices in the upcoming periods.

Results revealed that the mean annual maximum and minimum temperature, and precipitation have shown statistically significant (at 5% significant level) increasing trend in all the nine ESM-RCP scenarios in the 2020s 2050s and 2080s time slices. GFDL-ESM2M, projects the highest mean annual value for both temperatures and precipitation in all the RCP scenarios in future time slices; GFDL-ESM2G, projects the lowest increase in value of these parameters and CanESM2, projects an intermediate (median) increase. The variability of both temperatures and precipitation is higher in all ESMs of RCP8.5 than RCP4.5 and RCP2.6. The mean annual actual evapotranspiration, ground water contribution to the streamflow (baseflow), percolation, soil water content and water availability in the stream have been found to increase for all the nine ESMs-RCP scenarios in the entire basin and in all the sub-basins. However, surface runoff and potential evapotranspiration have shown a decreasing trend.

The future (mean of 3 ESMs) total annual water availability in the basin is observed to increase ranging from 15.04 to 21.61%, 20.08 to 23.34% and 16.21 to 39.53% by the 2020s, 2050s and 2080s time slice respectively from the available water resources (2333.39 Mm^3) of the base period. Sub-basin level analysis has shown that the annual, seasonal and monthly variations of hydrological processes in all the six sub-basins are similar in terms of direction but different in magnitude as compared to that of the entire basin analysis. In addition, it is observed that there is a larger monthly and seasonal variability in climatic variables and hydrological processes as compared to the variation in annual scale. Analysis has also revealed that the future total annual water demand of the basin will increase by 83.47% after 15 years, 200.67% after 45 years and 328.78% after 75 years, i.e., by the 2020, 2050 and 2080 respectively from the base period water demand of 289 Mm^3. This is primarily due to high pace of population increase (40.81%, 130.80% and 229.12% by the 2020, 2050 and 2080 respectively) in the basin and also due to change in climatic parameters.

The current water availability per capita per year of the basin is about 3112.23 m^3 and tends to decline ranging from 11.78 to 17.49%, 46.02 to 47.45% and 57.18 to 64.34% by the 2020s, 2050s and 2080s respectively from base period per capita per year water availability. This indicated that there is a possibility that the basin may face water stress condition in the long term. The increase of rainfall is comparatively higher in the dry season which might have positive impact on lowland region of the study area and it might affect the highland areas negatively since this season is specifically main crop harvesting period. Net water availability tends to decrease in all months on the dry season this might cause water shortage in the lowland region, and greater increase of water availability in intermediate and rainy seasons this might cause flooding to some flood prone region of the basin. Since the variation of net water availability among the six sub-basins in upcoming period is high, there is a scope of meeting agriculture water demand through water transfer from sub-basin having more available water in small area to the sub-basin having less available water in a larger agricultural area.

Keywords CMIP5-ESMs-RCPs Scenario · SDSM · Climate Change Scenarios · ArcSWAT Hydrologic Model · Hydrological Processes · Entire River Basin and Sub-basin Scale · Water Demand-Water Availability Scenario · Water Resources Status · Weyib River basin · Southeastern Ethiopia

Chapter 1: Introduction

1.1 Introduction

In recent days the word climate change is gaining importance in different fields because of its expected impacts on various sectors of economy. This section highlights on causes and projection of climate change effect with particular emphasis on the impact of climate change on the water resources availability as well as on current and future estimates of total annual water demand in the study area of Weyib River basin. Giving a background of the research need, objectives of the study is presented in this chapter. The research work is divided into different parts and presented in different chapters. Outline of the thesis organization is also presented towards end of this chapter.

1.2 Background of the Study

It is hard to talk about the 21st-century water issue without mentioning climate change. Climate change already knocked every corner of sectors in Ethiopia, mainly water resources, and agriculture. Almost 90% of the study area is agricultural land and extensively cultivated for cereal crops like barley and wheat. Therefore, having information about future variability of climatic variables, particularly precipitation is essential to sustain agriculture in the basin. The present unpredictable climate is striking plenteous threat to Ethiopia. The recent flooding incidences, as well as the very frequent drought in Ethiopia, could remain placed as visible indications for these influences (Ethiopian National Meteorological Agency, 2007). The Weyib River, water from which is utilized for diverse water resources schemes, is one of the important rivers of Ethiopia. However, increase in temperature and change in both magnitude and its spatiotemporal distribution of rainfall under changing climate are adversely affecting the water resources scenario. Climate change is aggravating the standing pressure on water resources resulting from growing populations and economic development. The increased variability in rainfall and streamflow caused by climate change may lead to water scarcity and flooding over the longer term.

Considering ensembles of multiple Global Circulation Models/ Earth System Models (GCMs/ ESMs) output for climate change impact studies is of paramount importance (Brekke et al., 2008; Maurer et al., 2007; Pierce et al., 2009; Reichler and Kim, 2008) to minimize uncertainty arise due to GCM/ESM. Therefore, in this study, three bias-corrected ESMs

(GFDL-ESM2M, CanESM2, and GFDL-ESM2G) for the Representative Concentration Pathway of Radiative Forcing Levels 8.5, 4.5 and 2.6 W/m^2 (watts per meter square) by the year 2100 (i.e., RCP8.5, RCP4.5 and RCP2.6, respectively) scenarios from coupled model inter-comparison project 5 (CMIP5) have been used. Ludwig et al. (2009) noted that the temporal and spatial distribution and availability of water resources, as well as the frequency of extreme events, will be affected by changing climate. Changing rainfall patterns, river hydrology, drought, reduced crop yields caused by drought are affecting food security (Africa), increasing frequency and intensity of storms is resulting in more severe flooding (Caribbean and Southeast Asia) and a decline in critical ecosystems are certain to have an adverse impact on the poor. Changes in rainfall patterns and amounts and rising of temperatures have reduced the reliability, and quality of water resources and these effects are predicted to become worse in future.

The projected mean annual temperature in Ethiopia is found to be in the ranges 0.9-1.1, 1.7-2.1 and 2.7-3.4°C by 2030, 2050 and 2080 time slices respectively (Ethiopian National Meteorological Agency, 2007). The projected mean annual maximum and minimum temperature shows rising trend in Southeastern part of Ethiopia (Shawul et al., 2016). In general, global mean temperatures revealed an increasing trend (IPCC, 2013; Kruger and Shongwe, 2004; New et al., 2006; Unganai, 1996) which points towards glacier to melt, sea level to rise and alteration in circulation pattern which influence precipitation, water availability, and extremes of floods and droughts; just to name a few.

The climate drives the hydrological cycle (Crosbie et al., 2010) and projected changes in spatial and temporal patterns of the climate variables will effect on local water resources, in particular, changes in precipitation has amplified as an impact on hydrological components. Rainfall is the largest factor in the water balance of catchment hydrology (Mpelasoka and Chiew, 2009). It is observed that there is a substantial variability in precipitation (rise about 20% and also declined by about 20%) in the globe (Bates et al., 2008). Larger spatial variation of precipitation (from a drop of about 25-50% to rise to 25-50%) has been reported in East Africa (Faramarzi et al., 2013). Increase in rainfall has been observed (Shongwe et al., 2009) in the tropics. Rainfall variability is more in the African continent and resulted in variation in water availability. For instance, a decline in water availability (streamflow) by 2050s is reported (Beck and Bernauer, 2011). Nevertheless, a rise of water availability (Graham et al., 2011) has also been stated. As seen in different literatures, it is difficult to

draw a general conclusion on the extent of decline or rise of water availability over the globe. The impact of climate change on water variability was studied (Setegn, 2010) in Lake Tana basin, Ethiopia using Soil and Water Assessment Tool (SWAT) model from coupled model inter-comparison project 3 (CMIP3) GCMs model for the future world of very rapid economic growth and global population with balanced across energy sources (A1B), convergent world with very rapid global population but with rapid changes in economic structures (B1), and very heterogeneous world with continuously increasing global population (A2) scenarios and he found that significant changes in stream flow and other hydrological parameters in the period between 2045-2100.

Farjad et al. (2016) investigated the average annual and seasonal variations of hydrological processes in the west and east sub-catchments using System Hydrologique European (MIKE-SHE) Model in Elbow River basin, Canada for the ensembles of CMIP3-GCMs up to the year 2070. They have reported that the mean annual surface runoff found to decrease. However, groundwater contribution to the streamflow (baseflow) and actual evapotranspiration tends to increase for the future world of very rapid economic growth and global population with alternative developments of energy technologies (fossil intensive) (A1F1) and world which emphasis on local solutions to economic, social, and environmental sustainability (B2) scenarios and which leading to a 50% net increase in total water yield. Aich et al. (2014) compared impacts of climate change on stream flow in four African River basins (Niger, Upper Blue Nile, Oubangui, and Limpopo) using Soil and Water Integrated Model (SWIM) from ensembles of CMIP5-ESMs for the RCP 8.5 and RCP2.6 scenarios. They found that a tendency for increased stream flows in three of the four basins (not for the Oubangui). Faramarzi et al. (2013) modeled the whole African continent using SWAT model from ensembles of coupled model inter-comparison project 4 (CMIP4) GCMs and they found that the same amount of mean annual water availability increment (about 10-20%) and decrement (about 10-20%), but with significant spatial variability. Faruqui et al. (2001) explained that one of the challenges in water resources management is an increasing water demand mainly due to a rapid increase of population, settlement patterns, wealth, industrial activity, technology, increasing demand for irrigation and climate change.

Therefore, in this study, statistical downscaling technique using multiple linear regression (MLR) based statistical downscaling model (SDSM) has been used to downscale daily temperatures (maximum and minimum) and precipitation data for 12 meteorological stations

found inside study area of Weyib River basin using ensembles of CMIP5-ESMs for the RCP8.5, RCP4.5, and RCP2.6 scenarios. These future downscaled temperatures, and precipitation data has been used as an input for SWAT hydrological model to simulate future, various surface and subsurface hydrological processes. Finally, total annual current and projected water demand were estimated and compared with available water in the stream so as to know water resources status of the basin. The analysis of climatic variables (maximum and minimum temperature and precipitation), hydrological processes and water resources status of Weyib River basin is carried out on an annual, seasonal and monthly basis in the 2020s (represents 2011-2040 time series data), 2050s (represents 2041-2070 time series data) and 2080s (represents 2071-2100 time series data) time slices in upcoming periods so that people and society can foresee and respond the tentative future challenges either by mitigating the worst condition that is likely to happen in future or at least be well prepared and resilient to face the possible challenges. These 30-year data (climatologically normal) is considered to be long enough to define local climate because it likely to have dry, wet, cool and warm period as suggested by many scientists and later recommended by IPCC.

1.3 Statement of the Problem

Climate change is exacerbating the existing pressure on water resources resulting from growing populations and economic development. The increased variability in rainfall and river flows caused by climate change may well increase water scarcity and flooding over the longer-term. Climate change that reduces either the overall quantity of water or the timing of water availability for use will have significant effects on agriculture, industrial and urban development.

The Weyib River, one of a tributary of Genale-Dawa River basin, water from which is utilized for diverse water resources schemes, is one of the important rivers of Ethiopia. The schemes include many existing and proposed irrigation systems (for instance, Bale Gadula; 4500 ha, Tegona; 2500 ha and Tebel; 1000 ha), tourism and fish farming at the different parts of the river. Farm Africa Sahel Ethiopia (2007) described that among the prior ecological services of the Bale Mountain National Park (BMNP) found in the study basin, the afro-alpine ecosystem is one of its hydrologic systems. It is sources of over 40 streams on which more than 12 million people depend on it.

The importance of the hydrological services that the area provides to Southeastern Ethiopia and parts of Somalia and Kenya have gradually recognized over the subsequent years, and their conservation is now a primary purpose of the park. The rapid urbanization encroaching into cultivated lands, expansions of cultivated areas into shrublands are the main causes that make the hydrologic system of the area in under continuous transformation. Though, there is a consensus on the need for proper planning of the water resources development as well as their utilization; there is still an urgent need to consider other factors like the impact of climate change on their sustainability. Many hydro-meteorological variables (for instance, stream flow, soil moisture and actual evapotranspiration) have inadequately measured in the study area. The recording period of hydro-meteorological data is very short and available for only a few stations, which impedes complete analysis of changes in water availability and water demand.

As reported in the Africa Climate Change Environment Security (ACCES) report (Ndaruzaniye, 2011), climate change is increasing the frequency and intensity of climate-related hazards, and hence, the level and patterns of often interrelated risks, particularly water and food security, exacerbate levels of vulnerability, mainly for rural communities in Ethiopia. Current climate variability is now imposing a significant challenge to Ethiopian communities by affecting water and food security, and energy supply. Over exploitation of land including deforestation associated with changing weather pattern have increased soil degradation and has inflicted water stress and crop failure. In Sub-Saharan Africa, i.e., the Eastern African region, particularly the Horn of Africa, is stated as highly geographically exposed to climate change and its impact on water resources is therefore expected to be high. Out of 160 million people living in the Horn of Africa, 70 million has located in areas prone to 'extreme drought leading to water insecurity and food shortages'. It is interesting to note that in this region both floods and droughts can occur in the same area within a very short period and these events can worsen water availability scenario both in terms of quality and quantity. Such temporal variability can adversely affect agricultural activities and power sector.

1.4 Significance of the Study

The effect of spatial data availability on climate change projection for any study area (watershed or basin) has not been studied yet. However, practical knowledge about impact of spatial data availability on future climate change projection in a specific study area is so

essential. Hence, this study tried to provide good understanding how spatial data availability affects the future climate change projection for the study area of Weyib River basin in Ethiopia.

The study aims to examine the variation of hydrological processes (in terms of mean annual, seasonal and monthly) under changing climate within the Weyib River basin at both basin and sub-basin level. Such analysis, therefore, could help us to have sufficient knowledge about the hydrological processes and their responses to climate change in each sub-basin can guide water resources management in providing a more rigorous assessment and more efficient decision-making.

Most research aims to address the problems related to the water availability side while neglecting the water demand side. But, the latter has also significant policy implications in terms of water demand management. Hence, this study tried to examine both water availability and water demand scenarios of the basin thereby status of water resources need of the basin was estimated.

Most of the climate change impact studies assess the hydrological processes on an annual basis in different regions. Analysis at higher temporal resolution (seasonal or monthly) scale is desirable, as seasonal or monthly variation of hydrological processes may not become visible in an annual basis analysis and thus may not provide the required information for managing water for agricultural and other needs. In this study, therefore, annual, seasonal and monthly temporal resolution have been considered to help a better planning for water resources management in the basin.

There is no study has been done in the Weyib River basin regarding future characteristics of climatic variables (mainly precipitation and temperatures) and their impact on various hydrological processes (at both basin and sub-basin level) under ensembles of CMIP5-ESMs-RCPs scenario to the year 2100 and water demand analysis, but this study tried.

This study noticeably culminates that different features between sub-basins in a basin such as land use land cover (LULC), soil non-homogeneity, topographic, surface-subsurface water interactions, drainage area, shape, and networks can result in different hydrological responses to climate change in each sub-basins, and consequently the changes in mean annual and seasonal climate variables may not always bring about the same change in hydrological

processes in the Weyib River basin. Therefore, calculating the water balance components (mainly water availability) in each sub-basin, along with the entire basin provides a better understanding of the hydrological processes in response to climate change. This study would not only provide the comprehensive analysis of the climatic change, hydrological processes, and water demand estimate but also would be helpful for the better management of water resources in the Weyib River basin.

1.5 Research Questions

This study primarily focused on downscaling large-scale atmospheric climatic variables to project the future climatic condition in the Weyib river basin and then investigated resulting changes in different surface and subsurface hydrological processes in future as compared to present condition. Finally, spatial distribution of total annual water demand at Wereda (the third-level administration division of Ethiopia) level in the basin was estimated. Therefore, the study was directed by the following research questions:

1. What are the most appropriate predictor variables to be considered for the downscaling of daily precipitation and temperatures based on the relationship between large-scale global atmospheric variables and local scale observed precipitation and temperatures?
2. How well do CMIP5-ESMs simulate present climate variables using SDSM in Weyib River Basin?
3. How alarming the future temperatures and precipitation change of the study area can be? (Is there a warming trend in the Weyib River Basin?)
4. How ArcSWAT hydrologic model perform to simulate historical hydrological processes in Weyib River basin?
5. How will the changes in climatic variables affect the hydrological processes in the study area?
6. How water demand and availability resemble in the basin?
7. What is the present and future water resources status of Weyib River basin (Is water abundance or water stress basin?)?
8. What are the adaptation options to be taken up to alleviate the adverse impacts of climate change on water availability?

1.6 Research Objectives

To address the questions mentioned above, the general and specific objectives have been drawn as stated below:

1.6.1. Broad objective

Against these backgrounds, the broad aim of this study was, therefore, to investigate climate change impacts on the hydrological processes and water demand estimates until the year 2100 in Weyib River Basin, Southeastern Ethiopia.

1.6.2. Specific objectives

To meet the broad objective of the study, the following specific objectives were set to:

1. Downscale daily temperatures (maximum and minimum) and precipitation from CMIP5-ESMs-RCPs scenario.
2. Develop temporal (in the 2020s, 2050s and 2080s time slices) temperatures and precipitation scenarios using CMIP5-ESMs-RCPs experiment in the Weyib River basin
3. Evaluate the performance of ArcSWAT model in simulating catchment hydrology in Weyib River Basin.
4. Investigate the response of surface and subsurface hydrological processes under ensembles of CMIP5-ESMs-RCPs scenario in the entire basin and sub-basin scale.
5. Analyze the annual, seasonal and monthly net water availability (in the 2020s, 2050s, and 2080s time slices) in the entire basin and sub-basin scale under ensembles of CMIP5-ESMs-RCPs scenario.
6. Assess current and projected (in the 2020s, 2050s, and 2080s time slices) total annual water demand of the Weyib River basin under increasing population.
7. Estimate current and projected water resources status of the basin under CMIP5-ESMs-RCPs scenario.
8. Suggest possible adaptation options to alleviate the adverse impacts of climate change on water availability.

1.7 Organization of the Thesis

The thesis has been organized to have seven chapters including the introductory section. General overviews of each chapter have discussed as follows.

Chapter 1 comprises the background of the study, statement of the problem, significance of the study, research questions and research objectives (general and specific).

Chapter 2 is the literature review and discusses about climate change impacts on the hydrology and water resources (climate change impacts on the hydrologic cycle and water resources management), climate change impact in Africa, Ethiopia and Weyib River basin, GCMs and ESMs, future emission scenarios (update on scenario development from SRES to RCPs), the new representative concentration pathway scenarios (RCPs) and benefits of using RCPs), downscaling approaches (dynamical (RCM) and statistical (transfer functions, weather typing and weather generators)), hydrology and water resources modelling and water demand assessment for selected and Weyib River basin.

Chapter 3 discusses about statistical downscaling of daily temperatures and precipitation data from CMIP5-ESMS-RCPs experiment: in Weyib River basin, Southeastern Ethiopia. The chapter also provides detail description of study area, types of ESMs and RCP scenarios used, types of data used, downscaling methods, SDSM and its approach and performance evaluation, statistical bias correction, climate change scenario statistics, Mann-Kendall trend test, selected common potential predictor variables, calibration and validation results of SDSM for both temperatures and precipitation and scenarios developed for future temperatures and precipitation (2006-2100) for different averaged spatial weather stations.

Chapter 4 gives the detail explanation about ArcSWAT hydrologic model description, approaches, and hydrological components, input data (spatial and weather) used and model set-up. Hydrological simulation of the Weyib River catchment carried out using SWAT model is presented along with analysis done for identifying SWAT's most sensitive streamflow Parameters, final calibrated fitted values obtained through variation methods. Statistical and hydrograph technique used to evaluate the performance of ArcSWAT hydrologic model is detailed here. Four statistical model performance evaluation criteria were used during the calibration and validation periods namely: coefficient of determination (R^2), Nash and Sutcliffe simulation efficiency (NSE), RMSE-observations standard deviation ratio (RSR) and Percent bias (Pbias). Hydrograph analysis was also made to provide a visual comparison of simulated and measured constituent data, to identify differences in timing and magnitude of peak flows, to visualize the shape of hydrograph and to identify model bias throughout model calibration and validation period and presented in this chapter.

Chapter 5 investigated the entire basin (EB) and sub-basin (SB) scale current and projected future changes in surface and subsurface water hydrological processes under climate change scenarios in Weyib River basin, Southeastern Ethiopia. In this chapter, therefore, EB and SB scale major hydrological processes such as surface runoff contribution to the streamflow (QSURF), groundwater contribution to the streamflow (GWQ), actual and potential evapotranspiration (ET and PET), water that percolates past the root zone (PERC), soil water content (SW), and net water yield of the basin (WYLD) have been studied using distributed deterministic ArcSWAT hydrologic model for both current and future (under Ensembles of GFDL-ESM2M, CanESM2 and GFDL-ESM2G for the RCP8.5, RCP4.5 and RCP2.6 scenarios from CMIP5) have been detailed.

Chapter 6 examines spatial and temporal variation of current and projected water demand and water availability under climate change scenarios in the study area. In this chapter, spatial distribution of current (2005) and projected (in 2020s, 2050s and 2080s time slice) population, water demand and water availability of the Weyib River basin is discussed in detail. Irrigation, domestic (which includes drinking, sanitation, bathing and food preparation), commercial and public institutions (public schools, clinics, hospitals, offices, shops, bars, restaurants and hotels), industrial, livestock uses, water losses through water supply system have been considered. Current and future water availability resulted from mean of three downscaled ESMs climatic variables under the RCP8.5, RCP4.5 and RCP2.6 scenarios for three future time slices are also investigated in this chapter. Finally, water resources status of the basin based on 'Water Stress Index Analysis' (total water available divided by total number of population residing in the basin) has been outlined.

Following these chapters, a summary, conclusion, and recommendation from results obtained and challenges faced during this study is presented in **Chapter 7**. Some contributions (publications) from this Ph.D. thesis work have been provided in 'Publications and Award Based on the Present Thesis Work' section after references. Pertinent detail tables, figures and photos/pictures are presented in appendices at the back of the thesis after 'Publications and Award Based on the Present Thesis Work' section.

Chapter 2: Literature Review

2.1. Introduction

To carry out a systematic study of all possible relevant past work, available in the literature, review has been carried out by dividing it into different sub-headings. Review of climate change impacts on the hydrologic cycle and water resources management in general is first done. Then, climate change impact in Africa, Ethiopia and Weyib River Basin is carried out. Following this, literatures, reviewed to understand development and application of ESMs, future emission scenarios (update on scenario development from SRES to RCPs), benefits of using RCPs, downscaling approaches (dynamic (RCM) and statistical), are presented. To know state of the art in hydrological modelling, literatures containing works related to hydrology and water resources modeling are reviewed. Literature available on water demand assessment for selected river basin as well as Weyib River basin have also been reviewed and presented in this chapter.

2.2. Climate Change Impacts on the Hydrology and Water Resources

2.2.1. Climate change impacts on the hydrologic cycle

Precipitation, evapotranspiration, runoff, groundwater and soil moisture are the key components of hydrology cycle, and they have linked with changes in atmospheric temperature and radiation balance. The climate drives the hydrological cycle (Crosbie et al. 2010), and projected changes in spatial and temporal patterns of the climate variables will impact on regional hydrological processes, in particular, changes in rainfall will be amplified as an impact on hydrological components (Chiew, 2006; Wang et al., 2011). Precipitation pattern over a 21st century has shown substantial spatial variability and the risks of extreme events due to increase of the intensity and variability of the rainfall also projected to rise (IPCC, 2008). For instance, results from 15 AOGCM runs for the future warmer climate show that the extreme drought increased from 1% at the current day land area to 30% in 2100 for the A2 emission scenario (IPCC, 2008). In addition to this, precipitation has shown increased by 2% and 7-12% for the area found between 0 to 55°S and 30 to 85°N respectively (IPCC, 2001). Summer precipitation characteristics have been done using 15 GCMs outputs for the A1B scenario in the sub-tropical and South Asian monsoon and noted that rainfall decreases over several sub-tropical areas and an increment in tropical oceans and some monsoon regimes such as South Asian monsoon has observed.

The impact of climate change on the precipitation characteristics of Dhansiri River has been studied (Vinnarasir and Sarma, 2011). A future climate projection from three GCMs under the one IPCC emission scenarios which have been downscaled by regression analysis and Artificial Neural Network was used to study future precipitation characteristics in the basin and they found that about 20% increase in average annual precipitation by the year 2100. It is observed that there is a substantial variability in rainfall (rise about 20% and also declined by about 20%) in the glob (Bates et al., 2008).

The impact of climate change on freshwater availability in Africa at the subbasin level for the period of 2020-2040 has been studied (Faramarzi et al., 2013). Future climate projections from five GCMs under the four IPCC emission scenarios were fed into an existing SWAT hydrological model to project the impact on different components of water resources across the African continent. The results show that for East Africa, the larger spatial variation of precipitation (from a drop of about 25-50% to rise to 25-50%). Projected changes in mean precipitation in Africa under Global Warming was investigated (Shongwe et al., 2009) from CMIP4 GCM models using Bayesian approach to downscale precipitation. The results revealed that the mean annual precipitation is likely to increase. Rainfall is the largest factor in the water balance of catchment hydrology (Mpelasoka and Chiew, 2008).

Projecting impacts of future climate change onto hydrological systems can be undertaken in different ways and a variety of effects can be expected. Although simulation results from GCMs are typically used to project future climate, different outcomes from these projections may be obtained depending on the GCMs themselves and how they are applied, including different ways of downscaling from global to regional scales. Projections of climate change from different downscaling methods, different GCMs and different future emissions scenarios were used as input to simulations in a hydrological model to assess climate change impacts on hydrology. Rainfall variability is more in the African continent and resulted in variation in water availability. For instance, a decline in water availability (streamflow) (Beck and Bernauer, 2011) by 2050s has been reported. Nevertheless, the rise of water availability (Graham et al., 2011) has also been stated. From the above literatures it is clear that spatiotemporal changes in respect of water availability due to climate change impact vary over the globe and it is difficult to suggest a general trend.

Future projected characteristics of various climate variables, especially global mean surface temperature, have been investigated (IPCC, 2013b) from ensembles of multi-model CMIP5 GCM models under the four RCP scenarios. The results revealed that the increment of global mean surface temperature observed to be range between 2.6-4.8°C (RCP8.5), 1.1-2.6°C (RCP4.5) and 0.3-1.7°C (RCP2.6). This resulted sea level has to be projected to continue rising ranges between 0.45-0.82 m (RCP8.5), 0.33-0.63 m (RCP6.0), 0.32-0.63 m (RCP4.5) and 0.26-0.55 m (RCP2.6) and this sea level substantially will rise due to collapse of some sections of the Antarctic ice sheet by the end of the 21st century. In general, temperatures revealed an increasing trend (Kruger and Shongwe, 2004; New et al., 2006; Unganai, 1996) which tends to glacier to melt, sea level to rise and alteration in circulation pattern which influence precipitation, water availability, and extremes of floods and droughts; just to name a few. Higher temperatures increase evapotranspiration which may further lead to a reduction in surface and subsurface water resources (Chiew and McMahon, 2002; Crosbie et al., 2010).

Based on Indian Network for Climate Change Assessment Report (INCCA, 2010), which was used PRECIS (providing climate investigation studies) based on HadRM (Hadley Regional climate Model) under the A1B SRES to generate climate change scenario for 2030s, climate change will affect four major regions (Himalayan, North Eastern (NE), Western Ghats, and Coastal Region) by 2030s. Temperature will increase from 1.7 to 2.0°C with greater seasonal variability, small increase in annual precipitation with fewer rainy days, increased frequency of extreme rainfall, fewer and more intense cyclones, storm surge (coastal) will increase from 5 to 20%, sea-level rise, on average, slight increase (50-80 mm), variable water availability (generally wetter will increase, and dryer will decrease), sediment yields will increase up to 25% in most areas, floods level will increase from 10 to 30% compared to 1970s in most regions, extreme drought in southern portion NE; West Coast; most severe in the Himalayas, crop water demand will increase from 5-20% in Himalayas and NE; variable Coastal Zone; increased land sliding, salinization coastal areas, overall declines in total yield for all regions and most crops (rice, sorghum, maize, mustard, wheat, apple) and increased land degradation and soil erosion from the area.

Global runoff under A1B scenario apparently reduced in Central American, part of Asia, part of Mexico, and Europe; however, it has increased in high-latitude Rivers. It has been noted that annual evaporation increases over most oceans (surface temperature increase). At the

global scale, mean evaporation changes balance global precipitation but it is different at the local level due to variations in the atmospheric transport of water vapor (IPCC, 2001).

Farjad et al. (2016) investigated the average annual and seasonal variations of surface and subsurface hydrological processes in the west and east sub-catchments along with the entire watershed under five plausible GCM-scenarios up to 2070 using the physically-based, distributed MIKE-SHE Model in Elbow River Basin, Canada. Future climate projections from seven CMIP4 GCM models under the six IPCC emission scenarios which have been downscaled by delta-change method were fed into an existing MIKE-SHE hydrological model to project the impact on different hydrological processes in the basin. They have been reported that the mean annual surface runoff found to be decreased by 10.50 and 10.60% (A1F1), and 4.60 and 9.90% (B2) in 2020s and 2050s time slices respectively, and increases by 3.70 and 17.90% (A1B), 6.00 and 6.68% (A2) and 0.60 and 3.85% (B2) in 2020s and 2050s time slice respectively. The mean annual groundwater contribution to the streamflow (baseflow) has been rise by 2.50 and 12.70% (A1B), and 2.10 and 2.30% (A2) in the 2020s and 2050s, respectively. The actual evapotranspiration has also been rise by 1.60 and 9.60% (A1B), and 2.40 and 4.80% (A2) in the 2020s and 2050s, respectively for the entire basin. They explained in their study also that with the 21% increase in precipitation, SWAT produced a 51% decline in surface runoff, and a 43% rise in recharge, leading to a 50% net increase in total water yield.

2.2.2. Climate change impacts on the water resources management

Vano et al. (2010) studied the effects of climate change impacts on water management and irrigation in the Yakima River Basin, Washington, USA using the Variable Infiltration Capacity (VIC) macro-scale hydrology model from the ensembles of different CMIP4 GCM models under the two IPCC SRES scenarios. They found that earlier snowmelt results in increased water delivery curtailments. Historically, the basin experienced substantial water shortages in 14% of years. Without adaptations, for A1B emission scenarios, water scarcity increases by 27, 33 and 68% in the 2020s, 2040s, and 2080s respectively. For B1 emissions scenarios, shortage tends to rise by 24, 31 and 43% in the 2020s, 2050s, and 2080s respectively. In India, Pakistan, Nepal and Bangladesh, water scarcity has attributed to issues due to rapid urbanization and industrialization, population growth and inefficient water use, which are all aggravated by climate impacted changes induced on demand, supply, and water quality. The decreased precipitation and increased temperature have been reported to increase

water shortages, particularly in parts of Asia where water resources are already under stress from growing water demands and inefficient water use (Manton et al., 2001).

The climate impact assessment has been performed by Vetter et al. (2013) for three river basins on three continents (Rhine in Europe, Upper Niger in Africa and Upper Yellow in Asia) using three hydrological models (HBV, SWIM and VIC) from five CMIP5 GCMs outputs (HadGEM2-ES, IPSL-CM5ALR, MIROC-ESM-CHEM, GFDL-ESM2M and NorESM1-M) which have been downscaled by trend-preserving bias-correction method with the WATCH reanalysis data and have been re-sampled on a 0.5°x0.5° grid (Hempel et al., 2013) for the RCP 8.5 were provided for this study. They found that the uncertainty resulting from climate models is larger compared to that of the hydrological models for all three basins. The impact of climate change on streamflow has been investigated (Liu et al., 2011) using SWAT model from HadCM3 GCM model under the B2 emission scenario which has been downscaled by SDSM in the headwater catchment of the Yellow River basin. The results revealed that an overall decreasing trend in annual streamflow in the headwater catchment of the Yellow River watershed in the 2020s, 2050s, and 2080s time slices was observed.

The impact of climate change on the water resources of twelve river basins in Indian River systems has been studied (Gosain et al., 2006) using SWAT from HadRM2 model under the GHG scenarios. The results revealed that severity of droughts and intensity of floods in various parts of the country might get worsened. Moreover, a general drop of the available runoff has predicted under the future climate scenario. Hydrological changes and its impact on water resources of Bagmati watershed in Nepal has been investigated (Sharma and Shakya, 2006). Due to climate change effect in Bagmati watershed, precipitation during monsoon decreased, and pre and post-monsoon rain increased, but mean yearly flow in river decreased, magnitude of flood decline but frequency and duration of flood increased. Hydropower generation reduction and concentration of pollution increased because of less water availability. Due to the increasing demand and dropped supply, water conflicts between India and Nepal are likely to increase in future. It has suggested that a proper modality of water sharing should design in advance.

Implications of climate change for sustainable water resources management in India has been reviewed (Mujumdar, 2008). The main findings of this review indicated that the severe water scarcity in one region and flood hazards in other areas has observed, and these affects mainly

water quality and agriculture, so he suggested that the research studies integrating the atmospheric and hydrological models to understand the climatic influence on hydrologic extremes are needed in the country.

The impact of climate and land use changes on the flood hazard of the middle Brahmaputra reach, India was studied (Ghosh and Dutta, 2012) using a physically based macro-scale distributed hydrological model (DHM), which works on the concept of hydrological similarity classes (HSCs), has been calibrated and validated and then used to assess the possible future changes in the flood characteristics and flood vulnerability of the Brahmaputra basin, India, due to climate and land use changes. The bias corrected climatological data from a regional climate model (RCM) simulation (PRECIS) was used to obtain future changes in flood generation and its propagation through the basin in the projected climatological scenario. After model verification, "best guess" land use change scenarios were used to assess potential changes in flood characteristics. Results show that at the middle reaches of the Brahmaputra, peak discharge increases by a maximum of 9% for land use change scenarios and peak discharge will increase by an average of 21% in the future projected climate change scenario.

According to Arnell (2008); Kundzewicz et al. (2008); Rutashobya (2008) review, the impact of climate change on water availability will knock all the biotic and abiotic surrounding in general. This has assured in some field of areas. For example, agriculture reported by Vermeulen et al. (2012), healthy by Gage et al. (2008), ecology by Eriksen and Watson (2009). De Jong et al. (2000); Freibauer et al. (2004); Jandl et al. (2007); Lasco et al. (2002) (as cited in Sarma et al., 2013) have been conducted research on removal of green cover becoming a matter of global concern, as it can accelerate the adverse impacts of climate change. People coming in search of work generally reside in the hills, as they cannot afford the high cost of land in plains. This has led to deforestation of the hilly area and has resulted in increased surface erosion from the upper catchments. Though sediment and water yield from these degraded watersheds could have been minimized by implementing ecologically sustainable management practices (EMPs), such as grass land, forest land and detention pond, poor economic conditions of the people stands in the way of field implementation. On the other hand, major industries, which can be held responsible for emission of greenhouse gases, can be asked to finance greenery development in the hilly watersheds through implementation of selected EMPs to earn carbon credit for them. And, finally, they suggested

that the climate change impacts on the water resources could have alleviated by implementing EMPs.

2.3. Climate Change Impact in Ethiopia and Africa

As reported in the Africa Climate Change Environment Security (ACCES) report (Ndaruzaniye, 2011), climate change is increasing the frequency and intensity of climate-related hazards, and hence, the level and patterns of often interrelated risks, particularly water and food security, exacerbate levels of vulnerability, mainly for rural communities in Ethiopia. Current climate variability is now imposing a significant challenge to Ethiopian communities by affecting water and food security, and energy supply. Over exploitation of land including deforestation associated with changing weather pattern have been increased soil degradation and has inflicted water stress and crop failure. In Sub-Saharan Africa, i.e., the Eastern African region, particularly the Horn of Africa, is stated as highly geographically exposed to climate change and its impact on water resources is therefore expected to be high. Out of 160 million people living in the Horn of Africa, 70 million has located in areas prone to extreme drought leading to water insecurity and food shortages. It is interesting to note that in this region both floods and droughts can occur in the same area within a very short period and these events can worsen water availability scenario both in terms of quality and quantity. Such temporal variability can adversely affect agricultural activities and power sector.

The present unpredictable climate is striking plenteous threat to Ethiopia by mainly disturbing water resources and agricultural sectors. Recent flooding incidences, as well as the widespread drought in Ethiopia, could remain placed as visible indications for these influences (Ethiopian National Meteorological Agency, 2007). The impact of future climate projections on temperature and precipitation characteristics of Ethiopia has been investigated (Ethiopian National Meteorological Agency, 2007) from CMIP3 GCM model under the A1B scenario which has generated by using the 'Model for the Assessment of Greenhouse-gas Induced Climate Change (MAGICC)' software. The results revealed that the mean annual temperature would increase in the ranges 0.9-1.1, 1.7-2.1 and 2.7-3.4°C by 2030, 2050 and 2080 time slices respectively with a small rise in annual precipitation has expected over the country Ethiopia.

Legesse et al. (2013) studied a downscaling of daily temperature and rainfall data from CMIP3 GCM model under the A2 and B2 emission scenarios which has been downscaled by

SDSM in north central Ethiopia, and they found that mean annual maximum and minimum temperatures showed an increasing trend with the amount of 6.17˚C and 5.65˚C respectively by 2080s. However, mean annual precipitation tends to decline range about 14.2-43.3% by the year the 2080s. Climate change impact on the hydrology of bale mountainous area in Ethiopia has been investigated (Shawul et al., 2016) using ArcSWAT hydrologic model from CMIP3 GCM model under the A2a and B2a emission scenarios which has been downscaled by SDSM. The results revealed that the projected mean annual maximum and minimum temperature shows rising trend in the 2020s, 2050s and 2080s time slices.

The impact of climate change on water variability was studied (Setegn, 2010, 2011) in Lake Tana basin, Ethiopia using SWAT model from CMIP3 GCMs model under the A1B, B1 and A2 emission scenarios which have downscaled by using historical-modification procedure and he found that significant changes in stream flow and other hydrological parameters in the period between 2045-2100. An attempt was made to investigate the sensitivity of water resources to climate change in the Awash River basin in Ethiopia (Hailemariam, 1999) using integrated water balance model (WatBal) from CMIP3 GCMs under the doubling of CO_2 and transient scenarios and they found that the mean annual runoff tends to decline ranges between 10 to 34%, with doubling of CO_2 and transient scenarios of CO_2 increase.

The impact of climate change on soil water availability and crop production in Anjeni Watershed, Blue Nile Basin, Ethiopia was investigated (Yakob, 2009) using SWAT hydrological model from CMIP3 GCM output under the A2 and B2 emission scenarios which have been downscaled by SDSM. The results indicated that the annual potential evapotranspiration observed to increase for future periods while soil water content tends to decline and resulted over all variant in crop production in the watershed. The impact of climate change on the hydrology of Gilgel Abbay catchment in Lake Tana basin in Ethiopia has been investigated (Abdo et al., 2009) using HBV hydrological model from CMIP3 GCM model under the A2 and B2 emission scenarios which has been downscaled by SDSM. The results revealed that the volume of runoff shown to decline by 11.6% and 10.1% for A2 and B2 scenarios respectively in the 2080s and there will also be high seasonal and monthly deviation of runoff compared to variation in annual scale.

According to review report by Boko et al. (2008); Dinar (2006), reported that the temperature projection in the upcoming period will be in the range 2-4.1°C in Africa. In recent study, Faramarzi et al. (2013) modeled the whole African continent using SWAT model from five

CMIP4 GCM models (HadCM3, PCM, CGCM2, CSIRO2, and ECHAM4) under the four IPCC emission scenarios. They found that the same amount of increment (about 10-20%) and decrement (about 10-20%) of streamflow, but with significant spatial variability. The impacts of climate change on stream flow in four African river basins (Niger, Upper Blue Nile, Oubangui and Limpopo) has been done (Aich et al., 2014) using Soil and Water Integrated eco-hydrological Model (SWIM) for all four basins independently from CMIP5 ESM model under the RCP8.5 and RCP2.6 scenarios which have been downscaled by means of trend preserving bias correction method (Hempel et al., 2013). Results revealed that is a tendency of increasing stream flows in three of the four basins (not for the Oubangui).

2.4. General Circulation Model (GCMs) and Earth System Models (ESMs)

GCM is a complex mathematical model which represents physical processes in the atmosphere, cryosphere, ocean and land surface (NOAA, 2009; IPCC, 2013d). GCMs were developed for the first time in 1956 (Xu, 1999a) to mimic mean synoptic-scale and atmospheric circulation patterns but later modified (Lupo and Kininmonth, 2013) to use for weather forecasting, understanding the climate and predicting future change in climatic variables. There are two major GCMs, namely atmospheric GCMs and Oceanic GCMs (NOAA, 2015). The combined form of these two GCMs has then called as Atmosphere-Ocean coupled general circulation model (AOGCM). The Geophysical Fluid Dynamics Laboratory of NOAA developed coupled atmospheric and oceanic GCM for the first time in the 1960s.

According to IPCC (2007), the coarser resolution GCMs have been divided into three-dimensional grids of cells to reveal climates horizontal resolution ranges between 250-600 km, 10 to 20 vertical layers in the atmosphere and up to 30 layers in the oceans and these has not properly modeled. Till a few years back, GCMs only included atmosphere, land surface components, and sometime oceanic component. However, these are not the only components to define the climate; there are biological and chemical processes as well which impacts on climate. Considering these GCMs recently started incorporating sophisticated models of sea ice, carbon cycle, ice-sheet and even atmospheric chemistry and all these processes are included in a new climate model called ESM (Heavens et al., 2013).

In the development of CMIP5, newly developed ESMs are incorporated (Taylor et al., 2012) and which provide additional components that describe the atmosphere's linkage with land

use and vegetation, atmospheric chemistry, aerosols and the carbon cycle. The ESMs were assembled regarding newly defined atmospheric composition forcings for the present climate (historical forcing) and the future scenarios (Representative Concentration Pathways; RCPs) (Moss et al., 2010). The details of the three ESMs used in this study have given in Chapter 3 in 'Earth System Models and RCP Scenarios' section.

2.5. Future Emission Scenarios

2.5.1. Update on scenario development: from SRES to RCPs

In the AR5 (IPCC 5th assessment report) a series of new RCPs are employed, and that replace the 'Special Report on Emission Scenarios' (SRES). They create a range of reactions from roughly stabilize forcing to a strict mitigation scenario ('RCP2.6') that stabilizes and then slowly reduces the radiative forcing (RF) after mid-21st century. Unlike to the AR3 and AR4, the climate change from the RCP scenarios in the AR5 is enclosed as a combination of adaptation and mitigation. Mitigation activities starting now in the several RCP scenarios do not create noticeably different climate change outcomes for the next '30 years' or so, whereas long-term climate change after mid-century is substantially diverse across the RCPs.

2.5.2. The newly developed representative concentration pathway scenarios (RCPs)

These RCPs represent a larger set of mitigation scenarios and were selected to have different targets regarding radiative forcing at 2100 (about 2.6, 4.5, 6.0 and 8.5W/m^2), and these scenarios should be considered reasonable and illustrative, and do not have probabilities attached to them (IPCC, 2014b). There are four types of Representative Concentration Pathways namely RCP8.5, RCP6.0, RCP4.5, and RCP2.6 (Peak and Decline scenario). The numbers refer to radiative forcings ('global energy imbalances'), measured in watts per square meter, by the year 2100. The RCPs which typically include economic, demographic, energy and climate components have developed through Integrated Assessment Models (IAMs). The emission scenarios they create are then run through a simple model to produce time series of GHG concentrations that can be a ride in AOGCMs. The detail information about each of the RCPs has given below and Table 2.1.

RCP2.6 ('peak and decline scenario'): It describes very low greenhouse gas concentration levels. Its radiative forcing level first reaches a value around 3.1 W/m^2 (peak) mid-centuries and declining to 2.6 W/m^2 by 2100. The final RCP is based on the publication (Van Vuuren

et al., 2007). It has developed by the Integrated Model to Assess the Global Environment (IMAGE) modeling team of the Netherlands Environmental Assessment Agency.

RCP4.5 (stabilization scenario): Stabilizes its radiative forcing target at 4.5 W/m2 in the year 2100 without ever exceeding this level by applying of a range of technologies and strategies for reducing GHG emissions. The scenario drivers and technical options are detailed in (Thomson et al., 2011; Wise et al., 2009). It is developed by the Mini-Climate Assessment Model (MiniCAM) modeling team at the Pacific Northwest National Laboratory's Joint Global Change Research Institute (JGCRI).

RCP6.0 (stabilization scenario): Stabilizes its radiative forcing target at 6.0 W/m2 in the year 2100 without ever exceeding this Level by applying of a range of technologies and strategies for reducing GHG emissions. The details of the 'scenario' are described in Fujihara et al. (2006) and Hijioka et al. (2008). It is developed by the Asian Pacific Integrated Model (AIM) modeling team at the National Institute for Environmental Studies (NIES), Japan.

RCP8.5 (very high emission scenario): It has categorized by increasing 'greenhouse gas emissions over time representative for scenarios' in the literature leading to high greenhouse gas concentration levels. The basic scenario drivers and ensuing development path are based on the A2r scenario detailed in Riahi et al. (2007). It has developed by the Integrated Assessment Framework at the International Institute for Applied Systems Analysis (IIASA) modeling team, Austria.

Table 2.1 Types of representative concentration pathways (IPCC, 2013b)

Name	Radiative Forcing[1]	Concentration[2]	Pathway shape
RCP8.5	>8.5 W/m^2 in 2100	>~1370 CO_2-eq in 2100	Rising
RCP6.0	~6.0 W/m^2 in 2100	~850 CO_2-eq (at Stabilization after 2100)	Stabilization without overshooting
RCP4.5	~4.5 W/m^2 at stabilization after 2100	~650 CO_2-eq (at stabilization before 2100)	Stabilization without overshooting
RCP3-PD[3]	the peak at ~3W/m^2 before 2100 and then decline	the peak at ~490 CO_2-eq before 2100 and then decline	Peak and decline

Notes: [1] approximate radiative forcing level has defined as ±5% of the stated level in W/m^2. 'Radiative forcing values include the net effect of all anthropogenic GHGs and other forcing agents, [2] Approximate CO_2 equivalent (CO_2-eq) concentrations. 'The CO_2-eq concentrations were calculated with the simple formula Conc = 278 * exp(forcing/5.325)'. 'Note that the best estimate of CO2-eq concentration in 2005 for long-lived GHGs only is about 455 ppm', while the corresponding value including the net effect of all anthropogenic forcing agents (consistent with the table)' would be 375 ppm CO2-eq., [3] PD = peak and decline.

How do they differ from the Special Report on Emissions Scenarios (SRES)?

The RCPs distance a wider range of opportunities than the SRES marker scenarios used in the modeling for the AR3 and AR4. RCPs instigate with atmospheric concentrations of GHG rather than socioeconomic processes. This is paramount important since every modeling step as of a socioeconomic scenario to climate change impacts enhances ambiguity. By instigating with concentrations, there are lesser steps to impacts and therefore less aggregate ambiguity in impact assessments. This way ambiguity is shared uniformly among the numerous components. RCPs are internally stable sets of projections of the components of radiative forcing that have used in subsequent phases of climate modeling. In contrary to SRES, some of the RCPs also include mitigation and adaptation policies.

2.5.3. Benefits of using RCPs

The RCPs are a significant advance in climate research and provide a base for emissions mitigation and impact analysis and can link with different expertise (physical, biological and social scientists). Scholars working on the implications, adaptation, and vulnerability, will obtain model outputs sooner and supplemented with extensions (Extended Concentration Pathways, ECPs), which allow climate modeling experiments through to the year 2300. Development of the RCPs also brings together a diverse range of research communities that will help create fully combined ESMs that contain a representation of the global economy and society, impacts, and vulnerabilities. In this study, therefore, three of four future emission scenarios namely RCP2.6, RCP4.5, and RCP8.5 to cover the low, median and high ends of possible future climatic projections from CMIP5 have been applied. As it has mentioned, the changes described above are at global scale. At the worldwide basis, several studies about changes in precipitation, runoff, and soil moisture using different emission scenarios have carried in the many basins.

2.6. Review of Downscaling Approaches

Most of the GCMs do not provide information on scales smaller than few hundred kilometers (Wilby et al., 2004). Due to this coarse resolution of GCM output, it is necessary to convert GCM output at least at the scale of watershed or region before using for impacts studies (Chen et al., 2011). This process of converting large scale GCM output into a small scale that can be used to examine impacts at a local level has called as downscaling (Abdo et al., 2009). It is simply a procedure to use information known at larger scales to make predictions at local

scales (Hoar and Nychka, 2008). The primary objective of downscaling is to bridge the scale mismatch of GCMs that climate change studies required (Wilby et al., 2004). The hydrological model can be driven by the output from GCMs (Watson et al., 1996) to investigate the impact of climate change on future water resources. However, the spatial resolution of GCMs (about 250 km) might be too coarse for hydrological modeling at the basin scale. This scale gap can be accomplished through downscaling. There are two prime methodologies accessible for the downscaling of large scale resolution GCMs output to the finer (local) scale resolution (Wilby and Dawson, 2007) namely dynamical and statistical downscaling methodologies.

2.6.1. Dynamical downscaling (DD)

The dynamical downscaling methodology involves a higher resolution regional climate model (numerical meteorological model) is enforced to use GCMs/ESMs output (Murphy, 1999) instead of using mathematical equations. A higher resolution regional climate model (RCM), driven by boundary conditions from a GCM, is used to derive finer spatial scale climatic variables (Schmidli et al., 2007). The merit of using RCM is that they can provide smaller-scale atmospheric features better than the host GCMs/ESMs whereas the demerit is that they demand significant computing resources and are expensive (Abdo et al., 2009; Wilby and Dawson, 2007). The Regional Spectral Model (RSM) and South Atlantic Convergence Zone (SACZ) in the family of dynamical downscaling technique to downscale sea surface temperature have been investigated (Misra et al., 2003) in the in Amazon River basin. The results revealed that the RSM had been found to be better than SACZ to downscale sea surface temperature.

2.6.2. Statistical downscaling (SD)

The SD forms empirical relationships between large-scale atmospheric GCMs/ESMs variables, the predictors and local (finer or catchment) scale climate variables, the predictands (Giorgi et al., 2001). The SD comprises two step processes (Hoar and Nychka, 2008), the first is to form a statistical relationship between the predictand and predictor variables, and next is to apply the formed relationship to the output of GCM/ESM to simulate future climatic data.

To date, many statistical models have been developed and are available. SDSM is being used widely throughout the world (Huang et al., 2011) to downscale the most important climate variables such as temperature, precipitation, and evaporation, etc. for assessing hydrologic

responses in climate change scenarios. This SDSM model is developed through a combination of multiple linear regressions and the stochastic weather generator. The SDSM was originally conceived as a regional climate change scenario generator to support climate risk assessment and adaptation planning. A meta-analysis of the first decade of published work using SDSM showed that over half the 200+ studies to date refer to water and flood impacts, often with regards to the production of climate scenarios, benchmarking with other scenario tools, or refinement of downscaling techniques. So far, the downscaling algorithm of SDSM has been applied to a host of meteorological, hydrological and environmental assessments, as well as a range of geographical contexts including Africa, Europe, North America and Asia.

The SDSM version 4.2.9- a decision support tool for the assessment of regional climate change impacts, which was supported by the Environment Agency of England and Wales as part of the Thames Estuary 2100 project (Wilby and Dawson, 2007) has been, therefore, used for this study. It facilitates the rapid development of multiple, low-cost, single-site scenarios of daily surface weather variables under present and future climate forcing. Additionally, the software performs ancillary tasks of data quality control and transformation, predictor variable pre-screening, automatic model calibration, basic diagnostic testing, statistical analyses and graphing of climate data. The detail description and setup of SDSM is presented in chapter 3.

The SD is highly dependent on the outputs of GCMs/ESMs (large scale atmospheric predictor variables) which are used as input data to the downscaling model (Sachindra et al., 2014). The key demerits of statistical downscaling contain the assumption that observed relations between large-scale predictors and local predictands will continue in a changing climate (assuming that predictor/predictand relationships will be unchanged in the future), require long/reliable observed data series, and affected by biases in the underlying GCM. Similarly some merits of statistical downscaling contains: it is easy to apply, have possibility to downscale from numerous ESMs and different emission scenarios, based on standard and accepted statistical procedures, may flexibly be crafted for specific purposes, able to directly incorporate the observational record of the region, downscale comparatively fast and inexpensive (Wilby et al., 2004). According to Giorgi et al. (2001), SD classified into three classes namely transfer functions, weather generators and weather typing. The details have been given below.

A. Transfer Function (TF)

The TF downscaling methods are reliant on the empirical relationships between local scale predictand and large-scale predictors (Wilby and Dawson, 2007). The TF has generated from multiple linear regressions (MLR), artificial neural network (ANN), canonical correlation analysis (CCA), and principal component analysis (PCA). It is very convenient to apply, but the models often describe only a fraction of observed climate variability especially for precipitation and also the downscaling is reliant on the choice of the predictor variables.

B. Weather Generators (WGN)

The WGNs are statistical models that derive a random number which can be used as a daily weather data at a particular station to extend the existing climate record where measured data are not existing (Dibike and Coulibaly, 2005; Schoof et al., 2005). They reproduce the statistical features of a local climate variable but not observed sequences of events (Wilby et al., 2004). Based on the modeling approach for daily precipitation, two major types of weather generators have identified; the first one is 'Markov chain approach' and next is the 'spell length approach.' The parameters of the WGN have trained on large-scale atmospheric predictors, weather states or rainfall properties. The efficacy and suitability of the models, however, depend on the climatic features of the study area.

C. Weather Typing (WT)

The WT approaches classify local meteorological data from specified period into definite WT or states according to the synoptic similarity, about main patterns of atmospheric circulation (Wilby and Dawson, 2007; Wilby et al., 2004). The WT assumes that the weather of specific period allotted to a particular type is more or less homogenous and the changes among the types are clearly visible (Ladd and Driscoll, 1980). Wilby and Dawson (2007) notes, climate change scenarios are created either by re-sampling from observed data or creating synthetic sequences of weather patterns and then re-sampling from observed data. The downscaling has then conducted by linking weather at the local scale with climate on a large scale.

Comparative studies on five different SDMs (B.circ, C.circ, WGEN, SPELL, and ANN) have done (Wilby et al., 1998) and they obtained that the B.circ and C.circ are giving better results than the others. Tisseuil et al. (2010) compared four (GLM, GAM, ANN, ABT) SDMs to predict streamflow in 51 hydrological gauging stations from CMIP3 GCMs output under the

A2 and A1B scenarios in southwest France. The results revealed that among these models ABT gives a better result (decreasing trend of streamflow has observed). Comparative studies on two SDMs (Autism spectrum disorder (ASD) and SDSM) have been investigated (Omani et al., 2007) in 10 meteorological stations to downscale precipitation and temperature from HadCM3 and CGCM1 model outputs. The results revealed that the ASD is better than SDSM for temperature (but not precipitation; neither of them gives a good result). An evaluation of linear regression methods as downscaling tools in temperature projections over the Pichola Lake Basin in India has been researched (Goyal and Ojha, 2011) using various linear regression approaches, namely direct, forward, backward and stepwise regression, for obtaining projections of mean monthly maximum and minimum temperatures to lake-basin scale in an arid region in India from CMIP3-GCM output under the A1B, A2, B1 and COMMIT emission scenarios.

An evaluation of statistical and dynamical techniques for downscaling local climate variables have been studied (Kidson and Thompson, 1998; Murphy, 1999). The dynamical and statistical methods are compared in terms of the correlation between the estimated and observed time series of monthly anomalies. The results revealed that, overall; the dynamical and statistical methods show similar levels of skill, although the statistical method is better for summertime estimates of temperature while the dynamical methods give slightly better estimates of wintertime precipitation. In general, therefore, the skill with which present day surface climate anomalies can be derived from atmospheric observations is not improved by using the sophisticated calculations of sub-grid scale processes made in climate models rather than simple empirical relationships. It does not necessarily follow that statistical and dynamical downscaling estimates of changes in surface climate will also possess equal skill. However, it is observed that there is a considerable differences between the two downscaling methods (statistical and dynamical) (Hay and Clark, 2003; Wilby and Wigley, 2000; Wood et al., 2004).

2.7. Hydrology and Water Resources Modeling

Once the GCMs data have downscaled, hydrology and water resources models have been used to assess the climate change impacts at local/catchment scale. Hydrological models which simulate the main components of the hydrological cycle, considering the physical and geomorphological characteristics of the study area have been developed using mathematical equations (Kharchaf et al., 2013). Application of hydrological models started before 1850

when Mulvany, an Irish engineer, developed the rational method (Xu, 2002) since then numerous models have established (Todini, 2007) and they have been used enormously in scientific studies while assessing the potential impacts of climate change on water resources (Xu, 1999b; Zhao et al., 2014).

For instance, the Hydrologic Modeling System (HEC-HMS) developed by the Hydrologic Engineering Centre from US Army Corps of Engineers. This model is designed to simulate the 'precipitation-runoff processes' in the basin systems. MIKE SHE, a spatially distributed and physically based model has a capable of simulating the full suite processes occurring in the land phase of the hydrological cycle. On the other hand, Water Evaluation and Planning System (WEAP) (Foster and Lane, 1987) is an integrated water resources model that simulates an entire water resources system ('water demands, groundwater, hydrology, water supply, water quality, and evaluate water management policies'). SWAT (Arnold et al., 1998) is physically based distributed watershed model which simulates hydrology, sediment and water quality for the complex river basin system are some of widely applied hydrology and water resources models.

Chemicals, Runoff, and Erosion from Agricultural Management Systems (CREAMS) (Knisel, 1980), Areal Nonpoint Source Watershed Environmental Response Simulation (ANSWERS) (Beasley et al, 1982), European Soil Erosion Model (EUROSEM) (Morgan et al., 1998) and Agricultural Nonpoint Source Pollution Model ('AGNPS') (Young et al, 1987) are also some of the physically based hydrologic and water resources models (as cited in Chekol et al., 2007). There are no hydrologic models to be best one among the others (Todini, 2007) since modeler have a tendency to emphasize their approaches. Hydrological model selection for a particular study mainly depends on hydrological data availability and goal of the survey (Xu, 1999b). In this study, therefore, SWAT hydrological model has been used for investigating the climate change impacts on surface and subsurface hydrological processes of Weyib River basin. The theoretical description and hydrological component of SWAT hydrologic model have been described in Chapter 4 of this study.

2.8. Water Demand Assessment for Selected and Weyib River Basin

Faruqui et al. (2001) explained in their study that one of the threats in water resources management is an increasing of water demand mainly due to the rapid increase of population, settlement patterns, wealth, industrial activity, technology, increasing demand for irrigation

and climate change. Research on cooperative water resources allocation among competing users has been studied (Wang, 2005) using Cooperative Water Allocation Model (CWAM) and he came to conclusion that conflicts often ascend when various water users of the river compete for limited water availability. Vaughn (2007) also strengthen this idea by forwarding that due to limited and unpredictable rainfall, unsustainable use of water, pollution, and rapid population growth are responsible for numerous conflicts.

Estimates of future water demand for selected water-service areas in the Upper Duck River Basin, Central Tennessee has been estimated (Hutson and Schwarz, 1996) using a single-coefficient requirement model with assumption of a steady growth pattern of population and they found that the mean annual water demand has increased ranges between 121 to 150% by the year 2050. The annual total water demand observed to be increased (Roy et al., 2010) by 32.8 and 54.8% in the 2030 and 2050 respectively as compared to baseline. The average annual water demand has also been assessed (Sebhat, 2015) using WEAP model for the Juba and Shabelle Rivers in Somalia. The results revealed that the irrigation water demands for the year 2035 are 3% and 63% of the current annual flow volume at the Juba and Shabelle Rivers, respectively. Considering population growth rate of 2.7% and increasing trend of urbanization, the total domestic water demand would be increased by 149% in the year 2035.

The Genale-Dawa River basin covers an area of about 172,880 km² which is 15% of the total land area of the country. Altitude-wise, it ranges from 180 to 4377 meters above sea level. The basin contains highlands in its upper part and lowlands in its lower part. It has an estimated population (mid-2004) of about 4.6 million, which is about 6.5% of the total population of Ethiopia. 89.6% and 10.4% of the basin population are rural and urban respectively. The population density of the basin is about 23 persons per km². The three most important rivers that form the basin are Genale, Weyib (present study basin) and Dawa. All the three rivers join near Dolo area and create the Juba River in Somalia which flows into the Indian Ocean.

The Genale-Dawa basin covers three regional States, Oromia, Somali and the Southern Region. The Oromia Regional State has three zones; Bale, Guji, and Borena; the Southern Regional State two zone; Sidama and Gedeo; and the Somali Regional State have two zones; Afder and Liben in the basin (GDRB-IRDMPSFR, VOL II.3.1, 2007). The estimates of the annual total water demand (i.e., water demand for domestic, commercial and public institutions, industrial, livestock, and system water losses) for current (2005) and projected

(in the 2020s, 2050s and 2080s time slices) in the study area of Weyib River basin were calculated as the product of the gross per capita water use derived from the Genal-Dawa River basin master plan development (GDMPD) study report for the year 2000-2007 and a population estimation for each of Wereda (districts) found inside the study basin.

According to Gleick (1996) and accepted by World Bank, water demand for basic human needs (drinking water for survival, water for human hygiene, water for sanitation services, and modest household needs for preparing food) shall be at least in the ranges 30-50 liter per capita per day (lpcd) in the 21st Century, this standard is also applied during Genale-Dawa Master Plan Development Study in which our study area (Weyib River basin) is part of it. The irrigation water demand of the study basin has determined for each three irrigation schemes (Bale Gadula (4500 ha), Tegona (2500 ha) and Tebel (1000 ha)) during master plan development period (2005-2007). In case of annual total water availability estimation, the ArcSWAT hydrologic model was used to simulate surface and subsurface hydrological processes of Weyib River basin both for current and projected time periods. The standard procedure of ArcGIS interface ArcSWAT hydrologic model was applied to simulate surface and subsurface water resources components of the Weyib River basin.

Chapter 3: Statistical Downscaling of Daily Temperatures and Precipitation Data from CMIP5-ESMs-RCPs Experiment: in Weyib River Basin, Southeastern Ethiopia

3.1. Introduction

It is observed that there is a substantial gap between what the large-scale spatial resolutions of ESMs supply and what the hydrological models required for simulating local catchment hydrological processes. This scale discrepancy sources to a sizeable trouble for the valuation of climate change effect through hydrological models. Hence, significant awareness should be drawn to the development of downscaling methodologies so as to obtain local scale climate variables (mainly precipitation and temperatures) from coarse resolution ESMs. There are two prime methodologies accessible for the downscaling of large scale resolution ESMs output to the finer (local) scale resolution (Wilby and Dawson, 2007) namely dynamic (a higher resolution regional climate model is enforced to use ESMs output) and statistical (develop empirical relationships between large-scale atmospheric ESMs variables, the predictors and local (finer or catchment) scale climate variables, the predictands) downscaling methodologies.

Practical knowledge about spatial weather data availability in a particular study basin is so essential in the area of future climate change projection. Some researcher may use a single weather station; some experts may use three or six or ten, twenty and so on spatial weather stations to represent their study area. Therefore, studying impacts of spatial weather data availability on climate change projections (for example, impacts on both maximum and minimum temperature, precipitation) is paramount important. To characterize the station wise impacts of spatial weather data availability on precipitation and temperatures (maximum and minimum) projections, it is important to obtain station wise future projection on both temperatures and precipitation. Therefore, in this study, the statistical spatial downscaling under CMIP5-ESMs (GFDL-ESM2M, CanESM2, and GFDL-ESM2G) models for the RCP8.5, RCP4.5 and RCP2.6 scenarios were used to generate future daily precipitation and both temperatures series for twelve spatial arbitrary stations in the basin. To investigate the effect of spatial data availability on climate change projection, averaging less number of stations was done by considering 6, 3 and single station. The analysis of future maximum and minimum temperature and precipitation were carried out on an annual, seasonal and monthly basis in the 2020s, 2050s and 2080s time slices.

Therefore, specific objectives of this chapter were to;

→ Downscale daily temperatures (maximum and minimum) and precipitation from CMIP5-ESMs-RCPs scenario

→ Develop temporal (in the 2020s, 2050s and 2080s time slices) temperatures and precipitation scenarios from the CMIP5-ESMs-RCPs experiment in the Weyib River basin

→ Characterize how future temperature and precipitation projection under CMIP5-ESMs-RCP model output varies against four different averaged arbitrary spatial weather stations

3.2. Materials and Methods

3.2.1. Description of study area (Weyib River basin)

Weyib River basin (Fig 3.1) had an area of 4215.93 km^2 and situated between 6.50-7.50°N latitude and 39.50-41.00°E longitude. The altitude variation ranges around 4389 m (a.m.s.l) at the highest point to 898 m at the confluence point. The study area has 22.30°C average annual maximum temperature and 7.55°C minimum temperature. The mean rainfall of the entire study basin ranges from 749.34 to 1368.90 mm (mean of 1037.40 mm) per annum. Study area experiences bimodal rainfall shapes of double peaking in the month of April and August. The Eutric Vertisol and Dystric Cambisol are the two most important soil types, and agriculture is a leading land use type (about 90%). Roughly, 70.54% of the basin area has covered with 0-15% land slope (Serur and Sarma, 2016a).

Mean annual net water availability in the entire basin (for the simulation period 1984-2004) has to be 553.46 mm of this contribution of surface runoff, subsurface soil flow (water flowing laterally within the soil profile that arrives the main channel) and groundwater flow (base flow) to the net water availability is 24, 55 and 21% respectively. The lateral flow contribution becomes a greater portion (about 55%) of the water availability in the basin. About 46.40% of the mean annual precipitation has been vanished through evapotranspiration from the entire basin. Several tributaries drain into Weyib, and some of them are identified as main tributaries, including the Shaya, Tegona, and Tebel. The Shaya River is a tributary of the Weyib that originates from the Sanete Mountain above Goba town. It is known to have a perennial flow.

From its source in the mountains, it crosses the Addis Ababa-Goba road and down through the Sheneka plains to finally join the Weyib around the plains. The Tegona River is another tributary of Weyib that originates from the high rainfall areas of the Bale Mountains just above the town of Goba. It flows across the plains of Sinnana Wereda (Bale zone) in a very shallow river course until it joins the Weyib. The Tebel River, otherwise known as Dinik, is a small tributary of the Weyib originating from the hills around Ginnir. It flows from 2,000 m to around 1,000 m at its confluence with the Weyib.

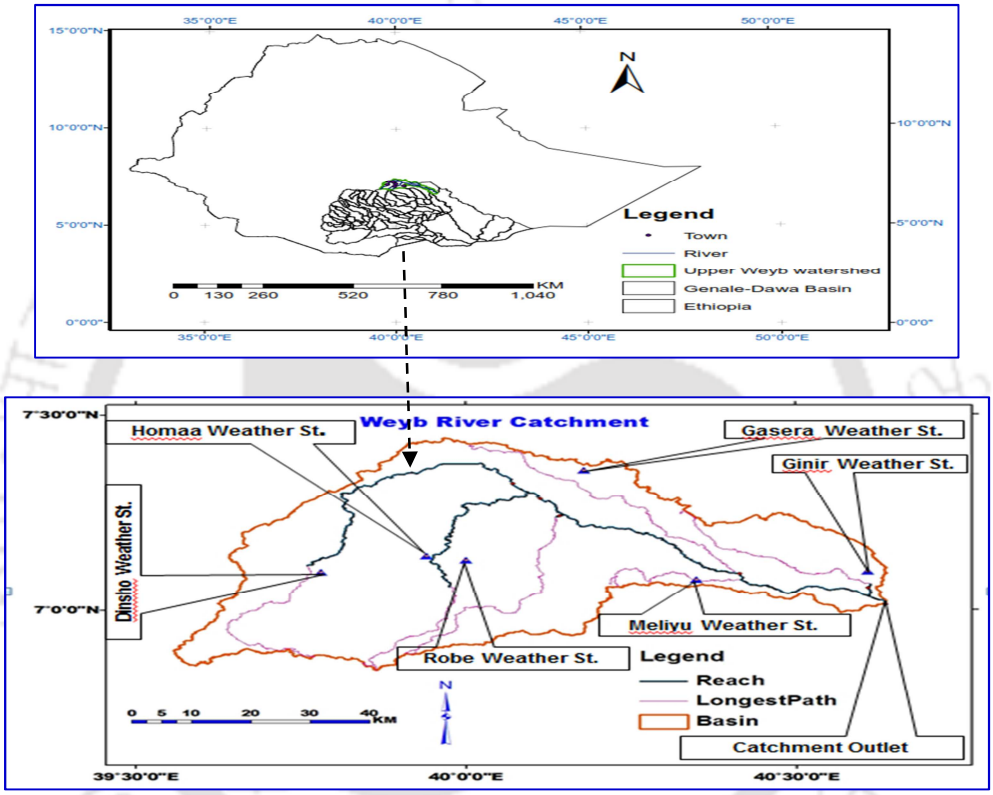

Figure 3.1 Location map, reaches and some of the weather stations in the study area

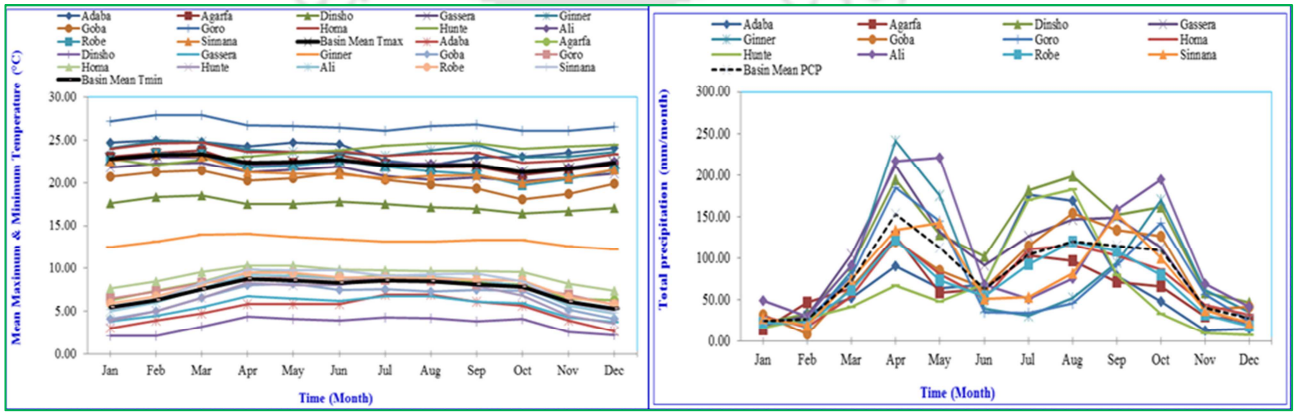

Figure 3.2 Spatial distribution of temperatures and rainfall characteristics of Weyib River basin

3.2.2. Types of Earth System Models (ESMs) and RCP scenarios used

In this study, three bias-corrected ESMs (GFDL-ESM2M, CanESM2 and GFDL-ESM2G) for the RCP8.5 (very high emission scenario) RCP4.5 (intermediate emission scenario) and RCP2.6 (very low emission scenario or peak and decline scenario) scenarios from CMIP5 have been used. These ESM models are adopted for two rationales. Firstly, the models are widely applied in various climate change impact studies, and second they offer large scale daily predictor variables which can be directly used into SDSM. The historical and future predictor variables are available for different regions of the world by providing latitude and longitude values that include the study area of Weyib River basin. These historical and future predictor variables have been downloaded through official website (http://ccds-dscc.ec.gc.ca/?page=pred-canesm2) of Canadian Centre for Climate Modelling and Analysis (CCCMA) for the CaESM2 ESM model. However, the predictor variables for GFDL-ESM2M and GFDL-ESM2G have been downloaded from NOAA-GFDL CMIP5 official data portal (https://pcmdi.llnl.gov/search/cmip5/). The downloaded predictor variables are then arranged as per the SDSM data file format to downscale local climate variables.

As explained by Grotch and MacCracken (1991), GCMs/ESMs are coarse in resolution and are unable to resolve significant sub-grid scale features such as topography, clouds, and land use. For instance, CanESM2 developed by the CCCMA has resolved at a spatial resolution of 2.81° longitude by 2.79° latitude; the NOAA Geophysical Fluid Dynamics Laboratory USA GFDL-ESM2M and GFDL-ESM2G have resolved at a spatial resolution of 2.50° longitude by 2.00° latitude. GFDL-ESM2M and GFDL-ESM2G models differ exclusively in the physical ocean component; ESM2M uses Modular Ocean Model version 4p1 with vertical pressure layers while ESM2G uses Generalized Ocean Layer Dynamics with a bulk mixed layer and interior isopycnal layers. Differences in the ocean mean state include the thermocline depth being relatively deep in ESM2M and relatively shallow in ESM2G compared to observations. Table 3.1 below shows the three different ESM models, institutions, and their spatial resolutions.

Table 3.1 The CMIP5 Earth System Models used in this study

Model	Institution	Spatial Resolution (Lon × Lat, degree)
CanESM2	Canadian Centre for Climate Modelling and Analysis, Canada	2.81×2.79
GFDL-ESM2M	NOAA Geophysical Fluid Dynamics Laboratory, USA	2.5×2.0
GFDL-ESM2G		2.5×2.0

3.2.3. Types of data used

Daily weather data and ESMs data have utilized for this chapter study. The daily weather data (daily precipitation, maximum and minimum temperature, mean wind speed, relative humidity and sunshine hours) for twelve weather stations (detailed in Table 3.2) that are established inside the basin and in nearby vicinity of the basin boundary of the Weyib River basin were collected from National Meteorological Service Agency of Ethiopia (NMSA). The source of ESMs data is the official website of CCCMA and NOAA-GFDL CMIP5 data portal as mentioned above in 'Earth System Model (ESM) and RCP Scenarios' section. The period of Fifth Assessment for future emission scenarios experiment is from 2006 to 2100. The spatial and temporal distribution of the 12 meteorological stations temperatures and rainfall characteristics of Weyib River basin have shown in Fig. 3.2.

Table 3.2 Details of the 12 meteorological stations and their data records

S.No.	Station name	Data recording periods	Latitude (°N)	Longitude (°E)	Altitude (m)	Total annual mean precipitation (mm)	Mean annual max. temp (°C)	Mean annual min. temp (°C)
1	Robe	1984-2011	7.133	40.000	2464	804.14	21.79	8.00
2	Goba	1998-2007	7.017	40.000	2613	980.03	20.13	6.52
3	Dinsho	1981-2007	7.100	39.783	3072	1368.90	17.43	3.43
4	Agarfa	1988-1997	7.267	39.817	2465	762.36	22.38	8.13
5	Sinnana	1982-2008	7.067	40.217	2364	894.35	21.39	8.02
6	Adaba	1980-2010	7.000	39.383	2415	823.65	23.87	5.10
7	Homa	1988-2010	7.133	39.933	2505	846.58	21.75	7.33
8	Ali	1988-2005	7.017	40.350	2460	1264.17	20.47	6.68
9	Gassera	1980-2010	7.367	40.183	2337	1181.12	20.67	6.95
10	Goro	1981-2005	7.000	40.467	1806	887.14	26.77	7.89
11	Ginnir	1980-2012	7.133	40.700	1929	1030.04	23.82	13.20
12	Hunte	1980-2011	7.100	39.417	2413	749.34	23.71	6.73

3.2.4. Downscaling methods

There are two prime methodologies accessible for the downscaling of large-scale spatial ESMs output to the local scale spatial resolution (Wilby and Dawson, 2007) and described in review literature chapter in 'review of downscaling approaches' section. The statistical downscaling method establishes empirical relationships between large-scale ESM outputs, the predictors, and local scale climatic variables (for instance, Tmax, Tmin, and

precipitation), the predictands with the help of some transfer function as shown in the following relation.

$$Y = f(X) \tag{3.1}$$

Where Y is dependent variables (predictands), i.e., the variables we are going to downscale (for instance, local Tmax, Tmin, and precipitation); X is independent variables (predictors), i.e., a set of large-scale potential predictor variables (for instance, mean sea level pressure, geopotential heights and specific humidity at the surface and 850 hpa) and f represents a stochastic function that relates the two (predictands and predictors).

The 'f' function is determined empirically from historical observations by training and validating the model. Thus, the achievement of the statistical downscaling method has based on the relationship used and choice of potential predictor variables, whose performance could have verified through estimation of various statistical indices (for instance, R^2, RMSE, and NSE). Regression analysis based statistical downscaling is very powerful for forecasting (Ghosh and Mujumdar, 2008) and it has divided into two categories namely simple regression (SLR) and multiple regressions (MLR). Therefore, in this study, the independent variables are more than one, so MLR using SDSM has been used to downscale daily temperatures and precipitation data from Ensembles of CMIP5-ESMs for the future RCP scenarios.

3.2.5. Statistical downscaling model (SDSM)

The SDSM describes a combination of the stochastic weather generator and regression based on the family of the transfer function (Liu et al., 2011). It performs the spatial downscaling through daily predictor-predictand relationships using MLR and creates predictands that represent the local weather condition. Regression-based in the family of transfer function method is the well-known technique of downscaling (Ghosh and Mujumdar, 2008) and that depends on the direct, measurable link between predictand and predictors through some form of regression (Eq.3.1). SDSM (version 4.2.9) a decision support tool (Wilby and Dawson, 2007) has been used for this study to downscale daily future Tmax, Tmin, and PCP. This model has downloaded from the website http://co-public.lboro.ac.uk/cocwd/SDSM/. There are seven major steps to be followed in developing the best performing MLR equation for the downscaling processes in this version of SDSM. Detailed discussions of the steps are given in (Wilby and Dawson, 2007; Wilby et al., 2002) and highlighted as well here below.

3.2.6. Statistical downscaling model setup (Model Approach)

A. Predictors' Files

The large-scale predictors, which used for SDSM model input, have been downloaded from the official website (http://ccds-dscc.ec.gc.ca/?page=pred-canesm2) of CCCMA for the CaESM2 climate model whereas NOAA-GFDL CMIP5 official data portal (https://pcmdi.llnl.gov/search/cmip5/) for the GFDL-ESM2M and GFDL-ESM2G climate models. Based on the availability of continuous time series data, the period from 1981-2005 is used for downscaling. Thus, the corresponding 25 years observed daily predictors' dataset and 95 years (2006-2100) future large-scale predictors under Ensembles of three ESMs from CMIP5 for the study area have been extracted. The downloaded predictor variables are then arranged as per the SDSM data file format to downscale local climate variables. Before constructing the relationship between given stations weather data called predictand and large scale atmospheric variables called predictors, some important model parameters have to be setup to achieve the best statistical agreement between observed and simulated climate data. The model setup has been described below, and these have based on the SDSM 4.2 manual (Wilby and Dawson, 2007).

Year length: The Gregorian calendar which consists of 365 days has been used while dealing with predictand and historical ESMs data and while working on scenario generation as the ESMs have a model year of 365 days.

Standard start and end date: The start date 01-01-1981 and the end date 31-12-2005 has been used in the model considering availability of continuously observed time series data.

Allow negative values: The negative values were allowed for simulation for maximum and minimum temperature whereas it was not allowed for precipitation.

Event threshold: The event threshold was set to zero for maximum and minimum temperature and 0.1 for precipitation (it means that the days with less than or equal to 0.1 mm per day of precipitation has treated as dry days).

Missing data identifier: The missing data have been given -99 for all the input data set. The model skipped this value whenever it finds this value in the input data during model calibration and calculating the summary statistics.

B. Data Quality Control

Quality control has been done for all the twelve meteorological stations (Table 3.2) before model calibration step. Few meteorological stations have 100% complete and/or fully correct data sets. Managing of missing and unsatisfactory data is necessary for most practical situations. Simple quality control checks in SDSM enable the identification of gross data errors, the specification of missing data codes and outliers before model calibration. After performing the quality control, the daily precipitation and temperatures (Tmax and Tmin) have been considered as predictand variables of interest. Table 3.2 shows the selected stations to downscale precipitation and both temperatures. All the selected stations lie within the basin except the three stations, which have found in close vicinity of the basin.

C. Screening the Downscaling Predictor Variables

The choice of appropriate downscaling potential predictor variables have been done with the help of the screen variables option of the SDSM using correlation analysis, partial correlation analysis and scatter plot. Screening the potential predictors have been done through choosing seven or eight predictors at a time and analyze their explained variance, then choice those predictors which have greater explained variance and drop the rest. Then partial correlation analysis has been done for nominated predictors to see the level of association with each other; these statistics identify the extent of the descriptive power of the predictor to describe the predictand. The selected predictor variables were then used to derive transfer function (parameter file ".PAR"). The parameter file has then used for generating ensembles of new synthetic daily weather data.

Let's take an example of minimum temperature for Goba Meteorological station. Among the available 26 predictor variables from the CanESM2-historical project, the five potential predictor variables namely; ceshp8thgl, ceshs850gl, ceshp8_zgl, ceshshumgl and ceshtempgl which have high explained variance were selected. These were then put forward for partial correlation analysis to identify the correlation among each other and found that *ceshp8_zgl* has significantly associated with other predictor variables (Table 3.3). Hence, this variable has been rejected from the selection. The rest four predictor variables were then checked individually in a scatterplot and showed that all of them have a good association with predictand and thus all four of them were selected as the final set of potential predictor variables. The same procedure has been followed for all the ESMs, predictands, and stations

to choose the most potential predictor variables. The list of all the selected potential predictor variables for all the ESMs, predictands and stations are given in Appendix Table 1-36.

Table 3.3 Example, correlation matrix obtained from SDSM for minimum temperature

Predictor Full Name	Notations	Parti.cor. (r-value)	p-value
850 hPa wind direction	ceshp8thgl.dat	0.078	0.000
Specific humidity at 850 hPa	ceshs850gl.dat	-0.116	0.000
850 hPa vorticity	*ceshp8_zgl.dat*	*-0.001*	*0.563*
Surface specific humidity	ceshshumgl.dat	0.146	0.000
Mean temperature at 2m	ceshtempgl.dat	0.323	0.000

Therefore, the predictors used for downscaling should be reliably generated by ESMs, freely accessible from ESM outputs archive and strongly linked with the local climate variables of concern (Tmax, Tmin, and precipitation in this case).

D. Calibration

After the routine screening procedure as mentioned above, the model calibration constructed a transfer function called ".PAR" (parameter) file based on the MLR equations with the help of predictand and predictor variables. There are two options in SDSM for optimizing the model namely dual simplex and ordinary least squares. The former one has been used for entire climatic variables and stations in this study. The model type determines whether the individual downscaling will be calibrated for each of the calendar months, seasonal or for the entire year. During this downscaling process, it was set to monthly for both temperatures and precipitation which means that twelve regression equations have developed for twelve months. Also, the model can either specify to unconditional or conditional process. The unconditional model process assumes that there is a direct link between predictor variables and predictand whereas conditional model assumes the existence of intermediate process between regional forcing and local weather. In this study, the model process has been set to unconditional for minimum and maximum temperature and conditional for precipitation. The significance level was set to default value 0.05. There was no transformation applied for all predictands considering the normal distribution.

E. Weather Generator

It helps to validate the calibrated model. This operation generates the ensembles of synthetic current daily weather data for the specified period based on inputs of the observed time series data and the MLR parameters produced during the calibration step. Each time series

data of the observed climate variable is linked to the regression model weights to generate the synthetic time series data into a series of ensembles (runs). The period of record to be synthesized and desired number of ensembles could have changed according to requirement. Twenty ensembles of synthetic daily weather data series were generated for the period of 1981 to 2005 for all the variables and stations to compare with the observed station data.

F. Scenario Generation

Similar to the weather generator function, the scenario generator operation also generates the ensembles of synthetic daily weather data series but for the future period. After validation of the model, the same parameter file or regression weight that has used during weather generation operation was used to downscale the future data. But this time, instead of using historical potential predictor variables for ensembles of ESMs, future ESMs (GFDL-ESM2M, CanESM2, and GFDL-ESM2G) output for the RCP8.5, RCP4.5, and RCP2.6) scenarios were used as large-scale atmospheric potential predictor variables. The twenty ensembles of synthetic daily time series data were generated for the period of 2006 to 2100 for all the variables and stations, and the mean of these twenty ensembles has used as final daily weather data for the specified period. According to Nigatu (2013), the average of 20 individual ensembles outputs perform well, and a large number of ensembles does not improve and have chances of significant deviation among ensembles. The same procedure was repeated to generate future precipitation, maximum and minimum temperature data for all the RCPs and in all stations. And then the future Tmax, Tmin, and precipitation scenarios have been established by dividing the future time series into three-time slices (in the 2020s, 2050s, and 2080s) for the 12, 6, and 3 averaged arbitrary spatial weather stations as well as for a single weather station.

3.2.7. SDSM performance evaluation

In order to evaluate the SDSM performance relative to the observed precipitation and temperatures data, three statistical model performance evaluation measures, in addition to graphical technique, were used during the calibration and validation periods (R^2; Krause and Boyle, 2005), NSE; Nash and Sutcliffe, 1970 and RMSE; Singh et al., 2004). In addition to statistical measures, the graphical technique also used to provide a visual comparison of simulated and measured constituent data. The detail scientific descriptions of statistical measures are given in Chapter 4 in 'Models performance evaluation' section.

3.2.8. Statistical bias correction

The bias correction approach is needed to remove the bias from the daily series of downscaled data (Salzmann et al., 2007). The linear scaling approach (Lenderink et al., 2007) operates with monthly correction values based on the differences between observed and present day downscaled (by SDSM) values for temperatures (Eq. 3.3). Precipitation is corrected with a factor based on the ratio of long-term monthly mean observed and downscaled data for baseline period (Eq. 3.2). The applied correction factors are assumed to remain unvaried even for future conditions.

$$P_{bc} = P_{downscaled}\left(\frac{P_{obs\ av}}{P_{cont\ av}}\right) \tag{3.2}$$

$$T_{bc} = T_{downscaled} + T_{obs\ av} - T_{cont\ av} \tag{3.3}$$

Where, P_{bc} and T_{bc} are bias corrected downscaled precipitation and temperature (for baseline and/or future condition), $P_{downscaled}$ and $T_{downscaled}$ are downscaled precipitation and temperature value with biases (for baseline and/or future condition), $P_{obs\ av}$ and $T_{obs\ av}$ are mean of observed (measured) precipitation and temperature data, $p_{cont\ av}$ and $T_{cont\ av}$ are mean of downscaled precipitation and temperature data for baseline (control) period.

3.2.9. Precipitation and temperatures scenario statistics

Percentage and absolute change have been used to calculate three-time slices of thirty years precipitation and temperatures, respectively.

Percentage difference has been used for precipitation;

$$\Delta 2020s = \frac{(V2020s - Vbase) \times 100}{Vbase} \tag{3.4}$$

$$\Delta 2050s = \frac{(V2050s - Vbase) \times 100}{Vbase} \tag{3.5}$$

$$\Delta 2080s = \frac{(V2080s - Vbase) \times 100}{Vbase} \tag{3.6}$$

Absolute difference has been used for temperatures,

$$\Delta 2020s = V2020s - Vbase \tag{3.7}$$

$$\Delta 2050s = V2050s - Vbase \tag{3.8}$$

$$\Delta 2080s = V2080s - Vbase \tag{3.9}$$

Where, Vbase is the mean of 20 ensembles of precipitation and temperature (max and min) for the base period for each ESM and each station. V2020s, V2050s, and V2080s are the mean of 20

ensembles of precipitation and temperature (max and min) for the period of 2011-2040, 2041-2070 and 2071-2100 respectively for each ESM-RCP experiment and each station.

3.2.10. Mann-Kendall trends test

A non-parametric rank-based procedure that has frequently been used to evaluate if there is a rise or decline trend in the time series of meteorological and hydrological data (Hamed, 2008; Karpouzos et al., 2010). The Mann-Kendall test was applied in this study to see the existing trends (rise or decline) of Tmax, Tmin, and precipitation for the RCP8.5, RCP4.5, and RCP2.6 scenarios in future periods.

Let X_1, X_2,…, X_n represent n data points where X accounts for the data point at time j. Then the Mann-Kendall statistic ('S') is given by equation (3.10):

$$S = \sum_{k=1}^{n-1} \sum_{j=k+1}^{n} sign(X_j - X_k) \tag{3.10}$$

Where:

$$sign(X_j - X_k) = \begin{cases} 1 & if(X_j - X_k) > 0 \\ 0 & if(X_j - X_k) = 0 \\ -1 & if(X_j - X_k) < 0 \end{cases}$$

A positive value of S is an indicator of an increasing trend, and a low negative value indicates a decreasing trend.

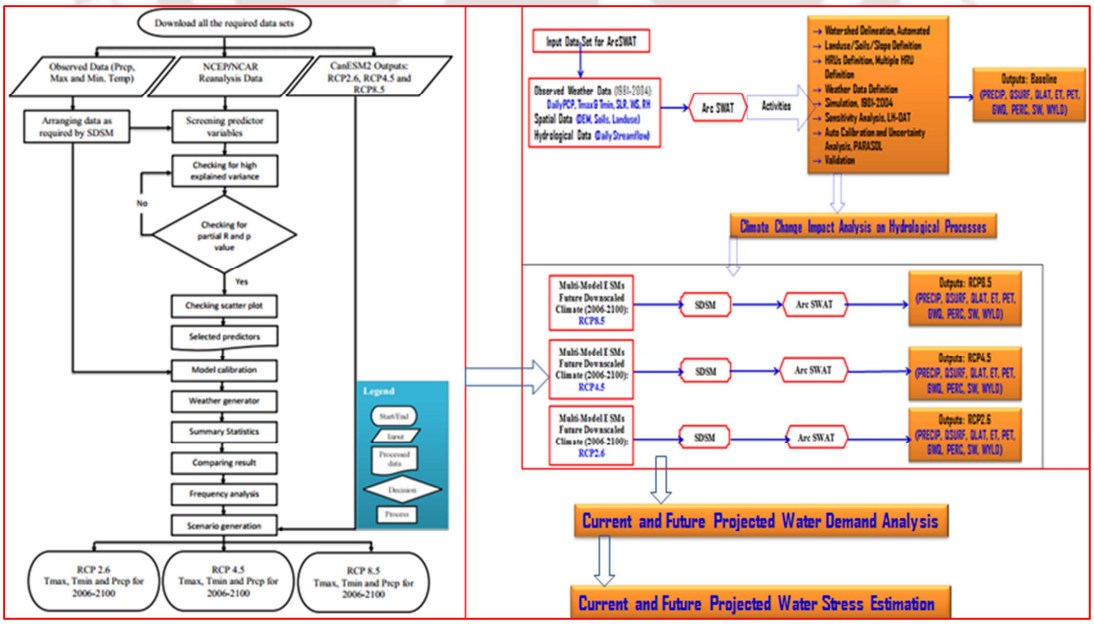

Figure 3 A comprehensive flow chart of SDSM downscaling processes, ArcSWAT hydrologic modeling, water demand analysis and water stress estimation

3.3. Results and Discussion

3.3.1. Selected common potential predictor variables

In this section lists of selected common potential predictor variables in the entire basin that gave better correlation results at $p<0.05$ for CanESM2, GFDL-ESM2M, and GFDL-ESM2G-historical models have presented below (Table 3.4, 3.5 and 3.6).

Results revealed that different atmospheric variables affect different local variables in all the ESMs (Table 3.4, 3.5 and 3.6). For example, precipitation is more sensitive to mean sea level pressure, specific humidity (at the surface and 850 hPa), zonal velocity (at 500 and 850 hPa) and geopotential heights (at 500 hPa). Mean sea level pressure, geopotential heights ('at 500 and 850 hPa'), average temperature (at 2m height), specific humidity (at near surface and 850 hPa) and wind direction (at 850 hPa) affect both the maximum and minimum temperature under the CanESM2-historical model.

Table 3.4 List of selected common potential predictor variables that gave better correlation results at $p<0.05$ from CanESM2-historical model for study area of Weyib River basin

Predictand	Predictor full name	Notations	Parti.cor. (r-value)	p-value
Precipitation	Mean sea level pressure	ceshmslpgl.dat	0.050	0.020
	Specific humidity at 850 hPa	ceshs850gl.dat	0.090	0.000
	Surface specific humidity	ceshshumgl.dat	0.077	0.002
	500 hPa zonal velocity	ceshp5_ugl.dat	-0.094	0.000
	850 hPa zonal velocity	ceshp8_ugl.dat	-0.119	0.000
	500 hPa geopotential height	ceshp500gl.dat	0.056	0.016
Maximum temperature	Mean sea level pressure	ceshmslpgl.dat	0.148	0.000
	500 hPa geopotential height	ceshp500gl.dat	0.134	0.000
	Specific humidity at 850 hPa	ceshs850gl.dat	-0.268	0.000
	Mean temperature at 2m	ceshtempgl.dat	-0.235	0.000
	850 hPa wind direction	ceshp8thgl.dat	0.110	0.000
	850 hPa geopotential height	ceshp850gl.dat	-0.200	0.000
	Surface specific humidity	ceshshumgl.dat	-0.274	0.000
Minimum temperature	Mean sea level pressure	ceshmslpgl.dat	-0.308	0.000
	500 hPa geopotential height	ceshp500gl.dat	0.222	0.000
	Surface specific humidity	ceshshumgl.dat	0.146	0.000
	Mean temperature at 2m	ceshtempgl.dat	0.323	0.000
	Specific humidity at 850 hPa	ceshs850gl.dat	-0.116	0.000
	850 hPa geopotential height	ceshp850gl.dat	-0.103	0.000
	850 hPa wind direction	ceshp8thgl.dat	0.078	0.000
	850 hPa zonal velocity	ceshp8_ugl.dat	-0.116	0.000

Table 3. 5 List of selected common potential predictor variables that gave better correlation results at p<0.05 from GFDL-ESM2M-historical model for study area of Weyib River basin

Predictand	Predictor full name	Notations	Parti.cor (r-value)	p-value
Precipitation	Sea level pressure	geshpslgl.dat	0.221	0.000
	Total cloud fraction	geshcltgl.dat	-0.131	0.000
	Daily-mean near-surface wind speed	geshsfcwindgl.dat	-0.243	0.000
	Eastward near-surface wind	geshuasgl.dat	-0.106	0.000
Maximum temperature	Sea level pressure	geshpslgl.dat	-0.143	0.000
	Near-surface relative humidity	geshrhsgl.dat	-0.418	0.000
	Daily maximum near-surface air temperature	geshtasmaxgl.dat	0.142	0.000
	Daily minimum near-surface air temperature	geshtasmingl.dat	0.143	0.000
	Daily-mean near-surface wind speed	geshsfcwindgl.dat	0.126	0.000
	Eastward near-surface wind	geshuasgl.dat	0.179	0.000
Minimum temperature	Sea level pressure	geshpslgl.dat	0.215	0.000
	Total cloud fraction	geshcltgl.dat	0.299	0.000
	Surface downwelling longwave radiation	geshrldsgl.dat	0.378	0.000
	Daily-mean near-surface wind speed	geshsfcwindgl.dat	-0.126	0.000

Table 3.6 List of selected common potential predictor variables that gave better correlation results at p<0.05 from GFDL-ESM2G-historical model for study area of Weyib River basin

Predictand	Predictor full name	Notations	Parti.cor. (r-value)	p-value
Precipitation	Total cloud fraction	geshcltgl.dat	-0.310	0.000
	Eastward near-surface wind	geshuasgl.dat	-0.418	0.000
	Daily-mean near-surface wind speed	geshsfcwindgl.dat	0.413	0.000
	Sea level pressure	geshpslgl.dat	-0.486	0.000
Maximum temperature	Sea level pressure	geshpslgl.dat	-0.415	0.000
	Near-surface relative humidity	geshrhsgl.dat	0.692	0.000
	Daily maximum near-surface air temperature	geshtasmax.dat	-0.429	0.000
	Eastward near-surface wind	geshuasgl.dat	0.721	0.000
	Daily-mean near-surface wind speed	geshsfcwindgl.dat	0.514	0.000
Minimum temperature	Surface downwelling longwave radiation	geshrldsgl.dat	0.523	0.000
	Sea level pressure	geshpslgl.dat	0.462	0.000
	Near-surface relative humidity	geshrhsgl.dat	-0.521	0.000
	Daily-mean near-surface wind speed	geshsfcwindgl.dat	-0.289	0.000

Note: The partial correlation coefficient (r) shows the explanatory power that is specific to each predictor. All are significant at $p \leq 0.05$. hpa: is a unit of pressure, 1 hPa = 1 mbar = 100 Pa = 0.1 kPa.

However, under GFDL-ESM2M and GFDL-ESM2G-historical models, precipitation is more impacted by sea level pressure, total cloud fraction, daily mean near-surface wind speed and

eastward near surface wind (Table 3.5 and 3.6). Sea level pressure, near surface relative humidity, daily maximum near-surface air temperature, daily mean near-surface wind speed and eastward near surface wind affect the maximum temperature whereas sea level pressure, surface downwelling longwave radiation and daily mean near-surface wind speed affect the minimum temperature (Table 3.5 and 3.6). Finally, these selected potential predictor variables are used to develop parameter files that can use for downscaling after validation with the independent dataset. The lists of selected potential predictor variables, their correlation coefficient and significance level for all the climatic variables (3 predictands) and 12 stations under all the three ESMs are given in Appendix Table 1-36.

3.3.2. Calibration and validation of SDSM for both temperatures and precipitation

For downscaling of maximum and minimum temperature and precipitation MLR, using SDSM was used to calibrate and validate the model. The entire length of the observed data was available from 1981 to 2005. This data has divided into two parts for calibration and validation. Data from 1981 to 1993 was used for calibration whereas data from 1994 to 2005 has used for validation of the model. *For brevity and explanation purposes only the average results of twelve meteorological arbitrary spatial stations and mean of three ESMs for the RCP8.5, RCP4.5 and RCP2.6 scenarios have been given in this section.*

Calibration and validation results of SDSM for twelve averaged spatial stations maximum temperature from the mean of 3 ESMs downscaling model are shown in (Fig 3.3a and b). The R^2, RMSE, and NSE values were 0.95, 0.44 and 0.82 respectively for calibration period whereas R^2, RMSE and NSE values of 0.94, 0.46 and 0.79 respectively for validation period. For minimum temperature (Fig 3.3c and d) the R^2, RMSE, and NSE values were 0.93, 0.58 and 0.88 respectively for calibration period whereas R^2, RMSE and NSE values were 0.92, 0.58 and 0.86 for validation period. Calibration and validation results for twelve averaged spatial stations precipitation downscaling model have shown in (Fig 3.3e and f). The R^2, RMSE, and NSE values were 0.86, 0.79 and 0.84 respectively for calibration period whereas R^2, RMSE and NSE values of 0.83, 0.98 and 0.78 respectively for validation period. From the statistical indices and graphical observation between simulated (by SDSM) versus measured value we can infer that SDSM has a good ability to replicate historical climate variables for the study area of Weyib River basin.

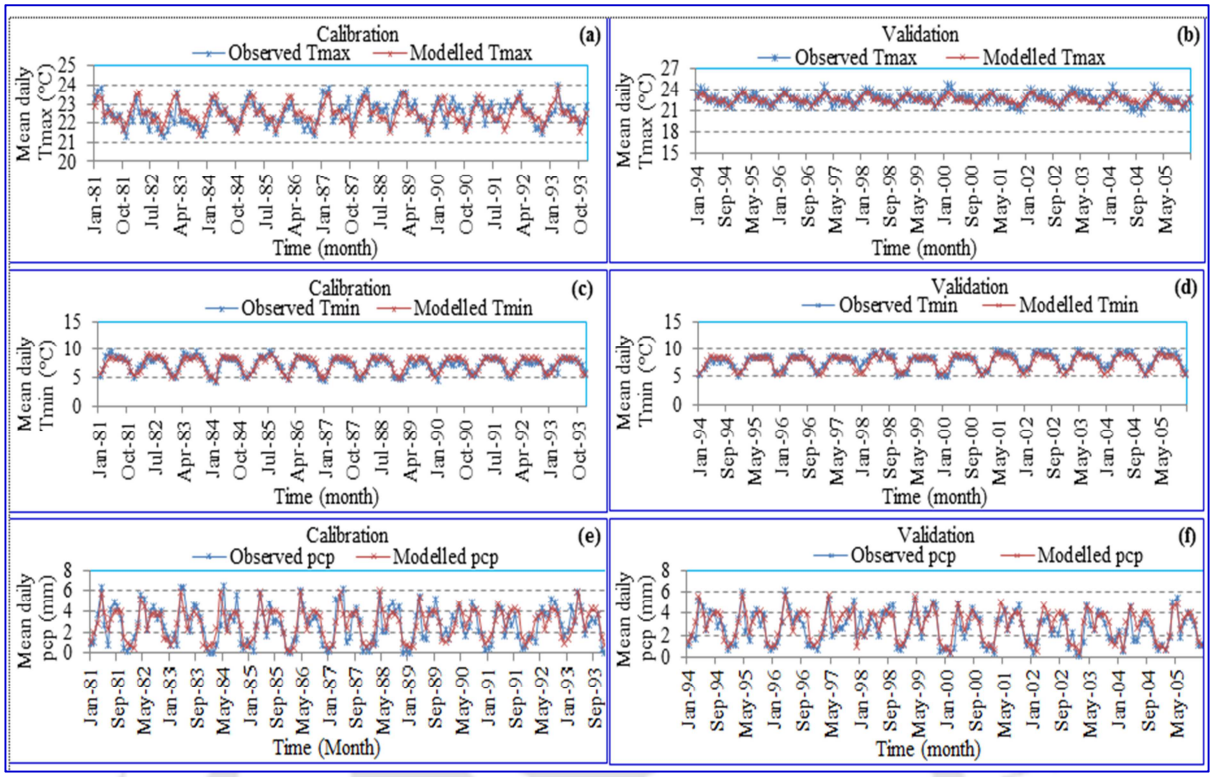

Figure 3.3a (top left): Calibration result of SDSM for maximum temperature from average of 3 ESMs (1981-1993), b (upper right): same as fig 3.3a but for validation period (1994-2005), c (middle left): Calibration result of SDSM for minimum temperature, d (middle right): same as c but for validation period, e (bottom left): Calibration result of SDSM for precipitation, f (bottom right): same as e but for validation period

Impact of Spatial Data Availability on Climate Change Projection

To characterize how future temperatures and precipitation projection under CMIP5-ESMs-RCP output varies against various averaged arbitrary spatial weather stations found in the Weyib River basin, it is essential to obtain station wise future projections on both temperatures (maximum and minimum), and precipitation. Therefore, for brevity reason, the results are summarized into four cases namely; case I (twelve averaged spatial weather stations), case II (six averaged spatial arbitrary weather stations), case III (three averaged spatial arbitrary weather stations) and case IV (for a single weather station) to describe both temperatures and precipitation.

3.3.3. Scenarios developed for future temperatures and precipitation (2006-2100) for twelve averaged spatial weather stations

A. Mean Annual, Seasonal, and Monthly Maximum Temperature Scenarios

The mean annual maximum temperature increases in all the nine ESM-RCP scenarios in the 2020s 2050s and 2080s relative to the baseline (Fig. 3.4). GFDL-ESM2M (G2M), projects

the highest mean annual value for maximum temperature and increased by 0.20, 0.32 and 0.42°C (G2M-RCP8.5), 0.20, 0.29 and 0.31°C (G2M-RCP4.5) and 0.22, 0.24 and 0.21°C (G2M-RCP2.6) in the 2020s, 2050s and 2080s time slices respectively; GFDL-ESM2G (G2G), projects the lowest increases in the value of this parameter by 0.04, 0.12 and 0.22°C (G2G-RCP8.5), 0.04, 0.09 and 0.11°C (G2G-RCP4.5) and 0.08, 0.04 and 0.03°C (G2G-RCP2.6) in the 2020s, 2050s and 2080s time slices respectively and CanESM2 (C2), projects an intermediate (median) increase of mean annual maximum temperature by 0.12, 0.22 and 0.32°C (C2-RCP8.5),0.12, 0.19 and 0.21°C (C2-RCP4.5) and 0.16, 0.14 and 0.13°C (C2-RCP2.6) in the 2020s, 2050s and 2080s time slices respectively (Fig. 3.4).

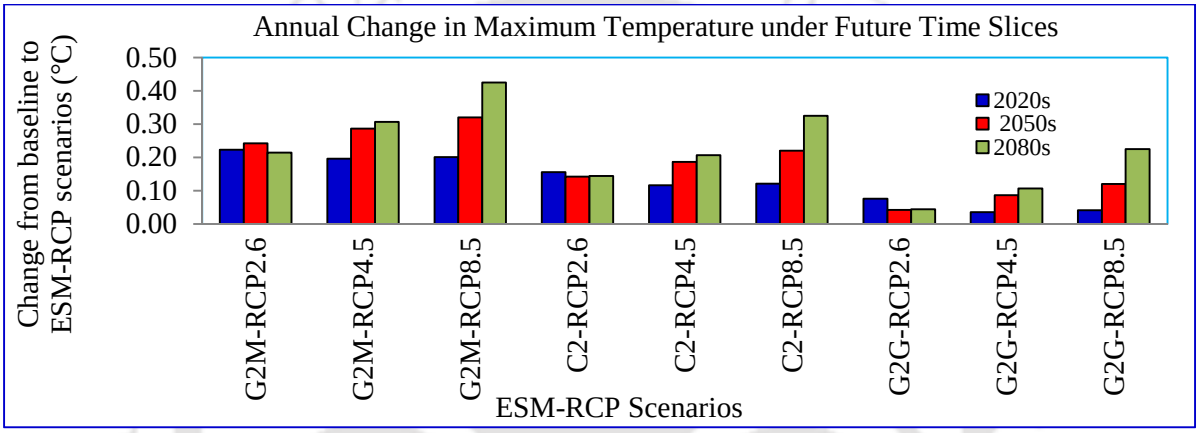

Figure 3.4 Absolute change from baseline simulation of annual maximum temperature in all the ESM-RCP scenarios in the 2020s, 2050s and 2080s time slices

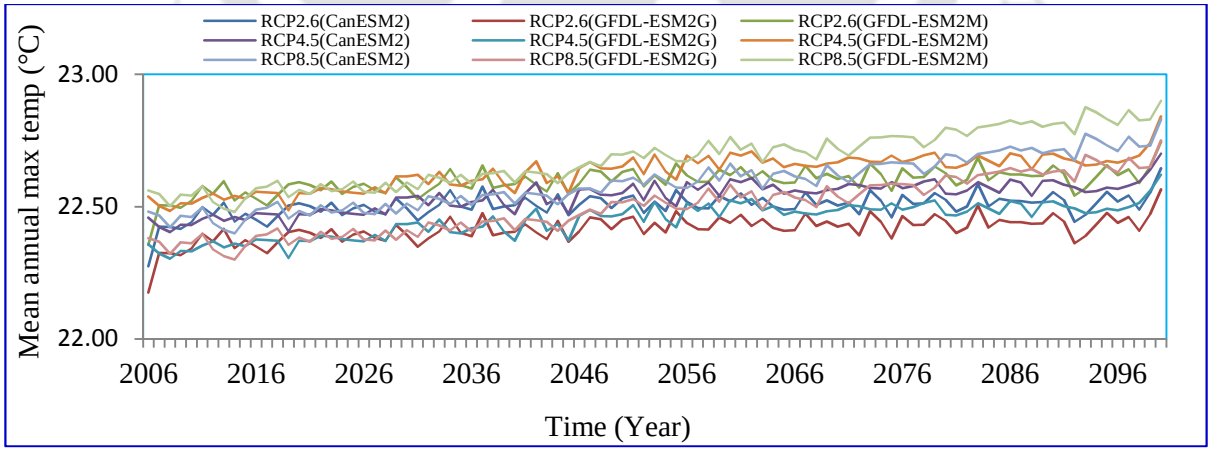

Figure 3.5 Future trend of mean annual maximum temperature (°C) in all the ESM-RCP scenarios

The variability of maximum temperature is higher for all ESMs of RCP8.5 than RCP4.5 and RCP2.6, and the future trend for RCP8.5 and RCP4.5 scenarios have been indicated a significantly (at 5% significant level) increasing trend of mean annual maximum temperature

until the end of the century (Fig. 3.5 and Table 3.10). Increasing trend but not significant (at 5% significant level) was observed for all ESMs of RCP2.6 scenario. Comparatively, RCP8.5 which is the high emission scenario (i.e., condition of very high GHG concentration level) prevail higher change in maximum temperature trend at the end of the century than the RCP4.5 which is an intermediate emission scenario (i.e., condition of medium to low GHG concentration level) and the RCP2.6 which is the lowest emission scenario (i.e., condition of very low GHG concentration level). *For brevity and explanation purposes only the average results of three ESMs for the RCP8.5, RCP4.5, and RCP 2.6 scenarios are given in the case of seasonal and monthly description of maximum and minimum temperatures and precipitation.*

The projected (mean of 3 ESMs) seasonal maximum temperature shows a decreasing trend in the dry season in all the three future time slices for the RCP2.6, RCP4.5, and RCP8.5 scenarios (but not for the RCP2.6 scenario which was an increasing trend in the dry season of the 2020s). However, it has shown an increasing trend for both an intermediate and wet seasons in all the three future time slices for the RCP2.6, RCP4.5 and RCP8.5 scenarios (except for the RCP2.6 scenario which was a decreasing trend in a Wet season of the 2020s) as shown in Fig. 3.6a-c and Table 3.7. The absolute changes of maximum temperature from the base period for three scenarios in future time slices for each season have presented in Table 3.7.

Table 3.7 Absolute changes in mean seasonal maximum temperature (°C) at different time slices from the base period

Scenario	Seasons in the 2020s			Seasons in the 2050s			Seasons in the 2050s		
	Dry	Intermediate	Wet	Dry	Interm.	Wet	Dry	Interm.	Wet
RCP2.6 (mean of 3ESMs)	+0.275	+0.194	-0.002	-0.017	+0.228	+0.215	-0.002	+0.224	+0.208
RCP4.5 (mean of 3ESMs)	-0.012	+0.192	+0.167	-0.001	+0.301	+0.257	-0.001	+0.338	+0.283
RCP8.5 (mean of 3ESMs)	-0.007	+0.202	+0.168	-0.036	+0.370	+0.326	-0.051	+0.529	+0.495

The projected (mean of 3 ESMs) monthly maximum temperature has a larger magnitude of increment on the month of Jun 2080s which was 0.58, 0.80 and 1.37°C for RCP2.6, RCP4.5 and RCP8.5 scenarios respectively at the end of the century. On the other hand, the larger decrement on Dec 2080s 0.75, 0.38°C and on Dec 2050s 0.32°C occurred for RCP8.5, RCP4.5, and RCP2.6 scenarios respectively Fig.3.6c, b and a. The absolute change in mean

maximum temperature was observed to be sizable due to there were a substantial increase and decrease of maximum temperature on different months. For instance, in the months of Jan, Feb, Nov and Dec, the decrement of the maximum temperature was observed and an increment on the rest of the months has observed.

Generally, the change in average monthly maximum temperature might range between -0.25°C on Dec and +0.48°C on Jun for the coming 2020s (2011-2040); -0.50°C on Dec and +0.91°C on Jun for 2050s (2041-2070) and -0.75°C on Dec and +1.37°C on Jun for 2080s (2071-2100) for the RCP8.5 scenario. The change in average monthly maximum temperature for RCP4.5 scenario varies between -0.25°C on Dec and +0.47°C Jun for the coming 2020s; -0.33°C on Dec and +0.70°C on Jun for 2050s and -0.38°C on Dec and +1.37°C on Jun for 2080s. For the RCP2.6, ranges -0.12°C on Aug and +0.42°C on Dec for 2020s; -0.32°C on Dec and +0.58°C on Jun for 2050s and -0.28 on Dec and +0.55°C on Jun for 2080s. As we can see in Fig 3.6d, there has been shown an increasing trend of maximum temperature in all months and seasons under all RCP scenarios, except in all months of the Dry season which experiences a decreasing trend.

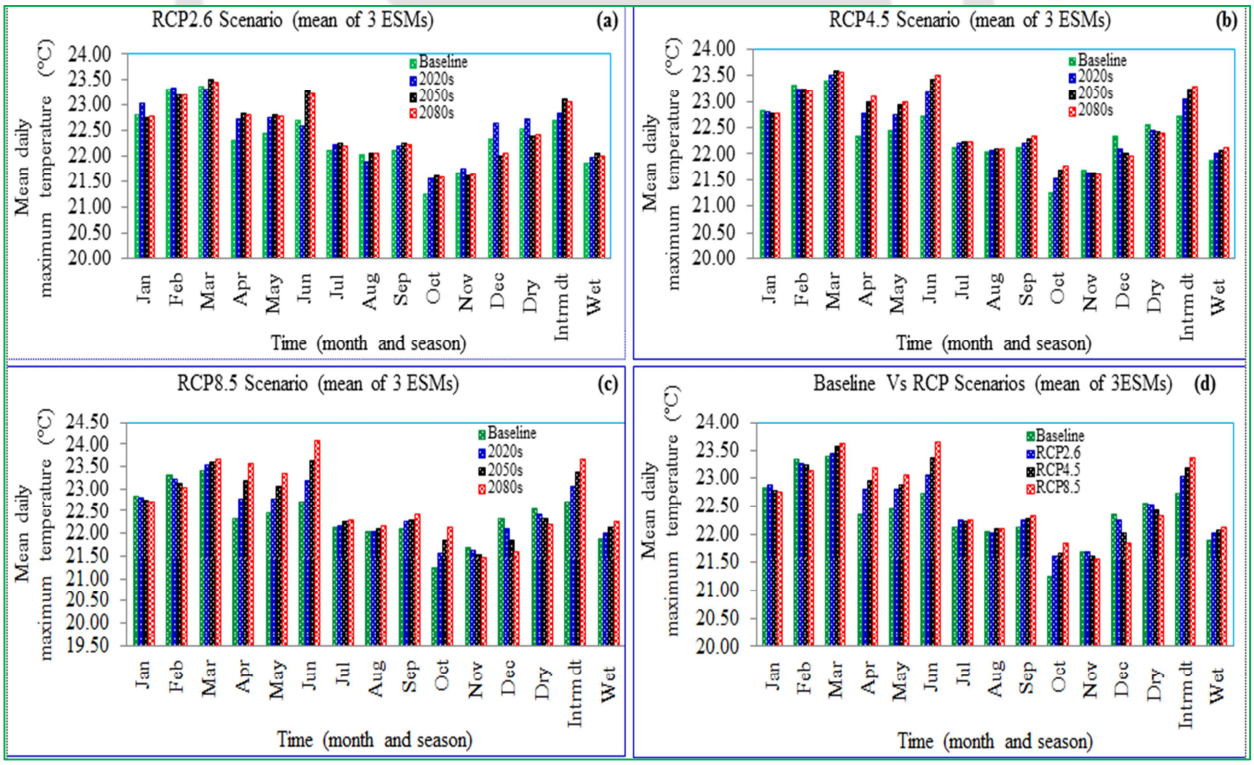

Figure 3.6a (top left): Maximum temperature (monthly and seasonal mean daily) during baseline (1981-2005) simulation and three future time slice under RCP2.6 scenario for twelve averaged spatial stations, b (top right): same as fig 3.6a but under RCP4.5, c (bottom left): same as fig 3.6a but under RCP8.5, d (bottom right): same as fig 3.6a but without time slice under RCP2.6, RCP4.5 and RCP8.5 scenarios.

B. Mean Annual, Seasonal, and Monthly Minimum Temperature Scenarios

Like maximum temperature, the mean annual minimum temperature also increases (Fig. 3.7) in all the nine ESM-RCP scenarios in the 2020s 2050s and 2080s relative to the baseline. GFDL-ESM2M (G2M), projects the highest mean annual value for minimum temperature and increased by 0.42, 0.75 and 1.14°C (G2M-RCP8.5), 0.39, 0.58 and 0.67°C (G2M-RCP4.5) and 0.38, 0.52 and 0.49°C (G2M-RCP2.6) in the 2020s, 2050s and 2080s time slices respectively; GFDL-ESM2G (G2G), projects the lowest increases in the value of this parameter by 0.26, 0.55 and 0.94°C (G2G-RCP8.5), 0.23, 0.38 and 0.47°C (G2G-RCP4.5) and 0.22, 0.32 and 0.29°C (G2G-RCP2.6) in the 2020s, 2050s and 2080s time slices respectively and CanESM2 (C2), projects an intermediate (median) increase in mean annual minimum temperature by 0.34, 0.65 and 1.04°C (C2-RCP8.5), 0.31, 0.48 and 0.57°C (C2-RCP4.5) and 0.30, 0.42 and 0.39°C (C2-RCP2.6) in the 2020s, 2050s and 2080s time slices respectively (Fig. 3.7).

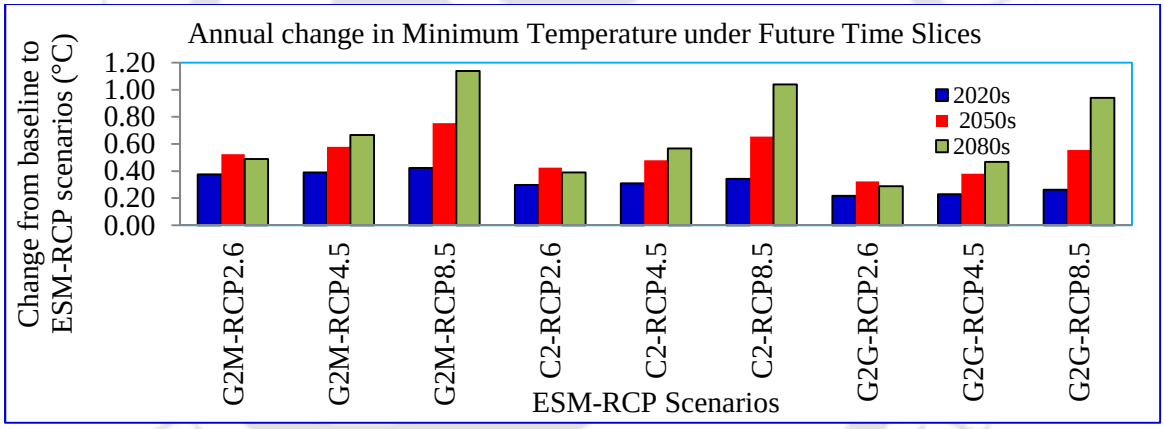

Figure 3.7 Absolute changes from baseline simulation of annual minimum temperature in all the ESM-RCP scenarios in the 2020s, 2050s and 2080s time slices

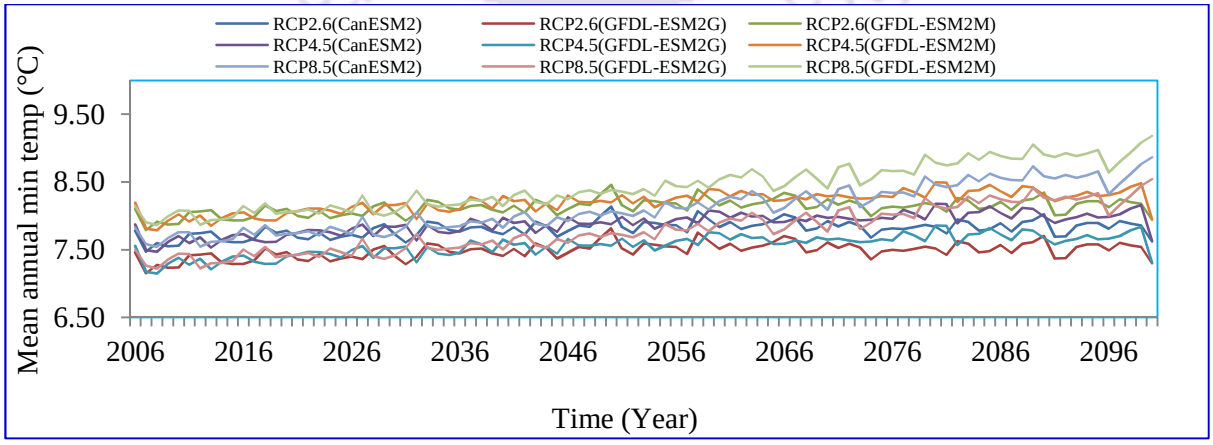

Figure 3.8 Future trend of mean annual minimum temperature (°C) in all the ESM-RCP scenarios

Variability of minimum temperature is more than the maximum temperature. Like maximum temperature, the variability of minimum temperature is also higher for all ESMs of RCP8.5 than RCP4.5 and RCP2.6 and the future trend for RCP8.5 and RCP4.5 scenarios have been indicated a significantly (at 5% significant level) increasing trend of average annual minimum temperature until the end of the century (Fig. 3.8 and Table 3.10). Increasing trend but not significant (at 5% significant level) was observed for all ESMs of RCP2.6 scenario. Comparatively, RCP8.5 prevail higher change in minimum temperature trend at the end of the century than the RCP4.5 and the RCP2.6.

As shown in Fig.3.9a-c, the projected (mean of 3 ESMs) seasonal minimum temperature shows an increasing trend in all the seasons (Dry, Intermediate, and Wet) in all the three future time slices for all the RCPs scenarios. The absolute change in mean seasonal minimum temperature from the base period for the three scenarios in three future time slice has presented in Table 3.8.

Table 3.8 Absolute changes in mean seasonal minimum temperature (°C) at different time slices from the base period

Scenario	Seasons in the 2020s			Seasons in the 2050s			Seasons in the 2050s		
	Dry	Intermediate	Wet	Dry	Interm.	Wet	Dry	Interm.	Wet
RCP2.6 (mean of 3 ESMs)	+0.307	+0.371	+0.213	+0.431	+0.544	+0.303	+0.418	+0.467	+0.283
RCP4.5 (mean of 3 ESMs)	+0.299	+0.390	+0.240	+0.488	+0.598	0.354	+0.567	+0.702	+0.431
RCP8.5 (mean of 3 ESMs)	+0.366	+0.425	+0.238	+0.682	+0.809	+0.473	+1.090	+1.332	+0.702

The projected (mean of 3 ESMs) monthly minimum temperature has a larger magnitude of increment on the month of Oct 2080s which was 2.13, 1.24 and +0.95°C for the RCP8.5, RCP4.5, and RCP2.6 scenarios respectively at the end of the century. On the other hand, the larger decrement on Feb 2080s 0.51, 0.48 and 0.36°C ensured for the RCP8.5, RCP4.5, and RCP2.6 scenarios respectively at the end of the century Fig.3.9c, b and a. The absolute change from the base period in mean minimum temperature was observed to be significant due to there were a substantial increase and decrease of minimum temperature on different months. For instance, in the months of Feb, Sep, and Dec, the decrement of the minimum temperature was observed and an increment on the rest of the months has observed. In both extreme conditions (rise or decline) the change in minimum temperature was higher in the 2080s.

Commonly, the change in average monthly minimum temperature might range between -0.30°C on Feb and +0.87°C on Oct for the coming 2020s; -0.41°C on Feb and +1.38°C on Oct for 2050s and -0.51°C on Feb and +2.13°C on Oct for 2080s for the RCP8.5 scenario. For RCP4.5 scenario, varies between -0.32°C on Feb and +0.69°C Oct for the coming 2020s; -0.42°C on Feb and +1.12°C on Oct for 2050s and -0.48°C on Feb and +1.24°C on Oct for 2080s. For the RCP2.6 scenario, ranges become -0.30°C on Feb and +0.74°C on Oct for the 2020s; -0.31°C on Feb and +0.94°C on Oct for 2050s and -0.36°C on Feb and +0.95°C on Oct for 2080s. However, there has shown an increasing trend of minimum temperature in all months and seasons under all RCP scenarios (Fig 3.9d).

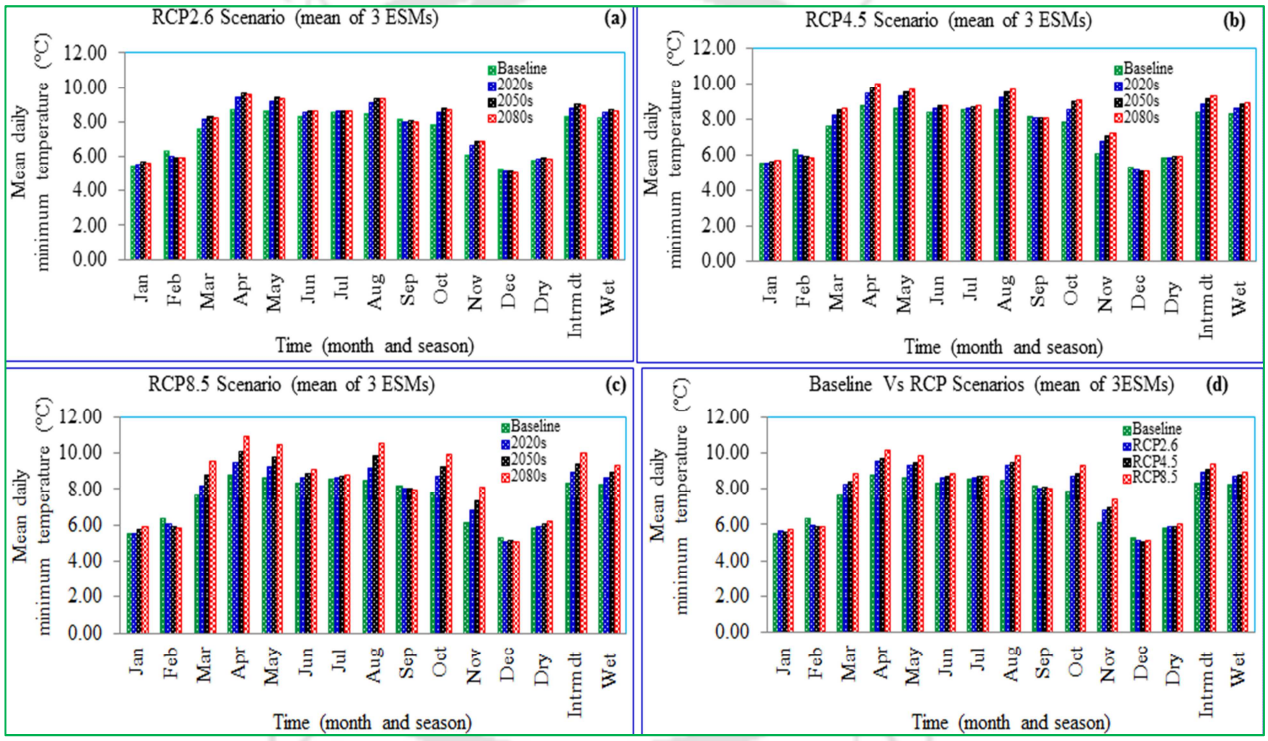

Figure 3.9a (top left): Minimum temperature (monthly and seasonal mean daily) during baseline (1981-2005) simulation and three future time slice under RCP2.6 scenario for twelve averaged spatial stations, b (top right): same as fig 3.9a but under RCP4.5, c (bottom left): same as fig 3.9a but under RCP8.5, d (bottom right): same as fig 3.9a but without time slice under RCP2.6, RCP4.5 and RCP8.5 scenarios

Mean annual future temperature projection observed to increase (Alexandrov and Genev 2003; Boko et al. 2008; Dinar 2006; Loukas et al. 2015; IPCC 2013; Kruger and Shongwe 2004; New et al. 2006; Unganai 1996) in Africa and in the globe. The future mean annual temperature projection in Ethiopia also witnessed to increase (e.g. Shawul et al., 2016; Legesse et al., 2013; ENMA, 2007). Boko et al. (2008) found that the temperature projection in the upcoming period will be in the range 2-4°C in Africa and Dinar (2006) obtained that

the temperature increase by the range of 2.2-4.1°C for most of Africa. The results of average temperature for this study come to an agreement, with the slight variation of RCP8.5 scenario, with the study reported (IPCC, 2013b) with increment of global average surface temperature by the end of the 21st century to be in the ranges 2.6-4.8°C (RCP8.5), 1.1-2.6°C (RCP4.5) and 0.3-1.7°C (RCP2.6). The average annual temperature in Ethiopia found to be in the ranges 0.9-1.1, 1.7-2.1 and 2.7-3.4°C by 2030, 2050 and 2080 time slices respectively (ENMA, 2007). The projected mean annual maximum and minimum temperature shows rising trend in Southeastern part of Ethiopia (Shawul et al., 2016). The average annual temperature of this study come to an agreement with all the literature given above regarding direction (pattern), but slight variation regarding magnitude (amount). This slight variation of mean annual temperature increment might arise due to types of GCM/ESM and emission scenarios used, a method of downscaling, and spatial variation of temperature.

C. Mean Annual, Seasonal and Monthly Precipitation Scenarios

Like maximum and minimum temperature, the average annual precipitation also increases (Fig. 3.10) in all the nine ESM-RCP scenarios in the 2020s 2050s and 2080s relative to the baseline. GFDL-ESM2M (G2M), projects the highest mean annual value for precipitation and increased by 19.70, 24.14 and 33.69% (G2M-RCP8.5), 14.54, 19.36 and 21.94% (G2M-RCP4.5) and 13.68, 17.93 and 16.34% (G2M-RCP2.6) in the 2020s, 2050s and 2080s time slices respectively; GFDL-ESM2G (G2G), projects the lowest increases in the value of this parameter by 12.70, 17.14 and 26.69% (G2G-RCP8.5), 7.54, 12.36 and 14.94% (G2G-RCP4.5) and 6.68, 10.93 and 9.34% (G2G-RCP2.6) in the 2020s, 2050s and 2080s time slices respectively and CanESM2 (C2), projects an intermediate (median) increase in mean annual precipitation by 14.70, 19.14 and 28.69% (C2-RCP8.5),9.54, 14.36 and 16.94% (C2-RCP4.5) and 8.68, 12.93 and 11.34% (C2-RCP2.6) in the 2020s, 2050s and 2080s time slices respectively (Fig. 3.10).

Like maximum and minimum temperature, the variability of precipitation is also higher for all ESMs of RCP8.5 than RCP4.5 and RCP2.6 and the future trend for RCP8.5 and RCP4.5 scenarios have been indicated a significantly (at 5% significant level) increasing trend of mean annual precipitation until the end of the century (Fig. 3.11 and Table 3.10). Increasing trend but not significant (at 5% significant level) was observed for all ESMs of RCP2.6 scenario. Comparatively, RCP8.5 prevail higher change in precipitation trend at the end of the century than the RCP4.5 and the RCP2.6.

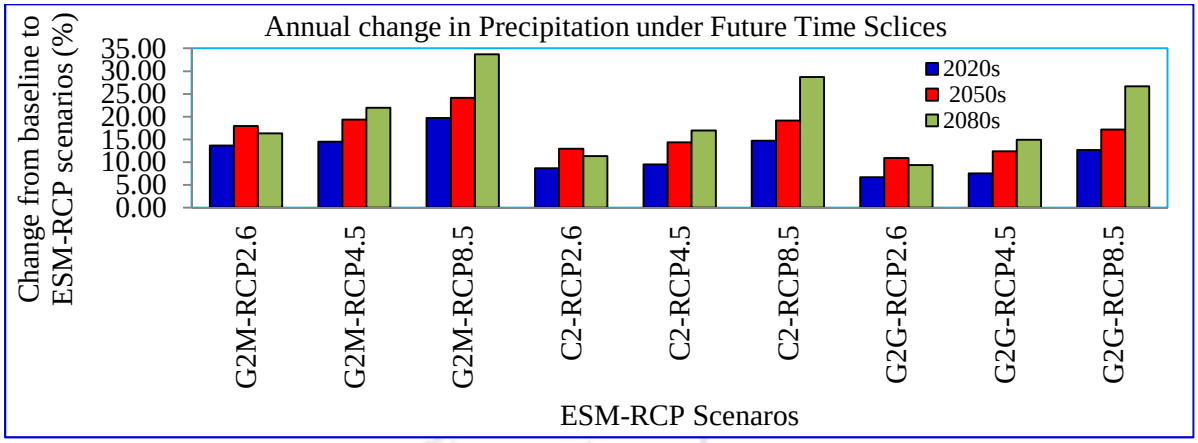

Figure 3.10 Percentage change from baseline simulation of annual precipitation in all the ESM-RCP scenarios in the 2020s, 2050s and 2080s time slices

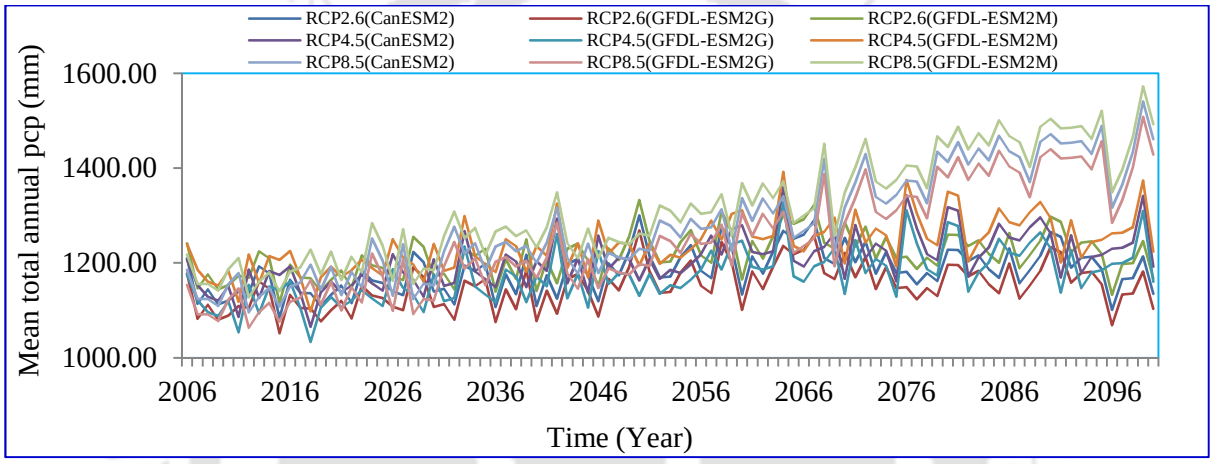

Figure 3.11 Future trend of mean annual total precipitation (mm) in all the ESM-RCP scenarios

As described in the IPCC Assessment Report (McCarthy et al., 2001), the projected future changes in mean seasonal rainfall in Africa are less well defined. The diversity of African climates, high rainfall variability, and a very sparse observational network make the predictions of future climate change difficult at the local scales. The seasonal (mean of 3 ESMs) rainfall scenarios have indicated that an increase of rainfall in all the seasons (Dry, Intermediate, and Wet) for the RCP2.6, RCP4.5, and RCP8.5 scenarios except for an intermediate season of the 2020s (a decreasing trend) for RCP2.6 and RCP4.5 scenarios (Fig.3.12a-c). The percentage changes of precipitation from the base period for the three scenarios in future time slice for each season have presented in Table 3.9.

Table 3.9 Percentage change in mean seasonal precipitation at different time slices from the base period

Scenario	Seasons in the 2020s			Seasons in the 2050s			Seasons in the 2050s		
	Dry	Intermediate	Wet	Dry	Interm.	Wet	Dry	Interm.	Wet
RCP2.6 (mean of 3 ESMs)	+15.19	-1.35	+8.83	+24.11	+2.57	+11.44	+21.14	+1.02	+9.81
RCP4.5 (mean of 3 ESMs)	+18.20	-0.32	+9.16	+26.63	+1.96	+13.50	+30.71	+4.55	+15.65
RCP8.5 (mean of 3 ESMs)	+20.68	+1.37	+9.10	+33.65	+6.23	+18.85	+53.74	+18.90	+27.06

The projected (mean of 3ESMs) monthly precipitation has a larger magnitude of increment on the month of Oct 2080s 81.02, 54.66 and 42.77% for RCP8.5, RCP4.5 & RCP2.6 scenarios respectively at the end of the century. On the other hand, the larger decrement on Feb 2020s 8.20, 10.35 and 10.80% occurred for RCP8.5, RCP4.5 & RCP2.6 scenarios respectively Fig.3.12c, b and a. The percentage change from the base period in mean monthly precipitation was observed to be significant due to there were a substantial rise and decline of precipitation on different months. For instance, in the months of Feb, Sep, and Dec, the decrement of precipitation was observed and an increment in the rest of the months has shown.

Characteristically, the percentage change in average monthly precipitation might range between -8.20% on Feb and +42.59% on Oct for the coming 2020s; -6.50% on Feb and +55.61% on Oct for 2050s and +1.58% on Aug and +81.02% on Oct for 2080s for the RCP8.5 scenario. For RCP4.5 scenario, the range tends to be between -10.35% on Feb and +34.53% Oct for the coming 2020s; -9.36% on Feb and +49.90 on Oct for 2050s and -7.42% on Feb and +54.66% on Oct for 2080s. For RCP2.6 scenario, percentage change in average monthly precipitation ranges between -10.80% on Feb and +35.41% on Oct for 2020s; -8.59% on Feb and +42.55% on Oct for 2050s and -9.37% on Feb and +42.77% on Oct for 2080s. But, there has been shown an increasing trend of precipitation in all months of dry, intermediate and wet seasons under all RCP scenarios, except in the month of Dec (under RCP2.6) and Feb of dry season which experiences a decreasing trend (Fig 3.12d).

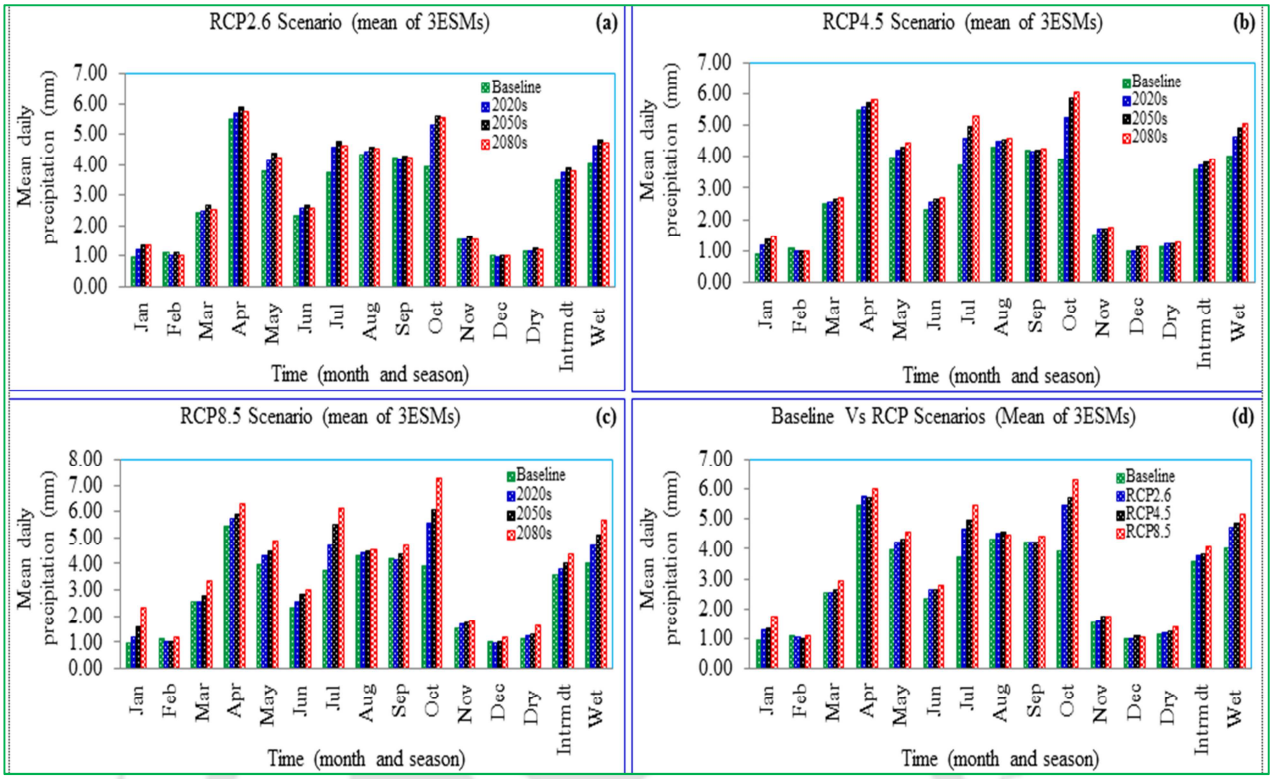

Figure 3.12a (top left): Precipitation (monthly and seasonal mean daily) during baseline period (1981-2005) simulation and three future time slice under RCP2.6 scenario for twelve averaged spatial stations, b (top right): same as fig 3.12a but under RCP4.5, c (bottom left): same as fig 3.12a but under RCP8.5, d (bottom right): same as fig 3.12a but without time slice under RCP2.6, RCP4.5 and RCP8.5 scenarios

Figure 3.11 indicated that the pattern of future (mean of 3ESMs) annual total precipitation with a range of 1124.00 to 1540.16 mm on the year 2028 and 2099 respectively for RCP8.5 scenario, 1065.43 to 1359.59 mm on the year 2018 and 2064 respectively for RCP4.5 scenario and 1100.74 to 1300.24 mm on the year 2096 and 2050 respectively for RCP2.6 scenario. It is observed that there is a substantial variability of mean annual total precipitation from year to year throughout the study area of Weyib River basin.

It is observed that there is a significant spatiotemporal variation in amount and distribution of precipitation (Faramarzi et al., 2013; Vinnarasir and Sarma, 2011; Wang et al., 2011; Shongwe et al., 2009; Bates et al., 2008; Mpelasoka and Chiew, 2008; Chiew, 2006), which is also the case in this study. Mean annual precipitation of this study come to an agreement with almost all literatures given above regarding direction (pattern), but slight variation interms of magnitude (amount).This slight variation might arise due to types of ESMs, RCPs and method of downscaling used. Mean of 3 ESMs of annual precipitation, in this study, substantially increased in the ranges 14.70-28.69% (RCP8.5), 9.54-16.94% (RCP4.5) and 8.68-13.00% (RCP2.6). The increase in annual total precipitation of the present study,

especially in the 2080s of RCP8.5 scenario, also comes to an agreement with various literatures regarding direction. Generally, the increment of rainfall comparatively higher in the dry season 20.68% in the 2020s, 33.65% in 2050s, and 53.74% in 2080s for the RCP8.5 scenario which might have positive impact on lowland region of the study area and it might affect the highland areas negatively since this season is specifically main crop harvesting period.

3.3.4. Mann-Kendall trend test of future temperatures and precipitation (2006-2100)

Based on the standardized test statistic, it is possible to conclude that Mann-Kendall test has revealed a statistically significant trend in the study area for both future precipitation and temperatures at the 5% significant level. The maximum and minimum temperature and precipitation for all the 3ESMs under RCP8.5 and 4.5 scenarios have revealed a significantly (at 5% significant level) increasing trend for future until the year 2100. Increasing but not significant has observed for all ESMs under the RCP2.6 scenario. For brevity reason, only mean of 3ESMs are given in Table 3.10.

Table 3.10 Mann-Kendall trend test for future average annual both temperatures and precipitation under three RCP scenarios for mean of 3 ESMs

scenarios	Kendall's tau	p-value	Alpha	Sen's slope	Trend
Tmax for rcp2.6	0.492	0.214	0.05	0.117	Increasing, but not significant
Tmax for rcp4.5	0.521	< 0.0001	0.05	0.117	Significantly increasing
Tmax for rcp8.5	0.634	< 0.0001	0.05	0.211	Significantly increasing
Tmin for rcp2.6	0.196	0.211	0.05	0.106	Increasing, but not significant
Tmin for rcp4.5	0.256	< 0.0001	0.05	0.109	Significantly increasing
Tmin for rcp8.5	0.435	< 0.0001	0.05	0.118	Significantly increasing
pcp for rcp2.6	0.186	0.572	0.05	0.378	Increasing, but not significant
pcp for rcp4.5	0.193	0.0005	0.05	0.546	Significantly increasing
pcp for rcp8.5	0.201	0.0009	0.05	0.607	Significantly increasing

3.3.5. Scenarios developed for future temperatures and precipitation (2006-2100) for six averaged arbitrary spatial weather stations

A. Mean Annual and Monthly Maximum Temperature Scenarios

The predicted absolute change in monthly mean daily maximum temperature has larger extent of increase for the month of Oct 2080s 2.10°C (RCP8.5) and 1.18°C (RCP4.5) at the end of the century but for the month of Oct in 2050s time slice by 0.85°C in case of RCP2.6 scenario then decline at the end of the century in all month and time slice because of history line of RCP2.6. Contrary, the larger decrease in Dec 2080s 0.99°C and 0.50°C occurred for RCP8.5 and RCP4.5 at the end of the century and greater decrease on the month of Dec in 2050s time slice by 0.37°C in case of RCP2.6 scenario (Fig 3.13a, b, and c).

Mostly, the absolute change in monthly mean daily maximum temperature for RCP8.5 scenario ranges -0.33 to +0.74°C in the 2020s, -0.68 to +1.35°C in 2050s and -0.99 to +2.10°C in 2080s. In case of RCP4.5 scenario, ranges-0.33 to +0.66°C in 2020s, -0.46 to +1.03°C in 2050s and -0.50 to +1.18°C in 2080s. The absolute change in monthly mean daily maximum temperature under RCP2.6 scenario ranges -0.26 to +0.68°C in the 2020s, -0.42 to +0.87°C in 2050s and -0.37 to +0.85°C in 2080s. An increase of mean annual maximum temperature was in the ranges 0.29-0.84°C (RCP8.5), 0.28-0.49°C (RCP4.5) and 0.29-0.36°C (RCP2.6) (Table 3.11). The deviation of maximum temperature is larger under RCP8.5 scenario than RCP4.5 and RCP2.6 scenarios as shown by the future trend in Fig 3.13d. Relatively, RCP8.5 revealed a higher change in maximum temperature trend at the end of the century than RCP4.5 and RCP2.6 scenario.

B. Mean Annual and Monthly Minimum Temperature Scenarios

The future predicted absolute change in monthly mean daily minimum temperature has larger extent of increase for the month of Nov 2080s 3.98°C (RCP8.5) and 2.21°C (RCP4.5) at the end of the century but for the month of Nov in 2050s time slice 1.54°C in case of RCP2.6 scenario then decline at the end of the century in all month and time slice. On the other hand, the larger decrease in Sep 2080s 1.61°C and 0.87°C ensued for RCP8.5 and RCP4.5 at the end of the century and larger decrease on the month of Sep in 2050s time slice by 0.74°C in case of RCP2.6 scenario (Fig 3.14a, b, and c).

Often time, the absolute change in monthly mean daily minimum temperature for RCP8.5 scenario ranges -0.61 to +1.39°C in the 2020s, -1.05 to +2.53°C in 2050s and -1.61 to +3.98°C in 2080s. In case of RCP4.5 scenario, ranges -0.51 to +1.26°C in 2020s, -0.83 to +1.87°C in 2050s and -0.87 to +2.21°C in 2080s. The absolute change in monthly mean daily minimum temperature under RCP2.6 scenario ranges -0.61 to +1.17°C in the 2020s, -0.72 to +1.62°C in 2050s and -0.74 to +1.54°C in 2080s. An increase of mean annual minimum temperature (Table 3.12) might vary 0.24-0.80°C (RCP8.5), 0.21-0.40°C (RCP4.5) and 0.19-0.31°C (RCP2.6). Like in maximum temperature scenario, the deviation of minimum temperature is greater under RCP8.5 scenario than RCP4.5 and RCP2.6 scenarios (Fig 3.14d).

C. Mean Annual and Monthly Precipitation Scenarios

The predicted percentage change in monthly mean daily precipitation has larger extent of increase on the month of Jan 2080s 100.00% (RCP8.5) and 99.53% (RCP4.5) at the end of the century but in the month of Jan in 2050s time slice 69.18% in case of RCP2.6 scenario then decline at the end of the century in all month and time slice. Conversely, the larger decrease on Sep 2080s 44.15% and 38.57% ensued for RCP8.5 and RCP4.5 at the end of the century and larger decrease on the month of Sep in 2050s time slice by 30.74% in case of RCP2.6 scenario (Fig 3.15a, b, and c).

Every so often, the percentage change in monthly mean daily precipitation for RCP8.5 scenario ranges -29.36 to +53.57% in 2020s, -39.36 to +97.81% in 2050s and -44.15 to +100.00% in 2080s. In case of an intermediate emission scenario (RCP4.5), varies -26.47 to +47.02% in 2020s, -35.91 to +77.48% in 2050s and -38.57 to +99.53% in 2080s. The percentage change in monthly mean daily precipitation under RCP2.6 scenario ranges -30.50 to +48.49% in 2020s, -32.75 to +69.18% in 2050s and -30.74 +64.75% in 2080s. A considerable increase of mean annual precipitation (Table 3.13) was found to be in the ranges 8.37-25.05% (RCP8.5), 5.95-14.00% (RCP4.5) and 4.91-8.12% (RCP2.6). As we can see from Fig 3.15d, the variability of precipitation is greater under RCP8.5 scenario than RCP4.5 and RCP2.6 scenarios. Fairly, RCP8.5 shows a higher change in precipitation trend at the end of the century than the RCP4.5 and RCP2.6 scenarios.

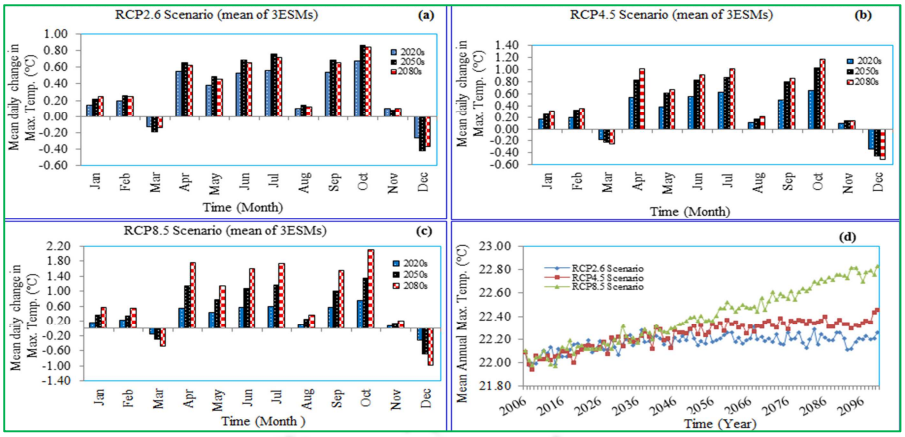

Figure 3.13a (top left): Monthly mean daily absolute change in maximum temperature from base period in three future time slice under RCP2.6 scenario for six averaged spatial stations, b (top right): same as fig 3.13a but for RCP4.5, c (bottom left): same as fig 3.13a but for RCP8.5, d (bottom right): future trend of mean annual maximum temperature for six averaged spatial stations

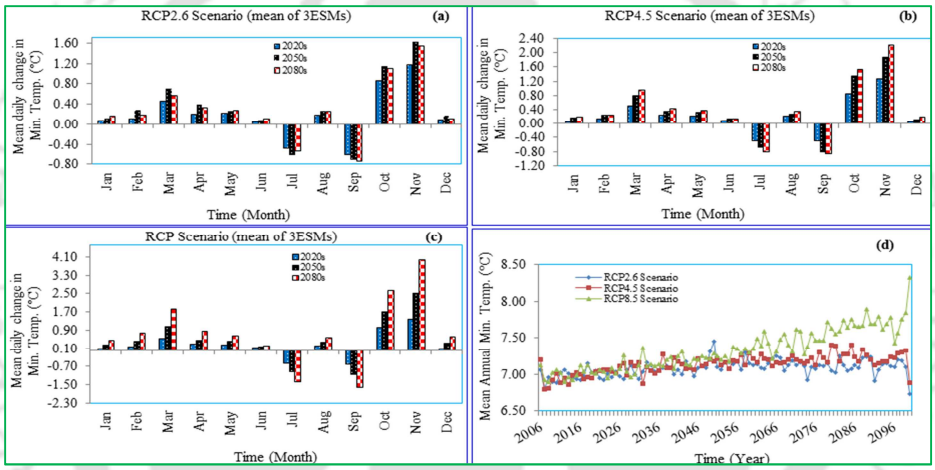

Figure 3.14a (top left): Monthly mean daily absolute change in minimum temperature from base period in three future time slice under RCP2.6 scenario for six averaged spatial stations, b (top right): same as fig 3.14a but for RCP4.5, c (bottom left): same as fig 3.14a but for RCP8.5, d (bottom right): future trend of mean annual minimum temperature for six averaged spatial stations

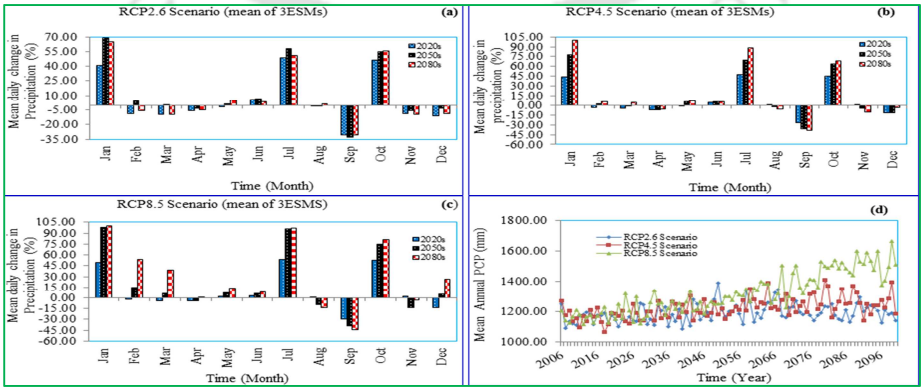

Figure 3.15a (top left): Monthly mean daily percentage change in precipitation from base period in three future time slice under RCP2.6 scenario for six averaged spatial stations, b (top right): same as fig 3.15a but for RCP4.5, c (bottom left): same as fig 3.15a but for RCP8.5, d (bottom right): future trend of mean annual precipitation for six averaged spatial stations

3.3.6. Scenarios developed for future temperatures and precipitation (2006-2100) for three averaged arbitrary spatial weather stations

A. Mean Annual and Monthly Maximum Temperature Scenarios

The predicted absolute change in monthly mean daily maximum temperature has larger extent of increase for the month of Apr 2080s 2.07°C (RCP8.5) and 1.29°C (RCP4.5) at the end of the century but for the month of Apr in 2050s time slice by 0.91°C in case of RCP2.6 scenario then decline at the end of the century in all month and time slice because of history line of RCP2.6. Opposing, the larger decrease in Sep 2080s 1.16°C and 0.67°C occurred for RCP8.5 and RCP4.5 at the end of the century and greater decrease on the month of Sep in 2050s time slice by 0.46°C in case of RCP2.6 scenario (Fig 3.16a, b, and c).

Characteristically, the absolute change in monthly mean daily maximum temperature for RCP8.5 scenario ranges -0.41 to +0.76°C in the 2020s, -0.79 to +1.41°C in 2050s and -1.16 to +2.07°C in 2080s. In case of RCP4.5 scenario, ranges -0.38 to +0.72°C in 2020s, -0.57 to +1.12°C in 2050s and -0.67 to +1.29°C in 2080s. The absolute change in monthly mean daily maximum temperature under RCP2.6 scenario ranges -0.40 to +0.70°C in the 2020s, -0.50 to +0.92°C in 2050s and -0.46 to +0.91°C in 2080s. A very slight increase of mean annual maximum temperature was in the ranges 0.03-0.06°C (RCP8.5), 0.04-0.07°C (RCP4.5) and 0.02-0.05°C (RCP2.6) (Table 3.11). The inconsistency of maximum temperature is almost same for RCP8.5 and RCP4.5 scenarios but a slight variation on the RCP2.6 scenario (Fig 3.16d).

B. Mean Annual and Monthly Minimum Temperature Scenarios

The future predicted absolute change in monthly mean daily minimum temperature has larger extent of increase on May 2080s 5.50°C (RCP8.5) and 3.24°C (RCP4.5) at the end of the century but on May in 2050s time slice 2.26°C in case of RCP2.6 scenario then decline at the end of the century in all month and time slice. Contrariwise, the larger decrease in Feb 2080s 1.77°C and 1.05°C ensued for RCP8.5 and RCP4.5 at the end of the century and larger decrease on the month of Feb in 2050s time slice by 0.79°C in case of RCP2.6 scenario (Fig 3.17a, b, and c).

Commonly, the absolute change in monthly mean daily minimum temperature for RCP8.5 scenario ranges -0.69 to +2.01°C in the 2020s, -1.17 to +3.62°C in 2050s and -1.77 to +5.50°C in 2080s. In case of an intermediate emission scenario, ranges -0.65 to +1.89°C in

2020s, -0.94 to +2.81°C in 2050s and -1.05 to +3.24°C in 2080s. The absolute change in monthly mean daily minimum temperature under RCP2.6 scenario ranges -0.60 to +1.79°C in the 2020s, -0.82 to +2.43°C in 2050s and -0.79 to +2.26°C in 2080s. An increase of mean annual minimum temperature (Table 3.12) might vary 0.78-2.15°C (RCP8.5), 0.74-1.28°C (RCP4.5) and 0.71-0.88°C (RCP2.6). Like in maximum temperature scenario, the deviation of minimum temperature is greater under RCP8.5 scenario than RCP4.5 and RCP2.6 scenarios (Fig 3.17d). Reasonably, RCP8.5 depicted the higher change in minimum temperature trend at the end of the century than the RCP4.5 and RCP2.6 scenarios.

C. Mean Annual and Monthly Precipitation Scenarios

The predicted percentage change in monthly mean daily precipitation has larger extent of increase on Sep 2080s 88.26% (RCP8.5) and 52.14% (RCP4.5) at the end of the century, but on Sep in 2050s time slice 45.26% in case of RCP2.6 scenario then decline at the end of the century in all month and time slice. In opposition, the larger decrease on Dec 2080s 36.22% and 13.47% resulted for RCP8.5 and RCP4.5 at the end of the century and larger decrease on Feb in 2050s time slice by 12.82% in case of RCP2.6 scenario (Fig 3.18a, b, and c).

Mostly, the percentage change in monthly mean daily precipitation for RCP8.5 scenario ranges -10.77 to +36.02% in 2020s, -29.31 to +62.46% in 2050s and -36.22 to +88.26% in 2080s. In case of RCP4.5 scenario, Varies -11.43 to +32.66% in 2020s, -12.82 to +50.68% in 2050s and -10.28 to +52.14% in 2080s. The percentage change in monthly mean daily precipitation under RCP2.6 scenario ranges -7.85 to +39.96% in 2020s, -13.47 to +45.26% in 2050s and -7.74 to +40.70% in 2080s. A sizeable increase of mean annual precipitation (Table 3.13) was found to be in the ranges 15.59-24.00% (RCP8.5), 11.04-15.16% (RCP4.5) and 9.84-13.32% (RCP2.6). As shown in Fig 3.18d the unevenness of precipitation is greater under RCP8.5 scenario than RCP4.5 and RCP2.6 scenarios. An interesting point here is that the variation of precipitation under RCP2.6 is higher than that of RCP4.5 at the end of the century. Accordingly, RCP8.5 shows a higher change in precipitation trend at the end of the century than the RCP4.5 and RCP2.6 scenarios.

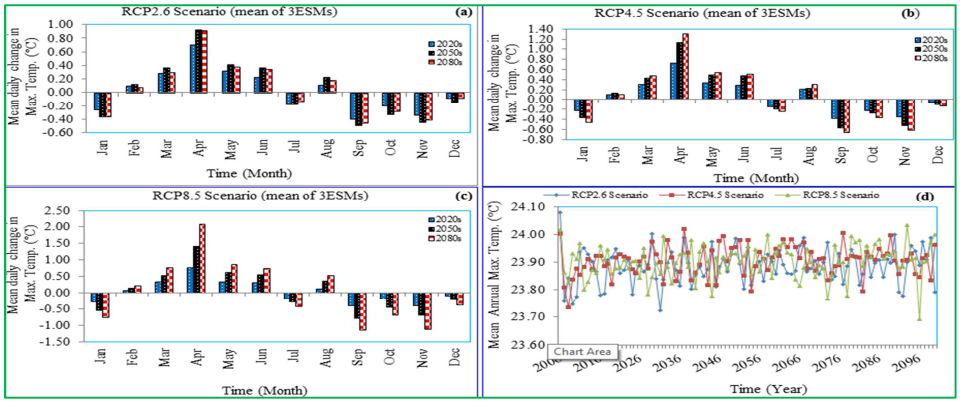

Figure 3.16a (top left): Monthly mean daily absolute change in maximum temperature from base period in three future time slice under RCP2.6 scenario for three averaged spatial stations, b (top right): same as fig 3.16a but for RCP4.5, c (bottom left): same as fig 3.16a but for RCP8.5, d (bottom right): future trend of mean annual maximum temperature for three averaged spatial stations

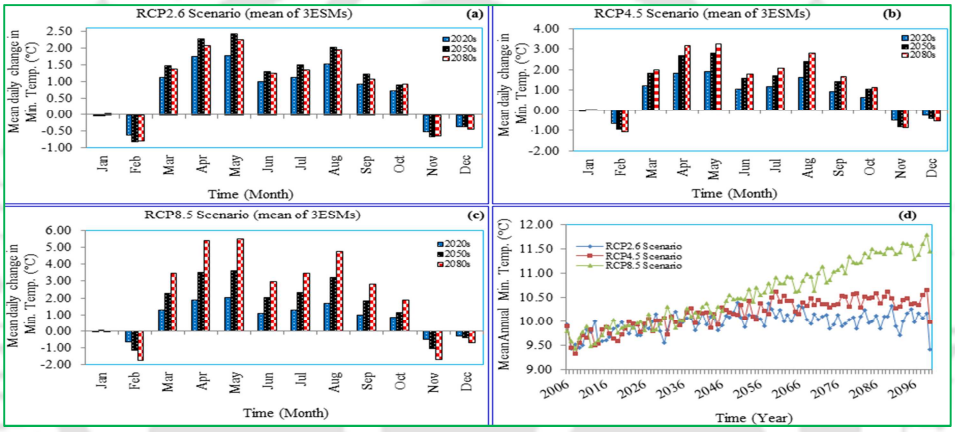

Figure 3.17a (top left): Monthly mean daily absolute change in minimum temperature from base period in three future time slice under RCP2.6 scenario for three averaged spatial stations, b (top right): same as fig 3.17a but for RCP4.5, c (bottom left): same as fig 3.17a but for RCP8.5, d (bottom right): future trend of mean annual minimum temperature for three averaged spatial stations

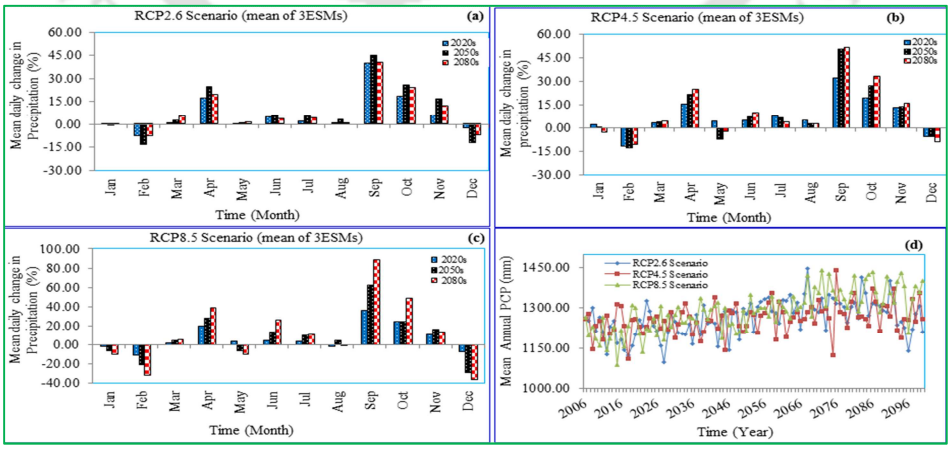

Figure 3.18a (top left): Monthly mean daily percentage change in precipitation from base period in three future time slice under RCP2.6 scenario for three averaged spatial stations, b (top right): same as fig 3.18a but for RCP4.5, c (bottom left): same as fig 3.18a but for RCP8.5, d (bottom right): future trend of mean annual precipitation for three averaged spatial stations

3.3.7. Scenarios developed for future temperatures and precipitation (2006-2100) for a single (Goba) weather station

A. Mean Annual and Monthly Maximum Temperature Scenarios

The predicted absolute change in monthly mean daily maximum temperature has a larger extent of increase on Mar 2080s 1.51°C (RCP8.5), 0.89°C (RCP4.5) and 0.70°C (RCP2.6). Contrasting, the larger decrease in Feb 2080s 5.16°C and Jul 3.11°C occurred for RCP8.5 and RCP4.5 and greater decrease on Feb in 2050s time slice by 2.40°C in case of RCP2.6 scenario (Fig 3.19a, b, and c).

Typically, the absolute change in monthly mean daily maximum temperature for RCP8.5 scenario ranges -2.03 to +0.66°C in the 2020s, -3.45 to +1.08°C in 2050s and -5.16 to +1.51°C in 2080s. In case of RCP4.5 scenario, ranges -1.88 to +0.65°C in 2020s, -2.65 to +0.85°C in 2050s and -3.11 to +0.89°C in 2080s. The absolute change in monthly mean daily maximum temperature under RCP2.6 scenario ranges -1.77 to +0.57°C in the 2020s, -2.40 to +0.69°C in 2050s and -2.21 to +0.70°C in 2080s. A sizeable decrease of mean annual maximum temperature was in the ranges 0.48-1.39°C (RCP8.5), 0.47-0.77°C (RCP4.5) and 0.44-0.60°C (RCP2.6) (Table 3.11). The changeability of maximum temperature is higher for RCP8.5 scenario than RCP4.5 and RCP2.6 scenarios and the future trend line for three scenarios has indicated a significant decrease of maximum temperature until the end of the century (Fig 3.19d).

B. Mean Annual and Monthly Minimum Temperature Scenarios

The future predicted absolute change in monthly mean daily minimum temperature has larger extent of increase on Jan 2080s 1.26°C (RCP8.5) and 0.62°C (RCP4.5) but on Jan in 2050s time slice 0.47°C in case of RCP2.6 scenario then decline at the end of the century in all month and time slice. Inversely, the larger decrease in Sep 2080s 2.27°C and 1.29°C arisen for RCP8.5 and RCP4.5 and larger decrease on the month of Sep in 2050s time slice by 1.01°C in case of RCP2.6 scenario (Fig 3.20a, b, and c).

Frequently, the absolute change in monthly mean daily minimum temperature for RCP8.5 scenario ranges -0.82 to +0.43°C in the 2020s, -1.55 to +0.69°C in 2050s and -2.27 to +1.26°C in 2080s. In case of an intermediate emission (RCP4.5) scenario, ranges -0.78 to +0.35°C in 2020s, -1.19 to +0.53°C in 2050s and -1.29 to +0.62°C in 2080s. The absolute

change in monthly mean daily minimum temperature under RCP2.6 scenario ranges -0.89 to +0.34°C in the 2020s, -1.01 to +0.47°C in 2050s and -0.93 to +0.41°C in 2080s. A slight decrease of mean annual minimum temperature (Table 3.12) might vary 0.08-0.15°C (RCP8.5), 0.10-0.14°C (RCP4.5) and 0.09-0.11°C (RCP2.6). The deviation of minimum temperature is higher for RCP8.5 scenario than RCP4.5 and RCP2.6 scenarios and the future trend line for three scenarios has indicated a slight decrease of minimum temperature until the end of the century (Fig 3.20d).

C. Mean Annual and Monthly Precipitation Scenarios

The predicted percentage change in monthly mean daily precipitation has a larger extent of increase on Oct 60.78% (RCP8.5), 38.14% (RCP4.5) and 23.73% (RCP2.6). In opposition, the larger decrease on Jan 2080s 34.54% and 29.41% resulted for RCP8.5 and RCP4.5 at the end of the century and larger decrease on Sep in 2050s time slice by 29.33% in case of RCP2.6 scenario (Fig 3.21a, b, and c).

Often time, the percentage change in monthly mean daily precipitation for RCP8.5 scenario ranges -25.86 to +35.02% in 2020s, -32.25 to +26.29% in 2050s and -34.54 to +60.78% in 2080s. In case of RCP4.5 scenario, Varies -21.81 to +19.99% in 2020s, -29.04 to +35.33% in 2050s and -29.41 to +38.14% in 2080s. The percentage change in monthly mean daily precipitation under RCP2.6 scenario ranges -26.16 to +19.23% in 2020s, -29.33 to +23.18% in 2050s and -22.68 +23.73% in 2080s. A slight increase of mean annual precipitation (Table 3.13) was found to be in the ranges 2.97-9.20% (RCP8.5), 1.48-5.41% (RCP4.5) and 0.52-3.06% (RCP2.6). As shown in Fig 3.21d the unevenness of precipitation is greater under RCP8.5 scenario than RCP4.5 and RCP2.6 scenarios. Accordingly, RCP8.5 shows a higher change in precipitation trend at the end of the century than the RCP4.5 and RCP2.6 scenarios.

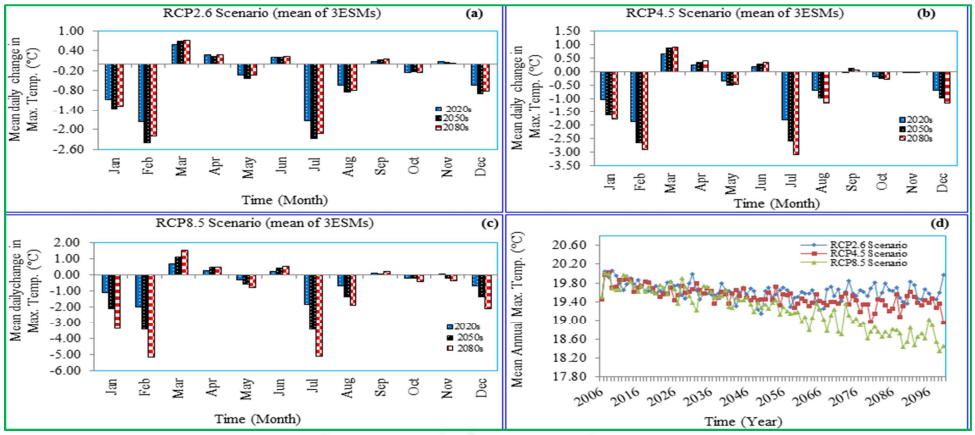

Figure 3.19a (top left): Monthly mean daily absolute change in maximum temperature from base period in three future time slice under RCP2.6 scenario for single station (Goba), b (top right): same as fig 3.19a but for RCP4.5, c (bottom left): same as fig 3.19a but for RCP8.5, d (bottom right): future trend of mean annual maximum temperature for single station (Goba)

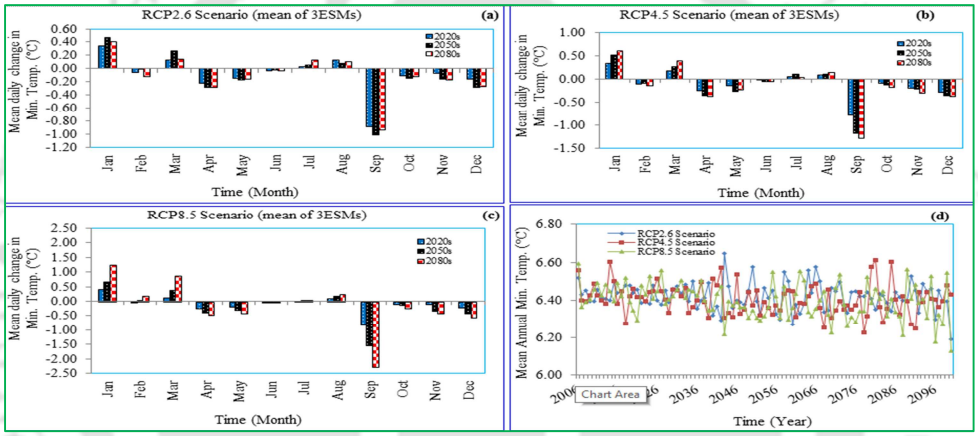

Figure 3.20a (top left): Monthly mean daily absolute change in minimum temperature from base period in three future time slice under RCP2.6 scenario for single station (Goba), b (top right): same as fig 3.20a but for RCP4.5, c (bottom left): same as fig 3.20a but for RCP8.5, d (bottom right): future trend of mean annual minimum temperature for single station (Goba)

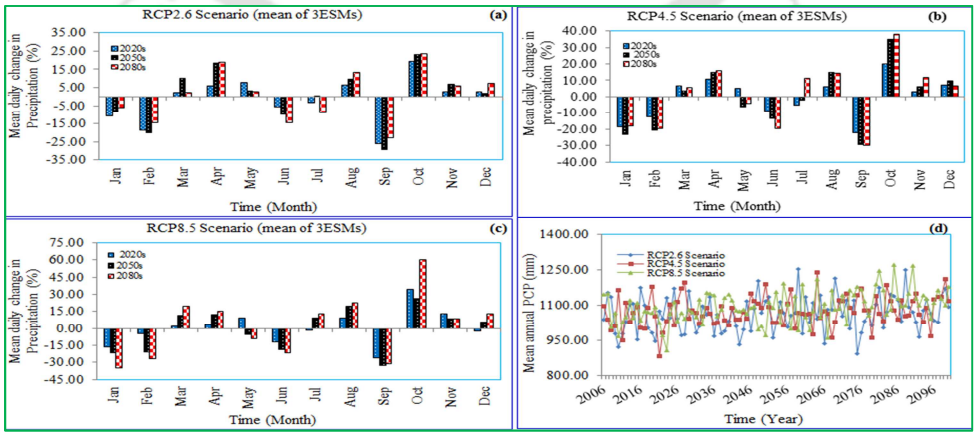

Figure 3.21a (top left): Monthly mean daily percentage change in precipitation from base period in three future time slice under RCP2.6 scenario for single station (Goba), b (top right): same as fig 3.21a but for RCP4.5, c (bottom left): same as fig 3.21a but for RCP8.5, d (bottom right): future trend of mean annual precipitation single station (Goba)

Mean of 3 ESMs of annual rainfall, in this study, substantially increased in the ranges 14.70-28.69% (RCP8.5), 9.54-16.94% (RCP4.5) and 8.68-13.00% (RCP2.6) for twelve averaged spatial weather stations, 8.37-25.05% (RCP8.5), 5.95-14.00% (RCP4.5) and 4.91-8.12% (RCP2.6) for six averaged spatial weather stations, 15.59-24.00% (RCP8.5), 11.04-15.16% (RCP4.5) and 9.84-13.32% (RCP2.6) for three averaged spatial weather stations and 2.97-9.20% (RCP8.5), 1.48-5.41% (RCP4.5) and 0.52-3.06% (RCP2.6) for a single weather station; coincide with the various literatures at the end of the century. Finally, comparison of current (i.e., base period of 1981-2005) and future projections (at 30 periods of 3 time slice) of mean of 3 ESMs (GFDL-ESM2M, CanESM2 GCM and GFDL-ESM2G) under three RCP scenarios for mean annual maximum and minimum temperature, and precipitation in case of twelve, six and three averaged spatial arbitrary weather stations, as well as future projection for a single weather station in Weyib River basin, is summarized in Table 3.11, 3.12 and 3.13.

Table 3.11 Comparison of current and future projections of mean of 3ESMs with three RCPs for annual mean daily maximum temperature (°C) at different averaged spatial observation stations in Weyib River basin

		For period (2011-2040):2020s			For period (2041-2070):2050s			For period (2071-2100):2080S		
Observation Stations	Current (°C) (1981-2005)	Rcp 2.6	Rcp4.5	Rcp8.5	Rcp 2.6	Rcp4.5	Rcp8.5	Rcp 2.6	Rcp4.5	Rcp8.5
12AS*	22.37	22.53(0.16)	22.49(0.12)	22.49(0.12)	22.52(0.14)	22.55(0.19)	22.59(0.22)	22.52(0.14)	22.58(0.21)	22.70(0.32)
6AS**	21.85	22.14(0.29)	22.13(0.28)	22.15(0.29)	22.21(0.35)	22.29(0.43)	22.40(0.55)	22.20(0.35)	22.35(0.49)	22.69(0.84)
3AS***	23.86	23.88(0.02)	23.90(0.04)	23.89(0.03)	23.89(0.04)	23.92(0.07)	23.91(0.05)	23.89(0.04)	23.91(0.06)	23.91(0.06)
1S****	20.13	19.69(-0.44)	19.66(-0.47)	19.65(-0.48)	19.53(-0.60)	19.47(-0.67)	19.22(-0.91)	19.59(-0.54)	19.36(-0.77)	18.74(-1.39)

Table 3.12 Comparison of current and future projections of mean of 3ESMs with three RCPs for annual mean daily minimum temperature (°C) at different averaged spatial observation stations in Weyib River basin

		For period (2011-2040):2020s			For period (2041-2070):2050s			For period (2071-2100):2080S		
Observation Stations	Current (°C) (1981-2005)	rcp 2.6	rcp4.5	rcp8.5	rcp 2.6	rcp4.5	rcp8.5	rcp 2.6	rcp4.5	rcp8.5
12AS*	7.44	7.74(0.30)	7.75(0.31)	7.79(0.34)	7.87(0.43)	7.92(0.48)	8.10(0.65)	7.83(0.39)	8.01(0.57)	8.48(1.04)
6AS**	6.83	7.02(0.19)	7.04(0.21)	7.07(0.24)	7.14(0.31)	7.16(0.34)	7.30(0.48)	7.11(0.28)	7.23(0.40)	7.62(0.80)
3AS***	9.15	9.86(0.71)	9.87(0.74)	9.93(0.78)	10.09(0.95)	10.25(1.11)	10.58(1.43)	10.02(0.88)	10.43(1.28)	11.30(2.15)
1S****	6.52	6.43(-0.09)	6.42(-0.10)	6.43(-0.08)	6.42(-0.10)	6.39(-0.13)	6.37(-0.15)	6.41(-0.11)	6.38(-0.14)	6.37(-0.15)

Table 3.13 Comparison of current and future projections of mean of 3ESMs with three RCPs for annual mean daily precipitation (mm) at different averaged spatial observation stations in Weyib River basin

		For period (2011-2040):2020s			For period (2041-2070):2050s			For period (2071-2100):2080S		
Observation Stations	Current (mm) (1981-2005)	rcp 2.6	rcp4.5	rcp8.5	rcp 2.6	rcp4.5	rcp8.5	rcp 2.6	rcp4.5	rcp8.5
12AS*	2.91	3.17(8.68%)	3.19(9.54%)	3.34(14.70%)	3.29(12.93%)	3.33(14.36%)	3.47(19.14%)	3.24(11.34%)	3.41(16.94%)	3.75(28.69%)
6AS**	3.04	3.19(4.91%)	3.22(5.95%)	3.29(8.37)	3.33(9.59%)	3.37(11.06%)	3.55(16.85%)	3.29(8.12%)	3.46(14.00%)	3.80(25.05%)
3AS***	3.06	3.36(9.84%)	3.39(11.04%)	3.79(24.00%)	3.46(13.32%)	3.46(13.27%)	3.53(15.59%)	3.42(11.80%)	3.52(15.16%)	3.73(22.09%)
1S****	2.85	2.86(0.52%)	2.89(1.48%)	2.93(2.97%)	2.94(3.06%)	2.94(3.21%)	2.95(3.70%)	2.93(2.93%)	3.00(5.41%)	3.11(9.20%)

Note: * represents the 12 averaged spatial arbitrary weather station, ** represents the 6 averaged spatial arbitrary weather station, *** represents the 3 averaged spatial arbitrary weather station, **** represents a single spatial weather station; number in the parentheses are the absolute change in mean annual maximum and minimum temperature and percentage change in case of precipitation for each time slice of each observation stations and each scenario; - sign in the parentheses represents the decrement of mean annual maximum and minimum temperature for each time slice and each RCP scenario

3.4. Conclusion

The mean annual maximum and minimum temperature and precipitation have shown an increasing trend in all the nine ESM-RCP scenarios in the 2020s 2050s and 2080s time slices about the baseline scenario (Fig. 3.4, 3.7 and 3.10). GFDL-ESM2M, projects the highest mean annual values for maximum and minimum temperature and precipitation increases in all the RCP (RCP8.5, 4.5 and 2.6) scenarios and in all the future time slices (in the 2020s, 2050s and 2080s); GFDL-ESM2G, projects the lowest increases in the value of this parameter and CanESM2, projects an intermediate (median) increase in all the RCP (RCP8.5, 4.5 and 2.6) scenarios and in all the future time slices (in the 2020s, 2050s, and 2080s) for twelve averaged spatial weather stations.

The variability of maximum and minimum temperature and precipitation is higher in all ESMs of RCP8.5 than RCP4.5 and RCP2.6 and the future trends for the RCP8.5 and RCP4.5 scenarios have been indicated a significantly (at 5% significant level) increasing trend of average annual maximum and minimum temperature, and precipitation until the end of the century (Fig. 3.5, 3.8 and 3.11 and Table 3.10). Increasing trend but not significant (at 5% significant level) was observed in all ESMs of RCP2.6 scenario. Comparatively, RCP8.5 scenario prevail higher change in maximum and minimum temperature and precipitation trend at the end of the century than the RCP4.5 and RCP2.6 scenarios. Seasonal and monthly variations of climate variables are more than the annual variation. The increment of rainfall comparatively higher in the dry season 20.68% in the 2020s, 33.65% in 2050s, and 53.74% in 2080s for RCP8.5 which might have a positive impact on the lowland region of the study area and it might affect the highland areas negatively since this season is specifically main crop harvesting period.

To investigate the effect of spatial data availability on climate change projection, averaging less number of stations was done by considering 6, 3 and single station. While trend was found same in 12 averaged, 6 averaged and 3 averaged stations cases, the magnitudes were observed to be different in all predicted parameters. In single station analysis the trend itself has changed from increasing trend to decreasing trend in case of maximum and minimum temperature. In case of precipitation, no visible trend has been observed in case of single station analysis.

Chapter 4: Evaluation of the ArcSWAT Model in Simulating Catchment Hydrology: in Weyib River Basin, Southeastern Ethiopia

4.1. Introduction

Climate change which is posing as a threat to water sector all over globe, including Ethiopia requires rapid assessment of available water for different sizes of catchment, so that its adverse impact on water resources can be mitigated through efficient planning, management and sustainable use. Therefore, seeking a suitable hydrological model that simulates the available water (streamflow) is also equally important and must go side by side with the assessment of available water. Hydrological models have become vital tools for understanding hydrologic processes at the catchment level. To apply model outputs confidently for various purposes ranging from regulation to research, models should be scientifically sound, robust, and reliable. Model evaluation is, therefore, beneficial in the acceptance of models to support scientific research and to guide policy, regulatory, and management decision making (Tetsoane, 2013).

The daily precipitation, minimum, and maximum temperature, solar radiation, relative humidity and wind speed are primary input climate data. Spatial ('Digital Elevation Model, Soil, and Land Use') data are pre-processed in Geographical Information Systems (GIS) and input into SWAT through the interface. The 24 years daily discharge data is used for model calibration. Sensitivity analysis and auto-calibration tools have incorporated into the SWAT model. Therefore, in this chapter, distributed ArcSWAT hydrologic model performance between observed and simulated data was evaluated using both statistical and graphical technique. Four statistical model performance evaluation criteria R^2, NSE, RMSE-observations standard deviation ratio (RSR) and Pbias have used during the calibration and validation periods. Hydrograph analysis was also made to provide a visual comparison of simulated and observed constituent data, to identify differences in timing and magnitude of peak flows, to visualize the shape of hydrograph and to identify model bias throughout model calibration and validation period.

The specific objectives of this chapter were to;

→Calibrate and validate the ArcSWAT model simulation results, and;

→Evaluate the performance of ArcSWAT model in simulating catchment hydrology in Weyib River Basin, Southeastern Ethiopia

4.2. Materials and Methods

The Weyib River originates from the northern sides of the Bale Mountains and first flows north-eastwards then flow to East and south-eastwards for the remainder of its course. Finally, it joins with Genale and Dawa Rivers near Ethiopia-Somalia border to strengthen its journey to Somali lowlands. The detail description of the study area has given in Chapter 3.

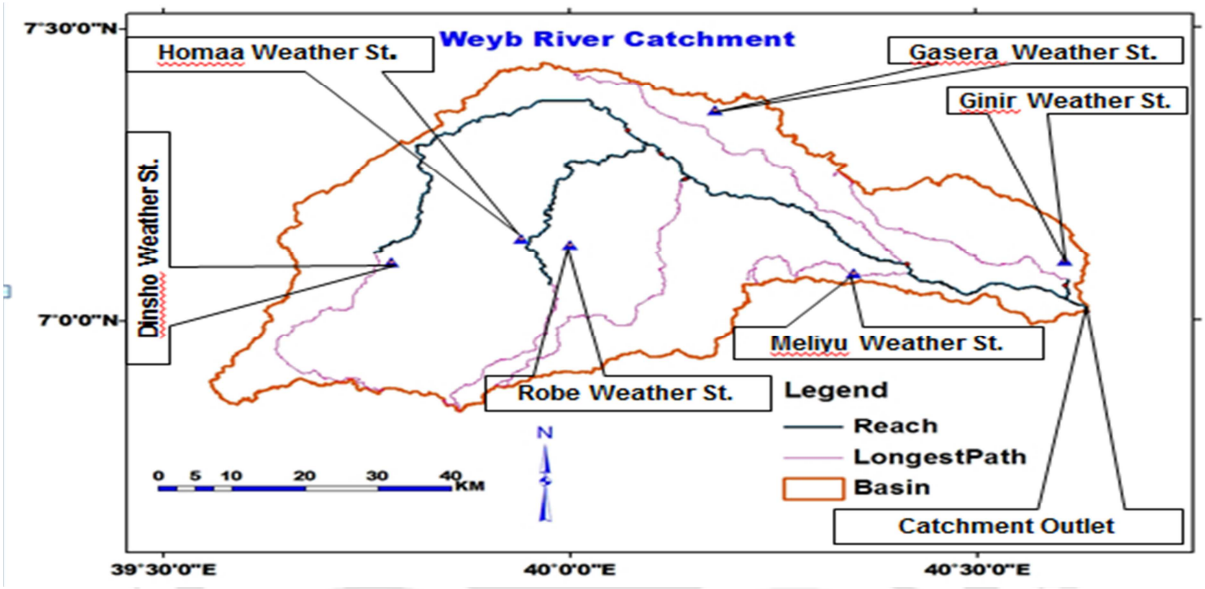

Figure 4.1 Study area: location map and weather stations of the study area

4.2.1. Materials and software program used

The materials employed in this study include Genale-Dawa River Basin Integrated Resources Development Master Plan Study Final Report from the Federal Democratic Republic of Ethiopia Ministry of Water Resources to extract some physicochemical properties of soil for different soil layers, soil and land use ArcGIS map layer that could be input to ArcSWAT hydrologic model.

The models/software programs used for this study are **(i)** Microsoft EXCEL to arrange meteorological and hydrological data as per the SDSM and ArcSWAT models data file format, develop various graphs, as well as to determine various statistical indices, for example R^2, RMSE, SRS, NSE, and Pbias, **(ii)** NetCDF4Excel to manipulate the large-scale atmospheric variables from global archive into the study area, **(iii)** SDSM to downscale temperatures (maximum and minimum) and precipitation for baseline and future time period under different RCP scenarios, **(iv)** XLSTAT 2015 used to conduct Mann-Kendall trend tests

to verify whether there is statistically significant increasing/decreasing trend on future temperatures (maximum and minimum) and precipitation under different RCP scenarios for the study area or not, **(v)** Baseflow Program (Allen, 1999) to determine the fraction of streamflow that is contributed by base flow from observed/measured discharge data, **(vi)** Global Mapper 11 to manipulate the DEM data (meaning to merge, fill, and also configure different grid-size DEM into one to represent study area), **(vii)** Rainbow software to check homogeneity of long-term annual precipitation series at different meteorological stations since knowing an expected behavior of hydro-meteorological processes, mainly precipitation is an important for hydrological modeling, **(viii)** pcpSTST program (Stefan Liersch, 2003) to calculate daily parameters of precipitation data used by the weather generator of the SWAT model; for instance to calculate average total monthly precipitation from daily time series, standard deviation for daily precipitation in month, skew coefficient for daily precipitation in month, probability of a wet day following a dry day, probability of a wet day following a wet day, and average number of days of precipitation in month, **(ix)** ArcGIS to prepare spatial data (DEM, LULC and Soil maps) that can be used in ArcSWAT model, **(x)** and ArcSWAT model to simulate entire river basin and sub-basin scale current (baseline) and future (up to year 2100) surface and subsurface hydrological processes under climate change scenarios.

4.2.2. SWAT model description

SWAT is a public domain model actively supported by the USDA (United States Department of Agriculture) ARS (Agricultural Research Service) at the Grassland, Soil and Water Research Laboratory in Temple, Texas, USA. SWAT is a river basin scale, a continuous time, a spatially distributed model developed to predict the impact of land management practices on water, sediment and agricultural chemical yields in a large complex basin with varying soils, land use and management conditions over long periods of time (Neitsch et al., 2005). SWAT can analyze both small and large basins by subdividing the area into homogenous parts. As a physically based model, SWAT uses hydrologic response units (HRUs) to describe spatial heterogeneity regarding land cover, soil type and slope within a watershed. The SWAT system embedded within geographic information system (GIS) that can integrate various spatial environmental data including soil, land cover, climate, and topographic features. Currently, SWAT has embedded in ArcGIS interface called ArcSWAT. SWAT is a physically based, continuous time (Lenhart et al., 2002) and computationally efficient hydrological model, which uses readily available inputs.

4.2.3. SWAT model approach

Basin can be subdivided into sub-basins and further divided into hydrologic response units (HRUs) to consider differences in soils, land use, crops, topography, and weather. The model has a weather generator that generates daily values of precipitation, temperatures, solar radiation, wind speed, and relative humidity from statistical parameters derived from mean monthly values. Depending on the data availability, SWAT model uses either SCS curve number method or the Green and Ampt infiltration method to estimate surface runoff. There are two approaches (variable storage coefficient method or the Muskingum routing) embedded in SWAT model to route flow through the channel. The model also has three methods (Penman-Monteith, Priestley-Taylor, and Hargreaves) to estimate potential evapotranspiration. The main equations used by the model are given below. SWAT splits hydrological simulations of a basin into two major phases: the land phase and the routing phase. The difference between the two lies in the fact that water storage and its influence on flow rates have considered in channelized flow (Neitsch et al., 2002). The detailed and complete descriptions have given in the SWAT technical documentation.

4.2.4. Hydrological components of SWAT model

Depending on the criterion given for hydrological model and taking into account the objective of the research SWAT model (distributed physically based) has been used for simulation of the hydrological processes of Weyib River basin. The SWAT model calibrated and validated to be applicable and efficient for simulation of streamflow in Bale Mountainous area of Shaya River basin (one of the tributaries of Weyib River basin) (Shawul et al., 2013). The land phase which simulates the hydrology of the basin controls the amount of water, sediment, and nutrient and pesticide loadings to the main channel in each sub-basin whereas the routing phase monitors the movement of water, sediments, nutrients and organic chemicals through the channel network of the basin to the outlet.

In the land phase of hydrological cycle, SWAT simulates based on the water balance equation (Eq.4.1a) and hydrological components simulated includes, for instance, canopy storage, infiltration, redistribution, evapotranspiration, lateral subsurface flow, surface runoff, ponds, tributary channels and return flow (Arnold et al., 1998; Neitsch et al., 2005).

$$SW_t = SW_0 + \sum_{i=1}^{t}\left(R_{day} - Q_{surf} - E_a - w_{seep} - Q_{qw}\right) \quad (4.1a)$$

Where, SW_t is the final soil water content, SW_o is the initial soil water content on day, t is the time (days), R_{day} is the amount of precipitation on day, Q_{surf} is the amount of surface runoff on day i, Ea is the amount of evapotranspiration on day i, W_{seep} is the amount of water entering the vadose zone from the soil profile on day i, and Q_{gw} is the amount of return flow on day i. All parameter are in mm.

Since sub-daily rainfall data was not available in the study area that can use for Green and Ampt infiltration method ('Green and Ampt, 1911'), Soil Conservation Service curve number equation (USDA, 1972) has been used to estimate the surface runoff of the catchment. Penman-Monteith method (Monteith, 1965) which developed based on the temperature, solar radiation, and relative humidity and wind speed data records were used to estimate the PET. The SCS curve number has described in Eq.4.2.

$$Q_{surf} = \frac{(R_{day} - 0.2S)^2}{(R_{day} + 0.8S)} \tag{4.2}$$

In which, Q_{surf} is the rainfall excess, R_{day} is the rainfall depth for the day, S is the retention parameter. All parameter are in mm. More detailed descriptions of the different model hydrologic components are listed in SWAT user's manual (Neitsch et al., 2005). The retention parameter (mm) has defined in Eq.4.3.

$$S = 25.4\left(\frac{1000}{CN} - 10\right) \tag{4.3}$$

The CN SCS is a function of the soil's permeability, land use and antecedent soil moisture conditions. SCS describes three antecedent moisture conditions (1) dry (wilting point), (2) average moisture, and (3) wet (field capacity). The moisture condition 1 curve number is the lowest value that the daily curve number can assume in dry conditions whereas the moisture condition 3 curve number is the highest value that the daily curve number can consider in wet conditions. The curve numbers for moisture conditions 1 and 3 have calculated from Eq. 4.4 and 4.5.

$$CN_1 = CN_2 - \frac{20 \cdot (100 - CN_2)}{\left(100 - CN_2 + \exp\left[2.533 - 0.0636 \cdot (100 - CN_2)\right]\right)} \tag{4.4}$$

$$CN_3 = CN_2 \cdot \exp\left[0.00673 \cdot \left(100 - CN_2\right)\right] \tag{4.5}$$

In which, CN_1 is the moisture condition 1 curve number, CN_2 is the moisture condition 2 curve numbers, and CN_3 is the moisture condition 3 curve numbers. Typical curve numbers for moisture condition 2 have listed in various tables (Neitsch et al., 2005) which are appropriate to slope less than 5%. However, in the Weyib River basin, there are areas with slopes greater than 5%. To adjust the curve number for higher slopes an equation developed (Williams, 1995) was used (Eq. 4.6).

$$CN_{2S} = \frac{(CN_3 - CN_2)}{3} \cdot [1 - 2 \cdot \exp(-13.86 \cdot slp)] + CN_2 \quad (4.6)$$

In which CN_{2S} is the moisture condition 2 curve number adjusted for slope, CN_3 is the moisture condition 3 curve number for the default 5% slope, CN2 is the moisture condition 2 curve number for the default 5% slope, and *slp* is the average percent slope of the sub-basin.

The second phase of the SWAT hydrologic simulation, the routing phase, consists of the movement of water, sediment and other constituents (for instance, nutrients, pesticides) in the stream network. The rate and velocity of flow have calculated by using the Manning's equation. The main channels or reaches are assumed to have a trapezoidal shape by the model. The two kinematic wave model options (variable storage and Muskingum methods) are available to route the flow in the channel networks. The variable storage method uses a simple continuity equation in routing the storage volume, whereas the Muskingum routing method models the storage volume in a channel length as a combination of wedge and prism storages. For this study, therefore, the variable storage method (Williams, 1969) used in the ROTO (Routing Outputs to Outlets) (Arnold et al., 1995) model was applied as in Eq.4.1b.

$$\text{Vstored} = \text{Vinflow} - \text{Voutflow} \quad (4.1b)$$

Where: Vstored is the change in volume of storage during the time step, Vinflow is the volume of inflow during the time step, and Voutflow is the amount of outflow during the time step. All parameters are in m^3. Detail of the equation has given in SWAT manual.

4.2.5. SWAT model inputs

A. Digital Elevation Model

A Digital Elevation Model (DEM) which describes the elevation of any point in a given area at a particular spatial resolution as a digital file. A topographic feature of study basin (slope

steepness, slope length, and defining of the stream network) with its characteristics (channel slope, length, and width) has been derived from the DEM. A 30 m resolution DEM obtained from ASTER official website was used for this study (http://gdem.ersdac.jspacesystems.or.jp/

B. Soil Map and Soil Properties

Soil map and major soil physicochemical properties which SWAT required includes its depth, percentage clay, silt and sand content, bulk density, porosity, available water capacity, field capacity, and saturated conductivity for each of the soil layers and morphological characteristics of major soils of Weyib River basin were obtained from the Genale-Dawa river basin integrated resources development master plan soil database and digital soil map from the Federal Democratic Republic of Ethiopia Ministry of Water and Energy (MoWE) produced between the year 2004 and 2007 and presented in Appendix Table 37 and 38.

C. Land Use Land Cover Maps

Land use land cover (LULC) is one of the most significant spatial input data required by SWAT model that affect mainly surface runoff and evapotranspiration and other hydrological processes in a given basin. The LULC map used for this study has been obtained from MoWE, Genale Dawa River Basin master plan produced between the year 2004 and 2007. Current various land use feature of the study area is shown in Appendix Photos 1-5.

D. Weather Data

The SWAT model requires daily measured (observed) weather data which includes 'precipitation, maximum temperature and minimum temperatures, solar radiation, relative humidity and wind speed'. These daily meteorological data for twelve meteorological stations (detailed in chapter 3 in ‘types of data used section’) have been collected from Ethiopian National Meteorological Agency (2007). It is important to know that the expected behavior of hydro-meteorological processes, mainly precipitation. Due to these facts, in this study, 'homogeneity of long-term annual rainfall' series of the Weyib River basin has been investigated using Rainbow software and presented in Appendix Figure 1-12. The detailed meteorological information for the twelve different meteorological stations, their recording periods, and spatial and temporal distribution of temperatures and precipitation characteristics of Weyib River basin has presented in Chapter 3.

E. Hydrological Data

Daily river discharge data of the Weyib River basin at Alemkerem gaging station has been obtained from the Hydrology Department of the MoWE. This data has been used for performing sensitivity analysis, calibration, and verification of the SWAT model. An automated baseflow separation and recession analysis technique (Allen, 1999) was employed to separate the base flow and surface runoff using the total daily river discharge data.

4.2.6. SWAT model setup

A. Basin Delineation

The basin delineation process includes five main steps (i.e., DEM setup, stream definition, outlet and inlet definition, basin outlets selection and definition and calculation of sub-basin parameters). Automated basin (watershed) delineation embedded in ArcSWAT interface was used to delineate the basin. Delineation of the basin and sub-basin was done using DEM data. DEM was imported into the SWAT model and projected to the projection area of Ethiopia (UTM zone 37). A mask was manually delineated over the DEM to extract the particular area, to describe the boundary of the watershed and digitize the stream networks in the study area, which reduce the time of processing and burn-in a polyline stream dataset that in turn helps the sub-basin reach to follow the known stream reach. The ArcSWAT interface proposes the minimum, maximum, and suggested the size of the sub-basin area (in hectare) define the minimum drainage area required to form the origin of a stream and to decide the number of sub-basins within the basin. The smaller the threshold area, the more detailed are the drainage networks and the larger number of sub-basins and HRUs. However, this needs more processing time and space. As a result, an optimum size that compromises both was selected. Therefore for this study, suggested the size of the sub-basin area (9033 ha) to define the minimum drainage area required to form the origin of a stream has been used. On the given area of the basin, only one outlet is set, which has later taken as a point of calibration and validation of the simulated streamflow. As a result, actual Weyib River basin outlet has been delineated. Finally, sub-basin parameters were estimated.

B. Determination of Hydrological Response Units

After basin delineation, sub-basins were divided into areas having a unique land use, soil and slope so-called hydrologic response units (HRUs). The land use, soil, and slope data sets have been projected into the same projection as DEM. After projection of the land use, soil and

slope data sets were reclassified, overlaid and linked with the SWAT databases and ready for HRU definition. Multiple HRU definition options were selected to define the distribution of HRUs. The threshold level set for land use, soil and slope were used to establish the number of HRUs within the sub-basin as well as the basin. In addition to land use and soil, HRUs were also classified based on slope classes. The multiple slope classification based on the suggested minimum, maximum, mean and median slope statistics of the basin has been used in this study.

The interface can provide us two options (either assigning only one HRU for each sub-basin considering the dominant soil-land use-slope combinations or assigning multiple HRUs for each sub-basin considering the sensitivity of the hydrologic process based on certain threshold values of soil-land use-slope combinations) to determine HRUs for each sub-basins. For this study, the multiple HRUs for each sub-basin had assigned as it better describes the heterogeneity within the basin and as it accurately simulates the hydrologic processes. The minimum threshold area of 5% for land use over the sub-basin area, 10% for soil class over the land use area and 20% for slope over the soil area have been used The land use, soil and slopes percentage areas covering less than the threshold area level have been eliminated, and then the remaining areas were reclassified so that 100% of the land area in the sub-basin could have been used in the simulation.

C. Sensitivity Analysis

After all the input (spatial as well as weather) data required for the SWAT model were correctly loaded, the parameter sensitivity analysis was done using the ArcSWAT interface for the whole basin (van Griensven et al., 2006). Twenty-six hydrological parameters have been tested for sensitivity analysis for the simulation of the streamflow in the study area. Here, almost all the default lower and upper bound parameter values have been used. In addition to hydrologic parameters, observed and simulated daily streamflow values of Weyib River basin have been used as an input. The sensitivity analysis was made using a built in SWAT sensitivity analysis tool that uses the Latin-Hypercube-One-factor-At a-Time (LH-OAT) algorithm (Van Griensven, 2005). After running sensitivity analysis, the sensitivity parameters were ranked based on their mean relative sensitivity from high to low (Table 4.5.)

D. Model Calibration and Validation

During the calibration process, model parameters were subjected to adjustments to obtain model results that correspond better to the measured datasets. After the sensitive parameters were selected, the model simulates the stream flow using default parameter values for years 1981-2004. The default simulation output was compared with the observed stream flow data. In this study, manual calibration followed by automatic calibration were made on a daily basis from 01 January 1981 to 31 December 2004 until the mean simulated value came closer to the measured value. Periods from 1981 to 1983 was used as warm up periods (the period left for model stabilization). Automatic calibration makes use of a numerical algorithm to increase the performance of the model and to optimize the numerical objective functions. In manual calibration for each simulation result and parameter change, the corresponding performance evaluation criteria have been compared against the present values. This procedure continued until the acceptable calibration model performance statics of $R^2 > 0.6$, NSE > 0.5, RSR ≤ 0.70 and Pbias within the ±25 (Moriasi et al., 2007) were achieved (Table 4.1). After the simulation result for the calibration period had fulfilled the above statistical criteria, validation has been performed for an independent period of records from 01 January 1995 to 31 December 2004. The demonstration of ArcSWAT model for the entire Weyib River basin is presented in Appendix Figure 13.

4.2.7. Model performance evaluation

In order to evaluate the SDSM and ArcSWAT models performance relative to the observed climatic and hydrological variables, the following four statistical model performance evaluation measures, in addition to graphical technique, were used during the calibration and validation periods. The four statistical model evaluation indices were R^2, NSE, RMSE-observations standard deviation ratio (RSR), and Pbias. Two commonly used graphical techniques; provide a visual comparison of simulated and measured constituent data, hydrographs and percent exceedance probability curves are especially valuable. In this study, a hydrograph method was used to identify differences in timing and magnitude of peak flows, to visualize the shape of hydrograph and to identify model bias (Singh et al., 2004) throughout model calibration and validation period.

A. Coefficient of Determination (R^2)

It was given by (Krause and Boyle, 2005) as shown in Equation 4.7

$$R^2 = \frac{(\sum[Xi-Xav][Yi-Yav])^2}{\sum(Xi-Xav)^2 \sum(Yi-Yav)^2} \quad (4.7)$$

Where, Xi is measured value, Xav is average measured value, Yi is simulated value, and Yav is average simulated value.

B. Nash-Sutcliffe Coefficient (E)

It was provided by (Nash and Sutcliffe, 1970) as shown in Equation 4.8

$$E = 1 - \frac{\sum_{i=1}^{n} (X_{obs,i} - X_{model})^2}{\sum_{i=1}^{n} (X_{obs,i} - \overline{X_{obs}})^2} \quad (4.8)$$

Where X_{obs} is observed values and X_{model} is modeled values at time/place *i*.

C. RMSE-Observations Standard Deviation Ratio (RSR)

It was given by (Singh et al., 2004) as shown in Equation 4.9 and 4.10

$$RMSE = \sqrt{\frac{\sum_{i=1}^{n} (X_{obs,i} - X_{model,i})^2}{n}} \quad (4.9)$$

$$RSR = \frac{RMSE}{STDEVobs} \quad (4.10)$$

Where X_{obs} is observed values, X_{model} is modeled values at time/place *i* and n is number of observation.

D. Percent Bias (Pbias)

It was given by (Moriasi et al., 2007) as shown in Equation 4.11

$$Pbias = \frac{\sum_{i=1}^{n}(obs - sim) \times 100}{\sum_{i=1}^{n}(obs)} \quad (4.11)$$

Where obs is observed values, sim is simulated values at time *i*

Table 4.1 General model performance ratings for recommended statistics for a monthly time step (Moriasi et al., 2007)

Statistics	Statistics equation	Performance ratings			
		Unsatisfactory	Satisfactory	Good	Very good
R^2	$R^2 = \frac{(\sum[Xi - Xav][Yi - Yav])^2}{\sum(Xi - Xav)^2 \sum(Yi - Yav)^2}$	< 0.5	0.5-0.6	0.6-0.7	0.7-1.0
NSE	$E = 1 - \frac{\sum_{i=1}^{n}(X_{obs,i} - X_{mo\,del})^2}{\sum_{i=1}^{n}(X_{obs,i} - \overline{X_{obs}})^2}$	≤ 0.5	0.5-0.65	0.65-0.75	0.75-1.0
RSR	$\mathrm{RSR} = \frac{\mathrm{RMSE}}{\mathrm{STDEVobs}}$	> 0.7	0.6-0.7	0.5-0.6	0-0.5
Pbias	Where $RMSE = \sqrt{\frac{\sum_{i=1}^{n}(X_{obs,i} - X_{model,i})^2}{n}}$ $\mathrm{PBIAS} = \frac{\sum_{i=1}^{n}(obs - sim) \times (100)}{\sum_{i=1}^{n}(obs)}$	≥ ±25%	±15-±25%	±10-±15	< ±10

4.3. Results and Discussion

4.3.1. Simulation of the hydrology of the Weyib River catchment

From the suggested threshold area, six sub-basins have been delineated in the Weyib River Basin (4215.93 km^2). Each sub-basin boundary marks the end of reach, the end point of which the accumulation point for all flow from upstream which is then fed into downstream sub-basin and reach (Fig. 1, Chapter 5). Once the main reach and the longest paths (tributaries) have been formed, the model uses soil, land use, and land slope data to define HRUs. From the supposed threshold values for HRUs delineation of 5% land use, 10% soil and 20% slope we have been obtained 77 HRUs in 6 sub-basins. All HRU is a grouping of a unique land use, soil type, and slope features.

As shown in Table 4.2 and Fig. 4.2a the greater portion of the basin has occupied by two soil types Eutric Vertisol (19.93%) and Dystric Cambisol (17.85%). Unlikely, Calcaric Cambisol and Calcic Vertisol cover a comparatively minor percentage of the basin 1.91% and 1.77% respectively. About 91.21% of study basin has been occupied by the agricultural land close grown (mainly cultivated for wheat and barley). Farm village's covers relatively smaller portion about 0.01% of the total basin area Table 4.3 and Fig. 4.2b. Based on the slope statistics in the basin, the present study considered three slope partitions, by dividing land

slope partitions as partition 1: 0 -15%, partition 2: 15-30%, partition 3:30-9999%. The maximum value for the highest slope class ranges in SWAT database was assigned by default to be 9999%. From land slope classifications, about 70.54% of the watershed area covered by 0-15%, 16.46% of the area 15-30% slope class and the rest 12.99% of the watershed area covered with a land slope of 30-9999% Table 4.4 and Fig. 4.2c. As we can see in Fig. 4.2d the altitude/elevation variation of study catchment is found to be in a range from 898 to 4388.60 m as obtained from DEM (30mr).

Table 4.2 Major soil unit of Weyib catchment and their areal coverage in the catchment

No.	Soil unit name	Soil unit code	Area (ha)	Percentage catchment area (%)
1	Chromic Cambisol	CMx	52855.24	12.54
2	Dystric Cambisol	CMd	75257.57	17.85
3	Eutric Cambisol	CMe	20564.47	4.88
4	Haplic Luvisol	LVh	72401.70	17.17
5	Vertic Luvisol	LVv	40063.73	9.50
6	Calcaric Cambisol	CMc	8063.79	1.91
7	Leptosol	LP	26628.50	6.32
8	Eutric Vertisol	VRe	84026.42	19.93
9	Regosol	RG	34281.81	8.13
10	Calcic Vertisol	VRk	7449.74	1.77

Table 4.3 Major Landuses of Weyib catchment and their areal coverage in the catchment

No.	Land Use	SWAT Code	Area (ha)	Percentage catchment area (%)
1	Agricultural Land-Close-grown	AGRC	384541.33	91.21
2	Range-Brush	RNGB	19766.09	4.69
3	Forest-Mixed	FRST	17187.64	4.08
4	Range-Grasses	RNGE	64.84	0.02
5	Residential-Med/Low Density	URML	33.09	0.01

Table 4.4 Land slope classes of Weyib catchment and their areal coverage in the catchment

No.	Slope Class	Area (ha)	Percentage catchment area (%)
1	0-15	297396.54	70.54
2	15-30	69415.04	16.46
3	30-9999	135367.59	12.99

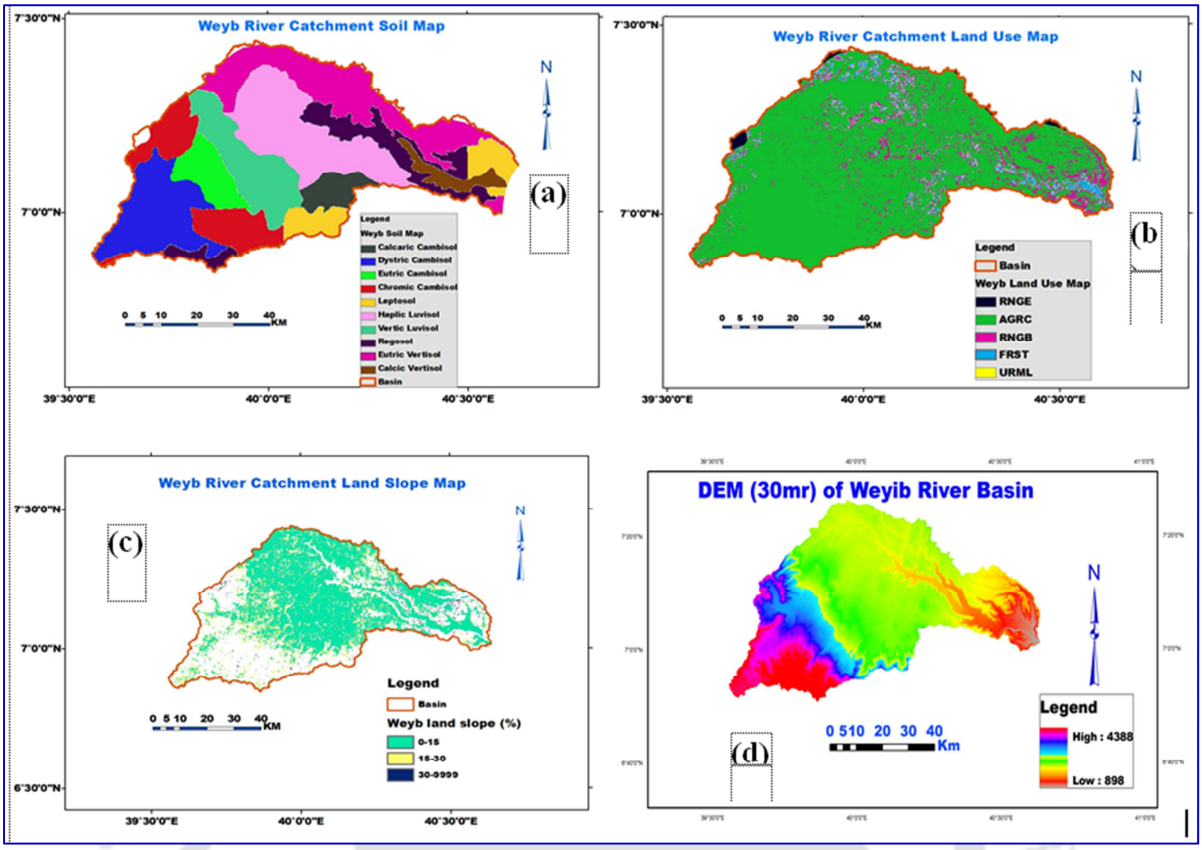

Figure 4.2a (top left): Soil map and its spatial distribution over the Weyib catchment, b (top right): the same as Fig.4.2a but for land use map, c (bottom left): the same as Fig.4.2a but for land slope map, d (bottom right): the same as Fig.4.2a but for DEM map (30mr)

4.3.2. Parameters sensitivity analysis

Sensitivity investigation has been made for the whole historical period of 1981-2004. About 270 iterations of sensitivity analysis have been done through sensitivity analysis tool which embedded in ArcSWAT model for flow. The model considered 26 flow parameters for basin sensitivity analysis; from which 20 of them were comparatively sensitive. Among 20 sensitive flow parameters, 13 were obtained to be the furthermost effective hydrologic parameters (detailed in Table 4.5) for the simulation of streamflow in the Weyib River basin. Moreover, then, these parameters were used for streamflow calibration and validation. The surface runoff parameter includes the curve number (Cn2), soil evaporation compensation factor (Esco) and available water capacity of the soil layer (Sol_Awc) are the top 3 most sensitive flow parameter over the others surface runoff and ground water parameters. A brief description of each hydrologic parameter is listed in the SWAT model user's manual (Neitsch et al., 2005).

Table 4.5 SWAT's most sensitive streamflow parameters and final calibrated fitted values

Flow Parameter	Description	Sensitivity Rank	Lower and Upper Bounds	Calibrated Value
CN2	SCS runoff curve number for moisture condition II	1	±25%	12%
Esco	Soil evaporation compensation factor	2	0 to1	0.9
Sol_Awc	Available water capacity of the soil layer	3	±25%	20%
Sol_Z	Depth from 'soil surface to bottom of layer'	4	±25%	9.5%
Canmx	Maximum canopy storage	5	0 to 10	2.5
Revapmn	threshold 'depth of water in the shallow aquifer' for revap to occur	6	±100	90.50
Gwgmn	Threshold 'depth of water in the shallow aquifer' required for return flow to occur	7	±1000	750
Blai	Maximum potential leaf area index	8	0 to1	0.45
Slope	Average slope steepness	9	±25%	15%
Sol_K	Saturated hydraulic conductivity	10	±25%	1.5%
GW_Revap	Groundwater revap coefficient	11	±0.036	0.03
Ch_K2	Effective hydraulic conductivity in the main channel alluvium	12	0 to 150	98
Alpha_Bf	Baseflow alpha factor	13	0 to 1	0.92

4.3.3. SWAT model calibration and validation

A. Model Calibration

The automatic baseflow separation technique based on the daily streamflow data measured at the outlet of the basin indicated that about 36-52% of the total discharge has contributed from the surface water source. The subsurface contribution (48 to 64% of total discharge) is more than the surface contribution. Daily streamflow data from the outlet of the study basin has been used for the calibration. Three-year data (i.e., 1981-1983 data) have been used as a spin up period (warm up time), and eleven years data (i.e., 1984-1994) have been used for testing (calibration). Some model parameters (e.g., CN2) can vary spatially depending on soil, land cover, slope, and other basin characteristics. During calibration, the baseline values initially assigned to the spatially varying parameters have been altered by multiplying or replacing the baselines by a sampled value as described in Table 4.5. This way, the parameters were adjusted for a realistic hydrologic simulation. Model parameters were first calibrated manually followed by automatic calibration using ParaSol (Parameter Solutions), an autocalibration tool which set-in ArcSWAT model. The calibration processes considered 13 flow parameters and their values were varied iteratively within the allowable ranges until a satisfactory agreement between measured and simulated streamflow has been obtained. The autocalibration processes significantly improved model efficacy. The results of four statistical analysis met model performance evaluation standards given (Moriasi et al., 2007) for

streamflow with R^2, NSE, RSR and Pbias values of 0.86, 0.83, 0.25 and 1.72 respectively for calibration period (Fig.4.3 and 4.4).

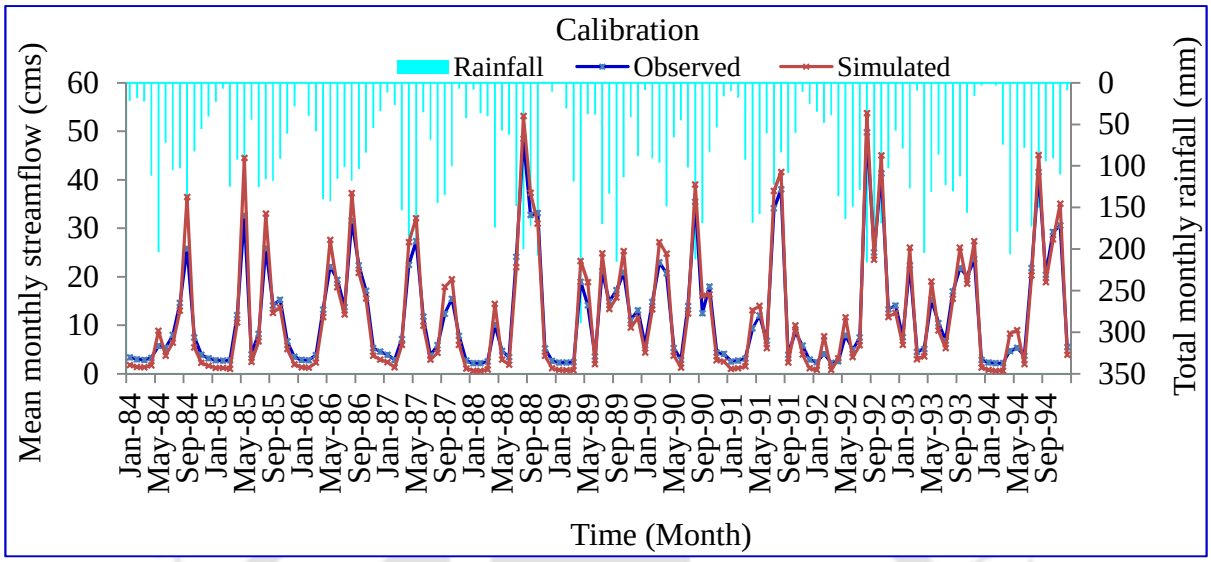

Figure 4.3 Hydrograph of the observed and simulated streamflow using calibrated parameters for the calibration period (1984-1994)

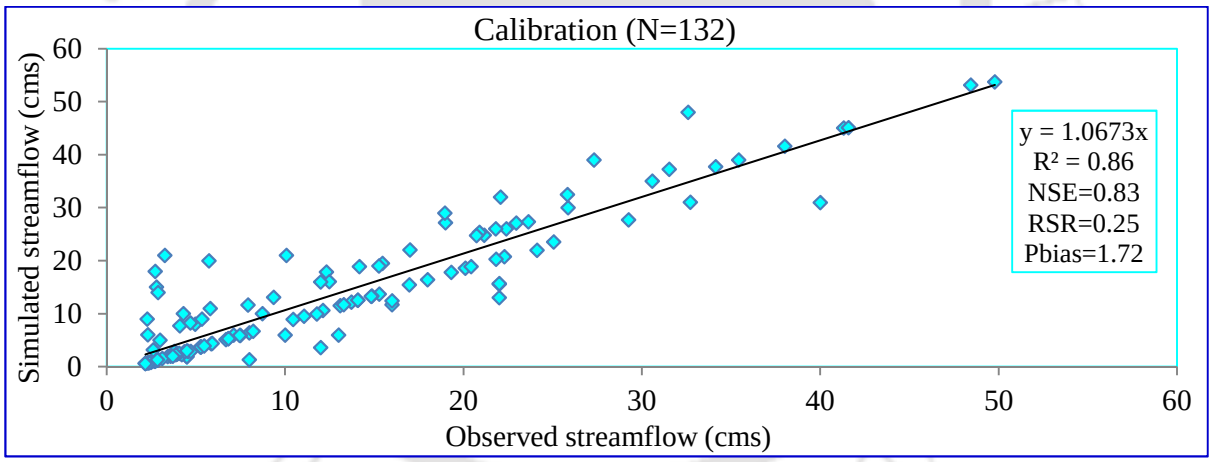

Figure 4.4 Regression line fit between observed and simulated streamflow during calibration period

An intensive hydrologic calibration resulted in good SWAT predictive efficiency at the daily time step of the basin when compared to measured flow data. The hydrograph and regression line between observed and simulated flow indicated that the ArcSWAT model is capable of simulating the hydrology of Weyib River basin as shown in Fig.4.3 and 4.4.

B. Model Validation

The performance of the calibration result has verified using the split-sampling approach (i.e., 1995–2004 data) was used for verification on a daily basis. It has found that the ArcSWAT

model has the high predictive capability with R^2, NSE, RSR and Pbias values of 0.84, 81, 0.31 and 2.69 respectively (Fig 4.5 and 4.6). Though rigorous calibration has undertaken for daily streamflow, simulated flow over predicts peak flow but under predicts all other time for both calibration and validation periods. The shape of the hydrograph of simulated flow was the same as the shape of hydrograph of measured daily streamflow (Fig.4.3 and 4.5).

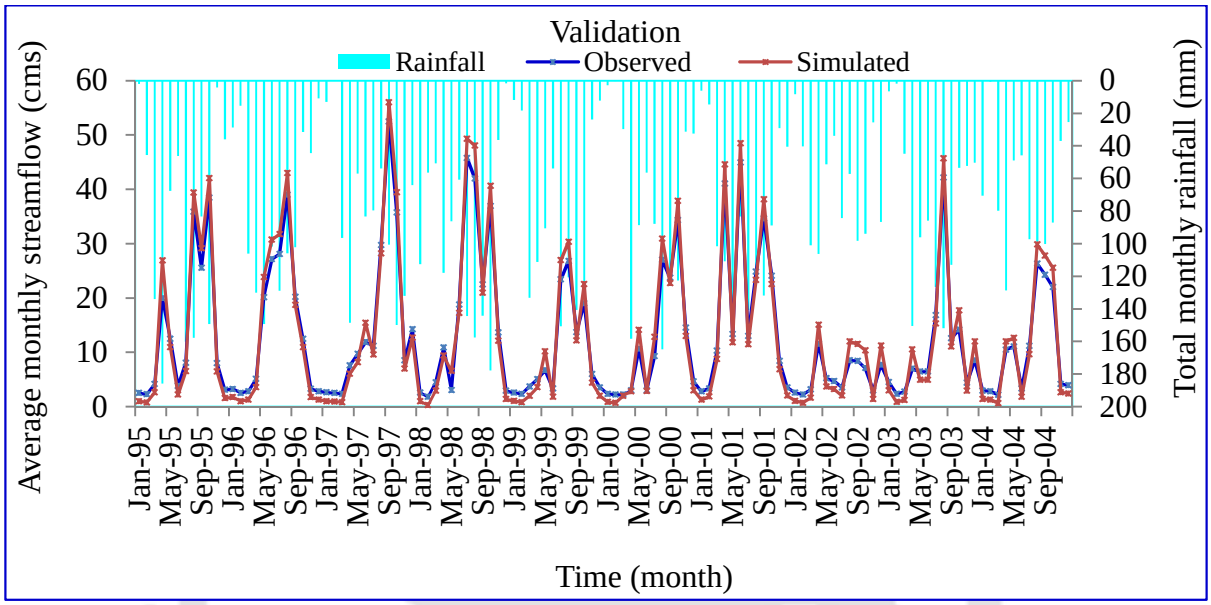

Figure 4.5 Hydrograph of the observed and simulated streamflow using calibrated parameters for the validation period (1995-2004)

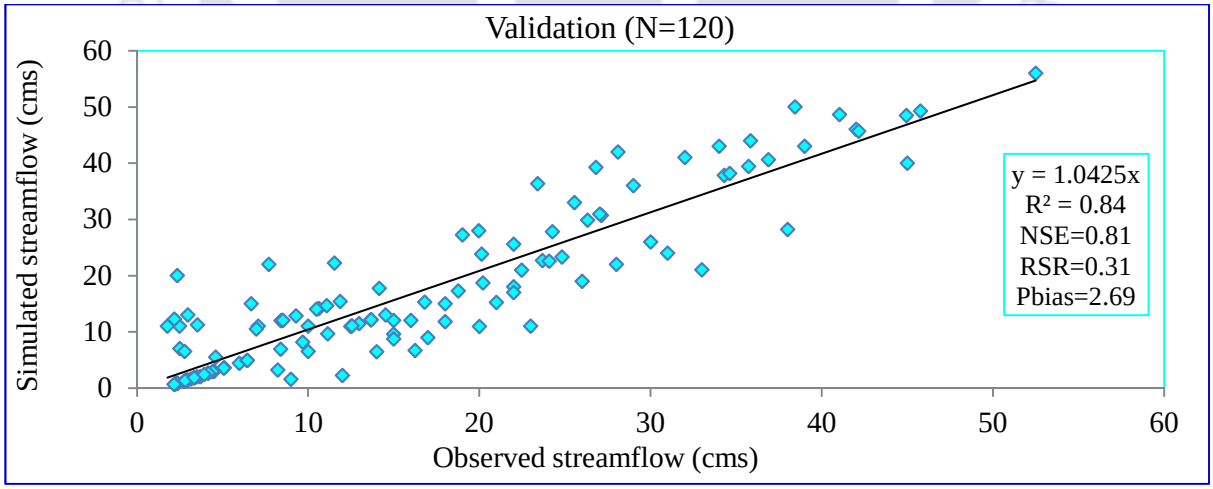

Figure 4. 6 Regression line fit between observed and simulated streamflow during validation period

Streamflow Simulations are considered satisfactory if $R^2 \geq 0.6$, NSE>0.5, RSR≤0.7 and Pbias are within ±25% (Moriasi et al. 2007). According to these criteria, Tables 4.1 and 4.6 indicate, for all evaluation criteria given, very satisfactory results for both calibration and

verification periods have been obtained. Therefore since the model performed as well in the validation period, as for the calibration period hence, the set of optimized parameters listed in Table 4.5 during the calibration process of Weyib River basin can be taken as the representative set of parameters for the similar basin. Altogether, when comparing the model's performance against the model evaluation criteria based on the guidelines (Moriasi et al., 2007) presented in Table 4.1 for the monthly time step, SWAT simulated streamflow very well in all the evaluation indices (Table 4.6).

Table 4.6 Summary of model performance ratings for simulations of streamflow

	Model Performance	
Statistics	Calibration for the Period of 1984-1994	Validation for the Period of 1995-2004
Coefficient of Determination (R^2)	0.86 (very good)	0.84 (very good)
Nash-Sutcliffe Coefficient (NSE)	0.83 (very good)	0.81 (very good)
RSR	0.25 (very good)	0.31 (very good)
Percent Bias (Pbias)	1.72 (very good)	2.69 (very good)

The Evaluation of the SWAT model in simulating catchment hydrology in case study of the Modder River basin has been investigated (Kusangaya et al., 2014) and they reported that the results of calibration and validation of the model at a monthly time step gave NSE of 0.65, Pbias of 15 and RSR of 0.4, while NSE of 0.5, Pbias of 31 and RSR of 0.5 have recorded for validation. Jha (2011) reported R^2 of 0.86 and NSE of 0.85 for calibrated monthly flows, and for validation the following monthly flows statistics have reported as R^2 of 0.69 and NSE of 0.61. Srinivasan et al. (2010) reported R^2 of 0.75 and NSE of 0.74 for calibrated monthly flows, and for validation the following monthly flows statistics have reported as R^2 of 0.58 and NSE of 0.69. Bouraoui et al. ('2005') reported R^2 of between 0.62 and 0.84 and NSE of between 0.41 and 0.84 for calibrated monthly flows. Setegn (2010) said R^2 of 0.80 and NSE of 0.73 for calibrated while R^2 of 0.80 and NSE of 0.71 for validation period. In an interrelated study, Shawul et al (2016) also reported that the SWAT model had a good performance in simulating the monthly, seasonal, and annual mean discharges with the R^2, NSE and D values of 0.81, 0.75 and 23 respectively in the calibration period, while R^2, NSE and D values of 0.65, 0.59 and 20 respectively in the validation period. In this study, the results of calibration and validation of the model at daily time step gave R^2 of 0.86, NSE of 0.83, and RSR of 0.25 and Pbias of 1.72 during the calibration period, while R^2 of 0.84, NSE of 0.81, RSR of 0.31 and Pbias of 2.69 during the validation period. There has been observed

a slight variation in statistical values among researchers, in this particular study too; this difference might be due to mainly spatial data used (predominantly LULC data), the disparity insensitive catchment parameters that affect calibration processes, uncertainty during data handling.

4.4. Conclusion

The assessment of SWAT hydrological model and investigation of its ability to simulate reliably the different components of water balance in general and streamflow, in particular, using different efficiency criteria gave an insight into how one can successfully generate useful information in catchments where there is little data available. To do so various efficiency criteria were implemented, namely, R^2, NSE, RSR and Pbias with hydrograph technique. The results suggest that the SWAT hydrological model can be a useful tool which, once calibrated effectively, can produce meaningful predictions of catchment hydrology to aid management decisions. The results obtained indicate that basin output simulated by ArcSWAT after calibration is comparatively consistent with recorded values.

This study provided a better understanding of SWAT model set-up, sensitive parameters that influence the model output, and hydrologic processes of the catchment. The most sensitive parameter found in this hydrological simulation exercise was Curve Number (CN) which is dependent on 'land management practice and soil parameters'. These parameters are found to influence hydrologic processes more than others. It is paramount that calibrated model results provide a reasonable reflection of actual hydrologic processes. Statistical evaluation criteria suggested (Moriasi et al., 2007) only provides the guidelines to which to evaluate model’s performance. Moreover, it is also essential to look at other statistical indices that can be used to assess the model's performance. It has inferred that further study is conducted to evaluate uncertainties in the model that affect model performance and the sensitivity of the 'distributed hydrologic' simulations to different calibration schemes under different catchment conditions.

Chapter 5: Climate Change Impact Analysis on Hydrological Processes of the Weyib River Basin, Southeastern Ethiopia

5.1. Introduction

The climate drives the hydrological cycle (Crosbie et al. 2010), and projected changes in spatial and temporal patterns of the climate variables will impact on 'regional hydrological processes, in particular, changes in rainfall will be amplified as an impact' on hydrological components (Wang et al., 2011). Rainfall is the largest factor in the water balance of catchment hydrology (Mpelasoka and Chiew, 2009). This chapter study investigated the response of hydrological processes under ensembles of three ESMs for the three RCP scenarios in the Weyib River Basin, Southeastern Ethiopia. Spatial (EB and SB) and temporal scale major hydrological processes (such as PRECIP, QSURF, GWQ, ET, PET, PERC, SW and WYLD) using ArcSWAT hydrologic model for the current and future (in the 2020s, 2050s and 2080s time slices) time period under Ensembles of three ESMs for the RCP8.5, RCP 4.5 and RCP 2.6 scenarios from CMIP5 have been considered. The hydrological processes for EB and six SBs were investigated separately to derive better in sight into the hydrological processes of the Weyib River. What is confident about study zone in general and study area of Weyib River Basin, in particular, is that our climate is changing. So far, however, there is no single study has been done in the study area about future hydrological processes under the CMIP5-ESMs-RCPs scenario, but this study tried.

The objectives of this chapter were to:

→ Examine the response of surface and subsurface hydrological processes under ensembles of CMIP5-ESMs-RCPs scenario in the entire basin and sub-basin scale.

→ Estimate the annual, seasonal and monthly water availability (in the 2020s, 2050, and 2080s time slices) under the CMIP5-ESMs-RCPs scenario in the entire basin and sub-basins scale up to the year 2100.

5.2. Materials and methods

5.2.1. Drainage area and hydrologic response unit description (HRUs)

Detail description of the study area (Weyib River basin) has been provided in chapter 3 and 4. There is no optimal number of sub-basins as it depends on the issues addressed in the modeling and scenario analysis, but for our case we have sub-divided the entire basin (4215.93 km^2) into six sub-basins (Fig 5.1) using suggested (by the ArcSWAT interface)

threshold value of 9033 ha (which basically controls the drainage density of the artificially constructed drainage system and thereby the number of sub-basins). The sub-basin 3 has a larger area of 1160.60 km^2 and 7 HRUs whereas sub-basin 6 has the smaller area of 284.27 km^2 and 17 HRUs. The drainage area (km^2) and HRUs (numbers) of sub-basin 1, 2, 4 and 5 were 942.35 and 10, 689.11 and 13, 742.44 and 17 and 397.12 and 13, respectively. The total number of HRUs in the entire river basin then becomes 77.

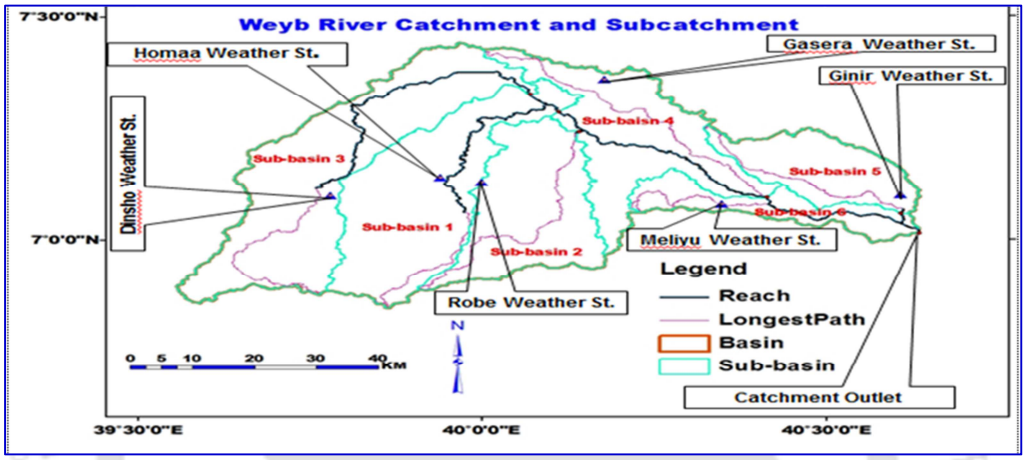

Figure 5.1 Entire basin, sub-basin and reach delineation, longest path, and selected weather stations

5.2.2. The Earth System Models (ESMs) and RCP scenarios

In this study, three bias-corrected Earth System Models (ESMs) for the RCP8.5, RCP4.5, and RCP2.6 scenarios from CMIP5 has been used. The historical and future predictor variables have been downloaded through official data portal (website) of CCCMA and NOAA-GFDL (refer chapter 3 for more detail in this regard).

5.2.3. The ArcSWAT hydrologic model

In this study, considering the aim we are going to achieve, ArcSWAT model was used to simulate various hydrological processes of Weyib River basin. SWAT model description, approach and various components are given in chapter 4. Data necessary for this chapter study comprises (i) daily weather data, (ii) spatial data (DEM, soil map and properties and LULC) and (iii) discharge/streamflow data. All these data sources are detailed in chapter 3 and 4. The standard procedure of ArcGIS interface ArcSWAT hydrologic model was applied to delineate the watershed, determination of hydrological response units (HRUs), sensitivity analysis, model calibration and validation and sensitivity analysis (detail explanation has given in chapter 4).

5.2.4. Investigation of future climate changes impact on hydrological processes

The CMIP5-ESMs output, which was downscaled to the Weyib River catchment level for twelve stations using SDSM, was used to generate the forthcoming hydrological processes in the basin. The ArcSWAT model first ran for historical (1981-2004) period for entire river basin and calibrated and validated accordingly. After successful validation, the model has then been re-run on the basins using Ensembles of three ESMs for the RCP8.5, RCP 4.5, and RCP2.6 scenarios climate data without changing the other parameters. The various outputs of hydrological processes have been analyzed firstly at the entire basin level to quantify the possible impacts of climate change on different hydrological processes. Successively, detailed analyses have been performed on the river basins to quantify the impacts at the sub-basin level. The analyses of the hydrological processes were then carried out on an annual, seasonal and monthly basis in the 2020s, 2050s and 2080s future time slices.

5.3. Results and Discussion

5.3.1. Entire river basin and sub-basin scale current annual hydrological processes

In this section, the analysis was performed on annual basis for all hydrological processes such as PRECIP, QSURF, GWQ, ET, PET, PERC, SW and WYLD for baseline (1981-2004) period. The three years (1981-1983) has left as a warming up (model stabilization) period. Results revealed in Fig 5.2a-g that the EB and SB scale analysis of all hydrological processes are found to be different in Weyib River basin. This is, probably, due to the basin characteristics that govern the hydrological regime of the EB and SBs. Therefore, we can pledge that there has been observed a significant spatial and temporal variability of all the hydrological processes in Weyib River basin during baseline simulation.

The PRECIP for EB was found to be 1061.12 mm with a range from 787.04 to 1421.45 mm (Fig 5.2a). Mean annual total PRECIP for SB 1, 2, 3, 4, 5 and 6 were observed to be 850.99 mm (ranges; 481.54 to 1237.89 mm), 818.39 mm (ranges; 550.19 to 943.93 mm), 1394.35 mm (ranges; 826.80 to 2320.86 mm), 1061.97 mm (ranges; 741.66 to 1751.23 mm), 853.45 mm (ranges; 609.79 to 1254.91 mm) and 1273.87 mm (ranges; 967.29 to 1740.07 mm) respectively during baseline simulation (Fig 5.2b-g). As can we seen Fig 5.2a, c and g maximum value of PRECIP was observed in the year 1992 in case of EB, SB2 and SB5 but in 1998 (SB1) (Fig 5.2b), 1989 (SB3), 1987 (SB4) and in 1997 (SB6) whereas a minimum

value of PRECIP has been observed in the year 2002 (in the EB and SB3), 1991 (in SB1 and 2), 1990 (in SB4), 2000 (in SB5) and 1988 (in SB6) (Fig 5.2a-g).

The mean annual total ET for EB is found to be 492.41 mm with a range from 445.77 to 522.01 mm. The mean annual total ET for SB 1, 2, 3, 4, 5 and 6 were observed to be 511.33 mm (ranges; 402.76 to 569.24 mm), 452.94 mm (ranges; 410.69 to 497.71 mm), 480.19 mm (ranges; 405.18 to 538.44 mm), 553.68 mm (ranges; 493.51 to 610.20 mm), 435.89 mm (ranges; 333.19 to 492.09 mm) and 494.22 mm (ranges; 393.04 to 557.77 mm) respectively. A maximum value of ET has been observed in year 1998 (in case of EB), 1986 (in SB1), 1992 (in SB2), 1990 (in SB3), 2001 (in SB4), 1996 (in SB5) and 1986 (in SB6) while a minimum value of ET was observed in year 1991 (in the EB and SB1), 1985 (in SB2), 1984 (in SB3), 1989 (in SB4) and 2000 (in SB5 and 6) (Fig 5.2a-g).

The mean annual total SURFQ for EB during baseline simulation was 132.95 mm (with a range from 66.63 mm in 2004 to 232.42 mm in 1989). The mean annual total SURFQ for SB1, 2, 3, 4, 5 and 6, respectively, were has to be 61.29 mm (ranges; 0.64 mm in 1991 to 182.17 mm in 1998), 68.10 mm (ranges; 20.10 mm in 1991 to 103.33 mm in 2000), 169.14 mm (ranges; 26.43 mm in 2004 to 575.46 mm in 1989), 170.55 mm (ranges; 58.94 mm in 1990 to 453.32 mm in 1987), 125.93 mm (ranges; 52.23 mm in 2001 to 298.24 mm in 1992) and 265.56 mm (ranges; 142.35 mm in 1986 to 472.29 mm in 1997) (Fig 5.2a-g). The average annual total SW for EB during baseline simulation was 3858.50 mm (with a range from 3580.33 mm in 1990 to 4307.77 mm in 1996). The mean annual total SW for SB1, 2, 3, 4, 5 and 6, respectively, were has to be 5014.88 mm (ranges; 3723.52 mm in 1991 to 5955.33 mm in 1996), 6364.11 mm (ranges; 5877.83 mm in 1988 to 6865.42 mm in 1996), 2355.53 mm (ranges; 1943.58 mm in 2002 to 2629.19 mm in 1996), 3295.69 mm (ranges; 3003.34 mm in 1990 to 3524.64 mm in 1996), 1297.21 mm (ranges; 1030.98 mm in 2002 to 1569.44 mm in 1996) and 4856.33 mm (ranges; 4470.42 mm in 2000 to 5146.58 mm in 1990) (Fig 5.2a-g).

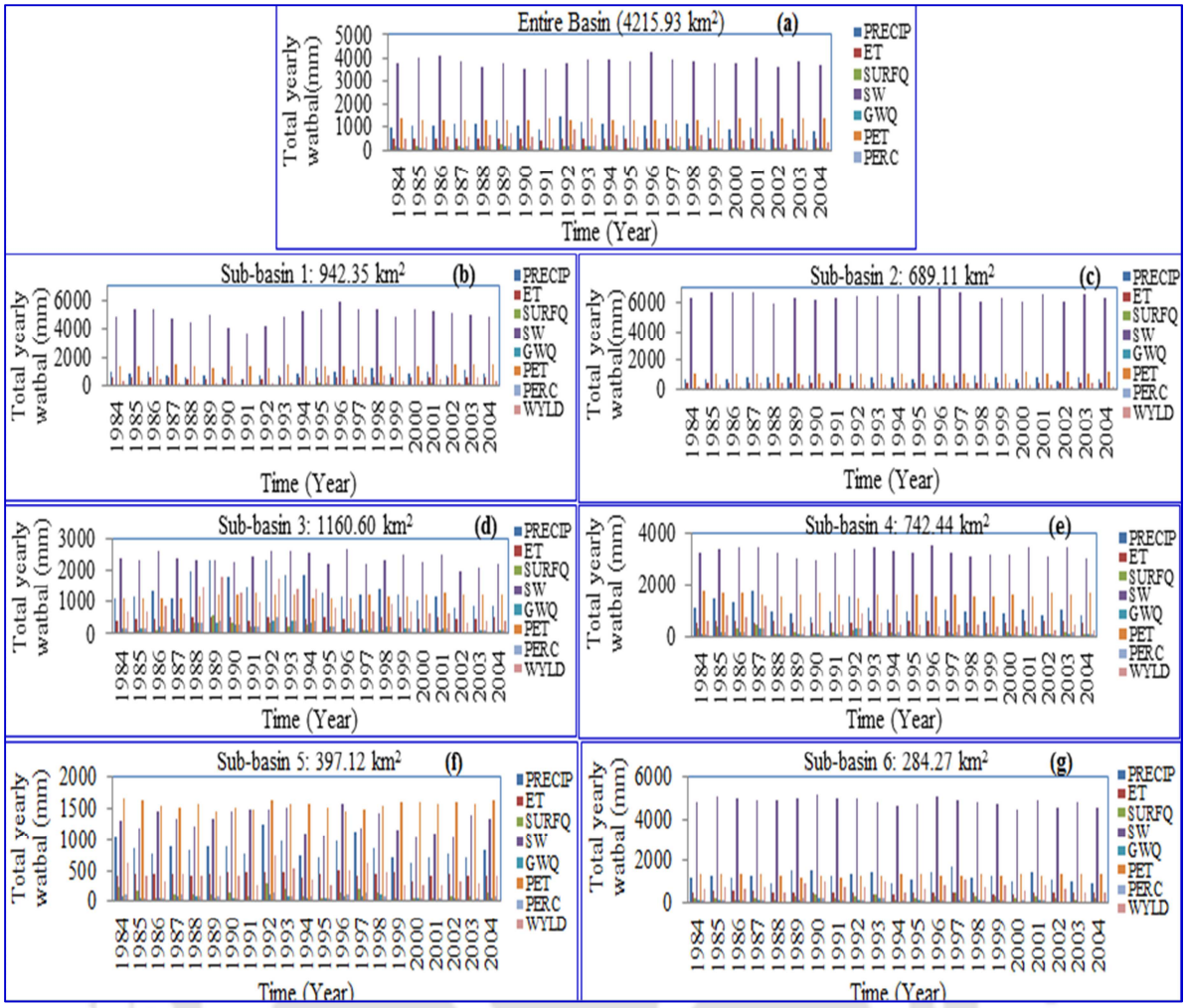

Figure 5.2a (top middle): Temporal variation of hydrological processes during base period (1984-2004) simulation for entire river basin, b (top left): same as fig 5.2a but for sub-basin 1, c (top right): same as fig 5.2a but for sub-basin 2, d (middle right): same as fig 5.2a but for sub-basin 3, e (middle left): same as fig 5.2a but for sub-basin 4, f (bottom left): same as fig 5.2a but for sub-basin 5, g (bottom right): same as fig 5.2a but for sub-basin 6

The average annual total GWQ for EB during baseline simulation was 117.94 mm with a range from 39.14 to 198.86 mm. The average total annual GWQ for SB1, 2, 3, 4, 5 and 6 were has to be 43.68 mm (ranges; 1.33 to 119.65 mm), 78.48 mm (ranges; 19.06 to 116.56 mm), 220.93 mm (ranges; 56.15 to 427.38 mm), 116.43 mm (ranges; 32.12 to 277.47 mm), 66.58 mm (ranges; 31.12 to 111.43 mm) and 125.19 mm (ranges; 65.03 to 190.34 mm) respectively. Fig 5.2a-g revealed that a maximum value of GWQ had been observed in the year 1992 (in case of EB, SB3 and SB5), 1998 (in SB1 and 2), 1987 (in SB4) and 1993 (in SB6) through a minimum value of GWQ was observed in year 2002 (in the EB and SB2, 3 and 4), 1991 (in SB1and 5) and 2004 (in SB6). The average annual total PET for EB during baseline simulation was 1333.27 mm (with a range from 1283.46 mm in 1996 to 1396.59 mm in 2002). The mean annual total PET for SB1, 2, 3, 4, 5 and 6, respectively, were has to be

1376.22 mm (ranges; 1251.25 mm in 1989 to 1492.02 mm in 2003), 1120.17 mm (ranges; 1059.99 mm in 1989 to 1189.36 mm in 2004), 1173.73 mm (ranges; 1089.70 mm in 1996 to 1279.69 mm in 1991), 1608.84 mm (ranges; 1735.98 mm in 1992 to 1470.24 mm in 1984), 1558.87 mm (ranges; 1455.56 mm in 1996 to 1668.92 mm in 1984) and 1323.53 mm (ranges; 1226.97 mm in 1989 to 1411.94 mm in 2004) (Fig 5.2a-g).

The average annual total PERC for EB during baseline simulation was 131.33 mm with a range from 52.02 to 231.51 mm. The average total annual PERC for SB1, 2, 3, 4, 5 and 6 were has to be 50.29 mm (ranges; 1.50 to 117.18 mm), 88.85 mm (ranges; 21.22 to 123.76 mm), 241.06 mm (ranges; 81.77 to 496.58 mm), 131.60 mm (ranges; 42.37 to 308.46 mm), 77.86 mm (ranges; 35.75 to 158.07 mm) and 140.20 mm (ranges; 64.65to 224.43 mm) respectively. Fig 5.2a-g revealed that a maximum value of PERC had witnessed in the year 1992 (in case of EB and SB3), 1998 (in SB1), 1994 (in SB2), 1987 (in SB4) and 1997 (in SB5 and 6) nevertheless a minimum value of PERC was observed in year 2002 (in the EB, SB3 and 4), 1991 (in SB1and 2), 1991 (in SB5) and 2004 (in SB6). The average annual total WYLD in Fig 5.2a-g for EB during baseline simulation was 553.47 mm (with a range from 281.38 mm in 2002 to 859.08 mm in 1992). The mean annual total WYLD for SB1, 2, 3, 4, 5 and 6, respectively, were has to be 327.96 mm (ranges; 84.06 mm in 1991 to 692.66 mm in 1998), 349.67 mm (ranges; 141.06 mm in 1991 to 447.90 mm in 1998), 905.79 mm (ranges; 340.75 mm in 2002 to 1800.51 mm in 1989), 491.59 mm (ranges; 196.30 mm in 2002 to 1144.88 mm in 1987), 409.00 mm (ranges; 251.67 mm in 1999 to 748.47 mm in 1992) and 753.30 mm (ranges; 493.37 mm in 2004 to 1155.82 mm in 1997).

As we can see in Fig 5.3a-d and Fig 5.4a-d, there has been observed a significant spatial and temporal variability of all the hydrological processes in Weyib River basin during baseline (1984-2004) simulation. The average total annual PRECIP was found to be higher in SB3 (1160.60 km^2) than the EB and other SBs throughout 1986-1995 time periods. However, all through 1987-2004 and in 1984 SB6 (284.27 km^2) has shown more PRECIP than the others. SB4 (742.44 km^2) has received more PRECIP than the entire river basin and other SBs in the year 1985 (Fig 5.3a).

The average annual total ET and PET were observed to be more in SB4 than the EB and other SBs throughout simulation period of 1984-2004 (Fig 5.3b and c). The average annual total SURFQ was more in SB4 during simulation period of 1984-1987 whereas in the simulation year 1988-2004 average annual total SURFQ observed to more in SB6 (Fig 5.3c) than the EB

and other SBs. From this point here, we can infer that the surface runoff production from the smaller area is more than the larger area; this is probably due to the time of concentration if other variables are assumed to be constant.

As shown in Fig 5.4a, the average annual total SW was found to be more in SB2 (having an area of 689.11 km^2) than the EB and other SBs throughout simulation periods (1984-2004). As relative to all other hydrological processes (such as PRECIP, ET, SURFQ, GWQ, PERC, PET and WYLD) magnitudes of SW for EB as well as for each SB are very high and this might be due to soil characteristics in the particular SB. Figure 5.4b and c described that in all the baseline simulation period (1984-2004) but except in the year 1987, 1997, 2002 and 2003 the mean annual total GWQ and PERC are more in SB3 than the others. In the year 1987 and 2003 SB4 has revealed more GWQ and PERC than the EB and other SBs while in the year 1997 and 2002 more GWQ and PERC have observed in S 6. The mean annual total WYLD in Fig 5.4d is found to be high in SB4 during baseline simulation (1984-1987) as relative to EB and other SBs. Between years 1988-1995 SB3 has shown relatively more WYLD than the others though in the remaining time series of baseline simulation (1996-2004) the SB6 revealed more WYLD than the EB and other SBs.

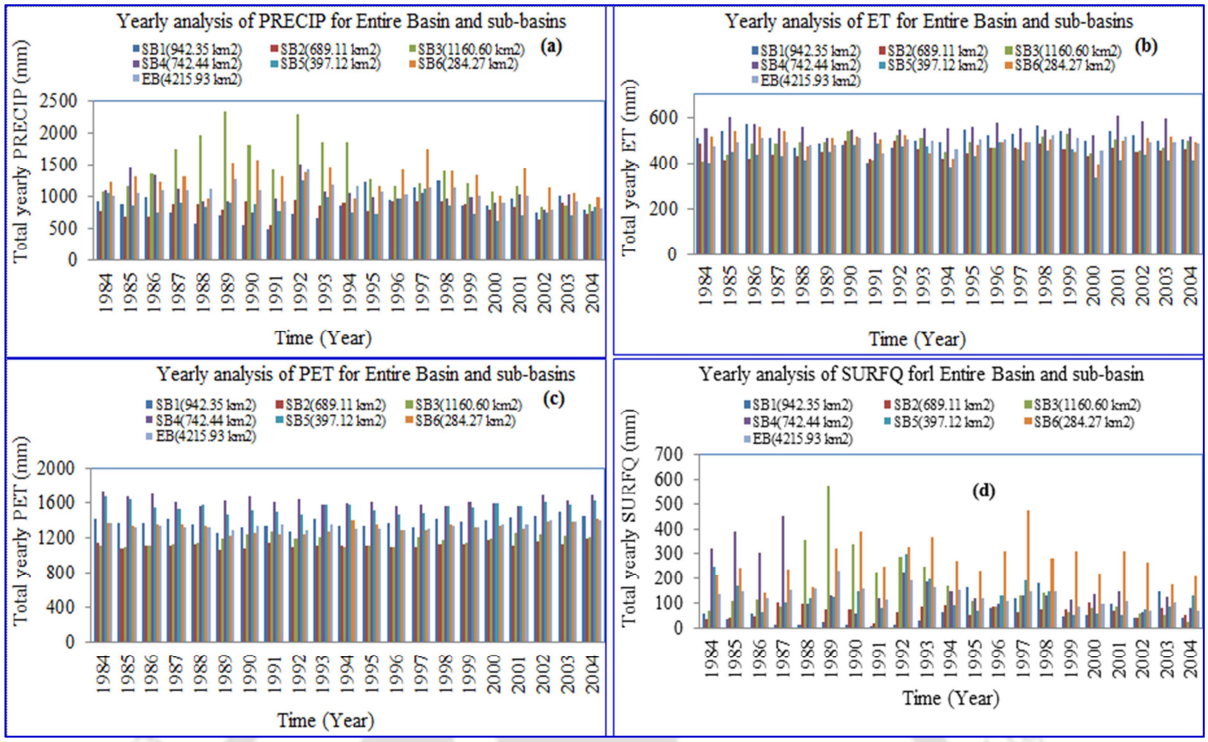

Figure 5.3a (top left): Spatial and temporal variation of total yearly precipitation (PRECIP) during baseline (1984-2004) simulation, b (top right): same as fig 5.3a but for actual evapotranspiration (ET), c (bottom left): same as fig 5.3a but for potential evapotranspiration (PET), d (bottom right): same as fig 5.3a but for surface runoff contribution to the streamflow (SURFQ)

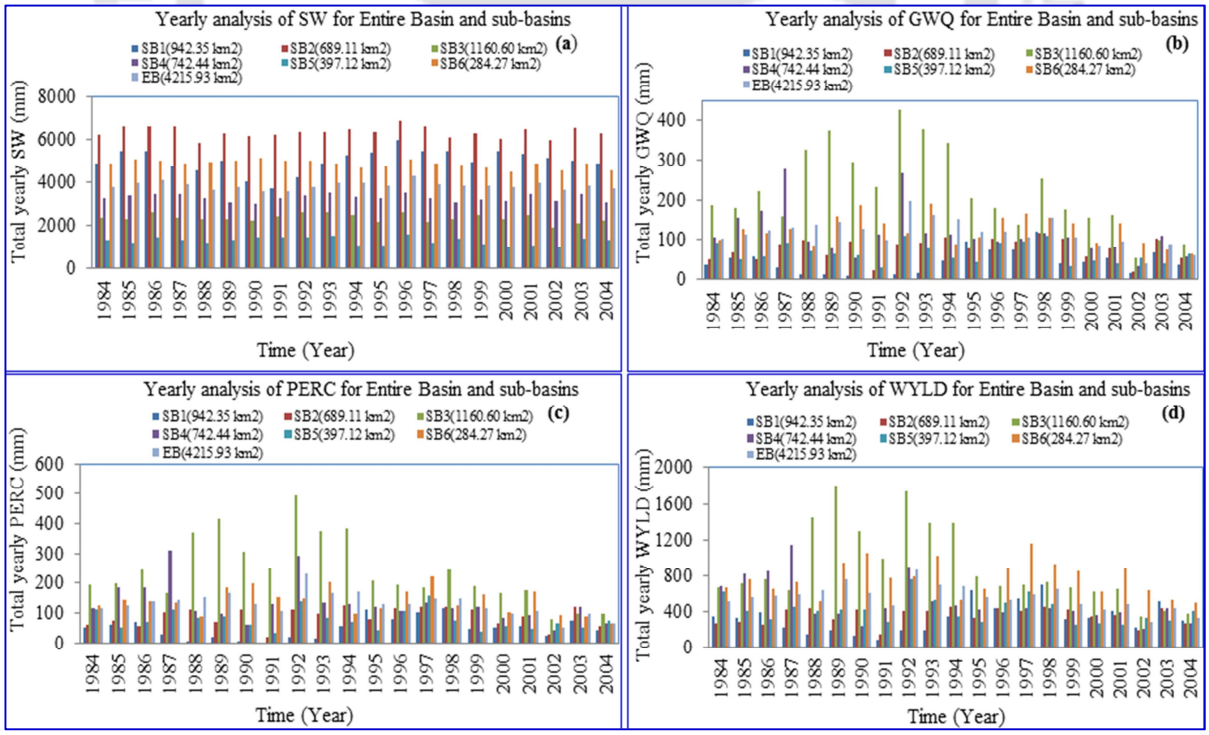

Figure 5.4a (top left): Spatial and temporal variation of total yearly soil water content (SW) during baseline (1984-2004) simulation, b (top right): same as fig 5.4a but for groundwater contribution to streamflow (GWQ), c (bottom left): same as fig 5.4a but for percolation (PERC), d (bottom right): same as fig 5.4a but for net amount of water availability (WYLD)

5.3.2. Entire river basin and sub-basin scale average annual future changes in hydrological processes under climate change scenarios

The downscaled future precipitation and both temperatures by SDSM from CMIP5-ESMs-RCPs scenario were the input variables for validated ArcSWAT model which was then used to simulate future diverse hydrological processes of the Weyib River Basin. The mean of ESMs outputs (hydrological processes) for the RCP8.5, RCP 4.5, and RCP 2.6 scenarios in annual, seasonal and monthly time scale in the 2020s, 2050s and 2080s time slices have beeb detailed in this section. *For simplicity and avoiding repetition reason results for each ESM have not included but mentioned as a mean of the ESMs with corresponding RCPs.*

As described in Table 5.1, the average SURFQ and PET will decrease in the EB and SBs in all the RCP scenarios with different magnitude. However, mean annual PRECIP, ET, GWQ, PERC, SW, and WYLD will increase with greater spatial variability in EB as well as in the SBs for all the RCP scenarios. Our ultimate goal here is to explain how climate change could affect the different hydrological processes of the Weyib River basin that control the final net water available in the stream. The actual EB and SB scale analysis of average annual simulated hydrological processes for baseline (1984-2004) and future period (2010-2100) under three RCP scenarios (for the mean of 3 ESMs) have presented in Table 5.1.

Table 5.1 Entire river basin and sub-basin scale analysis of mean annual simulated hydrological processes during baseline (1984-2004) and future period (2010-2100) simulation under Ensembles of ESMs for the RCP2.6, RCP4.5, and RCP8.5scenarios

Spatial Variation	Water Balance Components	Base Period	RCP2.6	RCP4.5	RCP8.5
Entire River Basin (4215.93 km²)	PRECIP(mm)	1061.1	1300.8	1318.4	1368.4
	ET(mm)	492.4	631	634.1	636.5
	PET(mm)	1333.2	1130.6	1140.2	1155.7
	SURFQ(mm)	132.98	36.41	39.6	48.62
	WYLD(mm)	553.46	647.86	662.01	708.24
	PERC(mm)	131.34	209.91	214.14	228.37
	GWQ(mm)	117.97	190.5	194.37	207.49
	SW(mm)	3858.50	4383.12	4384.14	4393.84
Subbasin 1 (942.35 km²)	PRECIP(mm)	850.99	1054.23	1078.50	1148.22
	ET(mm)	511.33	624.51	628.84	640.04
	PET(mm)	1376.22	1177.92	1191.57	1200.04
	SURFQ(mm)	61.29	12.31	14.79	21.93
	WYLD(mm)	327.96	410.77	429.86	485.93
	PERC(mm)	50.29	102.96	107.91	122.81
	GWQ(mm)	43.68	90.49	95.05	108.56
	SW(mm)	5014.88	5997.16	6002.62	6080.02
Subbasin 2 (689.11 km²)	PRECIP(mm)	818.39	1017.95	1030.67	1055.60
	ET(mm)	452.94	573.92	580.61	581.62
	PET(mm)	1120.17	1000.62	1000.91	1002.41
	SURFQ(mm)	68.10	21.78	28.95	32.79
	WYLD(mm)	349.67	422.66	428.46	453.40
	PERC(mm)	88.85	141.33	140.61	149.25
	GWQ(mm)	78.48	126.40	125.60	133.61
	SW(mm)	6364.11	6885.97	6893.05	6896.79
Subbasin 3 (1160.60 km²)	PRECIP(mm)	1394.35	1528.44	1539.46	1558.52
	ET(mm)	480.19	604.95	610.53	629.66
	PET(mm)	1173.73	959.58	974.16	996.76
	SURFQ(mm)	169.14	21.98	22.31	24.12
	WYLD(mm)	905.79	912.33	917.79	917.94
	PERC(mm)	241.06	305.43	306.60	305.26
	GWQ(mm)	220.93	281.78	282.68	281.17
	SW(mm)	2355.53	2708.15	2713.27	2708.63
Subbasin 4 (742.44 km²)	PRECIP(mm)	1061.96	1457.29	1486.90	1548.38
	ET(mm)	553.68	708.04	705.86	680.88
	PET(mm)	1608.84	1300.61	1313.25	1354.87
	SURFQ(mm)	170.55	67.25	72.73	94.37
	WYLD(mm)	491.59	719.82	750.81	834.77
	PERC(mm)	131.60	276.78	290.30	321.52
	GWQ(mm)	116.43	251.62	264.38	293.36
	SW(mm)	3295.69	3629.33	3619.80	3576.15
Subbasin 5 (397.12 km²)	PRECIP(mm)	853.45	1212.52	1213.32	1214.48
	ET(mm)	435.89	681.10	682.58	674.71
	PET(mm)	1558.87	1369.89	1370.19	1373.92
	SURFQ(mm)	125.93	36.40	35.93	37.12
	WYLD(mm)	409.00	516.13	518.32	524.00
	PERC(mm)	77.86	154.02	153.73	157.07
	GWQ(mm)	66.58	135.24	134.90	137.90
	SW(mm)	1297.21	1670.15	1662.16	1662.02
Subbasin 6 (284.27 km²)	PRECIP(mm)	1273.88	1589.07	1615.57	1827.26
	ET(mm)	494.22	625.83	621.29	621.40
	PET(mm)	1323.53	1207.78	1212.11	1214.42
	SURFQ(mm)	265.56	91.90	97.62	129.67
	WYLD(mm)	753.30	924.98	954.65	1159.51
	PERC(mm)	140.20	255.96	264.23	322.72
	GWQ(mm)	125.19	233.50	241.02	296.23
	SW(mm)	4856.33	5253.05	5248.27	5254.97

In the EB, the mean annual SURFQ and PET were decreased, respectively, by 63.44 and 13.31% (RCP8.5), 70.22 and 14.48% (RCP4.5) and 72.62 and 15.20% (RCP2.6). However, the mean annual PRECIP, ET, NWYLD, PERC, GWQ, and SW were observed to increase, respectively, by 28.96, 29.26, 27.97, 73.88, 75.88 and 13.87% for the RCP8.5 scenario, 24.45, 28.78, 19.61, 63.04, 64.76 and 13.62% for the RCP4.5 scenario and 22.59, 28.15, 17.06, 59.82, 61.48 and 13.60% for the RCP2.6 scenario (Fig 5.5a and Table 5.1). In the SB1,

the mean annual SURFQ and PET were decreased, respectively, by 64.22 and 12.80% (RCP8.5), 75.87 and 13.42% (RCP4.5) and 79.92 and 14.41% (RCP2.6). However, the mean annual PRECIP, ET, NWYLD, PERC, GWQ, and SW were observed to increase, respectively, by 34.93, 25.17, 48.17, 144.20, 148.53 and 21.24% for the RCP8.5 scenario, 26.73, 22.98, 31.07, 114.58, 117.61 and 19.70% for the RCP4.5 scenario and 23.88, 22.13, 25.25, 104.73, 107.17 and 19.59% for the RCP2.6 scenario (Fig 5.5b and Table 5.1).

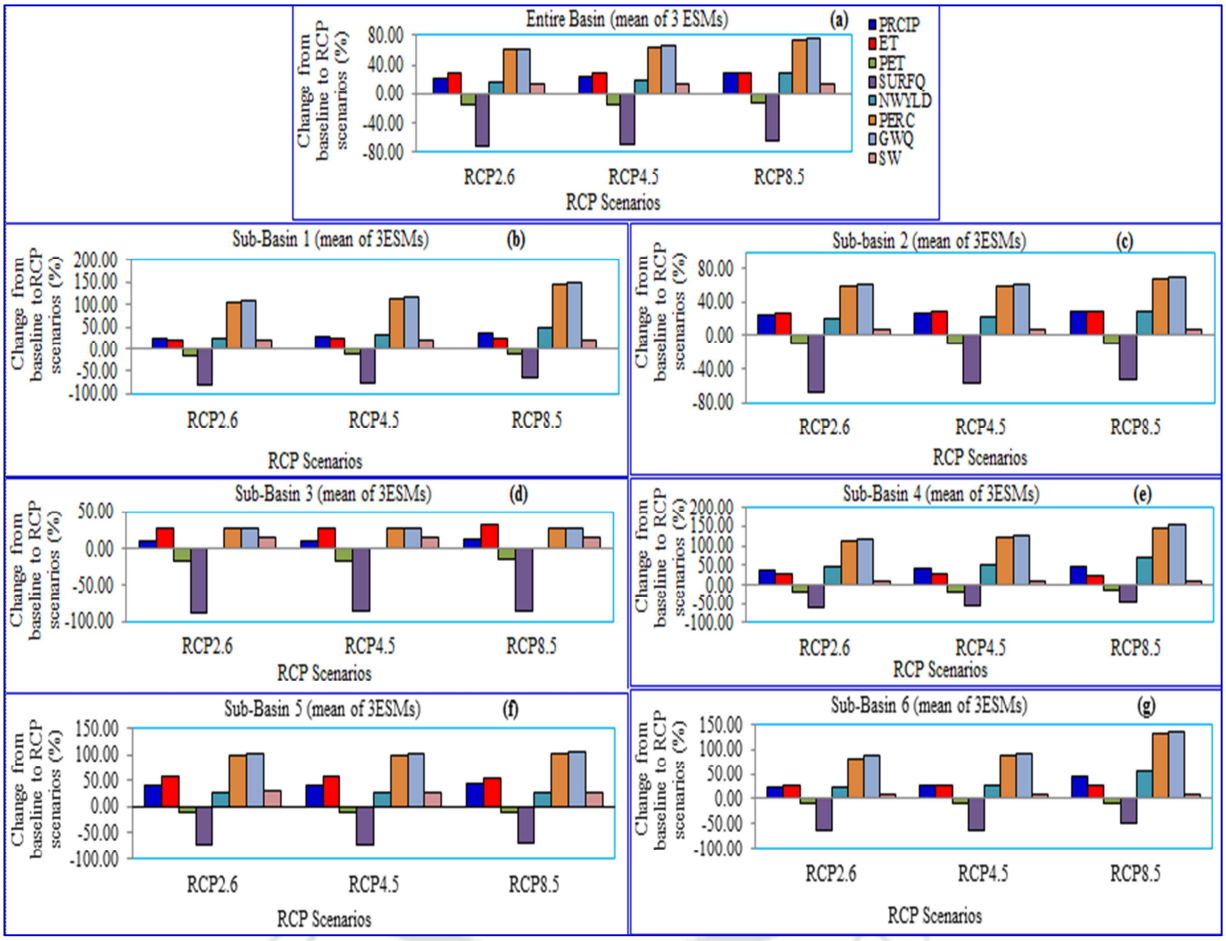

Figure 5.5a (top center): Percentage change from baseline simulation in the mean of three ESMs hydrological processes for the three RCP scenarios in the entire river basin, b (top left): same as fig 5.5a but for sub-basin 1, c (top right): same as fig 5.5a but for sub-basin 2, d (middle left): same as fig 5.5a but for sub-basin 3, e (middle right): same as fig 5.5a but for sub-basin 4, f (bottom left): same as fig 5.5a but for sub-basin 5, g (bottom right): same as fig 5.5a but for sub-basin 6. Legend given in (a) is the same as in all figures

In the SB2, the mean annual SURFQ and PET were decreased, respectively, by 51.85 and 10.51% (RCP8.5), 57.49 and 10.65% (RCP4.5) and 68.02 and 10.67% (RCP2.6). However, the mean annual PRECIP, ET, NWYLD, PERC, GWQ, and SW were observed to increase, respectively, by 28.98, 28.41, 29.67, 67.98, 70.25 and 8.37% for the RCP8.5 scenario, 25.94, 28.19, 22.53, 58.62, 60.04 and 8.31% for the RCP4.5 scenario and 24.38, 26.71, 20.87, 59.07, 61.06 and 8.20% for the RCP2.6 scenario (Fig 5.5c and Table 5.1). In the SB3, the mean

annual SURFQ and PET were decreased, respectively, by 85.74 and 15.08% (RCP8.5), 86.81 and 17.00% (RCP4.5) and 87.00 and 18.25% (RCP2.6). However, the mean annual PRECIP, ET, NWYLD, PERC, GWQ, and SW were observed to increase, respectively, by 11.77, 31.13, 1.34, 26.63, 27.27 and 14.99% for the RCP8.5 scenario, 10.41, 27.14, 1.32, 27.19, 27.95 and 15.19% for the RCP4.5 scenario and 9.62, 25.98, 0.72, 26.70, 27.54 and 14.97% for the RCP2.6 scenario (Fig 5.5d and Table 5.1).

In the SB4, the mean annual SURFQ and PET were decreased, respectively, by 44.67 and 15.79% (RCP8.5), 57.36 and 18.37% (RCP4.5) and 60.57 and 19.61% (RCP2.6). However, the mean annual PRECIP, ET, NWYLD, PERC, GWQ, and SW were observed to increase, respectively, by 45.80, 22.97, 69.81, 144.32, 151.96 and 8.51% for the RCP8.5 scenario, 40.01, 27.49, 52.73, 120.59, 127.07 and 9.83% for the RCP4.5 scenario and 37.23, 27.88, 46.43, 110.32, 116.11 and 10.12% for the RCP2.6 scenario (Fig 5.5e). In the SB5, the mean annual SURFQ and PET were decreased, respectively, by 70.52 and 11.86% (RCP8.5), 71.47 and 12.10% (RCP4.5) and 71.10 and 12.12% (RCP2.6). However, the mean annual PRECIP, ET, NWYLD, PERC, GWQ, and SW were observed to increase, respectively, by 42.30, 54.79, 28.12, 101.73, 107.12 and 28.12% for the RCP8.5 scenario, 42.17, 56.59, 26.73, 97.44, 102.61 and 28.13% for the RCP4.5 scenario and 42.07, 56.26, 26.19, 97.82, 103.12 and 28.75% for the RCP2.6 scenario (Fig 5.5f). In the SB6, the mean annual SURFQ and PET were decreased, respectively, by 51.17 and 8.24% (RCP8.5), 63.24 and 8.42% (RCP4.5) and 65.39 and 8.75% (RCP2.6). However, the mean annual PRECIP, ET, NWYLD, PERC, GWQ, and SW were observed to increase, respectively, by 43.44, 25.73, 53.92, 130.19, 136.62 and 8.21% for the RCP8.5 scenario, 26.82, 25.71, 26.73, 88.47, 92.52 and 8.07% for the RCP4.5 scenario and 24.74, 26.63, 22.79, 82.57, 86.52 and 8.17% for the RCP2.6 scenario (Fig 5.5g and Table 5.1).

5.3.3. Entire river basin and sub-basin scale mean monthly and seasonal future changes net water availability under climate change scenarios

The average ensembles of three Earth System Models (ESMs) outputs (net water available in the stream) for the RCP8.5, RCP4.5 and RCP 2.6 scenarios in monthly and seasonal time scale (in the 2020s, 2050s and 2080s time slice) for entire river basin and for all six sub-basins have been presented in this section.

A. The Entire River Basin (4215.93 km^2)

i. Surface runoff

The absolute change in mean daily surface runoff (mm) for upcoming periods (in each time slice of 2020s, 2050s and 2080s) under each RCP (RCP8.5, RCP4.5 and RCP2.6) scenarios have shown a decrease in every months and seasons as compare to the baseline (1984 2004) simulation (Fig 5.6a-c). Double peaking in surface runoff contribution to streamflow was observed on the months of Apr and Aug. The seasonal mean daily surface runoff (mm) decrease in dry season (for example, in the month of Nov, Dec, Jan and Feb) by 0.16mm (100.00%), 0.16mm (100.00%), 0.16mm (100.00%), and 0.12mm (84.67%), 0.16mm (100.00%), 0.15mm (99.47%) and 0.16mm (100.00%), 0.16mm (100.00%), 0.16mm (100.00%) in the 2020s, 2050s and 2080s for the RCP2.6, RCP4.5 and RCP8.5 scenarios respectively, and in an intermediate season (Mar, Apr, May and Jun) by 0.27mm (81.94%), 0.25mm (70.52%), 0.25mm (67.08%) and 0.27mm (79.57%), 0.26mm (73.27%), 0.22mm (51.13%) and 0.26mm (79.75%), 0.24mm (69.24%), 0.16mm (26.00%) in the 2020s, 2050s and 2080s for the RCP2.6, RCP4.5 and RCP8.5 scenarios respectively and Wet season (Jul, Aug, Sept and Oct) by 0.41mm (74.81%), 0.39mm (71.34%), 0.43mm (78.55%), and 0.42mm (76.46%), 0.39mm (69.96%), 0.39mm (70.25%) and 0.41mm (73.69%), 0.39mm (69.50%), 0.30mm (53.69%) in the 2020s, 2050s and 2080s for the RCP2.6, RCP4.5 and RCP8.5 scenarios respectively (Fig 5.6a-c).

ii. Lateral flow

Regarding to particular months absolute shift in monthly mean daily lateral flow (mm) between the baseline period and future time periods for the RCP2.6 scenario has shown a decrease in months of Jan and Feb (2020s time slice), Nov (in all the time slice) and Dec (in all the time slice) and an increase in the rest of the months and future time slices was observed (Fig 5.6d). The difference in monthly lateral flow was insignificant for the month of Jan (in the 2050s and 2080 time slice) in the RCP2.6 scenario. While in the case of RCP4.5, a decrease in the months of Jan and Feb (in the 2020s time slice), Nov (in the entire time slice) and Dec (in the entire time slice) and an increment on the rest of the months and future time slices was observed (Fig 5.6e). The variance in monthly lateral flow was insignificant for the month of Jan (in the 2050s and 2080 time slice) for the RCP4.5 scenario. In the case of very high emission level (RCP8.5), there has been a decrease of lateral flow for the months of Jan and Feb (in the 2020s time slice), Nov (in the entire time slice) and Dec (in the 2020s and

2050s time slice) and an increase in the rest of the months and future time slices was observed (Fig 5.6f). As compared to the base period, the variance in monthly lateral flow was minor for the month of Jan (in the 2050s time slice) and Dec (in the 2080s time slice) for the RCP8.5 scenario. Double peaking in lateral soil flow has observed in the months of Apr and Sep.

The seasonal mean daily lateral flow in Fig 5.6d-f might be decrease in dry season by 0.11mm (39.55%), 0.08mm (22.51%), 0.08mm (18.29%), and 0.10mm (34.84%), 0.10mm (28.72%), 0.06mm (8.45%) and 0.09mm (32.48%), 0.07mm (16.37%), 0.07mm (+41.54%) in the 2020s, 2050s and 2080s for the RCP2.6, RCP4.5 and RCP8.5 scenarios respectively, and increase in an intermediate season by 0.36mm (35.02%), 0.51mm (65.66%), 0.55mm (84.84%), and 0.37mm (35.88%), 0.52mm (66.30%), 0.60mm (94.41%) and 0.43mm (42.69%), 0.57mm (75.75%), 0.79mm (125.80%) in the 2020s, 2050s and 2080s for the RCP2.6, RCP4.5 and RCP8.5 scenarios respectively and wet seasons by 0.68mm (51.40%), 0.61mm (46.55%), 0.49mm (38.01%), and 0.68mm (51.70%), 0.64mm (49.56%), 0.55mm (42.55%) and 0.75mm (57.52%), 0.62mm (48.09%), 0.63mm (48.90%) in the 2020s, 2050s and 2080s for the RCP2.6, RCP4.5, and RCP8.5 scenarios respectively. Likewise, the mean annual percentage change from base period of lateral flow found to be increased by 15.62%, 29.90%, 34.86%, and 17.58%, 29.04%, 42.83% and 22.58%, 35.82%, 72.08% in the 2020s, 2050s, and 2080s in the RCP2.6, RCP4.5, and RCP8.5 scenarios respectively. Results indicate that there has been high monthly and seasonal variation of lateral flow as compared to the annual variation for all the three RCP scenarios and future time slices.

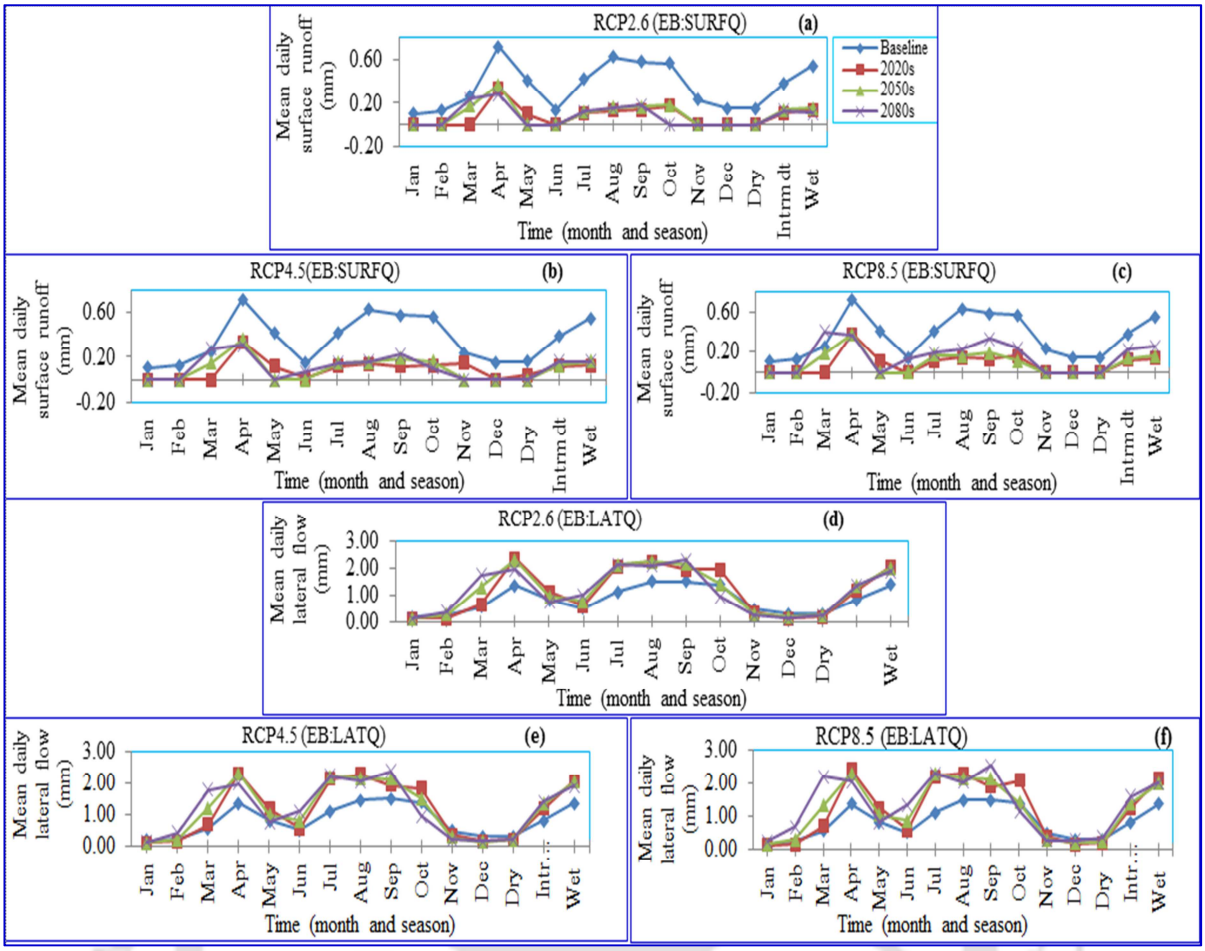

Figure 5.6a (top center): Entire river basin surface runoff (monthly and seasonal mean daily) during baseline (1984-2004) simulation and three future time slice under mean of 3 ESMs for the RCP2.6 scenario, b (top left): same as fig 5.6a but for RCP4.5 scenario, c (top right): same as fig 5.6a but for RCP8.5 scenario, d (middle center): same as fig 5.6a but for lateral flow RCP 2.6 scenario, e (bottom left): same as fig 5.6d but RCP4.5 scenario, f (bottom right): same as fig 5.6d but RCP8.5 scenario. Legend given in (a) is the same in all figures

iii. Groundwater flow

The absolute variation in monthly mean daily groundwater flow (mm) between the baseline period and future time periods for the RCP2.6 scenario has shown a decrease in months of Jan (in the 2080s time slice), Feb (in all the time slice) and Dec (in the 2080s time slice) and an increase in the rest of the months and future time slices was observed (Fig 5.7a). The difference in monthly groundwater flow was insignificant in the month of Dec (in the 2050s time slice) in the RCP2.6 scenario. While in the case of RCP4.5, a decrease in the months of Jan (in the 2050s and 2080s time slice), Feb (in the entire time slice) and Dec (in the 2080s time slice) and an increment on the rest of the months and future time slices was observed (Fig 5.7b). The variance in monthly groundwater flow was insignificant for the month of Jan (in the 2020s time slice) in the RCP4.5 scenario. In the case of very high emission level (RCP8.5), there has been a decrease of groundwater flow for the months of Jan (in the 2050s

time slice) and Feb (in the 2020s time slice) and an increase in the rest of the months and future time slices was observed (Fig 5.7c). As compared to the base period, the variance in monthly groundwater flow was minor for the month of Jan (in the 2020s and 2080s time slice), Feb (in the 2050s and 2080s time slice) and Dec (in the 2050s and 2080s time slice) for the RCP8.5 scenario. Double peaking in groundwater contribution to streamflow has observed in the months of May and Oct.

As explained in Fig 5.7a-c, the seasonal mean daily groundwater flow might be decrease in dry season (in the 2050s and 2080s time slice) for the three RCP scenarios but rises as compared to baseline scenario in the 2020s time slice. Mean daily groundwater flow increase in an intermediate season by 0.14mm (72.59%), 0.21mm (120.88%), 0.26mm (132.84%), and 0.15mm (75.85%), 0.21mm (117.59%), 0.27mm (139.08%) and 0.17mm (87.32%), 0.23mm (129.03%), 0.36mm (191.69%) in the 2020s, 2050s and 2080s for the RCP2.6, RCP4.5 and RCP8.5 scenarios respectively and wet seasons by 0.36mm (85.81%), 0.39mm (94.87%), 0.38mm (92.80%), and 0.38mm (89.55%), 0.41 mm (98.91%), 0.42mm (103.47%) and 0.40mm (96.85%), 0.41mm (102.11%), 0.49mm (121.44%) in the 2020s, 2050s and 2080s in the RCP2.6, RCP4.5 and RCP8.5 scenarios respectively.

iv. Net water resources availability

The net water availability of river catchment is estimated (Arnold et al., 2012) as the summation of surface runoff, lateral flow and groundwater flow minus losses (amount of water losses from tributaries by transmission). It is one of the supreme significant parameters to be studied for the sustainable water management (Adeogun et al., 2014).

Regarding to particular months absolute shift in monthly mean daily net water availability in upcoming periods in the EB for the RCP2.6 scenario has shown a decrease in months of Jan, Nov and Dec (in all the time slice) and Oct (in the 2050s and 2080s time slice) and an increase in the rest of the months and future time slices was observed (Fig 5.7d). The difference in monthly water availability was insignificant for the month of Feb and May in the RCP2.6 scenario. While in the case of RCP4.5, a decrease in the months of Jan (in all the time slice), Feb (in the 2020s and 2050s time slice), Oct (in the 2080s time slice), Nov (in the 2080s time slice) and Dec (in all the time slice) and an increment on the rest of the months and future time slices was observed (Fig 5.7e). The variance in monthly water availability was insignificant for the month of Feb (in the 2080s time slice), Mar (in the 2020s time slice),

May (in the 2080s time slice), and Nov (in the 2020s and 2050s time slice) for the RCP4.5 scenario.

In case of RCP8.5, there has been a decrease of net water availability in the EB on the months of Jan (in the 2020s and 2050s time slice) and Feb (in the 2020s and 2050s time slice and Dec (in all the time slice) and an increase in the rest of the months and future time slices was observed (Fig 5.7f). As compared to base period, the variance in monthly net water availability was minor for the month of Jan (in the 2080s time slice), Feb (in the 2050s time slice), Mar (in the 2020s time slice), May (in the 2080s time slice), Oct (in the 2050s and 2080s time slice) and Nov (in the entire time slice) in the RCP8.5 scenario. The double peaking in net water availability has observed in the months of Apr and Sep.

As revealed in Fig 5.7d-f, the future seasonal average daily net water availability might be decrease in dry season (Nov, Dec, Jan and Feb) by 0.20mm (29.58%), 0.26mm (33.81%), and 0.26 mm (34.17%) (RCP2.6), and 0.15mm (29.92%), 0.19mm (30.60%), 0.22mm (26.96%) (RCP4.5) and 0.12mm (25.94%), 0.18mm (26.10%), 0.01mm (+9.67%) (RCP8.5) in the 2020s, 2050s and 2080s respectively, but increase in intermediate season (Mar, Apr, May and Jun) by 0.47mm (36.73%), 0.55mm (51.74%), 0.53mm (49.75%) (RCP2.6), and 0.25mm (12.94%), 0.49mm (38.06%), 0.63mm (60.39%) (RCP4.5) and 0.34mm (19.48%), 0.59mm (47.16%), 0.98mm (91.69%) (RCP8.5) in the 2020s, 2050s and 2080s respectively as well as increase in wet seasons (Jul, Aug, Sept and Oct) by 0.61mm (28.31%), 0.46mm (22.53%), 0.47mm (22.47%) (RCP2.6), and 0.63 mm (28.92%), 0.66mm (30.90%), 0.57mm (27.76%) (RCP4.5) and 0.75mm (33.99%), 0.64mm (30.67%), 0.82mm (38.12%) under RCP8.5 scenario in the 2020s, 2050s and 2080s respectively. As we can see from the results above that there has been observed high monthly and seasonal variation of water availability as compared to the annual variation for all the three RCP scenarios and upcoming time slices.

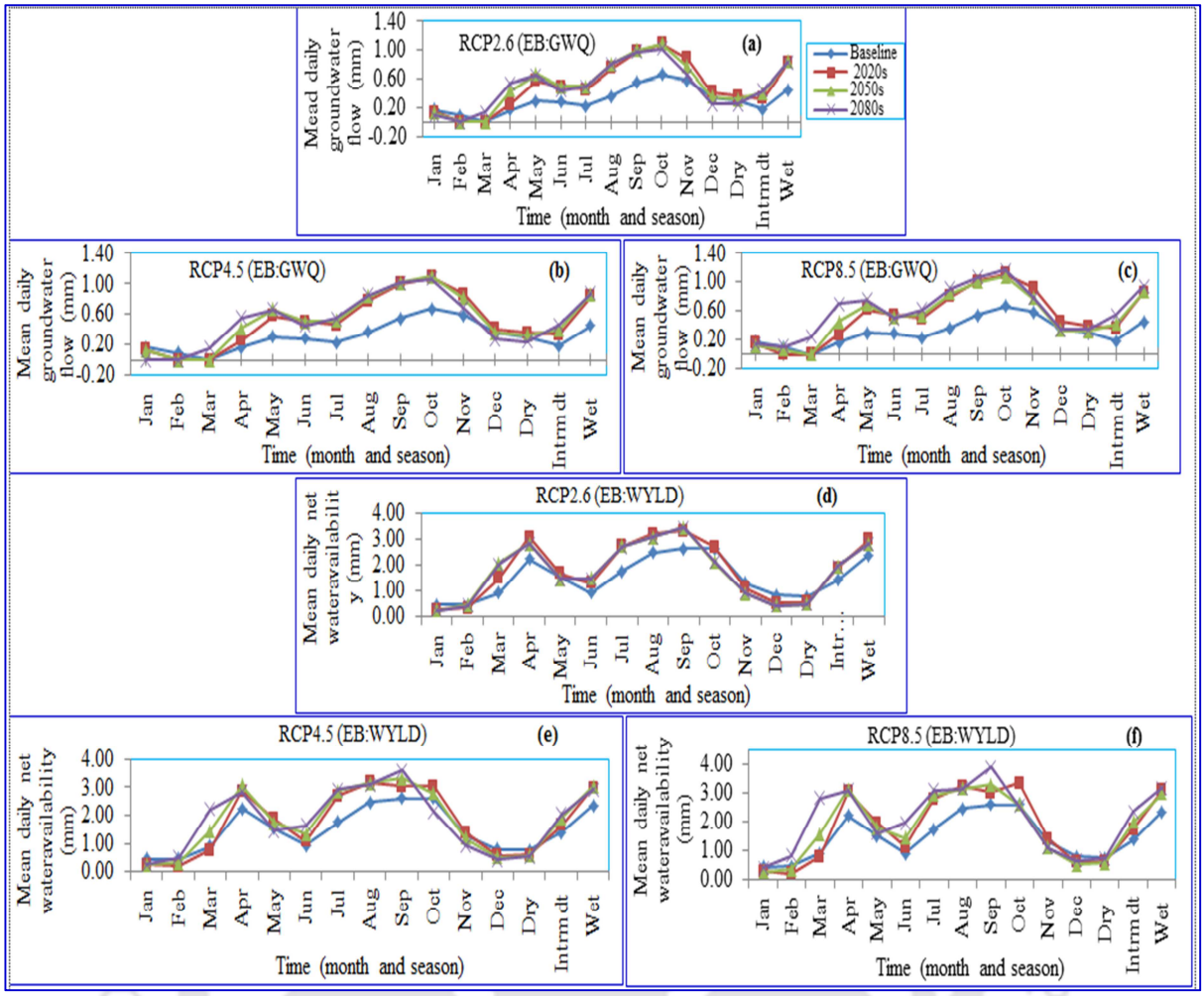

Figure 5.7a (top center): Entire river basin groundwater flow (monthly and seasonal mean daily) during baseline (1984-2004) simulation and three future time slice under mean of 3 ESMs for theRCP2.6 scenario, b (top left): same as fig 5.7a but for RCP4.5 scenario, c (top right): same as fig 5.7a but for RCP8.5 scenario, d (middle center): same as fig 5.7a but for net water availability RCP 2.6 scenario, e (bottom left): same as fig 5.7d but RCP4.5 scenario, f (bottom right): same as fig 5.7d but RCP8.5 scenario. Legend given in (a) is the same in all figures

B. The Sub-basin 1 (942.35 km^2)

The absolute change in monthly mean daily net water availability in upcoming periods for SB1 in the RCP2.6 scenario has shown a decrease in months of Jan, Feb, Nov and Dec (in all the time slice), Mar (2020s time slice) and Oct (in the 2050s and 2080s time slice) and an increase in the rest of the months and future time slices was observed (Fig 5.8a). The difference in monthly water availability was insignificant for the month of Oct (2020s time slice) for the RCP2.6 scenario. While in case of RCP4.5, a decrease in the months of Jan, Nov and Dec (in the entire time slice), Feb (in the 2020s and 2050s time slice) and Oct (in the 2050s and 2080s time slice) and an increment on the rest of the months and future time slices was observed (Fig 5.8b). The variance in monthly water availability was insignificant for the

months of Feb (at the 2080s time slice) and Oct (in the 2020s time slice) in the RCP4.5 scenario. In case of RCP8.5, there has been a decrease of net water availability for the months of Jan, Nov and Dec (in all the time slice), Feb (in the 2020s and 2050s time slice) and Oct (in the 2050s and 2080s time slice) and an increase in the rest of the months and future time slices was observed (Fig 5.8c).

As compared to the base period simulation, the variance in monthly net water availability was minor in the month of Mar (in the 2020s time slice), Aug (in the 2080s time slice) and Sep (in the 2050s and 2080s time slice) in the RCP8.5 scenario. As we can see in Fig 5.8d, there has been shown that an increasing trend of net water availability in all months and seasons for all the RCP scenarios, except in the months of Jan, Feb, Oct, Nov and Dec and Dry season which experiences a decreasing trend. The double peaking in net water availability ensues in Apr and Jul.

As revealed in Fig 5.8a-d, the future seasonal average daily net water availability might be decrease in dry season by 0.40mm (64.93%), 0.41mm (62.95%), and 0.42mm (62.90%) (RCP2.6), and 0.39mm (64.02%), 0.41mm (63.47%), 0.41mm (57.33%) (RCP4.5) and 0.37mm (61.75%), 0.40mm (58.91%), 0.23 mm (4.86%) (RCP8.5) in the 2020s, 2050s and 2080s respectively, but increase in intermediate season by 0.32mm (45.56%), 0.66mm (115.49%), 0.66mm (130.24%) (RCP2.6), and 0.27mm (37.26%), 0.69mm (121.36%), 0.99mm (207.13%) (RCP4.5) and 0.46mm (70.86%), 0.94mm (168.49%), 1.74mm (356.92%) (RCP8.5) in the 2020s, 2050s and 2080s respectively as well as increase in wet seasons by 0.70mm (52.22%), 0.60mm (46.33%), 0.33mm (26.85%) (RCP2.6), and 0.70mm (52.20%), 0.63mm (49.04%), 0.47mm (38.58%) (RCP4.5) and 0.86mm (64.21%), 0.62mm (50.04%), 0.30mm (27.94%) under RCP8.5 scenario in the 2020s, 2050s and 2080s respectively.

C. The Sub-basin 2 (689.11 km^2)

The absolute change in monthly mean daily net water availability in upcoming periods for SB2 in the RCP2.6 scenario has shown a decrease in months of Jan and Dec (in all the time slice), Feb (in the 2020s and 2050s time slice), Mar (in the 2020s time slice), Apr (in the 2080s time slice) and Nov (in the 2080s time slice) and an increase in the rest of the months and future time slices was observed (Fig 5.9a). The difference in monthly net water availability was insignificant for the month of Feb (in the 2080s time slice), Mar (in the

2050s time slice), Apr (in the 2020s and 2050s time slice), Mar (in the 2020s, 2050s, and 2080s time slice) and Nov (in the 2050s time slice) for the RCP2.6 scenario. While in case of RCP4.5, a decrease in the months of Jan, Feb, and Dec (in the entire time slice), Mar (in the 2020s time slice), Apr, May and Nov (in the 2080s time slice) and an increment on the rest of the months and future time slices has observed (Fig 5.9b).

The variance in monthly water availability was insignificant in the months of Mar (in the 2050s time slice), Apr and May (in the 2020s and 2050s time slice), Jun (in the 2020s time slice) and Sep (in the 2050s time slice) in the RCP4.5 scenario. In case of RCP8.5, there has been observed a decrease of net water availability for the months of Jan and Feb (in the 2020s and 2050s time slice), Mar (in the 2020s time slice), Apr (in the 2080s time slice) and Dec (in the 2050s time slice) and an increase in the rest of the months and future time slices was observed (Fig 5.9c). As compared to base period simulation, the variance in monthly net water availability was very minor for the month of Jan and Feb (in the 2080s time slice), Mar (in the 2050s time slice), Apr (in the 2020s and 2050s time slice), May and Sep (in the 2050s and 2080s time slice) and Dec (in the 2020s and 2080s time slice) in the RCP8.5 scenario. As we can see in Fig 5.9d there has been shown a significant increasing trend of net water availability for all the RCP scenarios in the months of Jun-Nov and dry season; a decreasing trend has observed otherwise.The double peaking in net water availability found in the months of Apr and Aug.

The future seasonal average daily net water availability might be decrease in dry season, except in the 2020s time slice (RCP4.5) and 2020s and 2080s time slice (RCP8.5), by 0.02mm (16.85%), 0.08mm (20.56%), and 0.16mm (33.88%) (RCP2.6) in 2020s, 2050s and 2080s time slice respectively, and 0.07mm (5.27%) and 0.11mm (21.47%) (RCP4.5) in the 2050s and 2080s time slice respectively and 0.01mm (13.25%) (RCP8.5) in the 2050s, but increase in intermediate season (except RCP2.6, 4.5 and 8.5 in the 2020s time slice) by 0.05mm (9.71%) and 0.11mm (26.93%) (RCP2.6), and 0.06mm (10.95%) and 0.05mm (17.21%) (RCP4.5) and 0.02mm (7.15%) and 0.10mm (25.71%) (RCP8.5) in the 2050s and 2080s respectively as well as increase in wet seasons by 0.61mm (39.64%), 0.69mm (46.84%), 0.62mm (45.06%) (RCP2.6), and 0.50mm (32.93%), 0.65mm (44.54%), 0.57mm (41.83%) (RCP4.5) and 0.68mm (42.24%), 0.62mm (43.84%), 0.89mm (61.64%) under RCP8.5 scenario in the 2020s, 2050s and 2080s respectively (Fig 5.9a-d).

D. The Sub-basin 3 (1160.60 km^2)

The absolute change in monthly mean daily net water availability in upcoming periods for SB3 in the RCP2.6 scenario has shown a decrease in months of Jan, Feb, Apr, May and Dec (in all the time slice), Mar (2020s time slice), Oct and Nov (in the 2080s time slice) and an increase in the rest of the months and future time slices was observed (Fig 5.10a). The difference in monthly water availability was insignificant in the month of Jun (in the 2020s time slice), Aug (in the 2050s and 2080s time slice), Oct (in the 2050s time slice) and Nov (in the 2020s and 2050s time slice) in the RCP2.6 scenario. While in case of RCP4.5, a decrease in the months of Jan, Apr and Dec (in the entire time slice), Feb (in the 2020s and 2050s time slice), Mar (in the 2020s time slice), May and Nov (in the 2080s time slice) and an increment on the rest of the months and future time slices was observed (Fig 5.10b). The variance in monthly net water availability was insignificant for the months of Feb (in the 2080s time slice), May (in the 2020s and 2050s time slice), Jun (in the 2020s time slice), Aug (in the 2080s time slice), Oct (in the 2050s time slice) and Nov (in the 2020s and 2050s time slice) in the RCP4.5 scenario. In case of RCP8.5, there has been observed a decrease of net water availability for the months of Jan, Apr, May and Dec (in the entire time slice), Feb (in the 2020s and 2050s time slice), Mar (in the 2020s time slice), Aug (2080s time slice) and Nov (in the 2050s and 2080s time slice) and an increase in the rest of the months and future time slices (Fig 5.10c).

As compared to the base period simulation, the variance in monthly net water availability was minor in the month of Jun and Sep (in the 2020s time slice), Oct (in the 2050s time slice) and Nov (in the 2020s time slice) in the RCP8.5 scenario. There has shown an increasing trend of net water availability in monsoon season (JASO) for all the RCP scenarios, but decreasing has found in the dry season (NDJF), and no clear signal has observed in an intermediate season (MAMJ) (Fig 5.10d). The double peaking in net water availability ensues in the months of Apr and Aug.

Figure 5.10a-d explained that the future seasonal average daily net water availability might be decrease in dry season by 0.24mm (36.09%), 0.32mm (39.72%) and 0.41mm (41.45%) (RCP2.6), 0.26mm (37.07%), 0.31mm (38.54%) and 0.39mm (38.66%) (RCP4.5) and 0.22mm (33.44%), 0.36mm (42.59%) and 0.29mm (28.34%) (RCP8.5) in the 2020s, 2050s and 2080s respectively, but increase in intermediate season (except RCP2.6, 4.5 and 8.5 in 2020s time slice) by 0.08mm (4.18%) and 0.14mm (21.52%) (RCP2.6), 0.05mm (10.81%) and 0.07mm (17.37%) (RCP4.5), and 0.00mm (9.32%) and 0.07mm (19.05%) (RCP8.5) in the 2050s and 2080s respectively as well as increase in wet seasons by 0.63mm (15.48%), 0.40mm (9.96%) and 0.27mm (7.87%) (RCP2.6), 0.55mm (13.70%), 0.49mm (12.61%) and 0.23mm (6.89%) (RCP4.5) and 0.70mm (17.07%), 0.28mm (7.00%) and 0.32mm (8.85%) for the RCP8.5 scenario in the 2020s, 2050s and 2080s respectively.

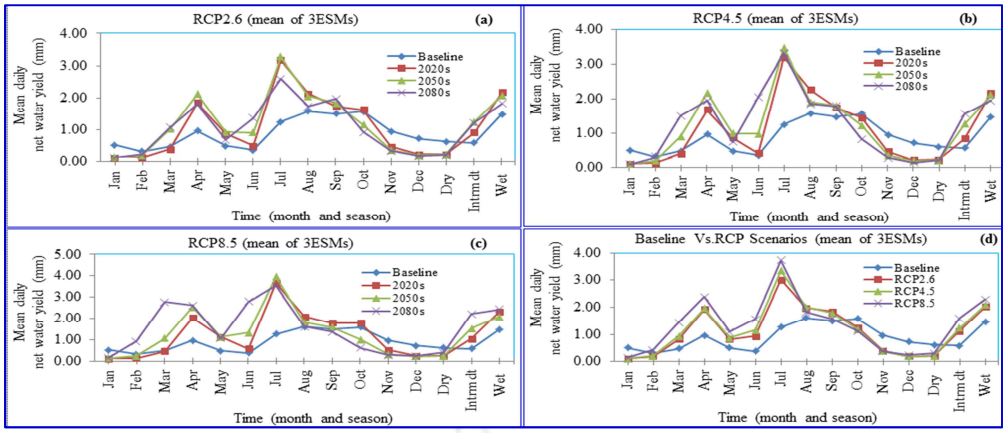

Figure 5.8a (top left): Sub-basin 1 water availability (monthly and seasonal mean daily) during baseline (1984-2004) simulation and three future time slice under mean of 3 ESMs for RCP2.6 scenario, b (top right): same as fig 5.8a but for RCP4.5 scenario, c (bottom left): same as fig 5.8a but for RCP8.5 scenario, d (bottom right): same as fig 5.8a but without time slice under RCP2.6, RCP4.5 and RCP8.5 scenarios

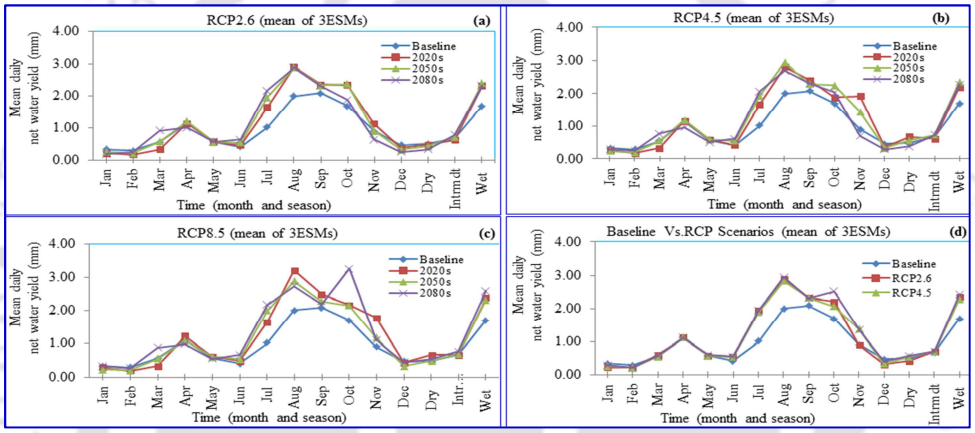

Figure 5.9a (top left): Sub-basin 2 water availability (monthly and seasonal mean daily) during baseline (1984-2004) simulation and three future time slice under mean of 3 ESMs for RCP2.6 scenario, b (top right): same as fig 5.9a but for RCP4.5 scenario, c (bottom left): same as fig 5.9a but for RCP8.5 scenario, d (bottom right): same as fig 5.9a but without time slice under RCP2.6, RCP4.5 and RCP8.5 scenarios

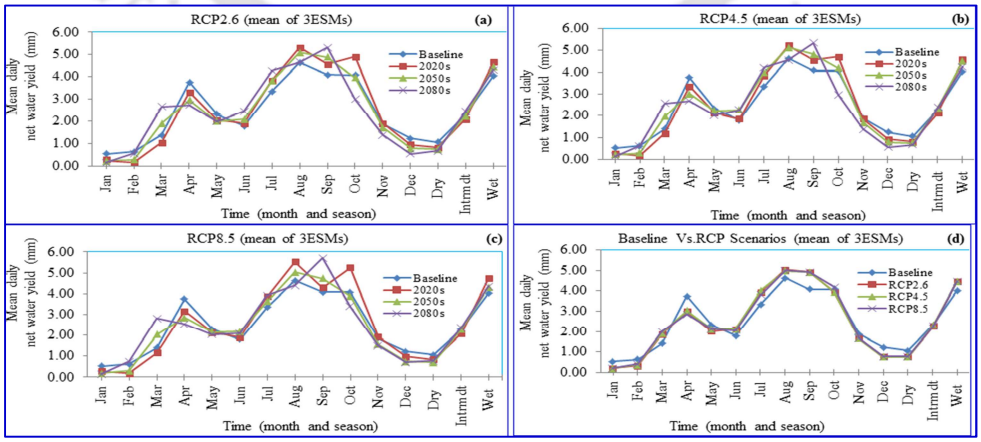

Figure 5.10a (top left): Sub-basin 3 water availability (monthly and seasonal mean daily) during baseline (1984-2004) simulation and three future time slice under mean of 3 ESMs for RCP2.6 scenario, b (top right): same as fig 5.10a but for RCP4.5 scenario, c (bottom left): same as fig 5.10a but for RCP8.5 scenario, d (bottom right): same as fig 5.10a but without time slice under RCP2.6, RCP4.5 and RCP8.5 scenarios

E. The Sub-basin 4 (742.44 km^2)

The change in monthly mean daily net water availability in upcoming periods for SB4 in the RCP2.6 scenario has shown a decrease in months of Jan (in all the time slice), Feb (in the 2020s and 2050s time slice), Mar (in the 2020s time slice), May and Nov (in the 2080s time slice) and Dec (in the 2050s and 2080s time slice) and an increase in the rest of the months and future time slices was observed (Fig 5.11a). The difference in monthly net water availability was insignificant for the month of Feb (in the 2080s time slice), May (in the 2050s time slice), Jun (in the 2020s time slice), Oct (in the 2080s time slice) and Nov (in the 2050s time slice) in the RCP2.6 scenario. While in case of RCP4.5, a decrease in the months of Jan and Feb (in the entire time slice), Mar (in the 2020s time slice), May and Dec (in the 2080s time slice) and an increment on the rest of the months and future time slices was observed (Fig 5.11b). The variance in monthly water availability was insignificant in the months of May (in the 2050s time slice), Jun (in the 2020s time slice), Oct (in the 2080s time slice) and Dec (in the 2050s time slice) in the RCP4.5 scenario. In case of RCP8.5, there has been a decrease of net water availability for the months of Jan and Feb (in the entire time slice), Mar (in the 2020s time slice) and May (in the 2080s time slice) and an increase in the rest of the months and future time slices was observed (Fig 5.11c). As compared to the base period simulation, the variance in monthly net water availability was minor for the month of May (in the 2050s time slice) and Dec (in the 2050s and 2080s time slice) in the RCP8.5 scenario. As we can see in Fig 5.11d, there has shown a significant increasing trend of net water availability for all the RCP scenarios in all months of monsoon season with double peaking on the months of Apr and Sep. A decreasing trend has observed in the dry season.

There was no clear ‘decreasing or increasing’ trend of net water availability for all the RCP scenarios and future time slices in dry season in case of bub-basin 4 (Fig 5.11a-d). But increase in intermediate season by 0.44mm (18.54%), 0.78mm (53.76%) and 0.75mm (69.86%) (RCP2.6), 0.41mm (17.20%), 0.66mm (41.79%) and 0.81mm (74.78%) (RCP4.5) and 0.64mm (31.55%), 0.77mm (52.00%) and 1.18mm (111.03%) (RCP8.5) in the 2020s, 2050s and 2080s, respectively and also increase in wet seasons by 1.25mm (54.47%), 1.41mm (62.00%) and 1.16mm (51.57%) (RCP2.6), 1.38 mm (62.31%), 1.57mm (69.64%) and 1.68mm (74.33%) (RCP4.5) and 1.40 mm (63.04%), 1.78 mm (79.15%) and 2.71 mm (119.98%) for the RCP8.5 scenario in the 2020s, 2050s and 2080s respectively

F. The Sub-basin 5 (397.12 km^2)

The change in monthly mean daily net water availability in future periods for SB5 in the RCP2.6 scenario has shown a decrease in months of Jan and Dec (in all the time slice), Feb (in the 2020s and 2050s time slice) and Nov (in the 2080s time slice) and an increase in the rest of the months and future time slices was observed (Fig 5.12a). The difference in monthly water availability was insignificant for the month of Feb (in the 2080s time slice), May (in the 2050s time slice), Jun (in the 2050s and 2080s time slice), Jul (in the entire time slice), Aug (in the 2020s and 2050s time slice), Oct (in the 2050s time slice) and Nov (in the 2020s and 2050s time slice) in the RCP2.6 scenario. While in case of RCP4.5, a decrease in the months of Jan and Dec (in the entire time slice), Feb (in the 2020s and 2050s time slice), May, Jun, Oct and Nov (in the 2080s time slice) and Aug (in the 2020s time slice) and an increment on the rest of the months and future time slices was observed (Fig 5.12b).

The variance in monthly water availability was insignificant for the months of Feb (in the 2080s time slice), May and Jun (in the 2050s time slice), Jul (in the entire time slice), Oct (in the 2050s time slice) and Nov (in the 2020s and 2050s time slice) in the RCP4.5 scenario. In the case of RCP8.5, there has been a decrease of net water availability for the months of Jan and Dec (in the entire time slice), Feb (in the 2020s and 2050s time slice) and May and Jun (in the 2080s time slice) and an increase in the rest of the months and future time slices was observed (Fig 5.12c). As compared to base period simulation, the variance in monthly net water availability was minor for the month of Feb (in the 2080s time slice), May and Jun (in the 2050s time slice), Jul and Nov (in the entire time slice), Aug (in the 2020s and 2050s time slice) and Oct (in the 2050s and 2080s time slice) in the RCP8.5 scenario. As we can see in Fig 5.12d, there has been shown a decreasing trend of net water availability in the dry season for all the RCP scenarios, but there was no difference between scenarios observed. Double peaking in net water availability has noted in the months of Apr and Oct. In this case; the significant increment has been found in an intermediate season instead of a wet season.

As revealed in Fig 5.12a-d, the future seasonal average daily net water availability might be decrease in dry season by 0.16mm (29.73%), 0.14mm (24.34%) and 0.42mm (62.90%) (RCP2.6), 0.15mm (28.84%), 0.15mm (25.64%) and 0.15mm (21.15%) (RCP4.5) and 0.13mm (27.13%), 0.18mm (28.95%) and 0.13 mm (18.55%) (RCP8.5) in the 2020s, 2050s and 2080s respectively, but increase in intermediate season by 0.69mm (42.40%), 0.78mm (61.32%) and 0.82mm (81.52%) (RCP2.6), 0.78mm (49.30%), 0.65mm (52.90%) and 0.74mm (71.71%) (RCP4.5) and 0.79mm (49.39%), 0.77mm (61.39%) and 0.72mm (70.79%) (RCP8.5) in the 2020s, 2050s and 2080s respectively as well as increase in wet seasons by 0.14mm (3.30%), 0.33mm (23.44%) and 0.38mm (36.90%) (RCP2.6), 0.17mm (6.52%), 0.28mm (20.73%) and 0.44mm (36.99%) (RCP4.5) and 0.24mm (10.14%), 0.29mm (22.16%) and 0.50mm (42.66%) under RCP8.5 scenario in the 2020s, 2050s and 2080s respectively.

G. The Sub-basin 6 (284.27 km^2)

The absolute change in monthly mean daily net water availability in future periods for SB6 in the RCP2.6 scenario has shown a decrease in months of Aug, Sep, Oct and Nov (in the entire time slice) and Dec (in the 2020s time slice) and an increase in the rest of the months and future time slices was observed (Fig 5.13a). The difference in monthly water availability was insignificant for the month of Feb and Mar (in the 2020s time slice), May (in the 2080s time slice) and Dec (in the 2050s and 2080s time slice) in the RCP2.6 scenario. While in case of RCP4.5, a decrease in the months of Aug, Sep, Oct and Nov (in the entire time slice) and Dec (in the 2020s and 2050s time slice) and an increment on the rest of the months and future time slices was observed (Fig 5.13b). The variance in monthly water availability was insignificant for the months of Dec (in the 2080s time slice) in the RCP4.5 scenario. In case of RCP8.5, there has been a decrease of net water availability for the months of Aug and Sep (entire time slice), Oct (in the 2050s and 2080s time slice), Nov (in the 2050s time slice) and Dec (in the 2020s time slice) and an increase in the rest of the months and future time slices was observed (Fig 5.13c).

As compared to the base period simulation, the variance in monthly net water availability was minor for the month of Oct (in the 2020s time slice) and Nov (in the 2020s and 2080 time slice) in the RCP8.5 scenario. As we can see in Fig 5.13d, there has been shown a decreasing trend of net water availability in the dry season for all the RCP scenarios, except RCP8.5 scenario. Double peaking in net water availability was observed in the months of Apr and Oct. In this case too; the significant increment has been noted in an intermediate season instead of a wet season. Large available water has been seen in a small area (284.27 km^2) of SB6.

The future seasonal average daily net water availability might be increase in intermediate and dry seasons, except under RCP2.6 and 4.5 in the 2020s time slice of dry season and decrease was observed in wet season (Fig 5.13a-d). In the dry season, increase by 0.27mm (38.39%) and 0.04mm (16.94%) (RCP2.6), 0.06mm (8.30%) and 0.27mm (42.52%) (RCP4.5) in the 2050s and 2080s time slice respectively and 0.07mm (13.50%), 0.43mm (58.39%) and 1.90 mm (210.29%) for the RCP8.5 in the 2020s, 2050s and 2080s respectively. In the intermediate season, increase by 1.38mm (55.10%), 2.21mm (98.71%) and 1.93mm (86.05%) (RCP2.6), 1.40mm (55.08%), 1.96mm (85.07%) and 2.50mm (118.47%) (RCP4.5) and 1.69mm (65.94%), 2.49mm (114.21%) and 3.99mm (198.50%) (RCP8.5) in the 2020s, 2050s and 2080s time slices respectively. In wet season, decrease by 0.49mm (15.40%), 0.36mm (12.70%) and 0.47mm (5.11%) (RCP2.6), 0.25mm (23.16%), 0.34mm (14.52%) and 0.40mm (4.71%) (RCP4.5) and 0.19mm (29.58%), 0.23mm (27.59%) and 0.05mm (36.46%) under RCP8.5 scenario in the 2020s, 2050s and 2080s time slices respectively.

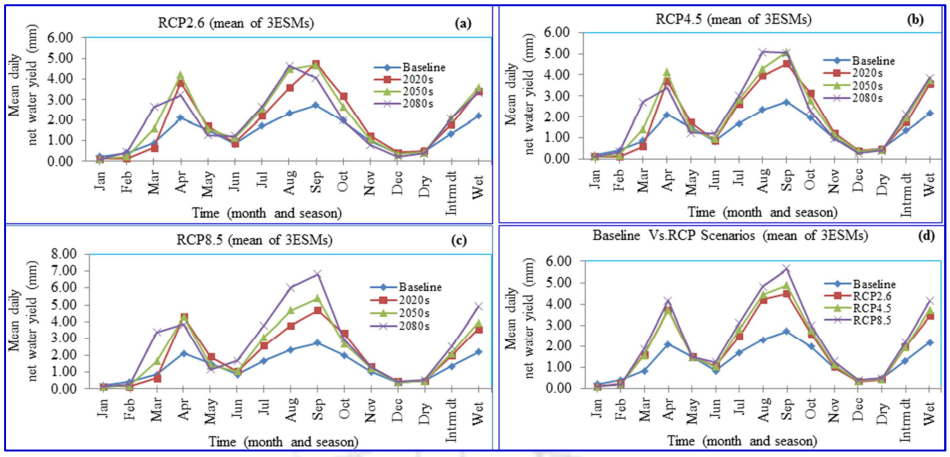

Figure 5.11a (top left): Sub-basin 4 water availability (monthly and seasonal mean daily) during baseline (1984-2004) simulation and three future time slice under mean of 3 ESMs for RCP2.6 scenario, b (top right): same as fig 5.11a but for RCP4.5 scenario, c (bottom left): same as fig 5.11a but for RCP8.5 scenario, d (bottom right): same as fig 5.11a but without time slice under RCP2.6, RCP4.5 and RCP8.5 scenarios

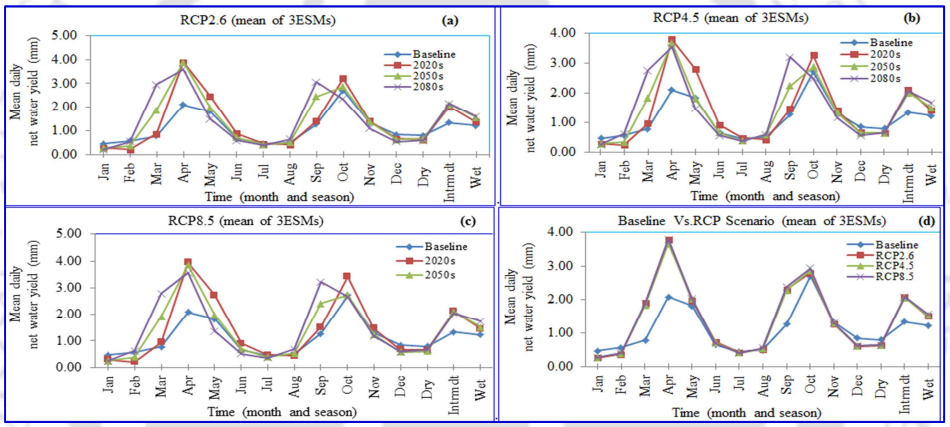

Figure 5.12a (top left): Sub-basin 5 water availability (monthly and seasonal mean daily) during baseline (1984-2004) simulation and three future time slice under mean of 3 ESMs for RCP2.6 scenario, b (top right): same as fig 5.12a but for RCP4.5 scenario, c (bottom left): same as fig 5.12a but for RCP8.5 scenario, d (bottom right): same as fig 5.12a but without time slice under RCP2.6, RCP4.5 and RCP8.5 scenarios

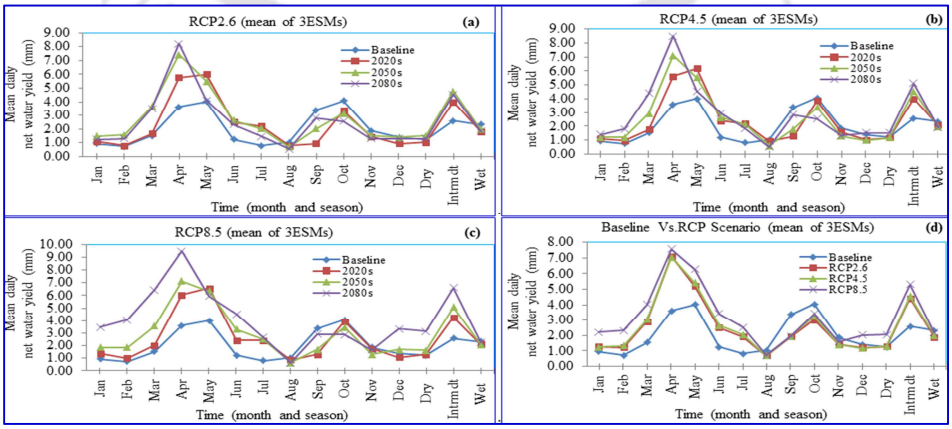

Figure 5.13a (top left): Sub-basin 6 water availability (monthly and seasonal mean daily) during baseline (1984-2004) simulation and three future time slice under mean of 3 ESMs for RCP2.6 scenario, b (upper right): same as fig 5.13a but for RCP4.5 scenario, c (bottom left): same as fig 5.13a but for RCP8.5 scenario, d (bottom right): same as fig 5.13a but without time slice under RCP2.6, RCP4.5 and RCP8.5 scenarios

The climate change impacts on streamflow (water availability) for various catchment hydrology in various regions considering different hydrological models were studied **(**Farjad et al., 2016**;** Aich et al., 2014; Faramarzi et al., 2013; Ghosh and Dutta, 2012; Graham et al., 2011; Setegn, 2010, 2011; Vano et al., 2010; Gosain et al., 2006) and they found that the mean annual streamflow of most river basins were observed to increase with significant spatial variability, which is also the case in this study.

Recent research has been done (Farjad et al., 2016) in Elbow River Basin, Canada and found that the SURFQ decreases by 10.50 and 10.60% (A1F1), 4.60 and 9.90% (B2) in 2020s and 2050s time slices respectively whereas GWQ has been rise by 2.50 and 12.70% (A1B), 2.10 and 2.30% (A2) in the 2020s and 2050s, respectively and AET has also been increasing by 1.60 and 9.60% (A1B), 2.40 and 4.80% (A2) in the 2020s and 2050s, respectively for Entire River basin. In this study too, SURFQ tends to decrease in all the three RCP scenarios for the entire river basin and sub-basins analysis (but in different magnitude) and an increment was observed in the case of GWQ and AET. Also, annual, seasonal and monthly variations of all hydrological processes in all the sub-basins are similar, regarding direction (pattern) but different in magnitude (amount), to the entire river basin in this study. Present results are not consistent with the studies has been done (Farjad et al., 2016) regarding magnitude. This dissimilarity might be due to different in GCMs, SRES, methods of downscaling and also hydrological modeling used in their study.

Farjad et al. (2016) explained in their study also with the 21% increase in PRECIP, SWAT produced a 51% increase in SURFQ, and a 43% increase in GWQ, leading to a 50% net increase in NWYLD, in this too; revealed that the increase in average annual PRECIP is not resulting always in an increase in the SURFQ in the entire river basin and all the sub-basins. This might be due to rising in temperatures in all the RCP scenarios, and that leads to increasing actual evapotranspiration resulted a decline in SURFQ even under increasing PRECIP. However, PET observed to decrease even increase in temperature. This indicated that PET affected by some other climatic factors in addition to temperature. For instance, due to increased cloudiness and reduced wind speeds and relative humidity PET tends to decrease even with increasing temperature.

In this study, however, with the 28.96% increase (mean of 3ESMs) in PRECIP for the RCP8.5 in the 2080s time slice, ArcSWAT produced a 63.44% decline in SURFQ, a 29.26% rise in AET, a 13.31% decline in PET, and a 75.88% rise in GWQ and leading to a 27.97%

rise in NWYLD in the ERB. This uneven change could have attributed to the non-linear nature of hydrological processes, such as evapotranspiration, surface runoff, and groundwater flow. Simulation of average annual streamflow (water availability) in the entire river basin shows increases by 3.00 and 14.70% (A1B) and 4.20 and 4.30% (A2) in the 2020s and 2050s time slices respectively (Farjad et al., 2016). There had been rises in streamflow ranges 10-20% (Faramarzi et al., 2009), this study also agreed with increment but in different magnitude.

In terms of seasonal and monthly changes, net water availability tends to decrease in all months of the dry season while an increase in all months of intermediate and wet seasons under ensembles of three ESMs and all RCP scenarios in entire river basin and similar trend has been observed in case of sub-basins analysis (but with variation in magnitude). In all the RCP scenarios, the double peaking in net water availability (risk of flooding) ensues in Apr and Sep in entire river basin and SB4, Apr and Jul in SB1, Apr, and Aug in SB2 and 3, Apr and Oct in SB5 and SB6. This shift in peak might be due to climate change effect. The results revealed that also there had been larger monthly and seasonal variation in net water availability than the annual variation for all the future RCP scenarios for EB and each SB is discussed in this study and taken to be an advantage over the other studies which focused only annual basis.

5.4. Conclusion

From the results found and challenges faced during this study the following conclusions have been made;

- ✓ Surface and subsurface hydrological processes in the EB and SB scale have been computed and which highlighted an enormous spatial variability among all the six sub-basins.
- ✓ The SB3 and SB6 showed a higher precipitation and resulting higher water availability than the others (SB4, EB, SB5, SB2, and SB).
- ✓ Study has shown a significant fluctuation of both surface and subsurface components for all SBs.
- ✓ Soil water content (SW) exhibits very high magnitude for all sub-basins as compared to other components.

- ✓ The SWAT based computation of both surface water and groundwater components for entire basin and sub-basin scale provide a comprehensive assessment to obtain a better understanding of surface water and groundwater interactions.
- ✓ Sub-basin scale analysis of surface and subsurface interactions could explore the long-term simulation of spatiotemporal variability of hydrological processes for the selected study basin.
- ✓ Annual, seasonal and monthly variations of all hydrological processes (PRECIP, QSURF, GWQ, ET, PET, PERC, SW, and WYLD) in all the SBs are similar in terms of direction but different in magnitude to the EB.
- ✓ Net water availability tends to decrease in the dry season in both basin and sub-basin analysis; this might cause water shortage in the lowland region and increase in intermediate and rainy seasons; this might cause flooding to some flood prone region of the basin
- ✓ Having sufficient knowledge about the hydrological processes and their responses to climate change in each SB can guide water resources management in providing a more rigorous assessment and more efficient decision-making.

This study noticeably culminates that different features between sub-basins in a basin such as LULC, soil non-homogeneity, topographic, surface-subsurface water interactions, drainage area, shape, and networks can result in different hydrological responses to climate change in each SB, and consequently the changes in mean annual and seasonal climate variables may not always bring about the same change in hydrological processes in the Weyib River basin. Therefore, calculating the water balance components (mainly water availability) in each SB, along with the EB provides a better understanding of the hydrological processes in response to climate change (helps to know which part of SB has high or low water availability) and this study would not only provide the comprehensive analysis of the climatic change and hydrological processes but also would be helpful for the better management of water resources in the Weyib River basin. Therefore, the physically based, deterministic, spatially distributed, and public domain ArcSWAT model is found to be a very appropriate tool to simulate both historical as well as impacted hydrological processes in the catchment of Weyib River basin.

Chapter 6: Current and Projected Water Demand and Water Availability Estimates under Climate Change Scenarios in the Weyib River Basin, Southeastern Ethiopia

6.1. Introduction

Integrated assessment of current and future projected water demand and water availability in a particular river basin is vital for sustainable water resources management (Latha et al., 2010). Investigation on the integration of both the water demand and water availability of Weyib River basin has not yet been studied. Through analyzing the water demand and available flow in a particular river basin helps to identify whether the basin falls under water stress or water surplus condition and it gives us also a detail assessment to manage the basin water resources accordingly.

Estimation of total annual water demand (i.e., water demand for domestic, commercial and public institutions, industrial, livestock, and system water losses) for current (2005) and projected (in the 2020s, 2050s and 2080s time slices) in the study area of Weyib River basin were calculated as the product of the gross per capita water use derived from the Genal-Dawa River Basin Master Plan Development (GDMPD) study report for the year 2000-2007 and number of population found in the basin. According to Gleick (1996), later accepted by Wold Bank, water demand for basic human needs (includes drinking water for survival, water for human hygiene, water for sanitation services, and modest household needs for preparing food) shall be at least in the ranges 30-50 lpcd in the 21st century, this standard has also taken by Genale-Dawa Master Plan Development Study in which Weyib River basin is part of it.

The irrigation water demand of the study basin has been determined for each of the three irrigation schemes (Bale Gadula; 4500 ha, Tegona; 2500 ha and Tebel; 1000 ha). ArcSWAT hydrologic model was used to simulate spatial water availability in the basin for both current (1981-2004) and projected (2006-2100) time periods under Ensembles of 3 ESMs for the RCP8.5, RCP4.5 and RCP2.6 from CMIP5. The current and future projected water resources status of the basin is then calculated based on Water Stress Index as suggested by IPCC (2007).

The objectives of this chapter were to:

→ Estimate the spatial distribution of current (2005) and projected (in the 2020s, 2050s and 2080s time slices) total annual water demand of the Weyib River basin under increasing population and;

→ Estimate current and projected water resources status of the basin under the CMIP5-ESMs-RCPs scenario.

6.2. Materials and Methods

6.2.1. Spatial distribution of current (2005) and projected (in the 2020s, 2050s, and 2080s) total population of Weyib River basin

Spatial distribution (Wereda level) of current population of the Weyib River basin has been compiled from Genale-Dawa River Basin Integrated Resources Development Master Plan Study Final Report (GDMP, 2007). According to the suggestion made by NU (2004), annual population growth rate of 2.6% has been used (for the period 2006-2020) to project total population for different Wereda found in the basin in 2020. To project total population in 2050 (for the period of 2021-2050) 2.13% annual population growth rate has been used whereas to project total population in 2080 (2051-2080) 1.42% annual population growth rate was used. The spatial distribution of current and projected total population of Weyib River basin is presented in Table 6.1.

6.2.2. Total annual water demand estimates of Weyib River basin

Water demand estimation of the basin comprises water demand for (i) irrigation, (ii) domestic (drinking, sanitation, bathing and food preparation), (iii) commercial and public institutions (public schools, clinics, hospitals, offices, shops, bars, restaurants and hotels), (iv) industrial, (v) livestock, and (vi) water losses in the water supply system. Additional factors such as climatic variations and the level of service have been provided affect water demand have been taken into account.

The crop water requirement at each irrigation scheme (Bale Gadula, Tegona, and Tebel) found in the Weyib River basin has been calculated using CropWat 4.3 for Windows during Genal-Dawa River basin master plan development (GDMPD) study period (2000-2007). The two crops used for this calculation was wheat (131-day crop) in Bale Gadula and Tegona irrigation schemes and Maize (135-day crop) in Tebel irrigation scheme depend on the geographical location of the site. Finally, irrigation water requirement has been estimated by

subtracting crop water requirement from available rainfall for a given period. The total annual irrigation water demand of the three irrigation schemes of Weyib River basin is detailed in Table 6.2.

A standard guideline of 30-50 lpcd has been used as an urban domestic water demand in this study. Water demand of 30 and 50 lpcd were used to estimate the current (2005) and projected total domestic water demand, respectively. The water demand for commercial and public institutions usually linked directly to the population and is taken as 5% of the domestic water demand. These allowances have therefore applied to all Wereda (districts) in the basin. Industrial water demand is not usually linked directly to the population. However, for the purpose of basin planning, it is assumed to use 10% of domestic water demand for all Wereda in the basin. To estimate livestock water demand, it has been taken a mean of 2 Livestock Unit (LU) per person for the whole basin. The average water demand for livestock has been taken as 25 litres per LU per day. In estimating water losses in the water supply system, a 20% of the totals of domestic, commercial and public institutions and industrial demands have been assumed.

Therefore, the average daily demand is taken to be the combined total of the domestic, commercial and public institutions, industrial, livestock demands and the system losses. The daily water demand in a Wereda varies depending on the time of day, the season and climatic conditions. Hence, the maximum daily demand has been taken as 1.15 times the average daily demand. The detail estimates for both current and projected water demand for each component (domestic, commercial and public institutions, industrial, livestock, system losses, average daily demand, maximum daily demand and total annual water demand) of the basin is presented in following boxes (Box A and B). The spatial distribution of current and projected total annual water demand of the Weyib River basin is shown in Table 6.3.

Box A: Year 2005

Domestic Water Demand (DWD) = 30 lpcd
= 0.030 m^3/c/d
CIWD = 5% DWD = 0.05 x 0.030 = 0.0015 m^3/c/d
IWD = 10% DWD = 0.10 x 0.030 = 0.003 m^3/c/d
LWD = 2 x 25 lpd = 50 lpcd = 0.053 m^3 pcd
System Losses = 20% (DWD + CIWD + IWD)
= 20% (0.030 + 0.0015 + 0.003)
= 20 x 0.0345 = 0.0069 m^3/d
Average Daily Demand (ADD) = 0.030 + 0.0015 + 0.003 + 0.050 + 0.0069
= 0.0914 m^3/c/d
Maximum Daily Demand (MDD) = 1.15 ADD
= 1.15x0.0914 m^3/c/d
= 0.105 m^3/c/d
Total water demand per capita per day =0.105 m^3/c/d
Maximum Demand person per year = 0.105 x 365 m^3
= 38.325 m^3/ year
Total water demand per capita per year =38 m^3

Box B: Year 2020, 2050 and 2080

Domestic Water Demand (DWD) = 50 lpcd
= 0.050 m^3/c/d
CIWD ……. 5% DWD = 0.0025 m^3/c/d
IWD …….. 10% DWD = 0.0050 m^3/c/d
LWD = 0.050 m^3/c/d
SL = 20% (DWD + CIWD + IWD) = 0.0115 m^3/c/d
ADD = DWD + CIWD + IWD + LWD + SL
= 0.119 m^3/c/d
MDD = 1.15 ADD = 1.15 x 0.119
= 0.13685 m^3/c/d
Total water demand per capita per day= 0.13685 m^3/c/d
Maximum Demand per person per year = 0.13685 x 365 m^3/ year
= 49.95 m^3/ year
Total water demand per capita per year = 50 m^3

Source: GDMP-II.3.1. Water Supply and Sanitation_Final Report

6.2.3.Water availability estimates of Weyib River basin

The standard procedure of ArcGIS interface ArcSWAT hydrologic model was applied to simulate spatial distribution of water availability in the basin for both current and future period under Ensembles of 3 ESMs for the RCP8.5, RCP4.5 and RCP2.6 scenarios. The theoretical description, hydrological component, data used and model set-up of ArcSWAT hydrologic model has been given in detail in chapter 4 of this study. The mean of 3 ESMs future downscaled daily maximum and minimum temperature and rainfall using SDSM have been applied into ArcSWAT model as an input to generate future water availability under various RCP scenarios considering that all other climatic and physiographic variables are supposed to be same in the upcoming period. The analysis of future water availability has then been carried out on an annual basis (Table 6.4 and 6.5) in the 2020s, 2050s and 2080s

time slices. Finally, the current (1984-2004) and future (in the 2020s, 2050s and 2080s time slice) water resources status of the basin is then calculated in Table 6.6 based on Water Stress Index (total available water divided by total number of population residing in the basin) as suggested by (IPCC, 2007) with the threshold value of 1000 m^3 per capita per year below which a basin might be considered to be water stressed.

6.3. Results and Discussion

6.3.1. Spatial distribution of current (2005) and projected (in the 2020s, 2050s, and 2080s) total population of Weyib River basin

Population plays a vital role in the estimation of water demand for specific basin/catchment. Wereda level spatial scale number of population is used to estimate water demands for domestic, commercial and public institutions, industrial, livestock consumption and water losses through water supply system in this study. Six Wereda, as shown in Table 6.1, population numbers are used in this case. There have been significant variations in population among Wereda in the year 2005. Sinnana-Dinsho Wereda (SB3) has the largest number of population than the others and followed by Gassera and Golelcha Wereda (SB4) whereas Goro Wereda (SB) has the smallest in population number as compared to the others. The Wereda level spatial distribution of current (2005) and projected (in the 2020s, 2050s, and 2080s) total population of Weyib River basin is presented in Table 6.1.

Table 6.1 Spatial distribution of current (2005) and projected (in the 2020s, 2050s, and 2080s) total population of Weyib River basin

			Current Total Population	Projected Total Population		
Region	Zone	Name of Wereda	2005	2020s	2050s	2080s
Oromia	Bale	Gassera and Golelcha	151648	211433	346539	494164
		Ginnir	110842	154540	253291	361193
		Adaba	117356	163622	268176	382420
		Sinnana and Dinsho	152489	212606	348461	496906
		Goro	89600	124923	204749	291972
		Goba	127813	178200	292070	416492
		Total	742338	1045324	1713286	2443146

Note: Current (2005) total population of the basin has compiled from GDMP-II, 5. P. (2007) and then projected based on annual population growth rate of Ethiopia: annual population growth rate of 2.6% has used for period 2006-2020, 2.13 and 1.42% of annual population growth rate have been considered for the period 2021-2050 and 2051-2080 respectively as suggested by (United Nations, 2004)

It is observed that there is a uniform increment in projected total populations in a future time slice of the 2020s, 2050s and 2080s in all Wereda from the year 2005. Meaning, for all Wereda (Table 6.1) in the basin have same population increment which has increased by 39.00% of total population of 2005 in the 2020s, 63.90% of total population of 2020s in

2050s and 42.60% of total population of 2050s in 2080s. Hence, a total number of projected population in the 2020s turns out to be the total number of population in 2005 plus 39% of total population of 2005. The projected number of population in 2050 tends to be a total number of population in the 2020s plus 63.90% of total population of 2020s whereas projected number of total population in 2080s becomes a total number of population in 2050s plus 42.60% of total population of 2050s. Therefore, the total projected population number of entire basin is increased by about 40.81% after 15 years in 2020, 130.80% after 45 years in 2050 and 229.12% after 75 years in 2080 from the base period (2005) population number.

6.3.2. Weyib River basin total annual water demand estimates

A. Current Total Annual Irrigation Water Requirement

The annual total irrigation water requirement for double cropping of 4,500 ha in Bale Gadula, 2500 ha in Tegona, 1000 ha in Tebel irrigation schemes of the Weyib River basin were 249.45, 0.02, and 11.04 Mm^3 respectively (Table 6.2). Greater irrigation water requirement (11.04Mm^3) is observed in small irrigated area (in Tebel irrigation scheme) due to less availability of rainfall in the area (lowland), and the reverse is true in Tegona irrigation scheme because of high rainfall availability (highland area). The total annual irrigation water demand of three irrigation schemes (Bale Gadula, Tegona, and Tebel) of the Weyib River basin, hence, tends to be 260.50 Mm^3.

Table 6.2 The annual total irrigation water requirement of three irrigation schemes in Weyib river basin

Name of Site/Scheme	Irrigation Water Requirement (Mm^3)	Irrigated Area (ha)
Bale Gadula	249.45	4500
Tegona	0.02	2500
Tebel	11.04	1000
Total	260.50	8000.00

Source: GDMP-II.3.H.Irrigation and Drainage_ Final Report, Mm^3= million cubic meter

B. Current and Projected Total Annual Water Demand Estimates

The current and projected total annual water demand estimations in Table 6.3 encompasses water demand for domestic, commercial and public institutions, industrial, livestock consumption and water losses in the water supply system. As we have seen in Table 6.3, water demand has highly correlated with population of the basin. A higher number of a population residing in the basin tends to have higher water demand. For instance, Sinnana and Dinsho Wereda (SB3) has higher (5.79 Mm^3) current total annual water demand due to

higher population (152489 in number) than the others followed by Gassera and Golelcha Wereda (SB4) with total annual water demand of 5.76 Mm^3.

The current total annual water demand of Ginnir (SB5), Adaba (SB1), and Goba (SB2) are 4.21, 4.46, and 4.85 Mm^3 in 2005 respectively whereas Goro Wereda (SB6) has the smallest (3.4 Mm^3) total annual water demand because of the smallest number of population than the others. There is a significant spatial variability in water demand within Wereda. Wereda level spatial distribution of current (2005) and projected (in the 2020s, 2050s, and 2080s) total annual water demand of Weyib River basin has presented in Table 6.3.

Table 6.3 Spatial distribution of current (2005) and projected (2020s, 2050s, and 2080s) total annual water demand estimates of Weyib River basin

			Weyib River Basin Annual Total (domestic, commercial & public institutions, industrial, livestock and water losses in the system) Water Demand Analysis							
			CTP and WD (in Mm^3)		Future PTP and WD (in Mm^3)					
State	Zone	Name of Wereda	TP in 2005	AWD in 2005	TP in 2020s	AWD in 2020s	TP in 2050s	AWD in 2050s	TP in 2080s	AWD in 2080s
Oromia	Bale	Gassera and Golelcha	151648	5.76	211433	10.57	346539	17.33	494164	24.71
		Ginnir	110842	4.21	154540	7.73	253291	12.66	361193	18.06
		Adaba	117356	4.46	163622	8.18	268176	13.41	382420	19.12
		Sinnana and Dinsho	152489	5.79	212606	10.63	348461	17.42	496906	24.85
		Goro	89600	3.4	124923	6.25	204749	10.24	291972	14.60
		Goba	127813	4.85	178200	8.91	292070	14.60	416492	20.82
		Total	749748	28.49	1045324	52.27	1713286	85.66	2443146	122.16

Note: Current domestic water demand per capita per day= 30 lpcd=0.03 m^3 pcd, current total water demand per capita per day =0.105 m^3 pcd, **current total water demand per capita per year = 38 m^3 pcy**, Projected domestic water demand per capita per day= 50 lpcd=0.05 m^3 pcd, projected total water demand per capita per day =0.13685 m^3 pcd, **projected total water demand per capita per year = 50 m^3 pcy**, CTP=current total population, WD=water demand, (Mm^3) = million cubic metre, PTP=projected total population, TP=total population, AWD=annual water demand

It is observed that there is a uniform increment in projected total annual water demand in the 2020s, 2050s and 2080s time slices in all Wereda from the year 2005 water demand. Meaning, for all Wereda (detailed in Table 6.3) in the basin have same water demand increment which is increased by 83.47% of total annual water demand of 2005 in the 2020s, 63.88% of total annual water demand of 2020s in 2050s and 42.61% of total annual water demand of 2050s in 2080s. Meanwhile, total annual water demand of entire basin is increased by about 83.47% after 15 years in 2020s, 200.67% after 45 years in 2050s and 328.78% after 75 years in 2080s from the base period (2005) annual total water demand (28.49 Mm^3).

6.3.3. Average annual total water availability estimates of Weyib River basin

Table 6.4 revealed that the current (1984-2004) average annual water availability of Weyib River basin is found to be 2333.39 Mm^3. The future projected average annual total water availability (mean of 3ESMs) has estimated to be 2837.61, 2878.04 and 3255.79 Mm^3

(RCP8.5), 2710.35, 2830.62 and 2838.43 Mm^3 (RCP4.5) and 2684.36, 2802.01 and 2711.70 Mm^3 (RCP2.6) in the 2020s, 2050s, and 2080s time slice respectively.

Table 6.4 Current and future average annual total water availability (mean of 3ESMs) in three future times slice under three RCP scenarios of Weyib River basin

Weyib River Basin Average Annual Total Water Availability (in Mm^3)									
Current	Future (Mean of 3ESMs)								
	2020s			2050s			2080s		
Base Period	rcp2.6	rcp4.5	rcp8.5	rcp2.6	rcp4.5	rcp8.5	rcp2.6	rcp4.5	rcp8.5
2333.39	2684.36	2710.35	2837.61	2802.01	2830.62	2878.04	2711.70	2838.43	3255.79
% Increment from base period	15.04	16.16	21.61	20.0833	21.31	23.34	16.21	21.644	39.53

Note: area of the basin=4215.93 km^2, Mm^3= million cubic meter

The average total annual water availability in the entire basin has been observed to increase by 21.61, 23.34 and 39.53% (RCP8.5), 16.16, 21.31 and 21.64% (RCP4.5) and 15.04, 20.08 and 16.21% (RCP2.6) in the 2020s, 2050s and 2080s time slice respectively from base period water availability (2333.39 Mm^3). It has shown that a substantial variability of current and future annual water availability from year to year in the Weyib River basin (Table 6.5). The variability of mean annual water availability is more in RCP8.5 than the RCP4.5 and RCP2.6. This might be due to the story line of RCP8.5 (very high emission scenario).

Table 6.5 Weyib River basin current and future (mean of 3ESMs) total yearly water availability in three future time slice under three RCP scenarios

Weyib River Basin Water Availability (in Mm^3)													
Current		Future (mean of 3 ESMs)											
Baseline		2020s				2050s				2080s			
Year	Bp	Year	rcp2.6	rcp4.5	rcp8.5	Year	rcp2.6	rcp4.5	rcp8.5	Year	rcp2.6	rcp4.5	rcp8.5
1984	2156.24	2011	2693.81	2428.54	2755.45	2041	2696.34	2611.09	2708.69	2071	2875.35	3025.56	3146.22
1985	2319.94	2012	2665.94	2985.93	2604.56	2042	2425.26	3242.35	3158.74	2072	2864.35	2802.20	3302.17
1986	2379.98	2013	3145.38	2629.31	2924.04	2043	2606.16	2772.27	2838.50	2073	2567.67	3090.99	3383.58
1987	2471.13	2014	2933.32	2902.50	3046.85	2044	3017.05	2888.29	2681.88	2074	2970.29	2933.02	3008.19
1988	2662.06	2015	2466.66	2845.42	2429.98	2045	2713.20	2746.85	2918.06	2075	2731.00	2473.06	3037.20
1989	3176.70	2016	2932.26	2987.24	2701.48	2046	2439.80	3106.93	2554.26	2076	2631.92	3297.45	3194.37
1990	2518.89	2017	2643.35	2711.22	2803.97	2047	2930.16	2628.84	2653.84	2077	2608.86	2942.89	3121.31
1991	1953.16	2018	2509.07	2394.23	2989.52	2048	2575.09	2900.10	2627.79	2078	2781.08	2622.18	2873.49
1992	3621.82	2019	2532.13	2711.56	2846.55	2049	2683.99	2858.91	2763.16	2079	2382.72	2567.88	3182.65
1993	2907.98	2020	2525.00	2715.61	2853.64	2050	3053.94	2603.34	2774.63	2080	2921.09	2938.50	3161.95
1994	2837.87	2021	2736.35	2541.53	2704.73	2051	2819.23	2733.65	2757.09	2081	3059.21	3062.45	3456.51
1995	2329.51	2022	2530.86	2541.74	2825.56	2052	2812.70	2618.60	3108.19	2082	2682.81	2556.71	3121.81
1996	2230.69	2023	2842.84	2790.06	2649.67	2053	2681.33	2673.95	3056.13	2083	2789.22	2828.09	3249.09
1997	2488.12	2024	2910.93	2725.47	3131.21	2054	2923.87	2879.35	3085.43	2084	2812.32	2794.91	3313.51
1998	2754.77	2025	2704.14	2491.28	3080.54	2055	3036.31	2938.50	2823.03	2085	2555.82	2754.14	3455.00
1999	1997.13	2026	2603.67	2891.79	2565.56	2056	2918.77	2957.01	2924.38	2086	2612.11	2712.57	3227.63
2000	1777.27	2027	2383.22	2854.86	3069.28	2057	2611.64	3111.23	2744.95	2087	2722.10	2980.96	3194.83
2001	2009.19	2028	2723.66	2547.73	2705.87	2058	2810.89	2753.59	2981.76	2088	2502.03	2858.44	2925.52
2002	1186.28	2029	2831.50	2415.81	2700.26	2059	2900.48	2852.88	2607.09	2089	2746.64	2958.82	3346.86
2003	1837.09	2030	2717.04	2720.16	2632.89	2060	2536.01	2756.88	3070.25	2090	2790.19	2960.34	3427.13
2004	1385.31	2031	2796.51	2653.17	2780.74	2061	2799.12	2807.13	2825.94	2091	3149.17	2649.46	3423.88
		2032	2423.19	2659.16	2980.11	2062	2775.81	2666.62	3046.47	2092	2898.16	3053.72	3351.75
		2033	2709.07	3103.09	2898.24	2063	2935.85	2661.56	2867.89	2093	2811.86	2277.70	3536.15
		2034	2618.39	2794.66	2984.96	2064	3180.96	3437.46	3273.54	2094	2621.93	2492.46	3377.97
		2035	2823.87	2891.92	2757.81	2065	2819.11	2833.99	2725.68	2095	2555.74	2858.95	3561.03
		2036	2353.75	2446.46	2947.44	2066	2942.30	2789.30	2980.92	2096	2265.26	2959.75	2909.24
		2037	2711.64	2686.39	2986.19	2067	3053.30	2575.85	2782.26	2097	2531.24	2990.11	3096.98
		2038	2525.13	2834.12	2936.02	2068	2848.07	2859.54	3246.14	2098	2589.89	2657.89	3210.30
		2039	3104.36	2613.03	3004.40	2069	2786.22	3104.61	2640.65	2099	2809.75	3379.45	3688.81
		2040	2433.60	2796.51	2830.91	2070	2727.29	2547.86	3113.89	2100	2511.30	2672.35	3388.68
Average	2333.39		2684.36	2710.35	2837.61		2802.01	2830.62	2878.04		2711.70	2838.43	3255.79

Note: area of the basin=4215.93 km^2, Mm^3= million cubic meter, BP= base period

6.3.4. Water stress index estimates (in m^3per capita per year) of Weyib River basin

The current (2005) and future projected (in the 2020s, 2050s and 2080s time slice) water resource status of Weyib river basin has been estimated based on Water Stress Index analysis (total available water divided by total number of population residing in the basin) and found to be water abundant basin currently (3112.23 m^3 per capita per year) and for the future too. The future water availability per capita per year of the entire basin in Table 6.6 is ranging from 2567.97 to 2714.58 m^3 by the 2020s, 1635.46 to 1679.84 m^3 by the 2050s and 1109.92 to 1332.62 m^3 by the 2080s.

Table 6.6 Estimates of water stress index (m^3per capita per year) in Weyib River basin

	Weyib River Basin Water Stress Index Calculation (in m^3 per capita per year)									
	Current	Future Projected								
		2020s			2050s			2080s		
Parameters	base period	rcp2.6	rcp4.5	rcp8.5	rcp2.6	rcp4.5	rcp8.5	rcp2.6	rcp4.5	rcp8.5
Average total water availability (Mm^3)	2333.39	2684.36	2710.35	2837.61	2802.01	2830.62	2878.04	2711.70	2838.43	3255.79
Total population	749748		1045 324			1713286			2443146	
Water Stress Index (m^3 pcy)	3112.23	2567.97	2592.83	2714.58	1635.46	1652.16	1679.84	1109.92	1161.8	1332.62
% Decrement in water availability per capita per year from base period		-17.49	-16.69	-11.78	-47.45	-46.91	-46.02	-64.34	-62.67	-57.18

Note: Mm^3= million cubic meter, m^3 pcy= cubic meter per capita per year

The greater magnitude of projected water availability per capita per year has been observed in the RCP8.5 scenario. Since magnitudes of projected water availability per capita per year in all the three-time slices and three RCP emission scenarios are above the threshold (1000 m^3 suggested by (IPCC, 2007) value, the basin then might be considered as water abundant basin. However, the water availability per capita per year in the entire river basin observed to decrease by 11.78, 46.02 and 57.18% (RCP8.5), 16.69, 46.19 and 62.67% (RCP4.5) and 17.49, 47.45 and 64.34% (RCP2.6) in the 2020s, 2050s and 2080s time slice respectively from base period per capita per year water availability (3112.23 m^3) as shown in Table 6.6.

The spatial analysis of mean annual water availability revealed to increase by 25.25, 31.07 and 48.17% (SB1), 20.87, 22.53 and 29.67% (SB2), 1.83, 2.43 and 4.65% (SB3), 46.43, 52.73 and 69.81% (SB4), 26.19, 26.73 and 28.12% (SB5) and 22.79, 26.73 and 53.92% (SB6) in the 2020s, 2050s and 2080s time slice respectively from base period water availability (Figure 6a). It is observed that there is a uniform increment of mean annual water demand by 83.61, 200.89 and 329.09% in the 2020s, 2050s and 2080s respectively in all the sub-basins (Figure 6b).

The spatial analysis of water availability per capita per year shown to decrease (except in SB4 in the 2020s time slice) by 10.17, 42.64 and 54.53% (SB1), 13.30, 46.38 and 60.21% (SB2), 14.58, 47.57 and 62.44% (SB3), 33.16 and 47.89% in the 2050s and 2080s (SB4), 9.49, 44.54 and 60.68% (SB5) and 11.93, 44.54 and 52.76% (SB6) in the 2020s, 2050s and 2080s time slices respectively from base period per capita per year water availability as shown in Figure 6c.

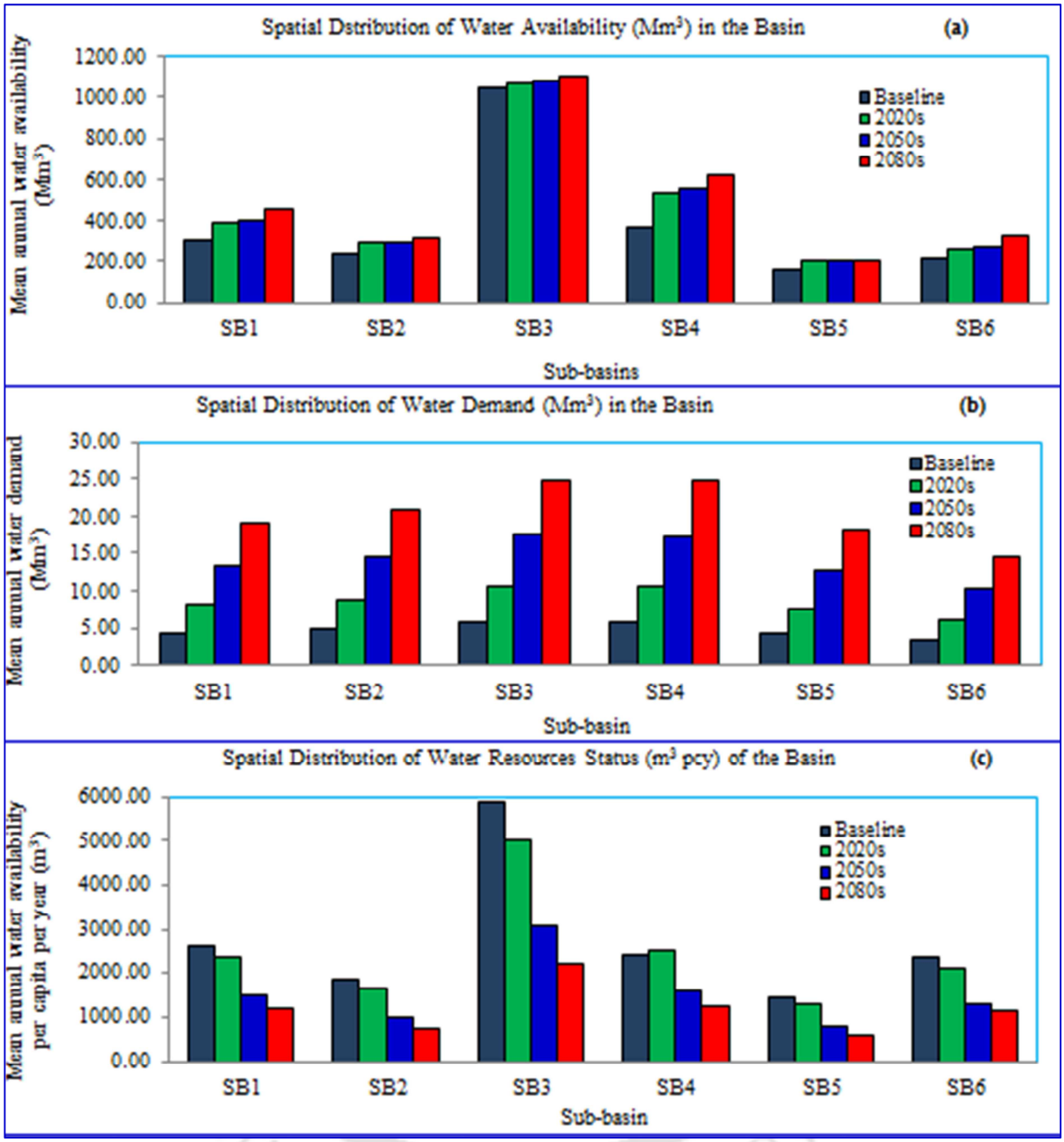

Figure 6 Spatial distribution of water availability (a), water demand (b) and water stress (water resources status of the basin) (c) during baseline and future time periods (in the 2020s, 2050s and 2080s time slices) of Weyib River basin

Based on the various literature reviews report, the mean annual water demand of any river basin is expected to increase (Sebhat, 2015; Roy et al., 2010; Faruqui et al., 2001; Hutson and Schwarz, 1996) mainly due to the rapid increase of population, settlement patterns, wealth, industrial activity, technology, increasing demand for irrigation and climate change.

A research output has been reported (Hutson and Schwarz, 1996) and showed that projected (in the 2050) average water demand for Duck River basin will increase ranging from 121 to 150%. Roy et al. (2010) reported that the total public water demand is projected to increase

by 32.8 and 54.8% in the 2030 and 2050 as compared to 2005 baseline. In this present study, but, the annual total water demand of the entire basin is found to be increased by 83.47% in 2020s, 200.67% in 2050s and 328.78% in 2080s from the base period. This result is in line with various literatures regarding direction (pattern) not coinciding with in terms of magnitude and this might be due to very rapid increasing population in the study area of Weyib River basin (for instance, the population of the basin was observed to increase by 40.81, 130.80 and 229.12% in the 2020s, 2050s and 2080s respectively). Irrigation water demands account for almost 90% of global consumptive water use (Shiklomanov and Rodda, 2003). In this study too, accounting for about 90.14% of total water demand of the basin.

Available water resources observed to increase about 10-20% during 2020-2040 in the East Africa (Faramarzi et al., 2013). Almost coincide with this study too in the 2020s time slice. The future mean annual total water availability in the entire basin is shown to rise by the ranges between 15.04 to 21.61%, 20.08 to 23.34% and 16.21 to 39.53% in the 2020s, 2050s, and 2080s time slice respectively from base period available water resources (2333.39 Mm^3). The current water availability per capita per year of the basin is about 3112.23 m^3 and tends to decline ranging from 11.78 to 17.49%, 46.02 to 47.45% and 57.18 to 64.34% in the 2020s, 2050s and 2080s time slices respectively from base period per capita per year water availability. This indicated that there might be a possibility to fall the basin under water stress condition in the long term.

6.4. Conclusion

In this chapter study, the spatial distribution of water demand, water availability and water stress (water resources status of the basin) during base period and future time period (in the 2020s, 2050s and 2080s time slices) under climate change scenario in the basin have been investigated as shown in Figure 6a, b and c.

Population number for six Wereda (the third-level administrative division of Ethiopia) found in the basin and water demand per capita per day data have been used to estimate current (2005) and future (in the 2020, 2050 and 2080 time slices) total annual water demands of the basin. The current total annual water demand of the basin is estimated to be 289 Mm^3. Irrigation is undoubtedly the leading user of water, accounting for about 90.14% of total water demand of the basin. The future projected total annual water demand of entire basin has been shown to increase by about 83.47% after 15 years in 2020s, 200.67% after 45 years in 2050s and 328.78% after 75 years in 2080s from base period total annual water demand. It is

observed that there is a significant spatial variation of mean annual water demand among sub-basins in the basin in base period and for future period with uniform percentage increment (Figure 6b).

The mean annual water availability in the entire basin is estimated to be about 2333.39 Mm^3 in the base period and this expected to increase in the future by 21.61, 23.34 and 39.53% (RCP8.5), 16.16, 21.31 and 21.64% (RCP4.5) and 15.04, 20.08 and 16.21% (RCP2.6) in the 2020s, 2050s and 2080s time slices respectively. Spatial scale analyses of water availability in all the sub-basins have shown an increasing trend but different in magnitude as compared to entire basin analysis. It is observed that there is also significant spatial variation of mean annual water availability among sub-basins (Figure 6a) in the basin in base period as well as for future period.

The current water availability per capita per year (water resources status) of the entire basin is about 3112.23 m^3 and tends to decline ranging from 11.78 to 17.49%, 46.02 to 47.45% and 57.18 to 64.34% in the 2020s, 2050s and 2080s respectively from base period per capita per year water availability (3112.23m^3). Spatial scale analyses of water resources status in all the sub-basins have shown a decreasing trend but different in magnitude as compared to entire basin analysis. It is observed that there is also significant spatial variation of mean annual water availability per capita per year among sub-basins in the basin in base period as well as for future period (Figure 6c).

The largest increment in case of mean annual water availability and water demand analysis and largest decrement in case of water availability per capita per year were observed at the end of the 21st century (in the 2080s time slice). Current total annual water availability is much more (about eight times) than the current total annual water demands in the basin. In case of future projection, however, the level of percentage increment in water demand is much more than the water availability. But still the available flow in the Weyib River is sufficient to provide water for irrigation, domestic, commercial and public institutions, and industrial and livestock uses.

Chapter 7: Summary, Conclusions, and Recommendations

7.1 Summary and Conclusions

This study is designed to address the following Eight specific objectives namely;

1. To downscale daily temperatures (maximum and minimum) and precipitation from CMIP5-ESMs-RCPs experiment.

The three bias corrected ESMs (GFDL-ESM2M, CanESM2 and GFDL-ESM2G) output in the RCP8.5 (very high emission scenario), RCP4.5 (an intermediate emission scenario) and RCP2.6 (very low emission scenario or peak and decline scenario) scenarios from CMIP5 using SDSM have been used to downscale future daily precipitation and both temperatures (maximum and minimum) for twelve different meteorological stations in the Weyib River Basin.

Calibration and validation results of SDSM for twelve averaged spatial stations maximum and minimum temperature, and precipitation from the mean of 3 ESMs downscaling model have been shown in (Fig 3.3a-f). SDSM has good ability to replicate historical local climate variables with R^2, RMSE and NSE values of 0.95, 0.44 and 0.79 respectively for calibration period whereas R^2, RMSE and NSE values of 0.94, 0.46 and 0.78 respectively for validation period in case of maximum temperature. For minimum temperature, R^2, RMSE and NSE values were 0.93, 0.58 and 0.86 respectively for calibration period whereas R^2, RMSE and NSE values were 0.92, 0.61 and 0.85 for validation period. In case of precipitation, R^2, RMSE and NSE values were 0.86, 0.92 and 0.84 respectively for calibration period whereas R^2, RMSE and NSE values of 0.83, 0.98 and 0.78 respectively for validation period. From the statistical indices and graphical observation between simulated (by SDSM) versus measured value we can infer that SDSM has a good ability to replicate historical climate variables for the study area of Weyib River basin.

The downscaling results revealed that different atmospheric variables affect different local variables in all the ESMs. For example, precipitation is more sensitive to mean sea level pressure, specific humidity (at the surface and 850 hPa), zonal velocity (at 500 and 850 hPa) and geopotential height (at 500 hPa). Mean sea level pressure, geopotential heights (500 and 850 hPa), the average temperature (at 2m height), specific humidity (at near surface and 850 hPa and 850 hPa) wind direction affect both the maximum and minimum temperature under

the CanESM2-historical model. However, under GFDL-ESM2M and GFDL-ESM2G-historical models, precipitation is more impacted by sea level pressure, total cloud fraction, daily mean near-surface wind speed and eastward near the surface wind. Sea level pressure, near surface relative humidity, daily maximum near-surface air temperature, daily mean near-surface wind speed and eastward near surface wind affect the maximum temperature whereas sea level pressure, surface downwelling longwave radiation and daily mean near-surface wind speed affects the minimum temperature.

2. To develop temporal (in the 2020s, 2050s and 2080s time slices) temperatures and precipitation scenarios using CMIP5-ESMs-RCPs experiment in the Weyib River basin.

The analysis revealed that the mean annual maximum and minimum temperature, and precipitation had shown an increasing trend in all the nine ESM-RCP scenarios in the 2020s 2050s and 2080s time slices relative to the baseline scenario (Fig. 3.4, 3.7 and 3.10). GFDL-ESM2M (G2M) projects the highest mean annual value for maximum temperature and increased by 0.20, 0.32 and 0.42°C (G2M-RCP8.5), 0.20, 0.29 and 0.31°C (G2M-RCP4.5) and 0.22, 0.24 and 0.21°C (G2M-RCP2.6) in the 2020s, 2050s and 2080s time slices respectively; GFDL-ESM2G (G2G), projects the lowest increases in the value of this parameter by 0.04, 0.12 and 0.22°C (G2G-RCP8.5), 0.04, 0.09 and 0.11°C (G2G-RCP4.5) and 0.08, 0.04 and 0.03°C (G2G-RCP2.6) in the 2020s, 2050s and 2080s time slices respectively and CanESM2 (C2), projects an intermediate (median) increase of mean annual maximum temperature by 0.12, 0.22 and 0.32°C (C2-RCP8.5),0.12, 0.19 and 0.21°C (C2-RCP4.5) and 0.16, 0.14 and 0.13°C (C2-RCP2.6) in the 2020s, 2050s and 2080s time slices respectively (Fig. 3.4).

GFDL-ESM2M (G2M) projects the highest mean annual minimum temperature to be increased by 0.42, 0.75 and 1.14°C (G2M-RCP8.5), 0.39, 0.58 and 0.67°C (G2M-RCP4.5) and 0.38, 0.52 and 0.49°C (G2M-RCP2.6) in the 2020s, 2050s and 2080s time slices respectively; GFDL-ESM2G (G2G), projects the lowest increases in the value of this parameter by 0.26, 0.55 and 0.94°C (G2G-RCP8.5), 0.23, 0.38 and 0.47°C (G2G-RCP4.5) and 0.22, 0.32 and 0.29°C (G2G-RCP2.6) in the 2020s, 2050s and 2080s time slices respectively and CanESM2 (C2), projects an intermediate (median) increase in mean annual minimum temperature by 0.34, 0.65 and 1.04°C (C2-RCP8.5),0.31, 0.48 and 0.57°C (C2-RCP4.5) and 0.30, 0.42 and 0.39°C (C2-RCP2.6) in the 2020s, 2050s and 2080s time slices respectively (Fig. 3.7).

GFDL-ESM2M (G2M) projects the highest mean annual value for precipitation and increases by 19.70, 24.14 and 33.69% (G2M-RCP8.5), 14.54, 19.36 and 21.94% (G2M-RCP4.5) and 13.68, 17.93 and 16.34% (G2M-RCP2.6) in the 2020s, 2050s and 2080s time slices respectively; GFDL-ESM2G (G2G), projects the lowest increases in the value of this parameter by 12.70, 17.14 and 26.69% (G2G-RCP8.5), 7.54, 12.36 and 14.94% (G2G-RCP4.5) and 6.68, 10.93 and 9.34% (G2G-RCP2.6) in the 2020s, 2050s and 2080s time slices respectively and CanESM2 (C2), projects an intermediate (median) increase in mean annual precipitation by 14.70, 19.14 and 28.69% (C2-RCP8.5),9.54, 14.36 and 16.94% (C2-RCP4.5) and 8.68, 12.93 and 11.34% (C2-RCP2.6) in the 2020s, 2050s and 2080s time slices respectively (Fig. 3.10). The variability of maximum and minimum temperature, and precipitation is higher in the RCP8.5 than RCP4.5 and RCP2.6 in all ESMs and the future trends for RCP8.5 and RCP4.5 scenarios have indicated a significantly (at 5% significant level) increasing trend of average annual maximum and minimum temperature, and precipitation until the end of the century (Fig. 3.5, 3.8 and 3.11 and Table 3.10). Increasing trend but not significant (at 5% significant level) was observed in the RCP2.6 scenario in all ESMs. Comparatively, RCP8.5 scenario prevail higher change in maximum and minimum temperature and precipitation trend at the end of the century than the RCP4.5 and RCP2.6 scenarios.

Seasonal and monthly variations of climate variables are more than the annual variation. The increment of rainfall comparatively higher in dry season (20.68, 33.65 and 53.74% increases in the 2020s, 2050s and 2080s time slices respectively for RCP8.5) and this might have positive impact on lowland region of the study area and it might affect the highland areas negatively since this season is specifically main crop harvesting period.

To investigate the effects of spatial data availability on climate change prediction, averaging less number of stations was done by considering 6, 3 and single station. While trend was found same in 12 averaged, 6 averaged and 3 averaged stations cases, the magnitudes were observed to be different in all predicted parameters. In single station analysis the trend itself has changed from increasing trend to decreasing trend in case of maximum and minimum temperature. In case of precipitation, no visible trend has been observed in case of single station analysis.

Therefore, the variation in amount and distribution of precipitation and temperature among the four averaged spatial stations in the same study area might affect the water resources and agriculture of the basin and also instead of using a single weather station to predict future climate variables for a particular study basin, it is more reliable using averages of numerous spatial weather stations data.

3. To evaluate the performance of ArcSWAT model in simulating catchment hydrology in the Weyib River basin in Ethiopia.

The ArcSWAT hydrologic model was employed to simulate streamflow in the entire basin to accomplish this objective. The assessment of SWAT hydrological model and investigation of its ability to simulate reliably the different components of water balance in general and streamflow, in particular, using different efficiency criteria gave an insight into how one can successfully generate useful information in catchments where there is little data available. To do so various efficiency criteria were implemented namely, R^2, NSE, RSR and Pbias with hydrograph technique.

The results obtained indicate that simulated basin output after calibration is comparatively consistent with recorded values. During the calibration period, the monthly streamflow gave R^2, NSE, RSR and Pbias of 0.86, 0.83, 0.25 and 1.72 respectively. The model also performed well during the validation period for the monthly streamflow simulation gave R^2, NSE, RSR and Pbias as 0.84, 0.81, 0.31 and 2.69 respectively. Based on statistical indices and hydrograph analysis results, ArcSWAT model has very good ability to replicate historical streamflow in the study area and which once calibrated effectively it can produce meaningful catchment predictions to aid management decisions.

4. To investigate the response of surface and subsurface hydrological processes under Ensembles of CMIP5-ESMs-RCPs scenario in the entire basin and sub-basin scale.

The future downscaled climate variables (precipitation and maximum and minimum temperature) have been used as an input to the ArcSWAT hydrological model to simulate various surface and sub-surface hydrological processes for both basin and sub-basin scale.

The analysis revealed that the mean annual surface runoff contribution to the streamflow and potential evapotranspiration will decrease in the entire basin and sub-basins for all the RCP scenarios with different magnitude. However, average annual precipitation, actual

evapotranspiration, groundwater contribution to streamflow, percolation from the root zone to shallow aquifer, soil water content and net water availability in the stream will increase with greater spatial variability in the basin. Annual variations of hydrological processes in all the sub-basins are similar regarding direction but different in magnitude as compared to entire basin analysis.

The 28.96% increase (mean of 3 ESMs) in precipitation at the end of the century (in the 2080s time slice) under RCP8.5 scenario, ArcSWAT produced 63.44% decline in surface runoff, 29.26% rise in actual evapotranspiration, 13.31% decline in potential evapotranspiration, 75.88% rise in groundwater contribution to the streamflow, and which leading to 27.97% rise in net water available in the stream. This uneven change can attribute to the non-linear nature of hydrological processes, such as evapotranspiration, surface runoff, and groundwater flow. Climate sensitivity has least pronounced in the basin; namely, a 28.96 % increase in precipitation under highest emission scenario (RCP8.5) results in 27.97% increase in annual discharge in the same scenario. However, high sensitivity has explained by the very low runoff coefficient (amount of runoff divided by rainfall; with a range from 0.07 to 0.21) of the entire basin and sub-basins, which makes the basin very sensitive to changes in precipitation.

Surface and subsurface hydrological processes in the entire basin and sub-basin scale have been computed and which highlighted an enormous spatial variability among all the six sub-basins. Soil water content (SW) exhibits very high magnitude for all sub-basins as compared to other components. Sub-basin scale analysis of surface and subsurface interactions could explore the long-term simulation of spatiotemporal variability of hydrological processes for the selected study basin. The SWAT based computation of both surface and subsurface components for entire basin and sub-basin scale provide a comprehensive assessment to obtain a better understanding of surface and subsurface hydrological interactions. Having sufficient knowledge about various hydrological processes and their responses to climate change in each sub-basin can guide water resources management in providing a more rigorous assessment and more efficient decision-making.

This study noticeably culminates that different features between sub-basins in a basin such as landuse land-cover and soil heterogeneity, topographic, surface-groundwater interactions, drainage area, shape, and stream networks can result in different hydrological responses to climate change in each sub-basin, and it is not at all logical to consider to have a linear

relationship between climate variables and hydrological processes of the entire river basin. This means that variations in the total average annual and seasonal climate variables may not necessarily translate into similar changes in hydrological processes in the entire basin. Therefore, calculating the water balance components in each sub-basin, along with the entire river basin provides a better understanding of the hydrological processes in response to climate change.

5. To analyze the annual, seasonal and monthly net water availability (in the 2020s, 2050s, and 2080s time slices) in the entire basin and sub-basin scale under ensembles of CMIP5-ESMs-RCPs scenario.

The mean annual water availability (mean of 3ESMs) possibly increased with the ranges 9.18 to 27.97% (RCP8.5), 3.98 to 19.61% (RCP4.5) and 11.82 to 17.06% (RCP2.6) in the entire basin. The spatial analysis of mean annual water availability revealed to increase by 25.25, 31.07 and 48.17% (SB1), 20.87, 22.53 and 29.67% (SB2), 1.83, 2.43 and 4.65% (SB3), 46.43, 52.73 and 69.81% (SB4), 26.19, 26.73 and 28.12% (SB5) and 22.79, 26.73 and 53.92% (SB6) in the 2020s, 2050s and 2080s time slice respectively from base period water availability (Figure 6a). It is observed that there is also significant spatial variation of mean annual water availability among sub-basins in the basin in base period as well as for future period.

In addition, it is observed that there is a larger seasonal and monthly variation in in water availability as compared to the variation in annual scale under all the future RCP scenarios for the entire basin as well as for each sub-basin is discussed in this study and taken to be an advantage over the other studies which focused only annual basis. Seasonal and monthly variations of net water availability in all the six sub-basins are similar regarding direction but different in magnitude to the entire basin. In all the RCP scenarios, the double peaking in net water availability (risk of flooding) ensues in Apr and Sep in the entire basin and sub-basin 4, Apr and Jul in sub-basin 1, Apr and Aug in sub-basin 2 and 3, Apr and Oct in sub-basin 5 and 6. Net water availability tends to decrease in the dry season in both basin and sub-basin scale analysis; this might cause water shortage in the lowland region and greater increase in intermediate and rainy seasons; this might cause flooding to some flood prone region of the basin.

6. To assess current and projected (in the 2020s, 2050s, and 2080s time slices) total annual water demand of the Weyib River basin under increasing population.

Current and projected population (human and livestock) number and water demand per capita per day data are considered to estimate the annual total water demand of the basin. Water demand estimation of the basin encompasses water demand for irrigation, domestic, commercial and public institutions, industrial, livestock consumption and water losses in the water supply system.

A 30 and 50 lpcd domestic water demands have been considered to estimate mean annual total water demand for current and future projection respectively as suggested by GDMP-II.3.1 (2007). For commercial and public institution water demand, a 5% of domestic water demand has considered. 10% of domestic water demand has deemed for industrial, and 20% of (domestic water demand plus commercial and public institutions water demand plus industrial water demand) has assumed for water losses in the water supply system. Two units of livestock have assumed for each population residing in Weyib River basin, and water consumption of each livestock has to be 25 lpd, a 50 lpcd (2×25 lpd) livestock water demand has considered in the estimation. Finally, 38 and 50 m^3 total water demand (considering domestic, commercial and public institutions, industrial, livestock, water losses in the system and water consumption variation based on time of day, the season and climatic conditions) per capita per year have been used to estimate current and future projection mean annual total water demand respectively.

As we have seen from water demand analysis results that it has highly correlated with number of population living in the basin. Higher number of population tends to have higher water demand. The total projected population of entire basin is increased by about 40.81% after 15 years in 2020, 130.80% after 45 years in 2050 and 229.12% after 75 years in 2080 from the base period population number (0.75 million in the year 2005).

The current total annual water demand (considering domestic, commercial and public institutions, industrial, livestock, water losses in the system and water consumption variation based on time of day, the season and climatic conditions) of the basin is found to be 28.49 Mm^3. The total annual irrigation water demand from three irrigation schemes (Bale Gadula, Tegona, Tebel) of the Weyib River basin is estimated to be 260.50 Mm^3 (Table 6.2). Therefore, total annual water demand of the Weyib River basin is estimated to be 289 Mm^3.

Irrigation is undoubtedly the leading user of water, accounting for about 90.14% of total water demand of the basin. The future projected total annual water demand of entire basin is increased by about 83.47% after 15 years in 2020, 200.67% after 45 years in 2050 and 328.78% after 75 years in 2080 from the base period water demand (detailed in Table 6.3). It is observed that there is a significant spatial variation of mean annual water demand among sub-basins in the basin in base period and for future period with uniform percentage increment (Figure 6b).

Current total annual water availability is much more (about eight times) than the current total annual water demands in the basin. In case of future projection, however, the level of percentage increment in water demand is much more than the water availability. But still the available flow in the Weyib River is sufficient to provide water for agriculture and domestic uses.

7. To estimate current and projected water resources status of the basin under CMIP5-ESMs-RCPs scenario.

The current (2005) and projected (in the 2020s, 2050s and 2080s time slice) water resources status of Weyib River basin were estimated based on Water Stress Index analysis (total water available divided by total number of population residing in the basin) for both basin and sub-basin scale and found to be water abundant basin currently (3112.23 m^3 per capita per year) and for the future too (Table 6.6) as compared to the threshold value of 1000 m^3 (IPCC, 2007) below which the basin considered to be water stressed. Since magnitude of current and projected water availability per capita per year in the entire basin is above the threshold value, therefore, the basin then might be considered as water abundant basin. However, the future water availability per capita per year (water resources status) was observed to decline by 11.78, 46.02 and 57.18% (RCP8.5), 16.69, 46.19 and 62.67% (RCP4.5) and 17.49, 47.45 and 64.34% (RCP2.6) in the 2020s, 2050s and 2080s time slice respectively from base period per capita per year water availability.

Spatial scale analyses of water resources status in all the sub-basins have shown a decreasing trend but different in magnitude as compared to entire basin analysis. It is observed that there is also significant spatial variation of mean annual water availability per capita per year among sub-basins in the basin in base period as well as for future period (Figure 6c). This

indicated that there might be a possibility to fall the basin under water stress condition in the long term.

8. To suggest possible adaptation options to alleviate the adverse impacts of climate change on water availability in upcoming period.

This objective is articulated based on (i) accomplishing the other objectives above specifically achieving objective number 5 and (ii) current various catchment activities in the basin. For instance, a key finding of objective number 5 is that 'net water availability tends to decrease in the dry season in both basin and sub-basin scale analysis; this might cause water shortage in the lowland region and greater increase in intermediate and rainy seasons; this might cause flooding to some flood prone region of the basin (specifically in the highland part of the basin)'. Based on this finding, therefore, possible adaptation options to alleviate these problems on water availability have been given in recommendation number 7 in section 7.2 below.

7.2 Recommendations

From the results found and challenges faced during this study the following recommendations have been forwarded:

1. Results of climate change impact analysis are very relying on the input data. Hence, more study in the area with the enhancement of existed data is necessary.

2. This study considered three CMIP5-ESMs (GFDL-ESM2M, CanESM2, and GFDL-ESM2G) output for the RCP8.5, RCP4.5, and RCP2.6 scenarios and SDSM has been used as a downscaling technique. Therefore, the additional study shall be carried out considering various CMIP5-ESMs outputs along with different downscaling techniques so as to minimize uncertainty arise due to GCM/ESM and downscaling technique.

3. ArcSWAT simulations for future various hydrologic components (for instance, surface runoff and groundwater contribution to the streamflow, actual and potential evapotranspiration, percolation to shallow aquifer and net available water in the stream; just to name a few) in the study area is subject to only future period (2006-2100) maximum and minimum temperature, and precipitation, keeping all other factors remain same. However, change in land use, management activities and other climate variables will

also enhance some impressions on different water balance components. So, achieving with these further researches might increase the certainty on the estimated results.

4. The landuse data used in this study is about 10 years old. Currently, a noticeable landuse change is going on in the basin, for instance, rapid urbanization encroaching into cultivated lands, increase of rural settlements and the expansion of cultivated areas into shrublands, natural resources management practices is being promoted (different catchment activities such as physical and biological soil and water conservation measures), land degradation is still an on-going process. These changes might have an effect on runoff generation and infiltration as well as evapotranspiration process. Therefore, further research has to be made considering recently developed landuse map.

5. The variation in water available in the stream among the six sub-basins in upcoming period is high. Therefore, there shall be water transfer from sub-basin having more available water in the small agricultural land to the sub-basin having less available water in a larger agricultural land to meet agricultural water demand in the basin.

6. Lack of measured and well-documented water demand data in the basin forced to make estimates from other data such as human and livestock population by applying unit water use rates. This may have an impact on the accuracy of estimated water demands, and therefore, further investigations are required in this regard.

7. Water resources availability will decrease in all months of the dry season, which might cause the water shortage in the lowland region. Increase in water availability in the intermediate and rainy seasons may lead to flooding in the flood-prone area of the basin. Therefore, to alleviate these problems an alternative source of water supply in the dry season like water harvesting technologies (to collect the available water during wet seasons with a view to use it in dry season) and the indigenous soil and water conservation technologies like cut-off drain/grassed waterways and water spreading bunds (contour bunds) are advisable to implement for the study area of Weyib River basin.

References

Abdo, K.S., Fiseha, B.M., Rientjes, T.H.M., Gieske, A.S.M., Haile, A.T., 2009. Assessment of climate change impacts on the hydrology of Gilgel Abay catchment in Lake Tana basin, Ethiopia. Hydrol. Process. 23, 3661–3669. doi:10.1002/hyp.7363

Adeogun, A.G., Sule, B.F., Salami, A.W., and Daramola, M.O., 2014. Validation of SWAT Model for Prediction of Water Yield and Water Balance: Case Study of Upstream Catchment of Jebba Dam in Nigeria. International Journal of Mathematical, Computational, Statistical, Natural and Physical Engineering, 8 (2), 264–270.

Aich, V., Liersch, S., Vetter, T., Huang, S., Tecklenburg, J., Hoffmann, P., Koch, H., Fournet, S., Krysanova, V., M??ller, E.N., Hattermann, F.F., 2014. Comparing impacts of climate change on streamflow in four large African river basins. Hydrol. Earth Syst. Sci. 18, 1305–1321. doi:10.5194/hess-18-1305-2014

Alexandrov, V., Genev, M., 2003. Climate Variability and Change Impact on Water Resources in Bulgaria. Eur. Water 12, 25–30.

Allen, J.G.A. and P.M., 1999. Automated methods for estimating baseflow and Florida is highly dependent on ground water mates of baseflow and recharge. Field. J. Am. Water Resour. Assoc. 35, 412–424.

Arnell, N.W., 2008. Climate change and global water resources 9.

Arnold, J.G., Kiniry, J.R., Srinivasan, R., Williams, J.R., Haney, E.B., and Neitsch, S.L., 2012. Soil & Water Assessment Tool: Input/output documentation, Version 2012. Texas Water Resources Institute, TR-439. Texas Water Resources Institute

Arnold, J.G., Srinivasan, R., Muttiah, R.S., Williams, J.R., 1998. Large area hydrologic modeling and assessment part I: model development. J. Am. Water Resour. Assoc. doi:10.1111/j.1752-1688.1998.tb05961.x

Arnold, J.G., Allen, P.M., Muttiah, R. and Bernhardt, G., 1995. Automated base flow separation and recession analysis techniques. Ground water, 33(6), pp.1010-1018.

Beasley, D.B. and Huggins, L.F., 1981. ANSWERS, areal nonpoint source watershed environment response simulation: user's manual.

Beck, L., Bernauer, T., 2011. How will combined changes in water demand and climate affect water availability in the Zambezi river basin? Glob. Environ. Chang. 21, 1061–1072. doi:10.1016/j.gloenvcha.2011.04.001

Boko, M., Niang, I., Nyong, A., Vogel, C., Githeko, A., Medany, M., Osman-Elasha, B., Tabo, R., Yanda, P., 2008. Africa. Clim. Chang. 2007 Impacts, Adapt. vulnerability. Contrib. Work. Gr. II to Fourth Assess. Rep. Intergov. Panel Clim. Chang. 433–467. doi:10.2134/jeq2008.0015br

Bouraoui, F., Benabdallah, S., Jrad, A., Bidoglio, G., 2005. Application of the SWAT model on the Medjerda river basin (Tunisia). Phys. Chem. Earth 30, 497–507. doi:10.1016/j.pce.2005.07.004

Brekke, L.D., Dettinger, M.D., Maurer, E.P., Anderson, M., 2008. Significance of model credibility in estimating climate projection distributions for regional hydroclimatological risk assessments. Clim. Change 89, 371–394. doi:10.1007/s10584-007-9388-3

Chekol, D.A., Tischbein, B., Eggers, H., Vlek, P., 2007. Application of SWAT for assessment of spatial distribution of water resources and analyzing impact of different land management practices on soil erosion in Upper Awash River Basin watershed. Water Resour. 110–117.

Chen, J., Brissette, F.P., Leconte, R., 2011. Uncertainty of downscaling method in quantifying the impact of climate change on hydrology. J. Hydrol. 401, 190–202. doi:10.1016/j.jhydrol.2011.02.020

Chiew, F.H., 2006. Estimation of rainfall elasticity of streamflow in Australia.Hydrological Sciences Journal, 51(4), pp.613-625.

Chiew, F.H. and McMahon, T.A., 2002. Modelling the impacts of climate change on Australian streamflow. Hydrological Processes, 16(6), pp.1235-1245.

Crosbie, R.S., McCallum, J.L., Walker, G.R. and Chiew, F.H., 2010. Modelling climate-change impacts on groundwater recharge in the Murray-Darling Basin, Australia. Hydrogeology Journal, 18(7), pp.1639-1656.

De Jong, B.H.J., Tipper, R., Montoya-Gómez, G., 2000. An economic analysis of the potential for

carbon sequestration by forests: Evidence from southern Mexico. Ecol. Econ. 33, 313–327. doi:10.1016/S0921-8009(99)00162-7

Dibike, Y.B., Coulibaly, P., 2005. Hydrologic impact of climate change in the Saguenay watershed: Comparison of downscaling methods and hydrologic models. J. Hydrol. 307, 145–163. doi:10.1016/j.jhydrol.2004.10.012

Dilnesaw Alamirew, (2006). Modelling of Hydrology and Soil Erosion of Upper Awash River Basin, PhD Thesis, University of Bonn

Dinar, A., 2006. District Level Hydroclimatic Time Series and Scenario Analysis to Assess the Impacts of Climate Change on Regional Water Resources and Agriculture in Africa. Discussion Paper No. 13. Special Series on Climate Change and Agriculture in Africa, 60 pp. ISBN 1-920160-01-09.

Eriksen, S.E.H., Watson, H.K., 2009. The dynamic context of southern African savannas: investigating emerging threats and opportunities to sustainability. Environ. Sci. Policy 12, 5–22. doi:10.1016/j.envsci.2008.10.009

Ethiopian National Meteorological Agency, 2007. Climate Change National Adaptation Programme of Action (Napa) of Ethiopia 1–73pp.

Faramarzi, M., Abbaspour, K.C., Ashraf Vaghefi, S., Farzaneh, M.R., Zehnder, A.J.B., Srinivasan, R., Yang, H., 2013. Modeling impacts of climate change on freshwater availability in Africa. J. Hydrol. 480, 85–101. doi:10.1016/j.jhydrol.2012.12.016

Farjad, B., Gupta, A., Marceau, D.J., 2016. Annual and Seasonal Variations of Hydrological Processes Under Climate Change Scenarios in Two Sub-Catchments of a Complex Watershed. Water Resour. Manag. 30, 2851–2865. doi:10.1007/s11269-016-1329-3

Farm Africa-SOS Sahel Ethiopia, 2007. Participatory Natural Resource Management Programme and Oromia Bureau of Agriculture and Rural Development, Six Months Report. 45p.

Faruqui, N.I., A.K. Biswas and M.J. Bino, Eds., 2001: Water Management in Islam. United Nations University Press, Tokyo, 149 pp.

Federal Democratic Republic of Ethiopia Ministry of Water Resources, Genale-Dawa River Basin Integrated Resources Development Master Plan Study Final Report, Vol. II.5.P. Social and Institutional Structures, July 2007

Federal Democratic Republic of Ethiopia Ministry of Water Resources, Genale-Dawa River Basin Integrated Resources Development Master Plan Study Final Report, Vol. II.3.1.Water Supply and Sanitation _ Final Report, July 2007

Federal Democratic Republic of Ethiopia Ministry of Water Resources, Genale-Dawa River Basin Integrated Resources Development Master Plan Study Final Report, Vol., II.3.H.Irrigation and Drainage_ Final Report, July 2007

Food agricultural Organization. FAO. Food Insecurity in the Horn of Africa. See: http://www.fao.org/docrep/003/x8530e/x8530e02.htm

Foster, G.R. and Lane, L.J., 1987. User requirements: USDA, water erosion prediction project (WEPP) Draft 6.3. NSERL report (USA).

Freibauer, A., Rounsevell, M.D.A., Smith, P., Verhagen, J., 2004. Carbon sequestration in the agricultural soils of Europe. Geoderma 122, 1–23. doi:10.1016/j.geoderma.2004.01.021

Fujihara, Y., Tanaka, K., Nagano, T., Watanabe, T., n.d. Assessing the impact of climate change on the water resources of the seyhan river basin, turkey 1.

Fujino, J., Nair, R., Kainuma, M., Masui, T. and Matsuoka, Y., 2006. Multi-gas mitigation analysis on stabilization scenarios using AIM global model.The Energy Journal, pp.343-353.

Gage, K.L., Burkot, T.R., Eisen, R.J., Hayes, E.B., 2008. Climate and Vectorborne Diseases. Am. J. Prev. Med. 35, 436–450. doi:10.1016/j.amepre.2008.08.030

Ghosh, S., Dutta, S., 2012. Impact of climate change on flood characteristics in Brahmaputra basin using a macro-scale distributed hydrological model. J. Earth Syst. Sci. 121, 637–657. doi:10.1007/s12040-012-0181-y

Ghosh, S., Mujumdar, P.P., 2008. Statistical downscaling of GCM simulations to streamflow using relevance vector machine. Adv. Water Resour. 31, 132–146. doi:10.1016/j.advwatres.2007.07.005

Giorgi, F., Hewitson, B., Christensen, J., Hulme, M., Storch, H. Von, Whetton, P., Jones, R., Mearns, L., and Fu, C., 2001. Regional Climate Information – Evaluation and Projections. In: J.T

Houghton, Y. Ding, D.J. Griggs, M. Noguer, P.J. van der Linden, X. Dai, K. Maskell, and C.A. Johnson, eds. Climate Change 2001: The Scientific Basis. New York: Cambridge University Press, Cambridge, 583 – 638

Gleick, P.H., 1996. Basic water requirements for human activities: meeting basic needs. Water Int. 21, 83–92. doi:10.1080/02508069608686494

Goosse H., P.Y. Barriat, W. Lefebvre, M.F.L. and V.Z., 2015. Introduction to climate dynamics and climate modeling [online].
Available from: http://www.climate.be/textbook (Accessed 30 Jun 2015).

Gosain, A K., Rao, S., Basuray, D., 2006. Climate change impact assessment on hydrology of Indian river basins. Current 90, 346–353.

Goyal, M.K., Ojha, C.S.P., 2011. Evaluation of linear regression methods as downscaling tools in temperature projections over the Pichola Lake Basin in India. Hydrol. Process. 25, 1453–1465. doi:10.1002/hyp.7911

Graham, L.P., Andersson, L., Horan, M., Kunz, R., Lumsden, T., Schulze, R., Warburton, M., Wilk, J., Yang, W., 2011. Using multiple climate projections for assessing hydrological response to climate change in the Thukela River Basin, South Africa. Phys. Chem. Earth 36, 727–735. doi:10.1016/j.pce.2011.07.084

Green, W.H. and Ampt, G.A., 1911. Studies on Soil Phyics. The Journal of Agricultural Science, 4(01), pp.1-24.

Grotch, S.L., MacCracken, M.C., 1991. The Use of General Circulation Models to Predict Regional Climatic Change. J. Clim.
doi:10.1175/1520-0442(1991)004<0286:TUOGCM>2.0.CO;2

Gupta, H.V., Sorooshian, S. and Yapo, P.O., 1999. Status of automatic calibration for hydrologic models: Comparison with multilevel expert calibration. Journal of Hydrologic Engineering, 4(2), pp.135-143.

Hamed, K.H., 2008. Trend detection in hydrologic data: The Mann–Kendall trend test under the scaling hypothesis. J. Hydrol. 349, 350–363. doi:10.1016/j.jhydrol.2007.11.009

Hay, L.E., Clark, M.P., 2003. Use of statistically and dynamically downscaled atmospheric model output for hydrologic simulations in three mountainous basins in the western United States. J. Hydrol. 282, 56–75. doi:10.1016/S0022-1694(03)00252-X

Heavens, N.G., Ward, D.S. and Natalie, M.M., 2013. Studying and Projecting Climate Change with Earth System Models. Nature Education Knowledge,4(5), p.4.

Hempel, S., Frieler, K., Warszawski, L., Schewe, J., Piontek, F., 2013. A trend-preserving bias correction – The ISI-MIP approach. Earth Syst. Dyn. 4, 219–236. doi:10.5194/esd-4-219-2013

Hijioka, Y., Y. Matsuoka, H. Nishimoto, M. Masui, and M. Kainuma, 2008. Global GHG emissions scenarios under GHG concentration stabilization targets, Journal of Global Environmental Engineering 13, 97-108

Hoar, T., Nychka, D., 2008. Statistical Downscaling of the Community Climate System(CCSM) monthly temperature and precipitation projections.

Hutson, B.S.S., Schwarz, B.G.E., 1996. Estimates of Future Water Demand for Selected Water-Service Areas in the Upper Duck River Basin , Central Tennessee With a section on Methodology Used to Develop Population Forecasts for Bedford , Marshall , and Maury Counties , Tennessee , From 1993 Though 1995.

Indian Network for Climate Change Assessment (INCCA), 2010. Climate Change and India: A 4X4 Assessment A sectoral and regional analysis for 2030s, Ministry of Environment & Forests Government of India, November 2010.

IPCC, 2014. Climate Change 2014: Synthesis Report. Contribution of Working Groups I, II and III to the Fifth Assessment Report of the Intergovernmental Panel on Climate Change, Core Writing Team, R.K. Pachauri and L.A. Meyer. doi:10.1017/CBO9781107415324.004

IPCC, 2013. Climate Change 2013: The Physical Science Basis. Contribution of Working Group I to the Fifth Assessment Report of the Intergovernmental Panel on Climate Change. Intergov. Panel Clim. Chang. Work. Gr. I Contrib. to IPCC Fifth Assess. Rep. (AR5)(Cambridge Univ Press. New York) 1535. doi:10.1029/2000JD000115

IPCC, 2008. Climate Change and Water. Intergovernmental Panel on Climate Change Working Group

II Technical Support. Cambridge University Press, Cambridge, United Kingdom and New York, NY, USA

IPCC, 2007. Climate change 2007 : impacts, adaptation and vulnerability : Working Group II contribution to the Fourth Assessment Report of the IPCC Intergovernmental Panel on Climate Change. Work. Gr. II Contrib. to Intergov. Panel Clim. Chang. Fourth Assess. Rep. 1, 976. doi:10.2134/jeq2008.0015br

IPCC, 2001. Climate Change 2001 : impacts , adaptation and vulnerability. Work. Gr. II Impacts Adapt. vulnerability 10. doi:10.1002/joc.775

Jandl, R., Lindner, M., Vesterdal, L., Bauwens, B., Baritz, R., Hagedorn, F., Johnson, D.W., Minkkinen, K., Byrne, K.A., 2007. How strongly can forest management influence soil carbon sequestration? Geoderma 137, 253–268. doi:10.1016/j.geoderma.2006.09.003

Jha, M.K., 2011. Evaluating Hydrologic Response of an Agricultural Watershed for Watershed Analysis. Water 3, 604–617. doi:10.3390/w3020604

Kabat, P., Ludwig, F., van der Valk, M. and van Schaik, H. eds., 2012.Climate change adaptation in the water sector. Routledge.

Karpouzos, D.., Kavalieratou, S., Babajimopoulos, C., 2010. Trend analysis of precipitation data in Pieria Region (Greece). Eur. Water 30, 31–40.

Kharchaf, Y., Rhinane, H., Kaoukaya, A. and Fadil, A., 2013. The Contribution of the Geospatial Information to the Hydrological Modelling of a Watershed with Reservoirs: Case of Low Oum Er Rbiaa Basin (Morocco).Journal of Geographic Information System, 5(3), p.258.

Kidson, J.W. and Thompson, C.S., 1998. A comparison of statistical and model-based downscaling techniques for estimating local climate variations.Journal of Climate, 11(4), pp.735-753.

Kim, U., Kaluarachchi, J.J., 2009. Climate change impacts on water resources in the upper Blue Nile River Basin, Ethiopia, Journal of the American Water Resources Association. doi:10.1111/j.1752-1688.2009.00369.x

Knisel, W.G., 1980. CREAMS: a field scale model for Chemicals, Runoff, and Erosion from Agricultural Management Systems [USA]. United States. Dept. of Agriculture. Conservation research report (USA).

Krause, P., Boyle, D.P., 2005. Advances in Geosciences Comparison of different efficiency criteria for hydrological model assessment. Adv. Geosci. 5, 89–97. doi:10.5194/adgeo-5-89-2005

Kundzewicz, Z.W., Mata, L.J., Arnell, N.W., Döll, P., Jimenez, B., Miller, K.A., Oki, T., Sen, Z., Shiklomanov, I.A., 2008. The implications of projected climate change for freshwater resources and their management. Hydrol. Sci. 53, 3–10. doi:10.1623/hysj.53.1.3

Kusangaya, S., Warburton, M.L., Archer van Garderen, E., Jewitt, G.P.W., 2014. Impacts of climate change on water resources in southern Africa: A review. Phys. Chem. Earth 67-69, 47–54. doi:10.1016/j.pce.2013.09.014

Ladd, J., Driscoll, D., 1980. A comparison of objective and subjective means of weather typing: an example from West Texas. J. Appl. Meteorol.

Lasco, R.D., Lales, J.S., Arnuevo, M.T., Guillermo, I.Q., de Jesus, A.C., Medrano, R., Bajar, O.F., Mendoza, C. V., 2002. Carbon dioxide (CO2) storage and sequestration of land cover in the Leyte Geothermal Reservation. Renew. Energy 25, 307–315. doi:10.1016/S0960-1481(01)00065-9

Latha, J., Saravanan, S., Palanichamy, K., 2010. A Semi – Distributed Water Balance Model for Amaravathi River Basin using Remote Sensing and GIS. Int. J. Geomatics Geosci. 1, 252–263.

Legates, D.R., 2005. Evaluating the Use of “Goodness of Fit” Measures in Hydrologic and Hydroclimatic Model Validation 35, 233–241.

Legesse, S.A., Rao, P.V.V.P., Rao, M.M.N., n.d. Statistical Downscaling of Daily Temperature and Rainfall Data From Global Circulation Models : in South Wollo Zone , North Central Ethiopia 27–39.

Lenderink, G., Buishand, a., van Deursen, W., 2007. Estimates of future discharges of the river Rhine using two scenario methodologies: direct versus delta approach. Hydrol. Earth Syst. Sci. 11, 1145–1159. doi:10.5194/hess-11-1145-2007

Lenhart, T., Eckhardt, K., Fohrer, N., Frede, H.-G., 2002. Comparison of two different approaches of sensitivity analysis. Phys. Chem. Earth, Parts A/B/C 27, 645–654. doi:10.1016/S1474-

7065(02)00049-9
Liersch, S., 2003. The Program pcpSTAT: user's manual. Berlin, August 2003, 5.
Liu, L., Liu, Z., Ren, X., Fischer, T., Xu, Y., 2011. Hydrological impacts of climate change in the Yellow River Basin for the 21st century using hydrological model and statistical downscaling model. Quat. Int. 244, 211–220. doi:10.1016/j.quaint.2010.12.001
Loukas, A., Sidiropoulos, P., Mylopoulos, N., Vasiliades, L., Zagoriti, K., 2015. Assessment of the effect of climate variability and change and human intervention in the lake Karla aquifer. Eur. Water 19, 31-54.
Lupo, A., Kininmonth, W., 2013. Global Climate Models and Their Limitations. Clim. Chang. Reconsidered II Phys. Sci. 1–142.
Manton, M.J., Della-Marta, P.M., Haylock, M.R., Hennessy, K.J., Nicholls, N., Chambers, L.E., Collins, D.A., Daw, G., Finet, A., Gunawan, D., Inape, K., Isobe, H., Kestin, T.S., Lefale, P., Leyu, C.H., Lwin, T., Maitrepierre, L., Ouprasitwong, N., Page, C.M., Pahalad, J., Plummer, N., Salinger, M.J., Suppiah, R., Tran, V.L., Trewin, B., Tibig, I., Yee, D., 2001. Trends in extreme daily rainfall and temperature in southeast Asia and the south Pacific: 1961-1998. Int. J. Climatol. 21, 269–284. doi:10.1002/joc.610
Maurer, E.P., Brekke, L., Pruitt, T., Duffy, P.B., 2007. Fine-resolution climate projections enhance regional climate change impact studies. Eos, Trans. Am. Geophys. Union 88, 504–504. doi:10.1029/2007EO470006
McCarthy, J.J., 2001. Climate change 2001: impacts, adaptation, and vulnerability: contribution of Working Group II to the third assessment report of the Intergovernmental Panel on Climate Change. Cambridge University Press.
Mearns, L.O., 2009. Methods of Downscaling Future Climate Information and Applications [online], Available from:
https://www.narccap.ucar.edu/users/user-meeting
09/talks/Downscaling_summary_for_NARCCAP_Users_Meet09.pdf (Accessed 10 Jun 2015).
Misra, V., Dirmeyer, P.A., Kirtman, B.P., 2003. Dynamic downscaling of seasonal simulations over South America. J. Clim. 16, 103–117.
doi:10.1175/1520-0442(2003)016<0103:DDOSSO>2.0.CO;2
Monteith, J.L., 1965. Eavaporation and the environment. In The State and Movement of Water in living Organisms, XIXth Symposium. Soc. For Exp. Biol., Swansea, Cam-bridge University Press. pp. 205-234
Morgan, R.P.C., Quinton, J.N., Smith, R.E., Govers, G., Poesen, J.W.A., Auerswald, K., Chisci, G., Torri, D., Styczen, M.E., 1998. the European Soil Erosion Model (Eurosem): a Dynamic Approach for Predicting Sediment Transport From. Earth Surf. Process. Landforms 23, 527–544. doi:10.1002/(SICI)1096-9837(199906)24
Moriasi, D.N., Arnold, J.G., Van Liew, M.W., Binger, R.L., Harmel, R.D., Veith, T.L., 2007. Model evaluation guidelines for systematic quantification of accuracy in watershed simulations. Trans. ASABE 50, 885–900. doi:10.13031/2013.23153
Moss, R.H., Edmonds, J. a, Hibbard, K. a, Manning, M.R., Rose, S.K., van Vuuren, D.P., Carter, T.R., Emori, S., Kainuma, M., Kram, T., Meehl, G. a, Mitchell, J.F.B., Nakicenovic, N., Riahi, K., Smith, S.J., Stouffer, R.J., Thomson, A.M., Weyant, J.P., Wilbanks, T.J., 2010. The next generation of scenarios for climate change research and assessment. Nature 463, 747–56. doi:10.1038/nature08823
Mpelasoka, F.S., Chiew, F.H.S., 2009. Influence of Rainfall Scenario Construction Methods on Runoff Projections. J. Hydrometeorol. 10, 1168–1183. doi:10.1175/2009JHM1045.1
Mujumdar, P.P., n.d. Modeling Climate Change Impacts on Regional Water Resources.
Murphy, J., 1999. An evaluation of statistical and dynamical techniques for downscaling local climate. J. Clim. 12, 2256–2284.
doi:10.1175/1520-0442(1999)012<2256:AEOSAD>2.0.CO;2
Nash, J.E. and Sutcliffe, J.V., 1970. River flow forecasting through conceptual models part I—A discussion of principles. Journal of hydrology,10(3), pp.282-290.
Neitsch, S.L., Arnold, J.G., Kiniry, J.R., Srinivasan, R., Williams, J.R., 2002. Soil and Water Assessment Tool User's Manual. TWRI Rep. TR-192 412.
Neitsch, S.L., Arnold, J.G., Kiniry, J.R., Williams., J.R., 2005. Soil and Water Assessment Tool

User's Manual Version 2005. Diffus. Pollut. Conf. Dublin 10, 494.
New, M., Hewitson, B., Stephenson, D.B., Tsiga, A., Kruger, A., Manhique, A., Gomez, B., Coelho, C.A.S., Masisi, D.N., Kululanga, E., Mbambalala, E., Adesina, F., Saleh, H., Kanyanga, J., Adosi, J., Bulane, L., Fortunata, L., Mdoka, M.L., Lajoie, R., 2006. Evidence of trends in daily climate extremes over southern and west Africa. J. Geophys. Res. Atmos. 111, 1–11. doi:10.1029/2005JD006289
Nigatu, Z.M., 2013. Hydrological Impacts of Climate Change On Lake Tana ' s Water Balance Hydrological Impacts of Climate Change On Lake Tana ' s Water Balance 57.
NOAA (National Oceanic and Atmospheric Administration), 2015. The First Climate Model [online]. Available from: http://celebrating200years.noaa.gov/breakthroughs/climate_model/welcome.html#model(Accessed 30 Jun 2015)
NOAA, 2009. Climate modeling [online]. Available from: http://www.gfdl.noaa.gov/climatemodeling\npapers2://publication/uuid/66FC00BF-F75E-42ED-8833-6DEE1013FB96 (Accessed 30 Jun 2015)
Omani, N., Tajrishy, M., Abrishamchi, A., 2007. Modeling of a River Basin Using SWAT Model and GIS. Rivers'07 510–517.
Pierce, D.W., Barnett, T.P., Santer, B.D., Gleckler, P.J., 2009. Selecting global climate models for regional climate change studies. Proc. Natl. Acad. Sci. 106, 8441–8446. doi:10.1073/pnas.0900094106
Reichler, T., Kim, J., 2008. How well do coupled models simulate today's climate? Bull. Am. Meteorol. Soc. 89, 303–311. doi:10.1175/BAMS-89-3-303
Hailemariam, K., 1999. Impact of climate change on the water resources of Awash River Basin , Ethiopia. Clim. Res. 12, 91–96. doi:10.3354/cr012091
Riahi, K., Grübler, A., Nakicenovic, N., 2007. Scenarios of long-term socio-economic and environmental development under climate stabilization. Technol. Forecast. Soc. Change 74, 887–935. doi:10.1016/j.techfore.2006.05.026
Roy, S.B., Chen, L., Girvetz, E., Maurer, E.P., Mills, W.B. and Grieb, T.M., 2010. Evaluating sustainability of projected water demands under future climate change scenarios. New York: Natural Resources Defense Council.
Rutashobya, D.G., 2008. Climate change scenarios impacts and adaptation strategies in Africa climate and water department. towards climate change adaptation building adaptive capacity in managing African Transboundary River Basins. In WEnt, Zschortau, Germany. International Water Management Institute (IWMI Research Report 126), 27.
Sachindra, D.A., Huang, F., Barton, A., Perera, B.J.C., 2014. Statistical downscaling of general circulation model outputs to precipitation-part 2: Bias-correction and future projections. Int. J. Climatol. 34, 3282–3303. doi:10.1002/joc.3915
Salzmann, N., Frei, C., Vidale, P.L., Hoelzle, M., 2007. The application of Regional Climate Model output for the simulation of high-mountain permafrost scenarios. Glob. Planet. Change 56, 188–202. doi:10.1016/j.gloplacha.2006.07.006
Sarma, B., Sarma, A.K., Singh, V.P., 2013. Optimal Ecological Management Practices (EMPs) for Minimizing the Impact of Climate Change and Watershed Degradation Due to Urbanization. Water Resour. Manag. 27, 4069–4082. doi:10.1007/s11269-013-0396-y
Schmidli, J., Goodess, C.M., Frei, C., Haylock, M.R., Hundecha, Y., Ribalaygua, J., Schmith, T., 2007. Statistical and dynamical downscaling of precipitation: An evaluation and comparison of scenarios for the European Alps. J. Geophys. Res. Atmos. 112, 1–20. doi:10.1029/2005JD007026
Schoof, J.T., Arguez, A., Brolley, J., O'Brien, J.J., 2005. A new weather generator based on spectral properties of surface air temperatures. Agric. For. Meteorol. 135, 241–251. doi:10.1016/j.agrformet.2005.12.004
Sebhat, M.Y., 2015. Assessments of Water Demandsfor the Jubaand Shabelle Rivers in Somalia. Integr. J. Br. 2, 16–29. doi:10.12895/jaeid.20152.318
Serur, A.B., Sarma, A.K., 2016a. Evaluation of the ArcSWAT Model in Simulating Catchment Hydrology : In Weyib River Basin , Bale Mountainous Area of Southeastern Ethiopia. Int. J. Innov. Emerg. Res. Eng. 3(2): 3-11

Setegn, S.G., Rayner, D., Melesse, A.M., Dargahi, B., Srinivasan, R., 2011. Impact of climate change on the hydroclimatology of Lake Tana Basin, Ethiopia. Water Resour. Res. 47, 1–13. doi:10.1029/2010WR009248

Setegn, S.G. 2010. Modeling Hydrological and Hydrodynamic Processes in Lake Tana Basin, Ethiopia, KTH. TRITA-LWR PhD Thesis 1057

Sharma, R.H., Shakya, N.M., 2006. Hydrological changes and its impact on water resources of Bagmati watershed, Nepal. J. Hydrol. 327, 315–322. doi:10.1016/j.jhydrol.2005.11.051

Shawul, A.A., Alamirew, T., Melesse, A.M. and Chakma, S., 2016. Climate Change Impact on the Hydrology of WeyibRiver Watershed, Bale Mountainous Area, Ethiopia. In Landscape Dynamics, Soils and Hydrological Processes in Varied Climates (pp. 587-613). Springer International Publishing

Shawul, A.A., Alamirew, T., Dinka, M.O., 2013. Calibration and validation of SWAT model and estimation of water balance components of Shaya mountainous watershed, Southeastern Ethiopia. Hydrol. Earth Syst. Sci. Discuss. 10, 13955–13978. doi:10.5194/hessd-10-13955-2013

Shiklomanov, I.A., Rodda, J.C., 2003. World Water Resources at the Beginning of the Twenty-First Century. Cambridge Univ. Press 452.

Shongwe, M.E., Van Oldenborgh, G.J., Van Den Hurk, B.J.J.M., De Boer, B., Coelho, C.A.S., Van Aalst, M.K., 2009. Projected changes in mean and extreme precipitation in Africa under global warming. Part I: Southern Africa. J. Clim. 22, 3819–3837. doi:10.1175/2009JCLI2317.1

Singh, J., Knapp, H.V., Arnold, J.G., Demissie, M., 2004. Hydrologic Modeling of the Iroquois River Watershed Using HSPF and SWAT. J. Am. Water Resour. Assoc. 41, 343–360. doi:10.1111/j.1752-1688.2005.tb03740.x

Srinivasan, R., Zhang, X., Arnold, J., 2010. Swat Ungauged: Hydrological Budget and Crop Yield Predictions in the Upper Mississippi River Basin. Am. Soc. Agric. Biol. Eng. 53, 1533–1546. doi:10.13031/2013.34903

Taylor, K.E., Stouffer, R.J., Meehl, G.A., 2012. An overview of CMIP5 and the experiment design. Bull. Am. Meteorol. Soc. 93, 485–498. doi:10.1175/BAMS-D-11-00094.1

Tetsoane, S.T., 2013. Evaluation of the SWAT model in simulating catchment hydrology: case study of the Modder River Basin (Doctoral dissertation, Bloemfontein: Central University of Technology, Free State).

Thomson, A.M., Calvin, K. V., Smith, S.J., Kyle, G.P., Volke, A., Patel, P., Delgado-Arias, S., Bond-Lamberty, B., Wise, M.A., Clarke, L.E., Edmonds, J.A., 2011. RCP4.5: A pathway for stabilization of radiative forcing by 2100. Clim. Change 109, 77–94. doi:10.1007/s10584-011-0151-4

Tisseuil, C., Vrac, M., Lek, S., Wade, A.J., 2010. Statistical downscaling of river flows. J. Hydrol. 385, 279–291. doi:10.1016/j.jhydrol.2010.02.030

Strzepek, K. and McCluskey, A., 2006. District level hydroclimatic time series and scenario analysis to assess the impacts of climate change on regional water resources and agriculture in Africa (Vol. 13). CEEPA Discussion Paper.

Todini, E., 2007. Hydrological catchment modelling : past , present and future 11, 468–482.

United Nations, 2004. World Population To 2300. New York 18, 553–561. doi:10.1016/j.asieco.2007.02.015

U.S. Army Corps of Engineers, 2000: Design and Construction of Levees, Manual No. 1110-2-1913, Washington, DC 20314-1000.

USDA-SCS (United States Department of Agriculture-Soil Conservation Service), 1972. National Engineering Handbook Section 4 Hydrology, Chapters 4-10.

Van Griensven, A., Meixner, T., Grunwald, S., Bishop, T., Diluzio, M., Srinivasan, R., 2006. A global sensitivity analysis tool for the parameters of multi-variable catchment models. J. Hydrol. 324, 10–23. doi:10.1016/j.jhydrol.2005.09.008

Van Griensven, A., 2005. Sensitivity, auto-calibration, uncertainty and model evaluation in SWAT2005. Unpublished report.

Van Vuuren, D.P., Den Elzen, M.G.J., Lucas, P.L., Eickhout, B., Strengers, B.J., Van Ruijven, B., Wonink, S., Van Houdt, R., 2007. Stabilizing greenhouse gas concentrations at low levels: An assessment of reduction strategies and costs. Clim. Change 81, 119–159. doi:10.1007/s10584-

006-9172-9
Vano, J.A., Scott, M.J., Voisin, N., St??ckle, C.O., Hamlet, A.F., Mickelson, K.E.B., Elsner, M.M., Lettenmaier, D.P., 2010. Climate change impacts on water management and irrigated agriculture in the Yakima River Basin, Washington, USA. Clim. Change 102, 287–317. doi:10.1007/s10584-010-9856-z
Vaughn, J., 2007. Conflicts over natural resources: A reference handbook. ABC-CLIO.
Vermeulen, S.J., Aggarwal, P.K., Ainslie, A., Angelone, C., Campbell, B.M., Challinor, A.J., Hansen, J.W., Ingram, J.S.I., Jarvis, A., Kristjanson, P., Lau, C., Nelson, G.C., Thornton, P.K., Wollenberg, E., 2012. Options for support to agriculture and food security under climate change. Environ. Sci. Policy 15, 136–144. doi:10.1016/j.envsci.2011.09.003
Vetter, T., Huang, S., Yang, T., Aich, V., Wang, X., Gu, H., Krysanova, V., Hattermann, F.F., 2013. Intercomparison of climate impacts and evaluation of uncertainties from different sources using three regional hydrological models for three river basins on three continents 1–11.
Vinnarasir and Arup Kumar Sarma, 2011: Impact of Climate Change on a Southern Tributary of Brahmaputra Basin, A Study Report, Department of Civil Engineering, Indian Institute of Technology Guwahati, December 2011
Wang, J., Wang, E., Liu, D.L., 2011. Modelling the impacts of climate change on wheat yield and field water balance over the Murray-Darling Basin in Australia. Theor. Appl. Climatol. 104, 285–300. doi:10.1007/s00704-010-0343-2
Wang, L., 2005. Cooperative Water Resources Allocation among Competing Users.
Watson, R.T., Zinyowera, M.C. and Moss, R.H., 1996. Climate Change 1995 impacts, adaptations and mitigation of climate change: Scientific-technical analysis. Cambridge University Press.
Wilby, R.L., Charles, S.P., Zorita, E., Timbal, B., Whetton, P., Mearns, L.O., 2004. Guidelines for Use of Climate Scenarios Developed from Statistical Downscaling Methods. Analysis 27, 1–27. doi:citeulike-article-id:8861447
Wilby, R.L., Dawson, C.W., 2007. SDSM 4.2-A decision support tool for the assessment of regional climate change impacts, Version 4.2 User Manual. Lancaster Univ. Lancaster/Environment Agency Engl. Wales 1–94.
Wilby, R.L., Dawson, C.W., Barrow, E.M., 2002. SDSM-a Decision Support Tool for the Assessment of Regional Climate Change Impacts. Environ. Model. Softw. 17, 145–157. doi:10.1016/S1364-8152(01)00060-3
Wilby, R.L., Hassan, H., Hanaki, K., 1998. Statistical downscaling of hydrometeorological variables using general circulation model output 205, 1–19.
Wilby, R.L., Wigley, T.M.L., 2000. Precipitation predictors for downscaling: Oberserved and General Circulation Model relationships. Int. J. Clim. 20, 641–661. doi:Doi 10.1002/(Sici)1097-0088(200005)20:6<641::Aid-Joc501>3.0.Co;2-1
Williams, J.R., 1969. Flood routing with variable travel time or variable storage coefficients. Transactions of the ASAE, 12(1), pp.100-0103.
Williams JR. The EPIC model. In: Singh VP. (Ed). Computer models of watershed hydrology. Water Resources Publications, Highlands Ranch, CO, 1995, Chapter 25, pp. 909-1000.
Wise, M., Calvin, K., Thomson, A., Clarke, L., Bond-lamberty, B., Sands, R., Smith, S.J., Janetos, A., Edmonds, J., 2009. T 25 20 324, 1183–1186. doi:10.1038/ncb2099
Wood, A.W., Leung, L.R., Sridhar, V., Lettenmaier, D.P., 2004. Hydrologic implications of dynamical and statistical approaches to downscaling climate model outputs. Clim. Change 62, 189–216. doi:10.1023/B:CLIM.0000013685.99609.9e
Xu, C.Y., 2002. Hydrologic models. Uppsala University, Department of Earth Sciences and Hydrology.
Xu, C., 1999a. Climate Change and Hydrologic Models : A Review of Existing Gaps and Recent Research Developments. Water Resour. Manag. 13, 369–382. doi:10.1023/A:1008190900459
Xu, C., 1999b. From GCMs to river flow: a review of downscaling methods and hydrologic modelling approaches. Prog. Phys. Geogr. 23, 229–249. doi:10.1191/030913399667424608
Yakob, M., 2009. Climate change impact assessment on soil water availability and crop yield in Anjeni watershed blue Nile basin.
Young, R.A., Onstad, C.A., Bosch, D.D. and Anderson, W.P., 1987. AGNPS, Agricultural Non-Point-Source Pollution Model: a watershed analysis tool. Research report (No. PB-88-135876/XAB; CONSERVATION/RR-35). Agricultural Research Service, Albany, CA (USA). Western Utilization Research and Development Div..
Zhao, G., Tian, P., Mu, X., Jiao, J., Wang, F., Gao, P., 2014. Quantifying the impact of climate variability and human activities on streamflow in the middle reaches of the Yellow River basin, China. J. Hydrol. 519, 387–398. doi:10.1016/j.jhydrol.2014.07.014

Publications and Award Based on the Present Ph.D. Thesis Work

The candidate (first author) and his supervisor (second author) have contributed the following publications to the knowledge of the area.

A. Journal Publication

I. **Abdulkerim B. Serur,** Arup Kr. Sarma, 2017. Impact of Spatial Data Availability on Climate Change Prediction in the Weyib River Basin in Ethiopia. Water Resources Management, 31 (6): 1809–1824 DOI: 10.1007/s11269-017-1613-x *(Status: Published, Springer)*

II. **Abdulkerim B. Serur**, Arup Kr. Sarma, 2017. Current and Projected Water Demand and Water Availability Estimates under Climate Change Scenarios in the Weyib River Basin in Bale Mountainous Area of Southeastern Ethiopia. Theoretical and Applied Climatology, 129 (1-2): 1-9, DOI: 10.1007/s00704-017-2219-1 *(Status: Published, Springer)*

III. **Abdulkerim B. Serur**, Arup Kr. Sarma, 2017. Climate Change Impacts Analysis on Hydrological Processes in the Weyib River Basin in Ethiopia *(Status: Under Review at **Water Resources Management Journal, Springer***)

IV. **Abdulkerim B. Serur**, Arup Kr. Sarma, 2016. Evaluation of the ArcSWAT Model in Simulating Catchment Hydrology: In Weyib River Basin, Bale Mountainous Area of Southeastern Ethiopia. Int. J. Innov. Emerg. Res. Eng. 3(2): 3-11 *(Status: Published)*

V. **Abdulkerim B. Serur**, Arup Kr. Sarma, 2016. Impact of Climate Change on Water Availability in the Weyib River Basin, Southeastern Ethiopia: Int. J. Innov. Res. Sci. Eng. Tech. 5(6): 9704-9712, DOI: 10.15680/IJIRSET.2016.0506028 *(Status: Published)*

B. International Conference

VI. **Abdulkerim B. Serur**, Arup Kr. Sarma, 2016. Statistical Downscaling of Daily Temperature and Precipitation Data from Coupled Model Inter-Comparison Project 5 (CMIP5): In Weyib River Watershed, Bale Mountainous Area, Ethiopia: A paper presented to *International Conference on Water, Environment, Energy and Society* ICWEES-2016 (Organized By Texas A&M University & AISECT University) March 15-18, 2016, Bhopal, India.

C. Book Chapter

VII. **Abdulkerim B. Serur**, Arup Kr. Sarma (2016) Statistical Downscaling of Daily Temperatures and Precipitation Data from CMIP5-RCP Experiment: In Weyib River Basin, Bale Mountainous Area, Ethiopia *(Status: Accepted for publication **in Water Science and Technology Library Book Series, Springer)***

D. Academic Award

VIII. **'Best Research Paper Awarded'** in the International Conference on Water, Environment, Energy and Society ICWEES-2016 (Organized By Texas A&M University & Aisect University) March 15-18, 2016, Bhopal, India.

Appendices

Appendix A

Appendix Tables

Selection of Predictor variables

In this section, station wise as well as the whole study area of Weyib River basin, lists of selected predictor variables that gave better correlation results at $p<0.05$ for CanESM2, GFDL-ESM2M and GFDL-ESM2G-historical models are presented below.

Appendix Table 1 Lists of selected potential predictor variables from CanESM2-historical model for station: Adaba

Predictand	Predictor full name	Notations	Parti.cor. (r-value)	p-value
Precipitation	Specific humidity at 850 hPa	ceshs850gl.dat	0.084	0.000
	Surface specific humidity	ceshshumgl.dat	-0.068	0.000
Maximum temperature	Mean sea level pressure	ceshmslpgl.dat	0.111	0.000
	500 hPa geopotential height	ceshp500gl.dat	0.072	0.000
	Specific humidity at 850 hPa	ceshs850gl.dat	-0.268	0.000
	Mean temperature at 2m	ceshtempgl.dat	0.120	0.000
Minimum temperature	Mean sea level pressure	ceshmslpgl.dat	-0.190	0.000
	500 hPa geopotential height	ceshp500gl.dat	0.177	0.000
	Surface specific humidity	ceshshumgl.dat	0.132	0.000
	Mean temperature at 2m	ceshtempgl.dat	-0.069	0.000

Appendix Table 2 Lists of selected potential predictor variables from GFDL_ESM2M-historical model for station: Adaba

Predictand	Predictor full name	Notations	Parti.cor. (r-value)	p-value
Precipitation	Daily minimum near-surface air temperature	geshtasmingl.dat	-0.056	0.003
	Eastward near-surface wind	geshuasgl.dat	0.056	0.003
Maximum temperature	Sea level pressure	geshpslgl.dat	-0.141	0.000
	Near-surface relative humidity	geshrhsgl.dat	-0.127	0.000
	Daily maximum near-surface air temperature	geshtasmaxgl.dat	0.142	0.000
	Eastward near-surface wind	geshuasgl.dat	-0.127	0.000
Minimum temperature	Surface downwelling longwave radiation	geshrldsgl.dat	0.222	0.000
	Daily maximum near-surface air temperature	geshtasmax.dat	-0.159	0.000
	Eastward near-surface wind	geshuasgl.dat	0.132	0.000

Appendix Table 3 Lists of selected potential predictor variables from GFDL_ESM2G-historical model for station: Adaba

Predictand	Predictor full name	Notations	Parti.cor. (r-value)	p-value
Precipitation	Daily minimum near-surface air temperature	geshtasmingl.dat	-0.256	0.000

	Total cloud fraction	geshcltgl.dat	0.591	0.000
	Eastward near-surface wind	geshuasgl.dat	0.096	0.000
Maximum temperature	Sea level pressure	geshpslgl.dat	-0.241	0.000
	Near-surface relative humidity	geshrhsgl.dat	-0.187	0.000
	Daily maximum near-surface air temperature	geshtasmaxgl.dat	0.192	0.000
	Eastward near-surface wind	geshuasgl.dat	-0.217	0.000
Minimum temperature	Surface downwelling longwave radiation	geshrldsgl.dat	0.382	0.000
	Daily maximum near-surface air temperature	geshtasmax.dat	-0.348	0.000
	Sea level pressure	geshpslgl.dat	0.460	0.000
	Eastward near-surface wind	geshuasgl.dat	0.172	0.000

Appendix Table 4 Lists of selected predictor variables from CanESM2-historical model for station: Agarfa

Predictand	Predictor full name	Notations	Parti.cor. (r-value)	p-value
Precipitation	500 hPa airflow strength	ceshp5_fgl.dat	0.064	0.040
	500 hPa zonal velocity	ceshp5_ugl.dat	0.097	0.001
Maximum temperature	850 hPa airflow strength	ceshp8_fgl.dat	0.126	0.000
	850 hPa wind direction	ceshp8thgl.dat	0.110	0.000
	850 hPa geopotential height	ceshp850gl.dat	-0.071	0.000
	Surface specific humidity	ceshshumgl.dat	-0.274	0.000
Minimum temperature	Mean sea level pressure	ceshmslpgl.dat	-0.043	0.020
	500 hPa meridional velocity	ceshp5_vgl.dat	0.048	0.009
	Specific humidity at 850 hPa	ceshs850gl.dat	-0.076	0.000
	Surface specific humidity	ceshshumgl.dat	0.111	0.000
	Mean temperature at 2m	ceshtempgl.dat	0.139	0.000

Appendix Table 5 Lists of selected predictor variables from GFDL_ESM2M-historical model for station: Agarfa

Predictand	Predictor full name	Notations	Parti.cor. (r-value)	p-value
Precipitation	Total cloud fraction	geshcltgl.dat	0.059	0.041
	Precipitation	geshprgl.dat	-0.069	0.022
	Daily-mean near-surface wind speed	geshsfcwindgl.dat	0.072	0.021
	Eastward near-surface wind	geshuasgl.dat	-0.071	0.022
Maximum temperature	Sea level pressure	geshpslgl.dat	-0.057	0.001
	Near-surface relative humidity	geshrhsgl.dat	-0.288	0.000
	Eastward near-surface wind	geshuasgl.dat	0.128	0.000
Minimum temperature	Sea level pressure	geshpslgl.dat	0.068	0.000
	Near-surface relative humidity	geshrhsgl.dat	0.196	0.009
	Daily-mean near-surface wind speed	geshsfcwindgl.dat	-0.115	0.000

Appendix Table 6 Lists of selected potential predictor variables from GFDL_ESM2G-historical model for station: Agarfa

Predictand	Predictor full name	Notations	Parti.cor. (r-value)	p-value
Precipitation	Total cloud fraction	geshcltgl.dat	0.095	0.011
	Daily minimum near-surface air temperature	geshtasmin.dat	0.148	0.000

	Daily-mean near-surface wind speed	geshsfcwindgl.dat	0.122	0.001
	Eastward near-surface wind	geshuasgl.dat	-0.159	0.000
Maximum temperature	Sea level pressure	geshpslgl.dat	-0.147	0.000
	Near-surface relative humidity	geshrhsgl.dat	-0.368	0.000
	Near-surface air temperature	geshtasgl.dat	-0.265	0.000
	Eastward near-surface wind	geshuasgl.dat	0.721	0.000
Minimum temperature	Sea level pressure	geshpslgl.dat	0.139	0.000
	Total cloud fraction	geshcltgl.dat	-0.211	0.000
	Near-surface relative humidity	geshrhsgl.dat	0.269	0.001
	Daily-mean near-surface wind speed	geshsfcwindgl.dat	-0.251	0.000

Appendix Table 7 Lists of selected predictor variables from CanESM2-historical model for station: Dinsho

Predictand	Predictor full name	Notations	Parti.cor. (r-value)	p-value
Precipitation	Mean sea level pressure	ceshmslpgl.dat	0.044	0.019
	500 hPa zonal velocity	ceshp5_ugl.dat	-0.059	0.011
	500 hPa vorticity	ceshp5_zgl.dat	-0.044	0.021
Maximum temperature	500 hPa geopotential height	ceshp500gl.dat	0.103	0.000
	850 hPa meridional velocity	ceshp8_vgl.dat	0.047	0.000
	850 hPa geopotential height	ceshp850gl.dat	-0.097	0.000
	850 hPa wind direction	ceshp8thgl.dat	-0.074	0.000
	Mean temperature at 2m	ceshtempgl.dat	-0.103	0.000
Minimum temperature	Mean sea level pressure	ceshmslpgl.dat	-0.156	0.000
	500 hPa geopotential height	ceshp500gl.dat	0.123	0.000
	Specific humidity at 850 hPa	ceshs850gl.dat	-0.066	0.000
	Surface specific humidity	ceshshumgl.dat	0.078	0.000

Appendix Table 8 Lists of selected predictor variables from GFDL_ESM2M-historical model for station: Dinsho

Predictand	Predictor full name	Notations	Parti.cor. (r-value)	p-value
Precipitation	Total cloud fraction	geshcltgl.dat	-0.131	0.000
	Daily-mean near-surface wind speed	geshsfcwindgl.dat	-0.079	0.000
	Near-surface air temperature	geshtasgl.dat	0.081	0.000
	Daily maximum near-surface air temperature	geshtasmax.dat	0.143	0.000
	Daily minimum near-surface air temperature	geshtasmin.dat	0.059	0.001
Maximum temperature	Total cloud fraction	geshcltgl.dat	-0.210	0.000
	Daily-mean near-surface wind speed	geshsfcwindgl.dat	-0.074	0.000
	Near-surface air temperature	geshtasgl.dat	-0.124	0.000
	Daily maximum near-surface air temperature	geshtasmax.dat	0.138	0.000
	Daily minimum near-surface air temperature	geshtasmin.dat	0.143	0.000
Minimum temperature	Total cloud fraction	geshcltgl.dat	-0.109	0.000
	Precipitation	geshprgl.dat	0.126	0.000
	Daily minimum near-surface air temperature	geshtasmin.dat	-0.087	0.000
	Daily maximum near-surface air temperature	geshtasmax.dat	0.048	0.000
	Northward wind at 500 hpa	geshva500gl.dat	-0.088	0.000

Appendix Table 9 Lists of selected potential predictor variables from GFDL_ESM2G-historical model for station: Dinsho

Predictand	Predictor full name	Notations	Parti.cor. (r-value)	p-value
Precipitation	Total cloud fraction	geshcltgl.dat	-0.191	0.000
	Daily-mean near-surface wind speed	geshsfcwindgl.dat	-0.146	0.000
	Near-surface air temperature	geshtasgl.dat	0.132	0.000
	Daily maximum near-surface air temperature	geshtasmax.dat	0.234	0.000
Maximum temperature	Total cloud fraction	geshcltgl.dat	-0.443	0.000
	Daily-mean near-surface wind speed	geshsfcwindgl.dat	-0.195	0.000
	Daily maximum near-surface air temperature	geshtasmax.dat	0.238	0.000
	Daily minimum near-surface air temperature	geshtasmin.dat	0.533	0.000
Minimum temperature	Precipitation	geshprgl.dat	0.099	0.000
	Daily minimum near-surface air temperature	geshtasmin.dat	-0.106	0.000
	Daily maximum near-surface air temperature	geshtasmax.dat	0.154	0.000
	Northward wind at 500 hpa	geshva500gl.dat	-0.097	0.000

Appendix Table 10 Lists of selected predictor variables from CanESM2-historical model for station: Gassera

Predictand	Predictor full name	Notations	Parti.cor. (r-value)	p-value
Precipitation	850 hPa zonal velocity	ceshp8_ugl.dat	-0.097	0.000
	Surface specific humidity	ceshshumgl.dat	0.077	0.002

Appendix Table 11 Lists of selected predictor variables from GFDL_ESM2M-historical model for station: Gassera

Predictand	Predictor full name	Notations	Parti.cor. (r-value)	p-value
Precipitation	Precipitation	geshprgl.dat	0.221	0.000
	Near-surface relative humidity	geshrhsgl.dat	-0.072	0.002
	Daily-mean near-surface wind speed	geshsfcwindgl.dat	-0.111	0.000
	Near-surface air temperature	geshtasgl.dat	0.097	0.000

Appendix Table 12 Lists of selected potential predictor variables from GFDL_ESM2G-historical model for station: Gassera

Predictand	Predictor full name	Notations	Parti.cor. (r-value)	p-value
Precipitation	Sea level pressure	geshpslgl.dat	0.471	0.000
	Near-surface relative humidity	geshrhsgl.dat	-0.212	0.000
	Daily-mean near-surface wind speed	geshsfcwindgl.dat	-0.342	0.000
	Eastward near-surface wind	geshuasgl.dat	-0.102	0.000

Appendix Table 13 Lists of selected predictor variables from CanESM2-historical model for station: Ginnir

Predictand	Predictor full name	Notations	Parti.cor. (r-value)	p-value
Precipitation	500 hPa vorticity	ceshp5_zgl.dat	-0.075	0.002
	850 hPa zonal velocity	ceshp8_ugl.dat	-0.094	0.000
Maximum temperature	Unknown	ceshp1_ugl.dat	0.063	0.000
	Unknown	ceshp1zhgl.dat	-0.074	0.000
	850 hPa zonal velocity	ceshp8_ugl.dat	-0.089	0.000
	850 hPa geopotential height	ceshp850gl.dat	-0.058	0.000
	Specific humidity at 850 hPa	ceshs850gl.dat	-0.114	0.000

	Mean sea level pressure	ceshmslpgl.dat	-0.130	0.000
Minimum temperature	500 hPa geopotential height	ceshp500gl.dat	0.074	0.000
	850 hPa vorticity	ceshp8_zgl.dat	-0.068	0.000
	850 hPa geopotential height	ceshp850gl.dat	0.058	0.000

Appendix Table 14 Lists of selected predictor variables from GFDL_ESM2M-historical model for station: Ginnir

Predictand	Predictor full name	Notations	Parti.cor. (r-value)	p-value
Precipitation	Sea level pressure	geshpslgl.dat	0.221	0.000
	Daily-mean near-surface wind speed	geshsfcwindgl.dat	-0.243	0.000
	Daily maximum near-surface air temperature	geshtasmax.dat	0.098	0.000
	Eastward near-surface wind	geshuasgl.dat	-0.106	0.000
Maximum temperature	Sea level pressure	geshpslgl.dat	-0.120	0.000
	Near-surface relative humidity	geshrhsgl.dat	-0.219	0.000
	Daily minimum near-surface air temperature	geshtasmin.dat	0.082	0.000
Minimum temperature	Sea level pressure	geshpslgl.dat	-0.112	0.000
	Near-surface relative humidity	geshrhsgl.dat	-0.138	0.000
	Surface downwelling longwave radiation	geshrldsgl.dat	0.198	0.000

Appendix Table 15 Lists of selected potential predictor variables from GFDL_ESM2G-historical model for station: Ginnir

Predictand	Predictor full name	Notations	Parti.cor. (r-value)	p-value
Precipitation	Sea level pressure	geshpslgl.dat	0.111	0.000
	Northward wind at 500 hpa	geshva500gl.dat	-0.240	0.000
	Daily maximum near-surface air temperature	geshtasmax.dat	0.104	0.000
	Eastward near-surface wind	geshuasgl.dat	-0.227	0.000
Maximum temperature	Sea level pressure	geshpslgl.dat	-0.216	0.000
	Near-surface relative humidity	geshrhsgl.dat	-0.412	0.000
	Surface downwelling longwave radiation	geshrldsgl.dat	0.385	0.000
Minimum temperature	Sea level pressure	geshpslgl.dat	-0.277	0.000
	Near-surface relative humidity	geshrhsgl.dat	-0.391	0.000
	Surface downwelling longwave radiation	geshrldsgl.dat	0.412	0.000

Appendix Table 16 Lists of selected predictor variables from CanESM2-historical model for station: Goba

Predictand	Predictor full name	Notations	Parti.cor. (r-value)	p-value
Precipitation	Unknown	ceshp1zhgl.dat	-0.100	0.007
	850 hPa divergence	ceshp8zhgl.dat	0.080	0.032
Maximum temperature	500 hPa geopotential height	ceshp500gl.dat	0.115	0.000
	850 hPa meridional velocity	ceshp8_vgl.dat	0.107	0.000
	850 hPa geopotential height	ceshp850gl.dat	-0.200	0.000
	Surface specific humidity	ceshshumgl.dat	-0.233	0.000
	Mean temperature at 2m	ceshtempgl.dat	-0.109	0.000
Minimum temperature	Unknown	ceshp1zhgl.dat	0.066	0.000
	850 hPa wind direction	ceshp8thgl.dat	0.078	0.000
	Specific humidity at 850 hPa	ceshs850gl.dat	-0.116	0.000
	Surface specific humidity	ceshshumgl.dat	0.146	0.000
	Mean temperature at 2m	ceshtempgl.dat	0.323	0.000

Appendix Table 17 Lists of selected predictor variables from GFDL_ESM2M-historical model for station: Goba

Predictand	Predictor full name	Notations	Parti.cor. (r-value)	p-value
Precipitation	Near-surface air temperature	geshtas.dat	0.075	0.041
	Northward wind at 500 hpa	geshva500gl.dat	-0.080	0.032
Maximum temperature	Near-surface relative humidity	geshrhsgl.dat	-0.318	0.000
	Daily-mean near-surface wind speed	geshsfcwindgl.dat	0.126	0.000
	Near-surface air temperature	geshtas.dat	0.103	0.000
	Daily minimum near-surface air temperature	geshtasmin.dat	0.112	0.000
	Eastward near-surface wind	geshuasgl.dat	0.179	0.000
Minimum temperature	Total cloud fraction	geshcltgl.dat	0.127	0.000
	Sea level pressure	geshpslgl.dat	-0.078	0.000
	Daily-mean near-surface wind speed	geshsfcwindgl.dat	-0.116	0.000
	Near-surface air temperature	geshtas.dat	0.182	0.000

Appendix Table 18 Lists of selected potential predictor variables from GFDL_ESM2G-historical model for station: Goba

Predictand	Predictor full name	Notations	Parti.cor. (r-value)	p-value
Precipitation	Near-surface air temperature	geshtas.dat	0.106	0.001
	Sea level pressure	geshpslgl.dat	-0.089	0.001
	Northward wind at 500 hpa	geshva500gl.dat	-0.1190	0.000
Maximum temperature	Near-surface relative humidity	geshrhsgl.dat	-0.523	0.000
	Daily-mean near-surface wind speed	geshsfcwindgl.dat	0.514	0.000
	Near-surface air temperature	geshtas.dat	0.235	0.000
	Eastward near-surface wind	geshuasgl.dat	0.621	0.000
Minimum temperature	Total cloud fraction	geshcltgl.dat	0.114	0.000
	Daily minimum near-surface air temperature	geshtasmin.dat	0.331	0.000
	Daily-mean near-surface wind speed	geshsfcwindgl.dat	-0.168	0.000
	Near-surface air temperature	geshtas.dat	0.292	0.000

Appendix Table 19 Lists of selected predictor variables from CanESM2-historical model for station: Goro

Predictand	Predictor full name	Notations	Parti.cor. (r-value)	p-value
Precipitation	500 hPa geopotential height	ceshp500gl.dat	0.056	0.016
	850 hPa zonal velocity	ceshp8_ugl.dat	-0.119	0.000
Maximum temperature	500 hPa geopotential height	ceshp500gl.dat	0.056	0.000
	850 hPa meridional velocity	ceshp8_vgl.dat	0.079	0.000
	Specific humidity at 850 hPa	ceshs850gl.dat	0.060	0.000
	Surface specific humidity	ceshshumgl.dat	-0.100	0.000
Minimum temperature	Unknown	ceshp1zhgl.dat	-0.047	0.000
	Specific humidity at 850 hPa	ceshs850gl.dat	-0.078	0.000
	Surface specific humidity	ceshshumgl.dat	0.081	0.000
	Mean temperature at 2m	ceshtempgl.dat	0.200	0.000

Appendix Table 20 Lists of selected predictor variables from GFDL_ESM2M-historical model for station: Goro

Predictand	Predictor full name	Notations	Parti.cor. (r-value)	p-value
Precipitation	Sea level pressure	geshpslgl.dat	-0.057	0.013
	Near-surface relative humidity	geshrhsgl.dat	-0.054	0.018
	Daily minimum near-surface air temperature	geshtasmin.dat	0.047	0.043
Maximum temperature	Precipitation	geshprgl.dat	-0.124	0.000
	Daily-mean near-surface wind speed	geshsfcwindgl.dat	0.122	0.000
	Daily minimum near-surface air temperature	geshtasmin.dat	-0.072	0.000
	Eastward near-surface wind	geshuasgl.dat	-0.118	0.000
Minimum temperature	Total cloud fraction	geshcltgl.dat	0.299	0.000
	Sea level pressure	geshpslgl.dat	0.215	0.000
	Near-surface air temperature	geshtas.dat	-0.201	0.000
	Daily minimum near-surface air temperature	geshtasmin.dat	-0.204	0.000

Appendix Table 21 Lists of selected potential predictor variables from GFDL_ESM2G-historical model for station: Goro

Predictand	Predictor full name	Notations	Parti.cor. (r-value)	p-value
Precipitation	Sea level pressure	geshpslgl.dat	-0.146	0.000
	Near-surface relative humidity	geshrhsgl.dat	-0.103	0.001
	Daily-mean near-surface wind speed	geshsfcwindgl.dat	0.314	0.000
Maximum temperature	Sea level pressure	geshpslgl.dat	-0.415	0.000
	Daily-mean near-surface wind speed	geshsfcwindgl.dat	0.247	0.000
	Daily minimum near-surface air temperature	geshtasmin.dat	-0.124	0.000
	Eastward near-surface wind	geshuasgl.dat	-0.286	0.000
Minimum temperature	Daily-mean near-surface wind speed	geshsfcwindgl.dat	0.117	0.000
	Sea level pressure	geshpslgl.dat	0.462	0.000
	Near-surface air temperature	geshtas.dat	-0.313	0.000
	Daily minimum near-surface air temperature	geshtasmin.dat	-0.584	0.000

Appendix Table 22 Lists of selected predictor variables from CanESM2-historical model for station: Homa

Predictand	Predictor full name	Notations	Parti.cor. (r-value)	p-value
Precipitation	Mean sea level pressure	ceshmslpgl.dat	0.056	0.042
	Unknown	ceshp1zhgl.dat	0.058	0.021
	Specific humidity at 850 hPa	ceshs850gl.dat	0.086	0.000
	Surface specific humidity	ceshshumgl.dat	-0.075	0.003

Appendix Table 23 Lists of selected predictor variables from GFDL_ESM2M-historical model for station: Homa

Predictand	Predictor full name	Notations	Parti.cor. (r-value)	p-value
Precipitation	Total cloud fraction	geshcltgl.dat	-0.100	0.000
	Sea level pressure	geshpslgl.dat	-0.082	0.000
	Daily-mean near-surface wind speed	geshsfcwindgl.dat	0.205	0.000

Appendix Table 24 Lists of selected potential predictor variables from GFDL_ESM2G-historical model for station: Homa

Predictand	Predictor full name	Notations	Parti.cor. (r-value)	p-value
Precipitation	Total cloud fraction	geshcltgl.dat	-0.310	0.000
	Sea level pressure	geshpslgl.dat	-0.119	0.000
	Eastward near-surface wind	geshuasgl.dat	0.231	0.000
	Daily-mean near-surface wind speed	geshsfcwindgl.dat	0.413	0.000

Appendix Table 25 Lists of selected predictor variables from CanESM2-historical model for station: Hunte

Predictand	Predictor full name	Notations	Parti.cor. (r-value)	p-value
Precipitation	850 hPa wind direction	ceshp8thgl.dat	0.048	0.017
	Convective Precipitation	ceshprcpgl.dat	-0.054	0.006
	Specific humidity at 850 hPa	ceshs850gl.dat	0.090	0.000
	Mean temperature at 2m	ceshtempgl.dat	-0.070	0.004
Maximum temperature	Mean sea level pressure	ceshmslpgl.dat	-0.053	0.000
	850 hPa geopotential height	ceshp850gl.dat	0.053	0.000
	850 hPa divergence	ceshp8zhgl.dat	-0.049	0.000
	Specific humidity at 850 hPa	ceshs850gl.dat	0.157	0.000
	Mean temperature at 2m	ceshtempgl.dat	-0.050	0.000
Minimum temperature	Mean sea level pressure	ceshmslpgl.dat	-0.033	0.004
	500 hPa geopotential height	ceshp500gl.dat	0.186	0.000
	850 hPa geopotential height	ceshp850gl.dat	-0.103	0.000
	Specific humidity at 850 hPa	ceshs850gl.dat	-0.062	0.000
	Surface specific humidity	ceshshumgl.dat	0.082	0.000

Appendix Table 26 Lists selected predictor variables from GFDL_ESM2M-historical model for station: Hunte

Predictand	Predictor full name	Notations	Parti.cor. (r-value)	p-value
Precipitation	Total cloud fraction	geshcltgl.dat	0.048	0.017
	Eastward near-surface wind	geshuasgl.dat	0.060	0.002
Maximum temperature	Sea level pressure	geshpslgl.dat	-0.143	0.000
	Near-surface relative humidity	geshrhsgl.dat	0.253	0.000
	Daily-mean near-surface wind speed	geshsfcwindgl.dat	0.100	0.000
	Daily maximum near-surface air temperature	geshtasmax.dat	-0.136	0.000
Minimum temperature	Total cloud fraction	geshcltgl.dat	-0.103	0.000
	Sea level pressure	geshpslgl.dat	0.126	0.000
	Surface downwelling longwave radiation	geshrldsgl.dat	0.230	0.000
	Daily-mean near-surface wind speed	geshsfcwindgl.dat	-0.084	0.000
	Eastward near-surface wind	geshuasgl.dat	0.146	0.000

Appendix Table 27 Lists of selected potential predictor variables from GFDL_ESM2G-historical model for station: Hunte

Predictand	Predictor full name	Notations	Parti.cor. (r-value)	p-value
Precipitation	Total cloud fraction	geshcltgl.dat	0.076	0.013
	Surface downwelling long wave radiation	geshrldsgl.dat	0.065	0.009
	Eastward near-surface wind	geshuasgl.dat	0.081	0.000
Maximum temperature	Sea level pressure	geshpslgl.dat	-0.265	0.000
	Near-surface relative humidity	geshrhsgl.dat	0.692	0.000
	Daily-mean near-surface wind speed	geshsfcwindgl.dat	0.098	0.000
	Daily maximum near-surface air temperature	geshtasmax.dat	-0.198	0.000
Minimum temperature	Total cloud fraction	geshcltgl.dat	-0.294	0.000
	Sea level pressure	geshpslgl.dat	0.283	0.000
	Surface downwelling longwave radiation	geshrldsgl.dat	0.230	0.000
	Daily-mean near-surface wind speed	geshsfcwindgl.dat	-0.118	0.000

Appendix Table 28 Lists of selected predictor variables from CanESM2-historical model for station: Ali

Predictand	Predictor full name	Notations	Parti.cor. (r-value)	p-value
Precipitation	Specific humidity at 850 hPa	ceshs850gl.dat	-0.078	0.003
	Surface specific humidity	ceshshumgl.dat	0.068	0.009

Appendix Table 29 Lists of selected predictor variables from GFDL_ESM2M-historical model for station: Ali

Predictand	Predictor full name	Notations	Parti.cor. (r-value)	p-value
Precipitation	Total cloud fraction	geshcltgl.dat	-0.067	0.011
	Surface downwelling longwave radiation	geshrldsgl.dat	0.078	0.004
	Eastward near-surface wind	geshuasgl.dat	-0.084	0.001

Appendix Table 30 Lists of selected potential predictor variables from GFDL_ESM2G-historical model for station: Ali

Predictand	Predictor full name	Notations	Parti.cor. (r-value)	p-value
Precipitation	Sea level pressure	geshpslgl.dat	-0.465	0.000
	Total cloud fraction	geshcltgl.dat	-0.098	0.001
	Surface downwelling longwave radiation	geshrldsgl.dat	0.105	0.000
	Eastward near-surface wind	geshuasgl.dat	-0.127	0.000

Appendix Table 31 Lists of selected predictor variables from CanESM2-historical model for station: Robe

Predictand	Predictor full name	Notations	Parti.cor. (r-value)	p-value
Precipitation	500 hPa zonal velocity	ceshp5_ugl.dat	0.051	0.009
	Convective Precipitation	ceshprcpgl.dat	0.049	0.013
Maximum temperature	Unknown	ceshp1_vgl.dat	0.083	0.000
	850 hPa geopotential height	ceshp850gl.dat	-0.185	0.000
	Specific humidity at 500 hPa	ceshs500gl.dat	-0.154	0.000
	Mean temperature at 2m	ceshtempgl.dat	-0.235	0.000
Minimum temperature	Mean sea level pressure	ceshmslpgl.dat	-0.308	0.000
	500 hPa geopotential height	ceshp500gl.dat	0.210	0.000
	850 hPa zonal velocity	ceshp8_ugl.dat	-0.116	0.000

	Specific humidity at 850 hPa	ceshs850gl.dat	-0.072	0.000
	Surface specific humidity	ceshshumgl.dat	0.103	0.000

Appendix Table 32 Lists of selected predictor variables from GFDL_ESM2M-historical model for station: Robe

Predictand	Predictor full name	Notations	Parti.cor. (r-value)	p-value
Precipitation	Sea level pressure	geshpslgl.dat	-0.154	0.000
	Near-surface relative humidity	geshrhsgl.dat	-0.235	0.000
	Northward wind at 500 hpa	geshva500gl.dat	-0.308	0.000
Maximum temperature	Near-surface relative humidity	geshrhsgl.dat	-0.350	0.000
	Daily-mean near-surface wind speed	geshsfcwindgl.dat	0.109	0.000
	Eastward near-surface wind	geshuasgl.dat	0.174	0.000
Minimum temperature	Total cloud fraction	geshcltgl.dat	-0.094	0.000
	Near-surface relative humidity	geshrhsgl.dat	-0.061	0.000
	Surface downwelling longwave radiation	geshrldsgl.dat	0.297	0.000
	Eastward near-surface wind	geshuasgl.dat	0.076	0.000

Appendix Table 33 Lists of selected potential predictor variables from GFDL_ESM2G-historical model for station: Robe

Predictand	Predictor full name	Notations	Parti.cor. (r-value)	p-value
Precipitation	Sea level pressure	geshpslgl.dat	-0.486	0.000
	Near-surface relative humidity	geshrhsgl.dat	-0.735	0.000
	Eastward near-surface wind	geshuasgl.dat	-0.418	0.000
Maximum temperature	Near-surface relative humidity	geshrhsgl.dat	-0.253	0.000
	Daily-mean near-surface wind speed	geshsfcwindgl.dat	0.103	0.000
	Eastward near-surface wind	geshuasgl.dat	0.224	0.000
Minimum temperature	Near-surface relative humidity	geshrhsgl.dat	-0.521	0.000
	Surface downwelling longwave radiation	geshrldsgl.dat	0.274	0.000
	Eastward near-surface wind	geshuasgl.dat	0.108	0.000

Appendix Table 34 Lists of selected predictor variables from CanESM2-historical model for station: Sinnana

Predictand	Predictor full name	Notations	Parti.cor. (r-value)	p-value
Precipitation	850 hPa divergence	ceshp8zhgl.dat	0.043	0.027
Maximum temperature	Mean sea level pressure	ceshmslpgl.dat	0.148	0.000
	Unknown	ceshp1_zgl.dat	-0.154	0.000
	500 hPa geopotential height	ceshp500gl.dat	0.134	0.000
	850 hPa geopotential height	ceshp850gl.dat	-0.175	0.000
	Surface specific humidity	ceshshumgl.dat	-0.192	0.000
Minimum temperature	Mean sea level pressure	ceshmslpgl.dat	-0.292	0.000
	500 hPa geopotential height	ceshp500gl.dat	0.222	0.000
	Surface specific humidity	ceshshumgl.dat	0.108	0.000

Appendix Table 35 Lists of selected predictor variables from GFDL_ESM2M-historical model for station: Sinnana

Predictand	Predictor full name	Notations	Parti.cor. (r-value)	p-value
Precipitation	Precipitation	geshprgl.dat	-0.043	0.037
	Sea level pressure	geshpslgl.dat	0.049	0.014
	Surface downwelling longwave radiation	geshrldsgl.dat	0.059	0.010
	Eastward near-surface wind	geshuasgl.dat	-0.041	0.039
Maximum temperature	Near-surface relative humidity	geshrhsgl.dat	-0.418	0.000
	Daily-mean near-surface wind speed	geshsfcwindgl.dat	0.089	0.000
	Daily maximum near-surface air temperature	geshtasmax.dat	-0.139	0.000
Minimum temperature	Total cloud fraction	geshcltgl.dat	-0.060	0.000
	Surface downwelling longwave radiation	geshrldsgl.dat	0.378	0.000
	Daily-mean near-surface wind speed	geshsfcwindgl.dat	-0.126	0.000
	Near-surface air temperature	geshtas.dat	0.080	0.000

Appendix Table 36 Lists of selected potential predictor variables from GFDL_ESM2G-historical model for station: Sinnana

Predictand	Predictor full name	Notations	Parti.cor. (r-value)	p-value
Precipitation	Sea level pressure	geshpslgl.dat	0.443	0.000
	Surface downwelling longwave radiation	geshrldsgl.dat	0.092	0.001
	Eastward near-surface wind	geshuasgl.dat	-0.103	0.000
Maximum temperature	Near-surface relative humidity	geshrhsgl.dat	-0.624	0.000
	Daily-mean near-surface wind speed	geshsfcwindgl.dat	0.107	0.000
	Daily maximum near-surface air temperature	geshtasmax.dat	-0.429	0.000
Minimum temperature	Surface downwelling longwave radiation	geshrldsgl.dat	0.523	0.000
	Daily-mean near-surface wind speed	geshsfcwindgl.dat	-0.289	0.000
	Near-surface air temperature	geshtas.dat	0.193	0.000

Note: The partial correlation coefficient (r) shows the explanatory power that is specific to each predictor. All are significant at $p \leq 0.05$. hpa: is a unit of pressure, 1 hPa = 1 mbar = 100 Pa = 0.1 kPa. Correlation matrix was used to investigate intervariable correlations for specified sub–periods (annual, seasonal or monthly).

Appendix Table 37 Morphological characteristics for the major soils of Weyib River basin

Soil group	Depth	Colour	Texture	Structure	Consistency	Drainage
Cambisols (CM)	Shallow to very deep	Dusky red to yellowish brown	Clay loam, sandy loam, silty loam	Moderate, fine and medium, granular and sub-angular blocky structure	Friable moist	Well/excessive
Leptosols (LP)	Very shallow	Dark brown to very dark brown	Sandy clay loam	Moderate, medium and coarse, granular structure	Very friable, slightly sticky and slightly plastic	Excessive/well
Luvisols (LV)	Moderately deep to Very deep	Dark red to very dark greyish brown	Clay/clay loam, loam,	Fine to medium, moderate to strong, sub-angular blocky structure	Friable to firm, sticky and plastic	Moderate to well
Regosols (RG)	Shallow	Dark brown to dark yellowish brown	Sandy clay loam/ loamy sand/ sandy loam	Weak, very fine, granular structure	Very friable, non-sticky and non-plastic	Excessive/some what excessive
Vertisols (VR)	Moderately deep to Very deep	Black to very dark brown.	Heavy clay/clay loam	Fine to coarse moderate to strong sub-angular and angular blocky structure	-Firm moist -Very firm moist -Friable moist	-Poorly drained -Poor -Moderate -Imperfect

Source: Federal Democratic Republic of Ethiopia, Ministry of Water Resources, Genale-Dawa River Basin Integrated Resources Development Master Plan, Part II Sector Reports

Appendix Table 38 Detail descriptions of soil physical and chemical characteristics of Weyib River basin used as an input for SWAT model

Profile No.	Soil Type	Depth cm	Sand	Silt %	Clay	Texture Class	pH H_2O	pH KCl	EC ms/cm	CEC	BS	ESP %	O.C	O.M.
GSP001	LVv	0-25	17.02	34.7	48.3	C	5.9	4.8	0.06	48.6	69.3	0.4	7.0	12.0
		25-110	2.94	17.0	80.1	HC	5.1	5.0	0.07	46.4	95.8	1.5	1.1	2.0
		110-200	2.09	10.2	87.7	HC	7.8	5.8	0.05	50.9	110.2	2.2	0.3	0.5
GSP003	Rg	0-50	52.42	25.4	22.2	SCL	6.1	4.9	0.05	18.1	86.1	1.5	1.6	2.8
GSP006	LVh	0-15	23.16	25.6	51.2	C	6.1	4.7	0.06	51.8	77.3	0.6	4.1	7.1
		15-80	7.45	16.8	75.7	HC	6.6	5.0	0.05	41.8	93.0	1.6	1.6	2.8
		80-110	3.73	14.4	81.8	HC	7.1	6.0	0.07	52.2	87.8	2.1	0.5	0.8
		110-200	10.13	12.1	77.7	HC	7.1	5.4	0.07	49.0	91.4	2.2	0.4	0.8
GSP012	CMc	0-15	27.08	57.1	15.5	SIL	8.1	7.2	0.18	59.4	111.4	0.3	3.5	5.9
		15-50	22.16	54.7	23.1	SIL	8.3	7.2	0.15	52.0	130.5	0.4	1.5	2.6
		50-80	34.39	47.0	18.6	L	8.5	7.3	0.16	47.9	133.0	1.0	0.6	1.0
		80-120	25	52.4	22.6	SIL	8.6		0.17	37.2	144.6	2.0	0.3	0.6
GSP049	CMd	0-30	62.29	10.2	27.5	SCL	6.8	6.0	0.04	9.9	76.3	0.3	1.2	2.0
		30-60	48.58	11.3	40.1	SC	6.5	5.1	0.02	12.3	45.2	0.8	0.9	1.5
GSP065	CMx	0-25	28.04	31.9	40.1	C	6.1	4.9	0.05	12.1	71.9	0.9	0.6	1.0
		25-90	26.04	31.2	42.7	C	6.2	5.0	0.08	14.5	74.6	1.6	0.5	0.8
		90-200	53.2	35.4	11.5	SL	8.5	7.3	0.09	22.2	83.3	1.5	0.2	0.4
GSP146	VRe	0-15	13.35	19.6	67.0	HC	8.6	7.08	0.19	87.7	102.5	3.4	2.2	3.7
		15-80	1.13	15.5	83.4	HC	8.5	7.0	0.67	95.0	97.0	9.2	2.3	3.9
		80-200	T	17.8	82.2	HC	8.3	7.1	1.18	87.0	104.0	10.3	1.8	3.2
GSP149	CMe	0-15	21.53	47.7	30.8	CL	7.3	6.1	0.06	32.0	97.7	0.5	1.9	3.3
		15-100	11.57	42.6	45.9	SC	7.5	5.8	0.06	45.3	95.3	1.9	1.6	2.7
		100-170	6.76	34.5	58.7	C	8.2	6.9	0.59	70.0	93.0	7.1	1.1	1.9
		90-200	7.43	11.4	81.1	HC	8.5	7.4	1.17	58.6	123.8	15.7	1.5	2.5
GSP205	Lp	0-20	41.4	34.53	24.07	L	8.64	7.64	0.20	40.7	98.3	1.6	0.58	1
GSP218	VRk	0-20	13.51	33.51	52.97	C	8.34	7.44	0.15	61.4	94.0	0.6	1.95	3.35
		20-80	2.48	24.92	72.6	C	8.33	7.49	0.58	57.8	108.8	4.9	1.54	2.65
		80-180	7.42	23.15	69.44	C	8.47	7.47	0.45	54.5	105.6	5	1.24	2.13

LVv: Vertic Luvisol, RG: Regosol, LVh: Haplic Luvisol, CMc: Calcaric Cambisol, CMd: Dystric Cambisol, CMx: Chromic Cambisol, VRe: Eutric Vertisol, CMe: Eutric Cambisol, Lp: Leptosol, VRk: Calcic Vertisol, **Source:** Federal Democratic Republic of Ethiopia, Ministry of Water Resources, Genale-Dawa River Basin Integrated Resources Development Master Plan, Part II Sector Reports

Appendix B

Appendix Figures

Knowing an expected behavior of hydro-meteorological processes, mainly precipitation is important for hydrological modelling. In this study, homogeneity of long-term annual precipitation series at different meteorological stations has been checked using Rainbow software. The rainfall data has been tested for homogeneity at different significance levels (at 0.1, 0.05 and 0.01alpha levels).

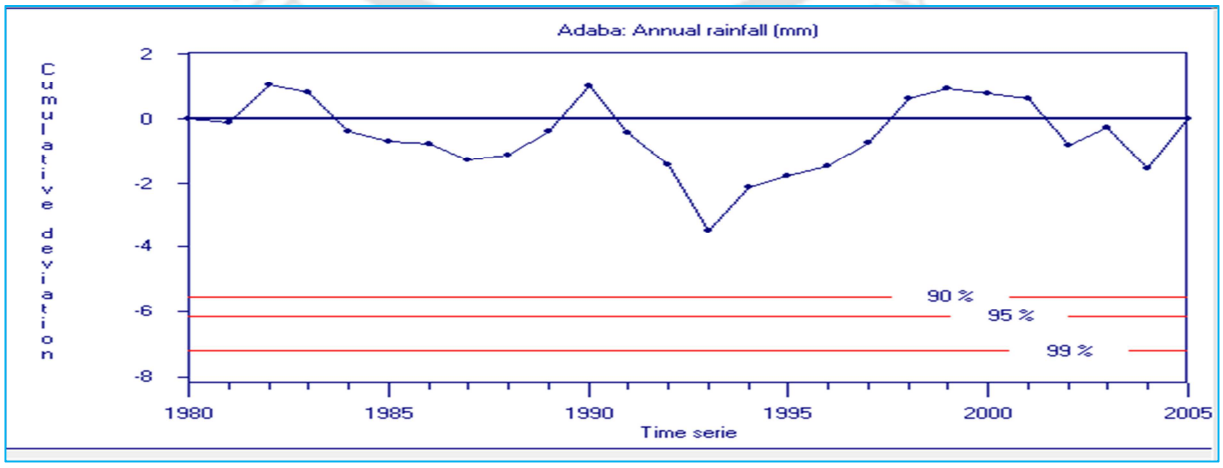

Appendix Figure 1 Homogeneity test of annual precipitation series at station Adaba (homogeneous)

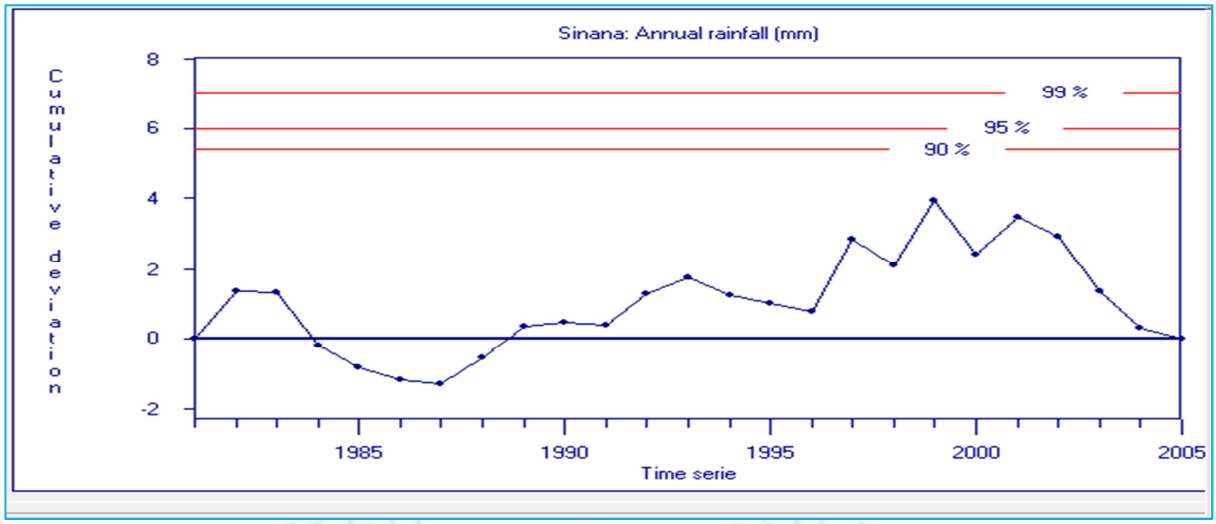

Appendix Figure 2 Homogeneity test of annual precipitation series at station Sinnana (homogeneous)

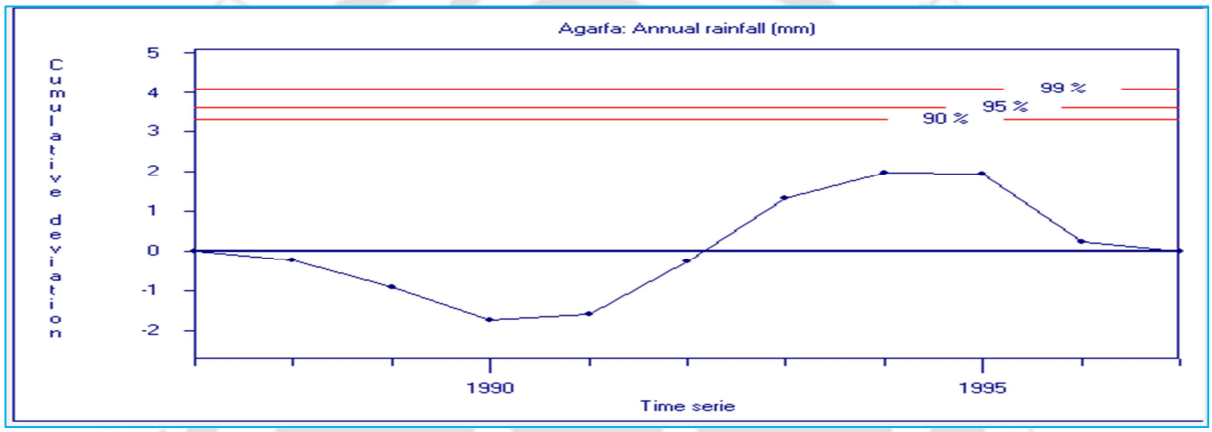

Appendix Figure 3 Homogeneity test of annual precipitation series at station Agarfa (homogeneous)

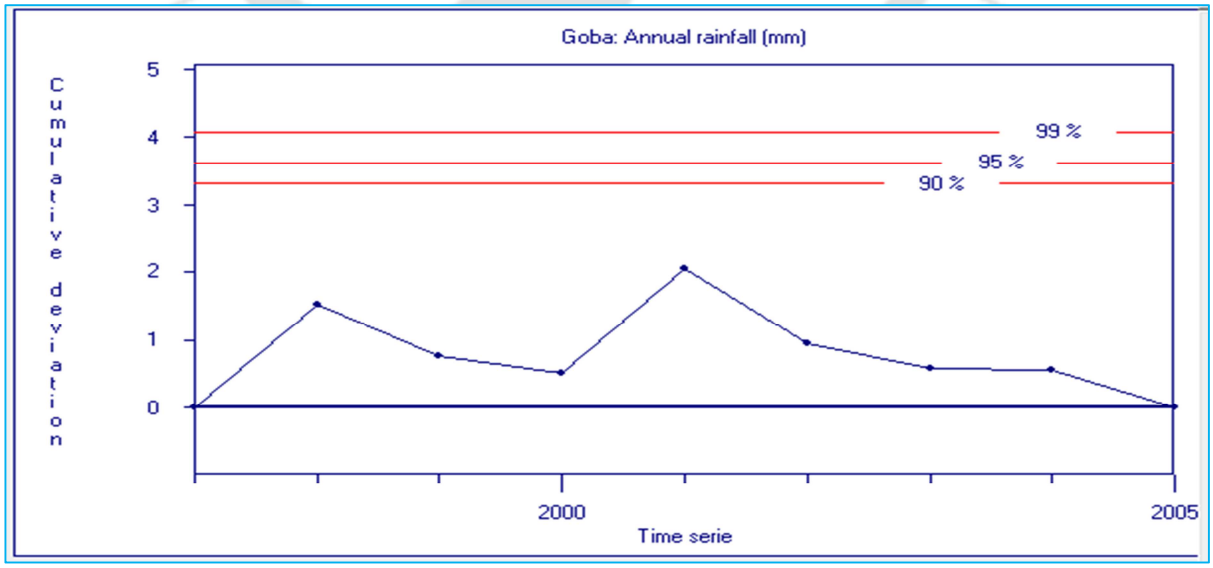

Appendix Figure 4 Homogeneity test of annual precipitation series at station Goba (homogeneous)

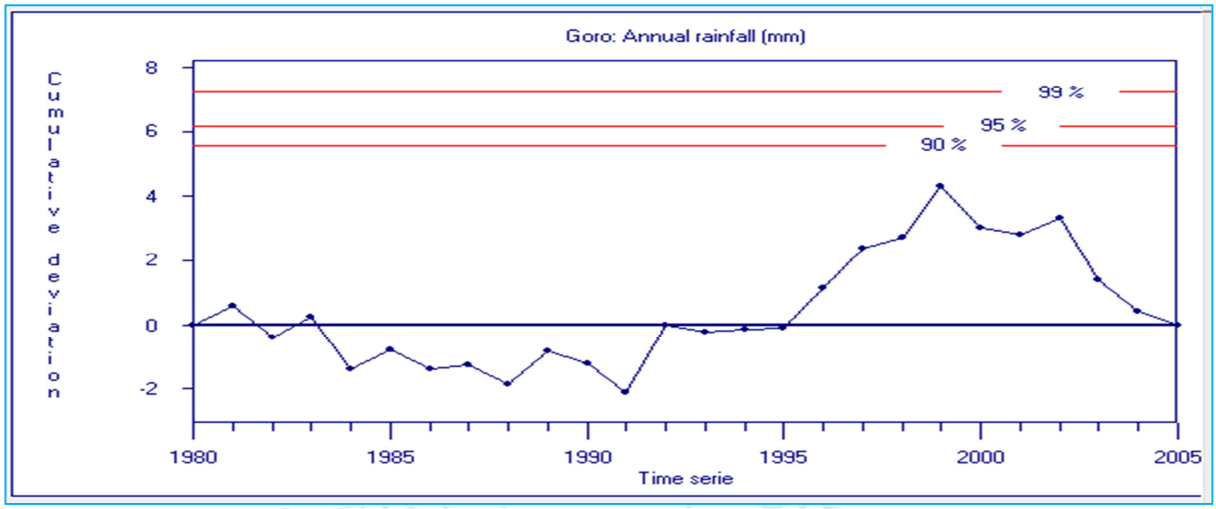

Appendix Figure 5 Homogeneity test of annual precipitation series at station Goro (homogeneous)

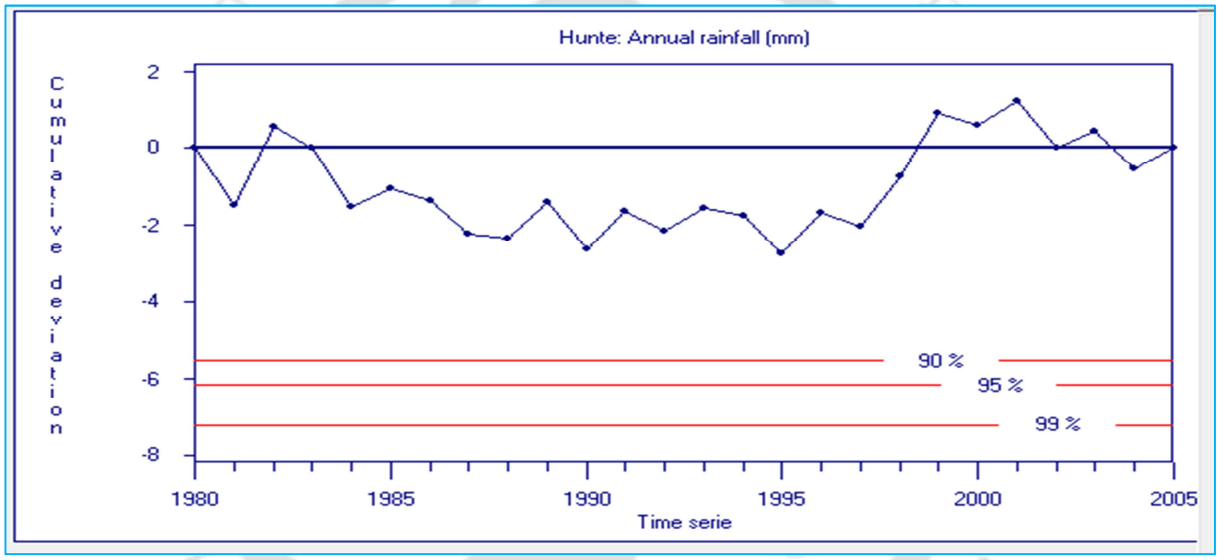

Appendix Figure 6 Homogeneity test of annual precipitation series at station Hunte (homogeneous)

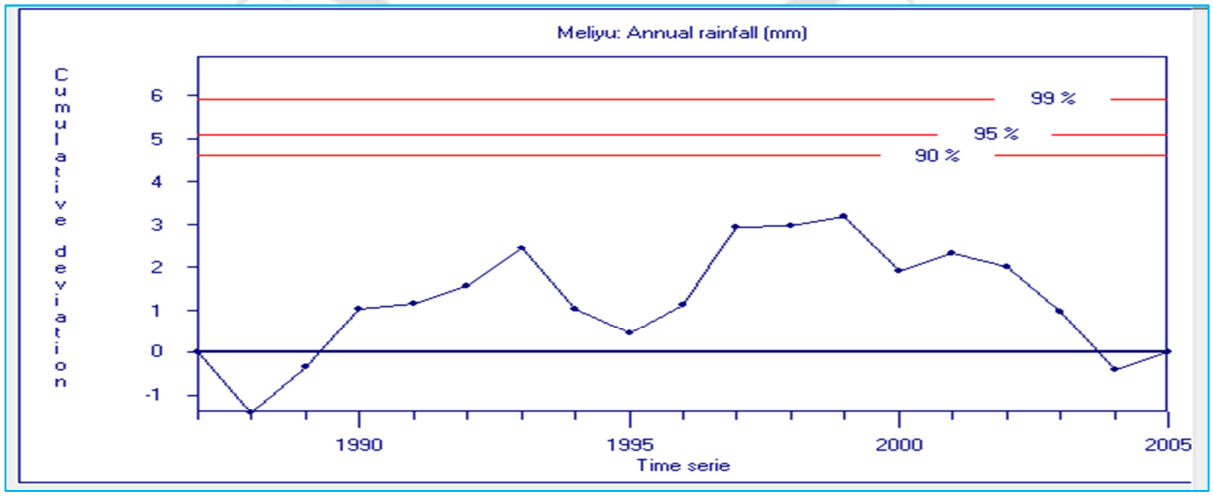

Appendix Figure 7 Homogeneity test of annual precipitation series at station Meliyu (homogeneous)

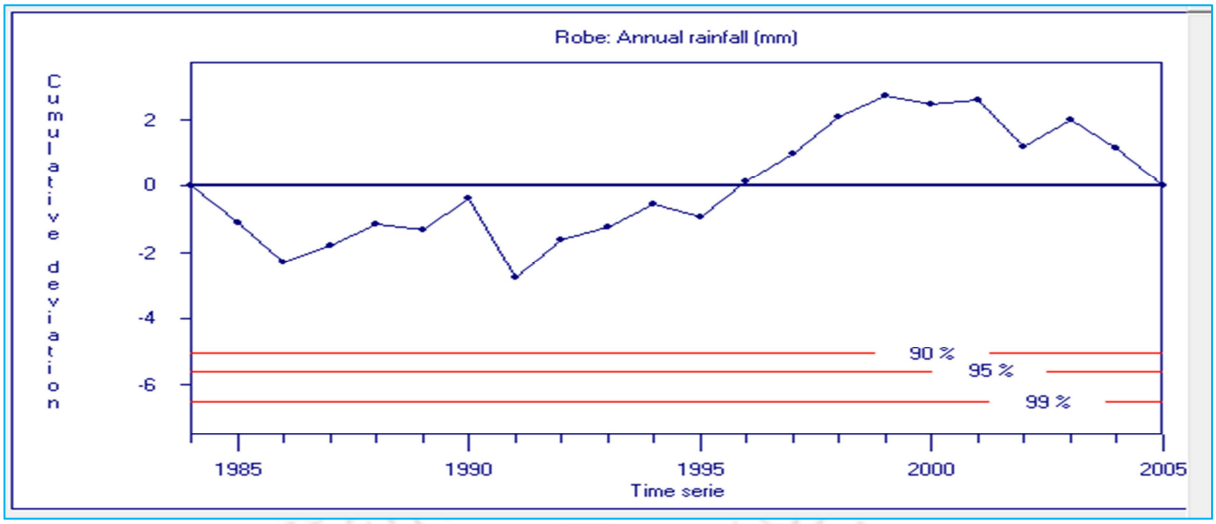

Appendix Figure 8 Homogeneity test of annual precipitation series at station Robe (homogeneous)

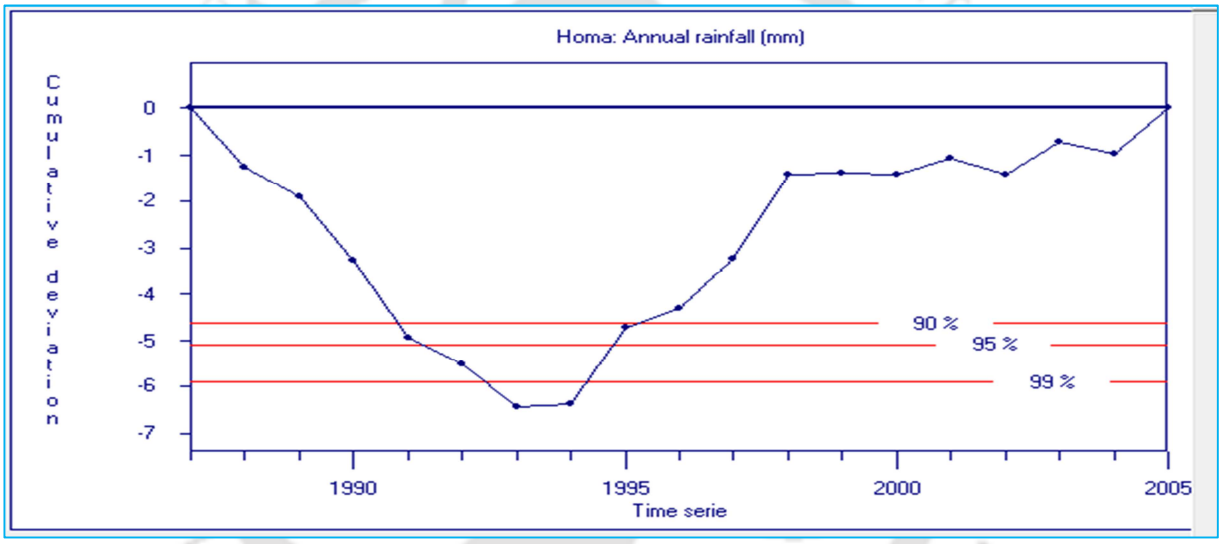

Appendix Figure 9 Homogeneity test of annual precipitation series at station Homa (non-homogeneous)

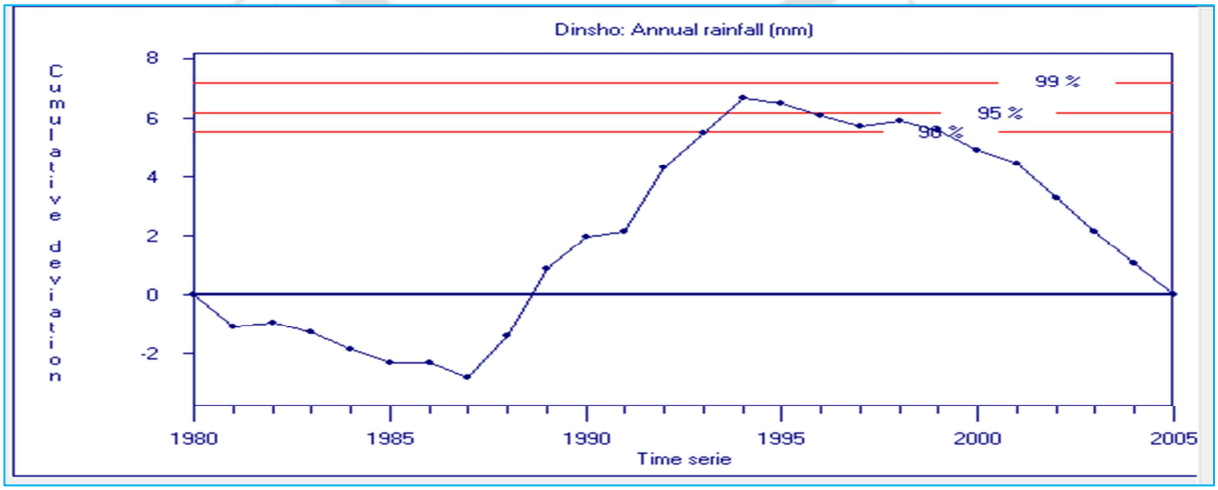

Appendix Figure 10 Homogeneity test of annual precipitation series at station Dinsho (non-homogeneous)

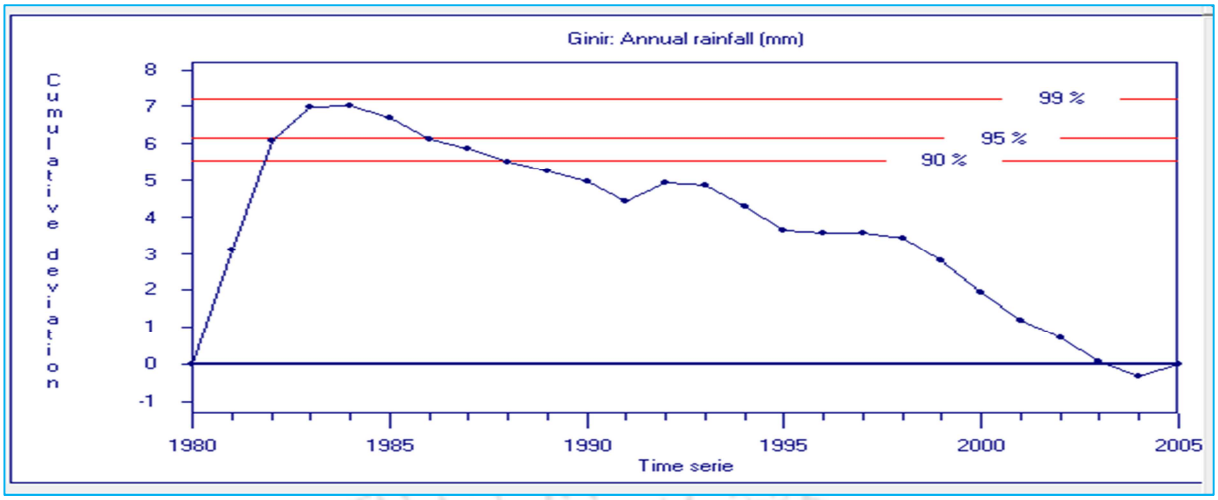

Appendix Figure 11 Homogeneity test of annual precipitation series at station Ginnir (non-homogeneous)

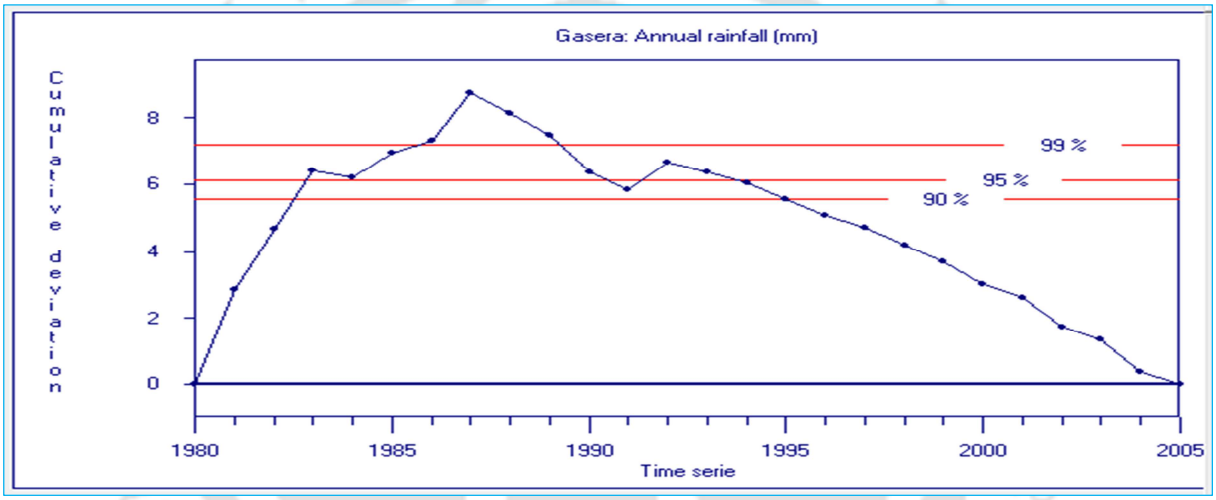

Appendix Figure 12 Homogeneity test of annual precipitation series at station Gassera (non-homogeneous)

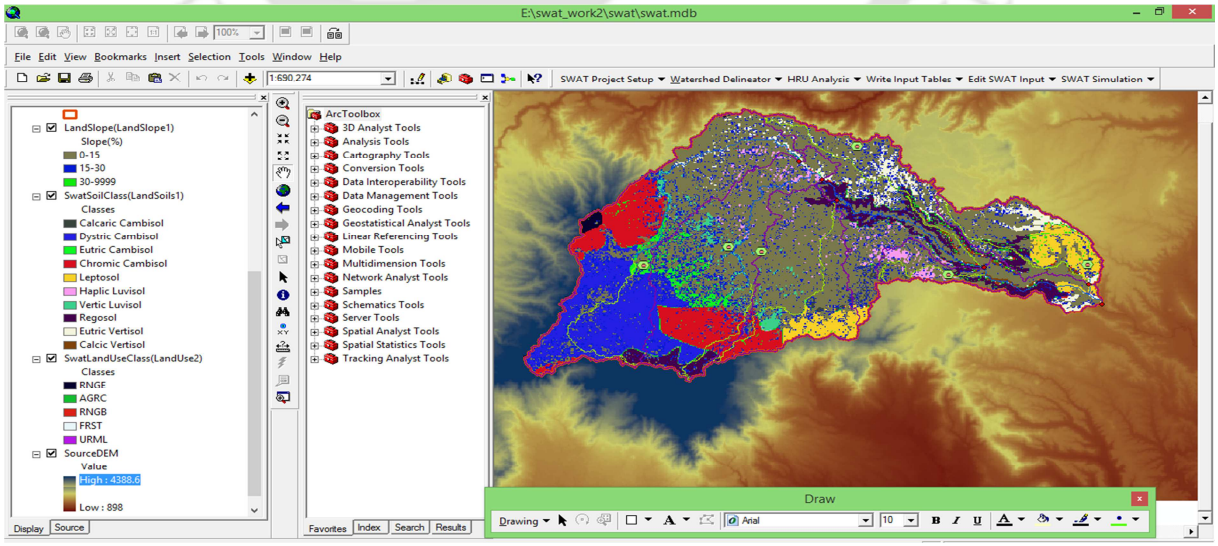

Appendix Figure 13 Demonstration of ArcSWAT model for Weyib River Basin

Appendix C

Appendix Photos

Some of the photos captured in side Weyib River basin during field trip are presented here under.

Appendix Photo 1 Bread wheat varieties in Sinnana Research Station, Bale zone of southern Ethiopia, in side Weyib River basin

Appendix Photo 2 Tegona river section, a tributary of Weyib River basin

Appendix Photo 3 Shaya river section, a tributary of Weyib River basin

Appendix Photo 4 Recent bale-robe flash flood, inside Weyib River basin

Appendix Photo 5 Mountain Nyala, Bale Mountains National park, Oromia regional state, inside Weyib River basin